EVALUATING THE ANTERIOR STABILITY PROVIDED BY THE GLENOHUMERAL CAPSULE: A FINITE ELEMENT APPROACH

by

Nicholas Joseph Drury

BS, University of Rochester, 2006

Submitted to the Graduate Faculty of

The Swanson School of Engineering in partial fulfillment

of the requirements for the degree of

Master of Science

University of Pittsburgh

2008

UNIVERSITY OF PITTSBURGH

SWANSON SCHOOL OF ENGINEERING

This thesis was presented

by

Nicholas Joseph Drury

It was defended on

July 7, 2008

and approved by

Patrick J. McMahon, MD, Assistant Professor, Department of Bioengineering

Rakie Cham, PhD, Assistant Professor, Department of Bioengineering

Jeffrey A. Weiss, PhD, Associate Professor, Department of Bioengineering, University of Utah

Thesis Advisor: Richard E. Debski, PhD, Associate Professor, Department of Bioengineering

EVALUATING THE ANTERIOR STABILITY PROVIDED BY THE GLENOHUMERAL CAPSULE: A FINITE ELEMENT APPROACH

Nicholas J. Drury, MS

University of Pittsburgh, 2008

The shoulder is the most dislocated joint in the body, with over 80% of dislocations occurring in the anterior direction. During anterior dislocation, the glenohumeral capsule within the shoulder is the primary joint stabilizer. Physical examinations following dislocation are crucial for clinicians to determine the location and extent of pathology in the capsule, and diagnoses from the examinations are used to decide the type, location, and extent of surgical repair to restore capsule function. These examinations, however, are not standardized for joint position among patients. Since capsule function is dependent upon joint position and can vary among patients, the lack of standardized joint positions for the examinations leads to misdiagnoses of the location and extent of capsule pathology that subsequently result in improper surgical procedures to restore capsule function. In fact, over 50% of redislocations and over 80% of pain and loss of motion following surgery have been shown to result from misdiagnoses of pathology to the capsule.

Therefore, the objective of the current work was to suggest joint positions where the stability provided by the capsule is consistent among patients in response to application of an anterior load. Two subject-specific finite element models of the glenohumeral joint were developed based on experimental data collected from two cadavers, using isotropic hyperelastic constitutive model to represent the capsule. The models were validated by comparing predicted capsule strains in the models to experimental capsule strains in clinically relevant joint positions.

The models were used to identify clinically relevant joint positions where the distributions of predicted capsule strain in the two models were correlated with an r^2 value greater than 0.7, and to further identify if strain was higher in specific regions of the capsule than others at these positions. The clinically relevant joint positions resulting from application of a 25 N anterior load at 60° of glenohumeral abduction and 10° - 40° of external rotation resulted in distributions of strain that were correlated with an r^2 value greater than 0.7. Of these positions, those with 20° - 40° of external rotation resulted in capsule strains that were significantly higher in the glenoid side of the anterior band of the inferior glenohumeral ligament than in other regions of the capsule. Therefore, the current work suggests that standardizing physical examinations for anterior instability at joint positions with abduction and a mid-range of external rotation may allow clinicians to more effectively diagnose the location and extent of capsule pathology resulting from anterior dislocation, and may ultimately lead to an improvement in surgical outcomes. The current work further provides an excellent foundation to evaluate the stability provided by the capsules of multiple subject-specific finite element models of the glenohumeral joint, to identify multiple joint positions for physical examinations that can be used to diagnose pathology throughout the glenohumeral capsule.

TABLE OF CONTENTS

PREFACE ..... **XX**

1.0 INTRODUCTION AND BACKGROUND **1**

1.1 DEMOGRAPHICS **3**

1.2 STRUCTURE OF THE GLENOHUMERAL CAPSULE **4**

1.2.1 Insertion Site **6**

1.3 FUNCTION OF THE GLENOHUMERAL CAPSULE **8**

1.3.1 Insertion Site **10**

1.4 DIAGNOSIS AND CLINICAL OUTCOMES **11**

1.4.1 Diagnosis **11**

1.4.2 Rehabilitation and Surgical Repair **12**

1.4.3 Clinical Outcomes and Relevance **14**

1.5 MOTIVATION FOR RESEARCH QUESTION **14**

1.6 RESEARCH QUESTION **17**

1.7 MOTIVATION FOR SPECIFIC AIMS **18**

1.8 SPECIFIC AIMS **25**

2.0 DEVELOPMENT AND VALIDATION OF FE MODEL 1 ..... **26**

2.1 INTRODUCTION **26**

2.2 MATERIAL COEFFICIENTS **28**

2.2.1 Available Data **29**

2.2.2 Computational Generation of Optimized Material Coefficients 30
2.3 FINITE ELEMENT MODEL DEVELOPMENT AND VALIDATION 31
2.3.1 Model Development 31
2.3.1.1 Mesh Development 31
2.3.2 Insertion Site Modification.....32
2.3.2.1 Labrum Inclusion 33
2.3.3 Finite Element Solution Procedure 33
2.3.4 Model Validation.....34
2.3.4.1 Predicted Strain Distribution 34
2.3.4.2 Finite Element Model Validation 35
3.0 DEVELOPMENT AND VALIDATION OF FE MODEL 2.....37
3.1 INTRODUCTION 37
3.2 SUBJECT-SPECIFIC EXPERIMENTAL INPUTS.....38
3.2.1 Reference Configuration 38
3.2.1.1 Specimen Preparation 38
3.2.1.2 Experimental Setup 40
3.2.1.3 Data Collection.....43
3.2.1.4 Determination of the Reference Configuration 43
3.2.2 Surface Geometry of Relevant Structures.....44
3.2.2.1 Structures of Interest.....45
3.2.2.2 CT Data Acquisition.....46
3.2.2.3 Surface Reconstruction and Development 48
3.2.3 Joint Positions for Validation 50
3.2.3.1 Robotic Universal Force/Moment Sensor System 52

3.2.3.1.1 Specimen Mounting 53

3.2.3.1.2 Application of Joint Motion 54

3.2.3.2 Measurement of Joint Kinematics and Capsule Strain 55

3.2.3.2.1 Experimental Setup 55

3.2.3.2.2 Data Collection 56

3.2.3.3 Determination of Experimental Capsule Strain 57

3.2.4 Material Coefficients to Constitutive Model 57

3.2.4.1 Tissue Sample Procurement 60

3.2.4.2 Experimental Setup 61

3.2.4.3 Data Collection.....63

3.2.4.4 Computational Generation of Optimized Coefficients.....65

3.3 FINITE ELEMENT MODEL DEVELOPMENT AND VALIDATION 67

3.3.1 Model Development 67

3.3.1.1 Mesh Development 67

3.3.2 Insertion Site Modification.....72

3.3.2.1 Preliminary Study.....72

3.3.2.1.1 Labrum Inclusion.....74

3.3.2.1.2 Sensitivity Study.....76

3.3.2.1.3 Sensitivity Study: Results.....79

3.3.2.2 Labrum Inclusion in FE Model 2.....82

3.3.3 Finite Element Solution Procedure 83

3.3.3.1 Joint Kinematics 83

3.3.3.2 Boundary Conditions 84

3.3.3.3 Finite Element Solution Procedure 85
3.3.4 Model Validation 86
3.3.4.1 Predicted Strain Distribution 86
3.3.4.2 Finite Element Model Validation 87
4.0 ANALYSIS OF JOINT POSITIONS 89
4.1 INTRODUCTION 89
4.2 KINEMATICS FOR INTERMEDIATE JOINT POSITIONS 92
4.2.1 Development of Anatomical Coordinate Systems 92
4.2.1.1 Scapular Anatomical Coordinate System 93
4.2.1.2 Humeral Anatomical Coordinate System 96
4.2.2 Joint Motions Using Anatomical Coordinate Systems 98
4.2.3 Rotations and Translations for Intermediate Joint Positions 99
4.2.3.1 Translations for Intermediate Joint Positions: FE Model 1 ... 100
4.2.3.2 Translations for Intermediate Joint Positions: FE Model 2 ... 103
4.3 ANTERIOR-INFERIOR CAPSULE STRAIN 105
4.3.1 Finite Element Model Output 105
4.3.2 Statistical Analyses 108
4.3.2.1 Joint Positions with Consistent Distribution of Strain 108
4.3.2.2 Localization of Stability Provided by Anterior Capsule 110
5.0 RESULTS 112
5.1 DEVELOPMENT OF FE MODEL 1 112
5.1.1 Computational Modifications 112
5.1.1.1 Material Coefficients 112
5.1.2 Finite Element Solution Procedure 114

5.2 VALIDATION OF FE MODEL 1 117

5.3 DEVELOPMENT OF FE MODEL 2 121

5.3.1 Reference Position 121

5.3.1.1 Scapular and Humeral Potting 121

5.3.1.2 Reference Position 122

5.3.2 Application of Joint Motion 122

5.3.2.1 Joint Kinematics 122

5.3.2.2 Experimental Strains 126

5.3.3 Material Coefficients 127

5.3.4 Finite Element Solution Procedure 133

5.4 VALIDATION OF FE MODEL 2 134

5.4.1 Initial Validation Attempt 134

5.4.2 FE Model 2 Modification 136

5.4.3 FE Model 2 Validation 145

5.5 ANALYSIS OF JOINT POSITIONS 148

5.5.1 Joint Positions with Consistent Strain Distributions 148

5.5.2 Localization of Stability at Clinically Relevant Joint Positions 152

5.5.2.1 Joint position with 10° of external rotation 153

5.5.2.2 Joint position with 20° of external rotation 155

5.5.2.3 Joint position with 30° of external rotation 157

5.5.2.4 Joint position with 40° of external rotation 159

5.5.2.5 Summary: Localization of Stability 161

6.0 DISCUSSION 163

6.1 FE MODEL VALIDATION 164

6.1.1 Advancements 164

6.1.2 Assumptions 165

6.1.3 Limitations 169

6.1.4 Future Directions 175

6.2 ANALYSIS OF JOINT POSITIONS 178

6.2.1 Advancements 178

6.2.2 Assumptions 179

6.2.3 Limitations 180

6.2.4 Future Directions 181

6.3 RELEVANCE OF FINDINGS 182

6.3.1 Engineering Relevance 182

6.3.2 Clinical Relevance 183

6.4 SUMMARY 186

APPENDIX A. EXPERIMENTAL ROBOT PROTOCOL 188

APPENDIX B. NIKE3D INPUT DECK FOR FE MODEL 2 198

APPENDIX C. FEBIO INPUT DECK FOR FE MODEL 2 208

APPENDIX D. MATLAB CODE FOR SIMULATION OF JOINT MOTION 215

BIBLIOGRAPHY 222

LIST OF TABLES

Table 2.1 Distribution of shell elements within the five capsule regions of FE Model 1 32

Table 3.1 Distribution of shell elements within the five capsule regions of FE Model 2 70

Table 3.2 Capsule region thicknesses obtained experimentally in the cadaver for FE Model 2 .. 72

Table 4.1 Humeral translations with respect to the scapular anatomical coordinate system for FE Model 1, resulting from application of a 25 N anterior load after the joint was abducted and externally rotated. Highlighted rows are for experimental joint positions..... 101

Table 4.2 Humeral translations with respect to the scapular anatomical coordinate system for FE Model 2, resulting from application of a 25 N anterior load after the joint was abducted and externally rotated. Highlighted rows are for experimental joint positions..... 103

Table 4.3 Distribution of elements in the sub-regions of FE Model 1 107

Table 4.4 Distribution of elements in the sub-regions of FE Model 2 107

Table 4.5 Joint positions in FE Model 1 and FE Model 2 where correlation tests were performed 109

Table 5.1 Material coefficients for the five capsule regions. For the axillary pouch and posterior region, the longitudinal and transverse Cauchy stress-stretch curves were used to create an average Cauchy stress-stretch curve to which material coefficients were generated 113

Table 5.2 Ranges of values for C1 and C2 in selected capsule regions obtained by Rainis [40] and during preliminary experiments in our research group 114

Table 5.3 Contact parameter modification at the joint position with 31.1° of external rotation 115

Table 5.4 FE Model 1 experimental and predicted strains in the anterior band of the inferior glenohumeral ligament, at the three clinically relevant joint positions for validation.... 119

Table 5.5 Quantitative 3-dimensional capsule strain marker motion at the three joint positions identified to have the lowest visual capsule strain marker motion. ER=external rotation, IR=internal rotation..... 122

Table 5.6 Average, standard deviation (SD), and peak maximum principal strains in the anterior-inferior capsule at the 3 clinically relevant joint positions with 0°, 25.1°, and 57.3° of external rotation 127

Table 5.7 Material coefficients for the five capsule regions. For the axillary pouch and posterior region, the longitudinal and transverse Cauchy stress-stretch curves were used to create an average Cauchy stress-stretch curve to which material coefficients were generated 132

Table 5.8 FE Model 2 experimental and predicted strains in the anterior band of the inferior glenohumeral ligament, at the three clinically relevant joint positions for validation.... 136

Table 5.9 FE Model 2 experimental and predicted strains in the anterior band of the inferior glenohumeral ligament, at the three clinically relevant joint positions for validation.... 147

Table 5.10 FE Model 1 strain ratios in the six sub-regions, at the four clinically relevant joint positions with an r^2 value greater than 0.7 152

Table 5.11 FE Model 2 strain ratios in the six sub-regions, at the four clinically relevant joint positions with an r^2 value greater than 0.7 152

Table 5.12 Magnitude (Ave ± SD) of strain in the glenoid side of the anterior band of the inferior glenohumeral ligament, as well as the minimum differences in strain when compared to the remaining five sub-regions, at the clinically relevant joint positions with 20°, 30°, and 40° of external rotation 162

Table 6.1 Average strains in the anterior band of the inferior glenohumeral ligament at the clinically relevant joint positions with 0°, 30°, and maximum external rotation. Specimen 1 – Specimen 5 = specimens used within our research group for an additional study [21] 171

LIST OF FIGURES

Figure 1.1 Lateral view of the left shoulder placed in abduction and external rotation 2

Figure 1.2 Capsule anatomy viewed laterally, with the humeral head removed (right shoulder). 1) Superior glenohumeral ligament (SGHL), 2) Middle glenohumeral ligament (MGHL), 3) Anterior band of the inferior glenohumeral ligament (AB-IGHL), 4) Posterior band of the inferior glenohumeral ligament (PB-IGHL), 5) Long head of the biceps tendon. The axillary pouch is between the AB-IGHL and PB-IGHL, the posterior region extends superiorly from the PB-IGHL, and the anterosuperior region extends superiorly from the AB-IGHL to include the SGHL and MGHL 5

Figure 1.3 Anterior-inferior capsulolabrum insertion types [48]..... 7

Figure 1.4 Anterior view (right shoulder) of the plicate and shift technique indicating "T" incision followed by a shift of the capsule tissue [77]..... 13

Figure 1.5 FE Model 1: Left shoulder, anterior view 22

Figure 1.6 Material response of capsule tissue, a hypoelastic constitutive model, and a hyperelastic constitutive model..... 23

Figure 2.1 Overview of finite element model development and validation process 27

Figure 3.1 Anterior view of the cadaver for FE Model 2 (right shoulder), after dissection down to the capsule and after the humerus and scapula were potted in epoxy putty 39

Figure 3.2 Inferior view of the 77 capsule strain markers applied to the anterior-inferior glenohumeral capsule for determination of the reference configuration..... 40

Figure 3.3 A) Joint mounted into custom fixture, with the air tank used for inflation shown B) Inflation via rubber hose inserted into rotator interval 41

Figure 3.4 Overlaid snapshots at two different joint positions showing relatively large (left) and small (right) capsule strain marker motion between the 4.8 kPa and 6.2 kPa pressures. Black ovals enclose the same capsule strain marker at the two different pressures..... 44

Figure 3.5 Joint, custom fixture, and air tank positioned in CT scanner..... 47

Figure 3.6 2-dimensional slice with the following structures segmented: humerus, humeral head cartilage, rubber tube, scapula, and capsule (capsule strain markers and registration blocks not shown) 49

Figure 3.7 A) Anterior view of the 3-dimensional surfaces created in Amira for FE Model 2, right shoulder (capsule strain markers and rubber tubes not shown). B) Capsule removed to expose humeral head cartilage 49

Figure 3.8 6-degree-of-freedom robotic/universal force-moment sensor testing system 53

Figure 3.9 Experimental motion and strain tracking setup 56

Figure 3.10 Veronda-Westmann isotropic hyperelastic strain energy function 58

Figure 3.11 Lateral view of the glenoid labrum, with the labrum radial thickness indicated 61

Figure 3.12 Material tensile testing apparatus setup 62

Figure 3.13 Typical load-elongation curve for tensile loading applied to capsule tissue, demonstrating toe and linear regions 64

Figure 3.14 Sample Cauchy stress-stretch plot of the posterior capsule region, demonstrating how the longitudinal and transverse curves were used to generate material coefficients from an average curve 66

Figure 3.15 Lateral view of FE Model 2 (right shoulder), indicating the projection of the green mesh of capsule quadrilateral shell elements to the red surface of the capsule. The posterior half of the mesh has already been projected to the capsule surface. Also shown are the humeral and scapular surfaces in red 69

Figure 3.16 Anterior, inferior, and posterior views of FE Model 2 capsule mesh (right shoulder) 71

Figure 3.17 Inferior view of maximum principal strains in capsule of FE Model 1 (left shoulder) at 60° of abduction and maximum external rotation. Black arrow indicates irregular strain concentration at glenoid insertion of axillary pouch 73

Figure 3.18 Left) Anterior view of FE Model 1 (left shoulder) Right) Newly added labrum regions 76

Figure 3.19 Labrum thickness modification comparisons. AB-L, AP-L, PB-L = labrum regions of the anterior band of the inferior glenohumeral ligament, the axillary pouch, and the posterior band of the inferior glenohumeral ligament. Capsule = mid-substance elements of the anterior band of the inferior glenohumeral ligament used for validation 80

Figure 3.20 Labrum modulus modification comparisons. AB-L, AP-L, PB-L = labrum regions of the anterior band of the inferior glenohumeral ligament, the axillary pouch, and the

posterior band of the inferior glenohumeral ligament. Capsule = mid-substance elements of the anterior band of the inferior glenohumeral ligament used for validation 81

Figure 3.21 Overview of the process to obtain joint kinematics. Registration blocks were digitized in the reference position and in the clinically relevant joint positions, and the joint kinematics were obtained by computing relative motion of the registration blocks from the reference position to the clinically relevant joint positions..... 84

Figure 3.22 Anterior-inferior views of experimental and computational validation elements for FE Model 2 (right shoulder), determined from the positions of the capsule strain markers 87

Figure 4.1 Anterior-medial view of FE Model 2 (right shoulder). Yellow arrow indicates medial axis of anatomical coordinate system, determined from the coordinates of the nodes on the medial face of the scapular registration block 94

Figure 4.2 Medial view of FE Model 2 (right shoulder). Yellow arrow indicates anterior axis of anatomical coordinate system, determined from the coordinates of the nodes located in the plane of the scapula..... 95

Figure 4.3 Nodes approximating the most anterior aspect of the lesser tuberosity (Anterior side) and most posterior aspect of the humeral ridge (Posterior side)..... 96

Figure 4.4 Posterior view of humerus (right shoulder) with circumferential rings of nodes identified, for use in determining the humeral axis of internal/external rotation 97

Figure 4.5 Inferior view of FE Model 1 (left shoulder) at six clinically relevant joint positions. The capsule is removed to show the positions of the humerus with respect to the scapula at each clinically relevant joint position. The intermediate joint positions with 10°, 20°, and 40° of external rotation appear to be interpolated between the joint positions with 0°, 31.1°, and 51.8° of external rotation..... 102

Figure 4.6 Lateral view of FE Model 2 (right shoulder) at six clinically relevant joint positions. The capsule is removed to show the positions of the humerus with respect to the scapula at each clinically relevant joint position. The intermediate joint positions with 10°, 20°, 40°, and 50° of external rotation appear to be interpolated between the joint positions with 0°, 25.1°, and 57.3° of external rotation 105

Figure 4.7 Inferior view of FE Model 2 (right shoulder), indicating six sub-regions of the anterior-inferior capsule formed by the anterior-inferior capsule halfway point. AB-IGHL = anterior band of the inferior glenohumeral ligament, AP = axillary pouch, PB-IGHL = posterior band of the inferior glenohumeral ligament..... 106

Figure 5.1 Inferior view of FE Model 1 (left shoulder) at the clinically relevant joint position with 31.1° of external rotation. The magnitude and distribution of strain in the anterior-inferior capsule was almost identical when either set of contact parameters was used that resulted in 100% convergence of the model..... 116

Figure 5.2 Inferior views of experimental and predicted strains in the anterior band of the inferior glenohumeral ligament for FE Model 1 (left shoulder), at the three clinically relevant joint positions for validation 118

Figure 5.3 Comparisons of experimental and predicted shape of the capsule for FE Model 1 (left shoulder), at the clinically relevant joint position with 51.8° of external rotation. The anterior band of the inferior glenohumeral ligament is outlined in black. Note that the capsule wraps around the humeral head during the joint motion 120

Figure 5.4 Radiograph with anterior view of joint (right shoulder) after potting procedure, demonstrating adequate potting 121

Figure 5.5 Anterior radiographs of joint (right shoulder) when mounted on robot, at 30° and 60° of glenohumeral abduction 123

Figure 5.6 Anterior-posterior humeral translation in response to 25 N anterior-posterior load, at the three clinically relevant joint positions with 0°, 25.1°, and 57.3° of external rotation 124

Figure 5.7 Superior-inferior humeral translation in response to 25 N anterior-posterior load, at the three clinically relevant joint positions with 0°, 25.1°, and 57.3° of external rotation 125

Figure 5.8 Medial-lateral humeral translation in response to 25 N anterior-posterior load, at the three clinically relevant joint positions with 0°, 25.1°, and 57.3° of external rotation... 125

Figure 5.9 Inferior view of the magnitude and direction of maximum principal strains at the clinically relevant joint positions with 0°, 25.1°, and 57.3° of external rotation (right shoulder). Black lines indicate margins of the anterior band of the inferior glenohumeral ligament..... 126

Figure 5.10 Experimental and optimized load-elongation curves for the anterosuperior region, anterior band of the inferior glenohumeral ligament (AB-IGHL), and posterior band of the inferior glenohumeral ligament (PB-IGHL) 129

Figure 5.11 Experimental and optimized load-elongation curves for the axillary pouch, with elongations in the longitudinal and transverse directions 130

Figure 5.12 Experimental and optimized load-elongation curves for the posterior region, with elongations in the longitudinal and transverse directions 131

Figure 5.13 Inferior view of FE Model 2 (right shoulder) at the clinically relevant joint position with 30° of external rotation. Black arrow indicates penetration of humerus through the capsule..... 133

Figure 5.14 Inferior views of experimental and predicted strains in the anterior band of the inferior glenohumeral ligament (right shoulder), at the three clinically relevant joint positions for validation 135

Figure 5.15 Inferior views of FE Model 2 (right shoulder) at the clinically relevant joint position with 25.1° of external rotation with modification of the simulated labrum. There were little if any qualitative differences when the labrum taper was decreased from 6.0 mm to 4.0 mm at the interface with the glenoid..... 137

Figure 5.16 Inferior views of FE Model 2 (right shoulder) at the clinically relevant joint position with 25.1° of external rotation with modification of the capsule thickness. There were little if any qualitative differences when the capsule thickness was decreased from 3.0 mm to 2.0 mm..... 138

Figure 5.17 Inferior views of FE Model 2 (right shoulder) at the clinically relevant joint position with 25.1° of external rotation with modification of the capsule bulk modulus. There were little if any qualitative differences when the bulk modulus was changed to 150, 500, or 1000..... 140

Figure 5.18 Inferior views of FE Model 2 (right shoulder) at the clinically relevant joint position with 25.1° of external rotation with modification of the capsule material coefficients. There were little if any qualitative differences in the magnitude and distribution of strain in the capsule when the values of C1 and C2 were scaled by 0.5X, 1.5X, or 2X of the initial values of C1 and C2..... 142

Figure 5.19 Inferior views of FE Model 2 (right shoulder) at the clinically relevant joint position with 25.1° of external rotation with region-specific modification of the capsule material coefficients. There was significant change in the magnitude and distribution of strain in the anterior-inferior capsule following the modification..... 143

Figure 5.20 Inferior views of FE Model 2 (right shoulder) at the clinically relevant joint positions with 0°, 25.1°, and 57.3° of external rotation, using initial material coefficients and the optimal region-specific material coefficients..... 144

Figure 5.21 Inferior views of experimental and predicted strains in the anterior band of the inferior glenohumeral ligament (right shoulder), at the clinically relevant joint positions with 0°, 25.1°, and 57.3° of external rotation..... 146

Figure 5.22 Comparisons of experimental and predicted shape of the capsule for FE Model 2 (right shoulder), at the clinically relevant joint position with 57.3° of external rotation. The anterior band of the inferior glenohumeral ligament is outlined in black. The large black arrows indicate discrepancies in the predicted and experimental shape of the axillary pouch..... 148

Figure 5.23 Inferior views of the distribution of strain in the anterior-inferior capsule in FE Model 1 (left) and FE Model 2 (right) at the six clinically relevant joint positions..... 150

Figure 5.24 Correlation of strain ratios in the sub-regions of the anterior-inferior capsule of FE Model 2 vs. FE Model 1, at each of the six clinically relevant joint positions. $r2 > 0.7$ indicates high correlation between the distribution of strain in the anterior-inferior capsule in FE Model 1 and FE Model 2. AB-IGHL: G, AB-IGHL: H = glenoid and humeral sides of the anterior band of the inferior glenohumeral ligament. AP: G, AP: H

= glenoid and humeral sides of the axillary pouch. PB-IGHL: G, PB-IGHL: H = glenoid and humeral sides of the posterior band of the inferior glenohumeral ligament 151

Figure 5.25 Strains in the six sub-regions of FE Model 1 and FE Model 2, at the clinically relevant joint position with 10° of external rotation. AB-IGHL: G, AB-IGHL: H = glenoid and humeral sides of the anterior band of the inferior glenohumeral ligament, AP: G, AP: H = glenoid and humeral sides of the axillary pouch, PB-IGHL: G, PB-IGHL: H = glenoid and humeral sides of the posterior band of the inferior glenohumeral ligament 154

Figure 5.26 Strains in the six sub-regions of FE Model 1 and FE Model 2, at the clinically relevant joint position with 20° of external rotation. AB-IGHL: G, AB-IGHL: H = glenoid and humeral sides of the anterior band of the inferior glenohumeral ligament, AP: G, AP: H = glenoid and humeral sides of the axillary pouch, PB-IGHL: G, PB-IGHL: H = glenoid and humeral sides of the posterior band of the inferior glenohumeral ligament 156

Figure 5.27 Strains in the six sub-regions of FE Model 1 and FE Model 2, at the clinically relevant joint position with 30° of external rotation. AB-IGHL: G, AB-IGHL: H = glenoid and humeral sides of the anterior band of the inferior glenohumeral ligament, AP: G, AP: H = glenoid and humeral sides of the axillary pouch, PB-IGHL: G, PB-IGHL: H = glenoid and humeral sides of the posterior band of the inferior glenohumeral ligament 158

Figure 5.28 Strains in the six sub-regions of FE Model 1 and FE Model 2, at the clinically relevant joint position with 40° of external rotation. AB-IGHL: G, AB-IGHL: H = glenoid and humeral sides of the anterior band of the inferior glenohumeral ligament, AP: G, AP: H = glenoid and humeral sides of the axillary pouch, PB-IGHL: G, PB-IGHL: H = glenoid and humeral sides of the posterior band of the inferior glenohumeral ligament 160

Figure 6.1 Inferior views of experimental and predicted strains in the anterior band of the inferior glenohumeral ligament of FE Model 2 (right shoulder), at the clinically relevant joint position with 30° of external rotation 173

Figure 6.2 Inferior views of FE Model 2 (right shoulder). For the current work, the strains in the validation elements were averaged within the region of the AB-IGHL. It is suggested for future direction that the strains in the validation elements are averaged within more refined regions of the anterior-inferior capsule 177

PREFACE

I would like to acknowledge my thesis advisor, Dr. Richard Debski, for all of his guidance, tutelage, support, and for providing me with the opportunity to perform my graduate work at the University of Pittsburgh. I have benefited both as a researcher and as an engineer, and my development is a testament to the time and effort he spent with me. I would also like to acknowledge the clinical advisor to my thesis, Dr. Patrick McMahon. In addition to helping me see "the forest through the trees," his clinical perspective and attitude towards helping others served as a reminder of why I chose the field of bioengineering. Thank you both for your time, commitment, and positive attitudes; it has truly been a pleasure working with you.

I would also like to thank the remaining members of my thesis committee, Dr. Rakie Cham and Dr. Jeffrey Weiss. Dr. Cham has contributed valuable knowledge and advice, an objective perspective, and an encouraging attitude, and has been a great complement to the rest of the committee. Dr. Weiss and his staff, particularly Ben Ellis, have played a critical role in the current work, providing tremendous input and time teaching and explaining the intricacies of computational modeling. Thank you all for your efforts and contributions to the work.

I would also like to thank Dr. Savio Woo for the opportunity to perform research in the Musculoskeletal Research Center, and Dr. Steve Abramowitch for his outstanding suggestions and willingness to help at all times. This work would not have been possible without the contributions of my coworkers in the MSRC, particularly the Shoulder Group. Carrie Voycheck

contributed her expertise in materials testing, PHAMD, and cookies, John Jolly contributed an endless supply of references, fitness advice, and a dynamic robot learning environment, and Andrew Brown contributed his tremendous knowledge of strain tracking. To the rest of the MSRC – Fisher, Feola, Alejandro, Serena, Antonio, Zegbeh, Lauren – thanks for your friendship, suggestions, and for making it enjoyable / bearable along the way. And for the golfers in the group….thank you for making me feel like Tiger Woods on the course.

A special thanks goes out to my fiancée Karen, who provided endless support, motivation, and encouragement from Day 1. Thank you for helping me to see the bigger picture and to keep things in perspective, for being my faith partner, and of course for feeding me along the way. Dave and Jim, thanks for making 940 Greenfield a fun place to live, even if we spent more time together out of the house than in the house over the last 2 years. And to Sara and Kelly, thanks for helping me remember my roots.

And of course I would like to thank my family. My parents have been outstanding role models who have always encouraged me to pursue my goals, to strive for success, and to keep a strong faith, and have been behind me through everything I've done. To my brothers and sisters: Colleen, Julie, Jean, Sarah, Chris, Meg, and Matt: thanks for providing a nationwide network of irreplaceable friendship, support, and entertaining life stories. You are all amazingly successful at what you do, both on professional and personal levels (thanks for raising the bar so high), and I thank God for the blessing of being in such a wonderful family.

1.0 INTRODUCTION AND BACKGROUND

The glenohumeral joint is the most dislocated major joint in the body, and dislocations occur across all age, gender, and race populations. Glenohumeral joint stability is provided by a complex combination of active and passive stabilizers, including muscular restraints, bony contact, negative intra-articular pressure, and the glenohumeral capsule. During the extreme joint positions associated with dislocation, however, primary stability is provided by the glenohumeral capsule. The capsule is a sheet of ligamentous tissue that connects the glenoid component of the scapula to the humerus, with several regions identified by variations in capsule thickness. The capsule truly functions as a composite sheet of tissue, however, acting to distribute loads across the joint multi-directionally and across the margins of the regions.

While the ball-and-socket nature of the glenohumeral joint allows for 6-degree-of-freedom motion, greater than 80% of all dislocations occur in the anterior direction [1, 2]. These traumatic events can result in rupture or tear of the capsule and/or its insertion site, as well as permanent deformation of the capsule resulting from excessive loading that stretches the capsule beyond its elastic limit [3-8]. Anterior dislocations frequently occur in joint positions where the arm is abducted and externally rotated, defined as the “apprehension position” due to patient concern that redislocation may occur when the joint is oriented in this position (Figure 1.1). The stability provided by specific regions of the capsule changes with joint positions, as regions of the capsule may be distributing load in some positions but may be unloaded in others. In joint

positions with abduction and external rotation, however, it is well-documented that anterior stability is provided by the anterior-inferior capsule [9-14].

Figure 1.1 Lateral view of the left shoulder placed in abduction and external rotation

Clinicians use multiple methods for diagnosing capsule pathology, including inquiries of patient history, radiographs, and arthroscopic examination. The use of physical examinations, however, is the most crucial step for diagnosing the location and extent of capsule pathology [15-17]. During these examinations clinicians apply load to the humerus while attempting to rigidly fix the scapula, and use the resulting humeral kinematics as a means of measuring the stability provided by the capsule in order to diagnose capsule pathology. In spite of their importance, the use of these examinations is problematic since they are unstandardized for joint position. Both the stability provided by the capsule and the glenohumeral kinematics during the examinations are dependent upon joint position [10, 11, 13, 14, 18-20], resulting in misdiagnosis of capsule pathology from the lack of standard joint positions for the examinations. Furthermore, the variability in the stability provided by the capsule from patient to patient may increase or decrease depending on joint position [11, 17, 18, 21], which may result in position-dependent

reliability of clinician diagnoses [22]. The lack of standard joint positions for the examinations where the stability provided by the capsule is consistent among patients may lead to misdiagnoses of capsule pathology, which in turn may result in poor outcomes following operative capsule repair since surgical procedures are based on the diagnoses [19, 23-25].

Therefore, there exists a need to identify clinically relevant joint positions where the stability provided by the capsule is consistent among patients, and to further identify at these positions the regions of the capsule that are providing stability. This may help establish physical examinations for capsule pathology that are standardized for joint position, that allow clinicians to more effectively diagnose the location and extent of pathology in the capsule which may in turn lead to an improvement in surgical outcomes.

1.1 DEMOGRAPHICS

Dislocations occur across all ages, genders, and races, thereby affecting all demographic groups. Approximately 34,000 shoulder dislocations occur per year in the young adult population between the ages of 15 to 25 years [26, 27], and approximately 2% of the general population (~5.6 million individuals in the United States) will dislocate their glenohumeral joint between the ages of 18-70 years [26, 28]. Due to the increased activity level in the general population, these values may underestimate future rates of dislocation, especially when considering the increases in the incidence of dislocation in the young adult population between the ages of 15 to 25 years [29, 30].

1.2 STRUCTURE OF THE GLENOHUMERAL CAPSULE

The glenohumeral capsule is composed of a variably thick layer of tissue that surrounds the ball-and-socket glenohumeral joint, with thickenings that have been termed the glenohumeral ligaments [13, 31] (Figure 1.2). Researchers, engineers, and clinicians have previously treated these thickenings as discrete uni-directional ligaments that stabilize the joint [14, 32-34], much like the collateral and cruciate ligaments in the knee. More recent work has suggested that the discretization of the capsule into separate ligamentous regions may not be appropriate, but rather that the capsule should be treated as a continuous sheet of ligamentous tissue that acts to distribute loads in multiple directions [13, 35, 36]. The capsule has therefore been divided into regions, including the anterior-inferior capsule (containing the anterior band of the inferior glenohumeral ligament (AB-IGHL), the axillary pouch, and the posterior band of the inferior glenohumeral ligament (PB-IGHL)), the posterior capsule, and the anterosuperior capsule (containing the superior glenohumeral ligament (SGHL) and middle glenohumeral ligament (MGHL)).

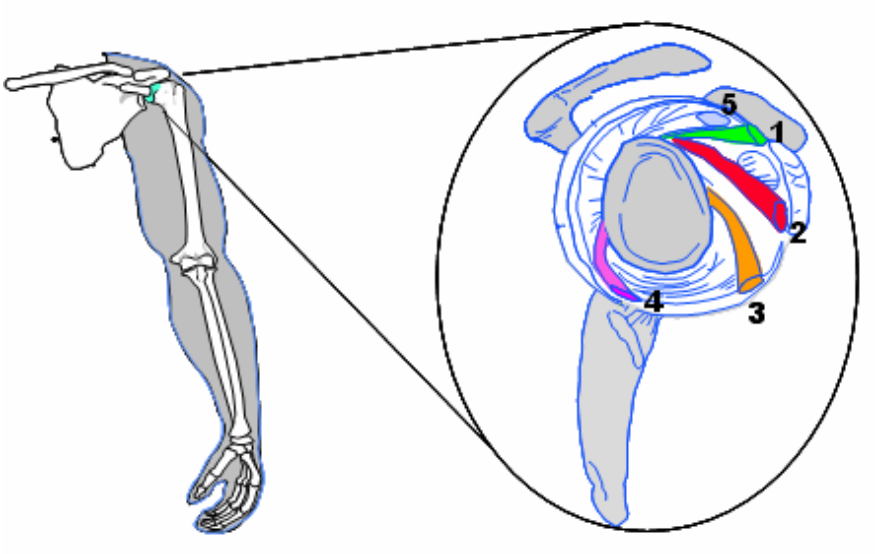

Figure 1.2 Capsule anatomy viewed laterally, with the humeral head removed (right shoulder). 1) Superior glenohumeral ligament (SGHL), 2) Middle glenohumeral ligament (MGHL), 3) Anterior band of the inferior glenohumeral ligament (AB-IGHL), 4) Posterior band of the inferior glenohumeral ligament (PB-IGHL), 5) Long head of the biceps tendon. The axillary pouch is between the AB-IGHL and PB-IGHL, the posterior region extends superiorly from the PB-IGHL, and the anterosuperior region extends superiorly from the AB-IGHL to include the SGHL and MGHL

Unlike traditional uni-directional ligaments such as the cruciate and collateral knee ligaments that have transversely isotropic material symmetry, the capsule tissue has isotropic material properties. O'Brien et al. [13] demonstrated a great deal of intermingling of the collagen fibers throughout the anterior-inferior capsule, and reported depth-dependent variations in collagen fiber architecture. Debski et al. [35] used a small angle light scattering (SALS) device to characterize the random orientation of collagen fibers throughout the anterior-inferior capsule. In addition, work by Malicky et al. [36] and Moore et al. [21] indicated that maximum principal strain directions on the surface of the anterior-inferior capsule in clinically relevant joint positions can be directed transversely to the longitudinal (glenoid to humerus) axis of the capsule, suggesting an underlying isotropic structure. Furthermore, arthroscopic examinations have confirmed the high variability in size and appearance of the thickenings [37-39].

Recent work has been performed in our research group on the material properties of the capsule tissue. Using a combined experimental and computational approach with a bi-directional testing protocol, Rainis [40] quantified the material response of the capsule to tensile and shear elongations applied in the longitudinal and transverse (perpendicular to the longitudinal) directions of the capsule. It was found that not only were there similarities in the material properties among different capsule regions, but that the material response within a capsule region was similar between longitudinal and transverse elongations. Additionally, Moore [41] compared the capsule surface strains and shape at a clinically relevant joint position in a cadaver and in a finite element model that was subject-specific to the cadaver. The finite element model was modified so that it could treat the capsule either as a composite sheet of tissue or as a collection of discrete ligaments. It was found that the experimentally measured capsule surface strains and shape were much better predicted by the model that treated the capsule as a composite sheet of tissue, as the lack of boundary conditions in the discrete ligament model resulted in unusual capsule bending and strain patterns that were not seen experimentally. The conclusions of these studies strongly confirm the need to treat the capsule as an isotropic continuous sheet of ligamentous tissue.

1.2.1 Insertion Site

The insertion of the glenohumeral capsule into the glenoid contains a fibrocartilagenous transition from the ligamentous capsule to the osseous glenoid. An integral component of the capsule's glenoid insertion is the glenoid labrum, a vascularized, pear-shaped ring of dense, predominantly fibrous tissue that extends laterally from the articular cartilage of the glenoid [24, 42-48].

There are three layers through the depth of the labrum [46, 49], and while collagen fiber architecture may be aligned at certain depths, overall the alignment is more irregular. The labrum constitutes approximately 50% of the depth of the glenoid cavity throughout the periphery [42], however the radial thickness can range from approximately 2 – 11 mm [43].

Eberly et al. [48] described two distinct types of capsule insertions into the glenoid at the anterior-inferior capsule-labrum complex, or capsulolabrum, shown in Figure 1.3. A Type I insertion has the capsule inserting primarily into the labrum, with the ligament fibers joining the labrum fibers to produce transitional zones of ligament, fibers, and fibrocartilage, much like the supraspinatus tendon insertion. However, part of the capsule continues on past the labrum and inserts into the neck of the glenoid.

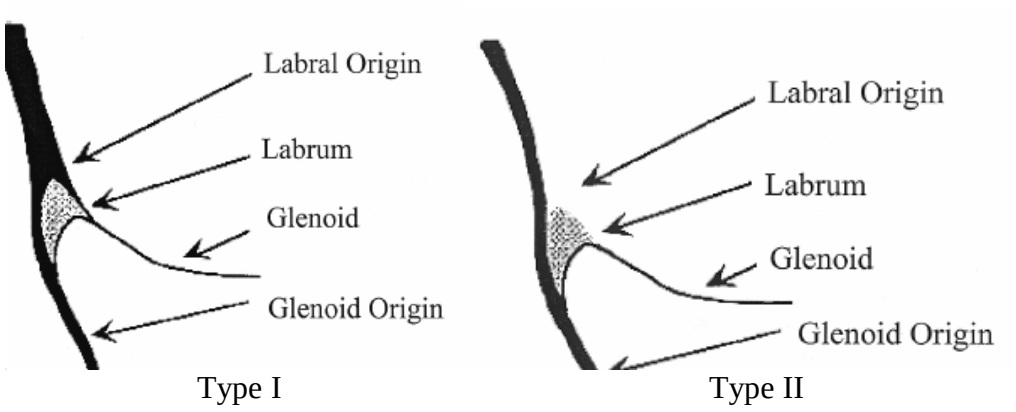

Figure 1.3 Anterior-inferior capsulolabrum insertion types [48]

A Type II insertion, on the other hand, has the capsule inserting primarily into the neck of the glenoid. The collagen fibers insert into the glenoid at acute angles, much like the tibial insertion of the medial collateral ligament. There is contact between the capsule and the labrum, but the capsule does not insert directly into the labrum. Both Type I and Type II insertions have

been documented in previous research [12, 24, 37, 46, 50], with the Type I insertion occurring in the anterior-inferior capsulolabrum more frequently at birth [51] and in adulthood [48].

1.3 FUNCTION OF THE GLENOHUMERAL CAPSULE

During glenohumeral joint motion, the capsule acts to provide stability to the joint by transferring load between the humerus and scapula. The rotation and/or translation of the humerus results in complex loading patterns applied to the capsule including tension, shear, twisting, and a radial pressure distribution caused from a wrapping of the capsule around the humeral head. The complex loading patterns further reinforce the capsule's multi-directional function and the need for its characterization as a 3-dimensional composite structure of ligamentous regions of variable thickness.

While the capsule is a sheet of ligamentous tissue, the stability provided by the capsule may be "localized" within the capsule, i.e. where the glenoid or humeral side of a particular capsule region provides greater stability to the joint than other regions of the capsule. This is reflected by the presence of Bankart lesions following anterior dislocation, where the glenoid side of the anterior-inferior capsule tears from its insertion into the glenoid [52, 53]. Furthermore, the local stability provided by the capsule is dependent upon joint position, as a given region of the capsule may be distributing load or may be unloaded depending on the orientation of the humerus with respect to the scapula. At the mid-range of motion, the entire capsule is relatively lax and plays a small role in stability [11, 14]. At 90° of humerothoracic abduction the anterior-inferior capsule is the primary anterior stabilizer, and the anterior stability

provided by the anterior-inferior capsule increases as the humerus is externally rotated [9-14, 21, 41, 54, 55].

Multiple biomechanical studies have attempted to quantify the contribution of each capsule region to joint stability, by examining elongation of the regions using strain or length changes using the distance between the origin and insertion. These elongation patterns were determined using radiographic markers [14, 37], electromagnetic tracking devices [56], Hall effect strain transducers [57], mercury strain gauges [58], and simple mathematical models [59]. A stereoradiogrammetric technique was also used to determine the strain field in the anterior-inferior capsule during anterior subluxation in the abducted joint [36]. Maximum principal strain fields were greater on the glenoid side of the anterior-inferior capsule than on the humeral side, suggesting stability provided by the anterior-inferior capsule at the joint position was localized to the glenoid side of the anterior-inferior capsule.

As direct measurement of capsule forces is experimentally challenging due to the complexity of the joint geometry [60], it has been suggested by Lew and coworkers [60] that a computational model or finite element analyses of the capsule be developed. While analytical models of the glenohumeral joint have been developed to predict joint kinematics and investigate the stability provided by the capsule regions and articular contact [61, 62], these models represented the capsule with uni-axial springs that wrapped around the articular surface of the humeral head. They also modeled only specific portions of the capsule, disregarding the interactions that occur between capsule regions [63].

More recently, a subject-specific finite element model of the glenohumeral joint that treated the capsule as a composite sheet of tissue was used to quantify the distribution of strain in the anterior-inferior capsule in multiple joint positions [41, 55, 64]. It was shown that strains in

the anterior-inferior capsule increased with external rotation when the shoulder was abducted, and were highest in the glenoid side of the anterior band of the inferior glenohumeral ligament and the axillary pouch when an anterior load was applied. This further reinforces that the stability provided by the anterior-inferior capsule may be localized in clinically relevant joint positions, and may help explain the presence of lesions to the glenoid side of the anterior-inferior capsule following traumatic anterior dislocation [53].

1.3.1 Insertion Site

The capsule's glenoid insertion, and specifically the glenoid labrum, helps to provide stability to the glenohumeral joint. The glenoid labrum provides added depth and concavity to the glenoid fossa at the articulation with the convex humeral head [24, 42-44, 46-48]. Not only does the labrum absorb humeral head forces and distribute them to the glenoid [42, 43, 46], it functions as a bumper [24, 46] to restrict humeral head translation and dislocation of the glenohumeral joint.

The labrum is also an integral component of the capsule's insertion into the glenoid, with its fibrillar connections to both structures helping to aid in the transfer of load across the joint during glenohumeral motion [42, 43, 46, 48]. The labrum thus provides stability to the glenohumeral joint both as a physical stabilizer and as an important constituent of the capsule's glenoid insertion. As a result, damage to the labrum is an important etiology to glenohumeral instability [42, 46]. Examples include Bankart lesions, in which the anterior-inferior capsulolabrum detaches from the glenoid [48], and SLAP lesions (Superior Labrum, Anterior and Posterior) [24], which occur at the superior aspect of the glenoid.

1.4 DIAGNOSIS AND CLINICAL OUTCOMES

1.4.1 Diagnosis

Clinicians use multiple methods for diagnosing anterior capsule pathology, including inquiries of patient history, radiographs, and arthroscopic examination. Following reduction, however, there is little radiographic evidence of dislocation, and while additional imaging techniques can be used to identify soft-tissue tears or avulsions [65], they are ineffective at identifying permanently deformed capsule tissue that may result in instability. Physical examinations are thus often employed, in order to diagnose the location and extent of capsule pathology [15-17].

During physical examinations, clinicians apply a manual maximum load to the humerus in certain joint positions while attempting to rigidly fix the scapula, and measure the resulting translations of the humeral head relative to the glenoid. Capsule pathology is diagnosed by grading the resulting humeral translations as a measure of the stability provided by the capsule, and through comparison to the contralateral joint [66]. These physical examinations are highly dependent on examiner skill and experience, and are not standardized for joint position [9, 67, 68]. Despite the importance of the physical examinations in making diagnoses, their use is problematic due to the lack of standardized joint positions. Different regions of the capsule act to provide stability to the joint at different joint positions, and humeral head translations have been shown to vary with joint orientation [18-20]. A lack of standard joint positions during the examinations may therefore hinder the clinician's ability to localize pathology in the capsule. In addition, the variability in the stability provided by the capsule from patient to patient may increase or decrease depending on joint position [11, 17, 18, 21]. The position-dependent variability may result in position-dependent reliability of clinician diagnoses that is poorest for

examinations performed in mid-ranges of humeral motion where the capsule is not the primary stabilizer [22, 69]. Therefore, the use of humeral head translations to diagnose capsule pathology at non-standardized joint positions where the distribution of load in the capsule is variable across the population provides an inaccurate means of determining the stability provided by the capsule. This poses significant problems for surgeries, since the location, extent, and type of surgical repair are often dependent on the diagnosed location and extent of the capsule pathology [9, 19, 66].

1.4.2 Rehabilitation and Surgical Repair

After diagnosis, treatment typically includes an initial immobilization period to allow for soft tissue healing. This is followed by a conservative treatment regimen with a rehabilitation program aimed at strengthening and conditioning the rotator cuff muscles and humerothoracic muscles such as the deltoid, latissimus dorsi, and pectoralis major [70, 71]. In spite of these efforts, disability after such treatments is common and becomes a severe hindrance to everyday activities, especially for physical laborers or throwing athletes. Recurrence occurs in 60% to 94% of the patients under 25 years of age [3, 65, 72-76], since the procedures do not specifically address the stability provided by the capsule, the primary joint stabilizer in positions of dislocation. Therefore, surgical repair to the capsule is often prescribed following anterior dislocations.

Surgical repair following anterior dislocations can involve a uni-directional shift, or tightening, of loose capsule tissue, or can involve plicating and shifting the capsule tissue [70, 77-79]. Repair procedures can be performed with either open or arthroscopic procedures. For a uni-directional shift procedure, excess capsule tissue resulting from permanent deformation is

pulled medially and sutured to the wall of the glenoid. For a typical plicate and shift procedure (Figure 1.4), the anterosuperior region is incised in the superior-to-inferior direction on either the glenoid or humeral side. This is followed by a medial-to-lateral incision, thus resulting in a "T" shape with an upper and lower tissue leaf. The lower leaf is then plicated, shifted in the superior direction, and sutured to the remaining tissue. The upper leaf is then plicated, shifted in the inferior direction, and sutured to the bone and lower leaf.

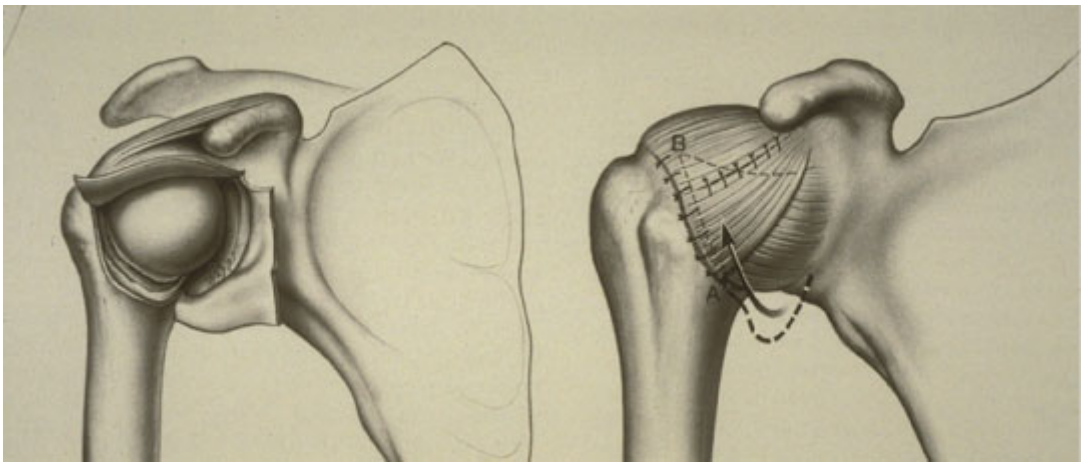

Figure 1.4 Anterior view (right shoulder) of the plicate and shift technique indicating "T" incision followed by a shift of the capsule tissue [77]

For the uni-directional shift procedure, it is often unclear where in the capsule the tissue should be shifted, as well as how much tissue should be shifted. For the plicate and shift procedure, it is often unclear as to which regions of the capsule should be plicated, how much of the tissue should be plicated, and how far the plicated tissue should be shifted. Such information could be obtained from physical examinations that can be used by clinicians to diagnose local pathology in the capsule as well to diagnose the extent of the pathology.

1.4.3 Clinical Outcomes and Relevance

While surgical repair has improved upon the poor outcomes from conservative treatment following dislocation, recurrence rates of 12% and 23% are still observed for open and arthroscopic repairs, respectively [80], and 20-25% of patients also suffer from pain, chronic instability, joint stiffness and osteoarthritis [66, 81, 82].

The less than adequate surgical outcomes may be directly due to the misdiagnoses that occur from the physical examinations, as the location, extent, and type of surgical repair are often dependent on the diagnosed location and the extent of the capsule pathology [9, 19, 66]. Reports have shown that over 38% of post-operative redislocations are due to misdiagnoses of the location of capsule pathology, and 35% of post-operative redislocations and over 80% of post-operative pain, motion loss, and or osteoarthritis cases are due to misdiagnoses of the extent of capsule pathology [23-25]. These misdiagnoses may be avoided if clinically relevant joint positions could be identified where the stability provided by the capsule is consistent among patients, since removal of the effects of unstandardized joint positions and patient variability would lead to more robust diagnoses. These joint positions could then be used in physical examinations that would provide more accurate diagnoses of capsule pathology, which may lead to improvement in surgical outcomes.

1.5 MOTIVATION FOR RESEARCH QUESTION

The anterior-inferior capsule is the primary anterior stabilizer to the glenohumeral joint in positions of anterior dislocation, and often requires surgical repair following dislocation to

restore normal joint stability. The current repair procedures are inadequate in restoring the normal stability provided by the anterior-inferior capsule, which may result from the current use of physical examinations that are not standardized for joint positions where the stability provided by the capsule is consistent among patients.

The capsule provides stability to the joint by transferring load between the humerus and scapula. Therefore, identifying joint positions where the distribution of load in the anterior-inferior capsule is consistent among patients may provide significant contribution towards establishing physical examinations for anterior instability that are standardized for joint position. The use of joint positions with consistent distribution of load in the anterior-inferior capsule is crucial for effective physical examinations, so that clinicians can make successful diagnoses of anterior-inferior capsule pathology that are not hindered by patient variability but depend only on the results of the physical examination. For the current work, joint positions with consistent distribution of load in the anterior-inferior capsule among patients are defined as those with a high correlation in how the distribution of load is localized within all regions of the anterior-inferior capsule, in each patient regardless of demographic background.

It is worth noting that establishing standard joint positions for use in effective physical examinations has previously been developed in the knee for anterior cruciate ligament instability, as the joint position of 30° of knee flexion is used with application of an anterior load to the tibia for robust diagnosis of anterior cruciate ligament instability independent of patient race, size, age, or gender. While the shoulder and knee joints are quite different in nature and function, it remains that identifying a joint position or positions where the distribution of load in the anterior-inferior capsule is consistent among patients would contribute significantly towards

establishing physical examinations that can be used for more effective diagnoses of anterior-inferior capsule pathology.

It has been shown that variability exists among patients in the structure of the capsule, particularly in the anterosuperior capsule region where the middle glenohumeral ligament and the superior glenohumeral ligament are often absent or vary in size and location [13, 31]. However, O'Brien et al. [13] described the anterior-inferior capsules of all subjects examined as having three distinct regions, the anterior and posterior bands of the inferior glenohumeral ligament and the axillary pouch. Similarities were also found in the locations of the glenoid and humeral insertions of these three regions. While slight differences in the types of glenoid and humeral insertions were discussed, the consistency in the structure and location of the anterior-inferior capsule among subjects suggests that the stability provided by the anterior-inferior capsule may also be consistent among patients in certain joint positions. The variability in the stability provided by the capsule among patients may change with joint position [11, 17, 18, 21], and may be highest in positions where the capsule is relatively lax. However, it remains that there may be joint positions at or near the end-range of motion of the glenohumeral joint where distribution of load in the anterior-inferior capsule is consistent among patients.

1.6 RESEARCH QUESTION

Therefore, the research question of the proposed work is as follows:

Research Question: **When an anterior load is applied, which glenohumeral joint positions result in consistent distribution of load in the anterior-inferior capsule among patients?**

For the current work, joint positions with consistent distribution of load in the anterior-inferior capsule among patients are defined as those with a high correlation in how the distribution of load is localized within all regions of the anterior-inferior capsule, in all patients regardless of demographic background. For example, a joint position will have consistent distribution of load among patients if for each patient certain regions of the anterior-inferior capsule (i.e. the glenoid side of the anterior band of the inferior glenohumeral ligament) carry relatively high load, while other regions (i.e. the humeral side of the posterior band of the inferior glenohumeral ligament) carry relatively little load. Identifying a joint position that results in transfer of load to a specific region or regions of the anterior-inferior capsule, regardless of the patient, will provide clinicians with an ability to diagnose local pathology to the anterior-inferior capsule during physical examinations.

1.7 MOTIVATION FOR SPECIFIC AIMS

The overall objective of the proposed work is to evaluate the distribution of load in the anterior-inferior capsules of multiple subjects, when an anterior load is applied in clinically relevant joint positions. As discussed previously, the distribution of load in the glenohumeral capsule is heavily dependent upon joint position. When defining joint positions for use in determining consistent distribution of load in the anterior-inferior capsule among patients, it is critical that the anterior-inferior capsule is loaded and thus providing stability to the joint. At the mid-range of motion the entire capsule is relatively lax and plays a small role in stability [11, 14], therefore it is of high importance that the joint positions evaluated in the current work place the joint at or near its end-range of motion, such as occurs in dislocation. It is well documented that the anterior-inferior capsule limits anterior humeral head translation when the joint is abducted and externally rotated [9-14, 17, 21, 41, 54, 55]. This is additionally supported by clinical outcomes of anterior-inferior capsulolabrum lesions and anterior-inferior capsule stretching following anterior dislocation [53]. The stability provided by the anterior-inferior capsule in the abducted shoulder has also been shown to vary with external rotation, with multiple authors indicating that the stability provided by the anterior-inferior capsule increases with external rotation [13, 17, 19, 20].

Furthermore, recent work performed by Moore et al. [21] measuring distribution of strain on the surface of cadaveric specimens suggests that there may be ranges of external rotation angles where the distribution of load in the anterior-inferior capsule is consistent among subjects. It was found that greater changes in strain occurred in subjects when rotated from 0° to 30° of external rotation than from 30° to 60° of external rotation in the abducted joint when an anterior load was applied. In this study the direction of the maximum principal strains was also

quantified as external rotation was increased. It was found that the direction of the maximum principal strains became aligned with the longitudinal margin of the anterior band of the inferior glenohumeral ligament when external rotation was increased, in all specimens. The results of this study indicate that the distribution of load in the anterior-inferior capsule is more consistent across subjects as external rotation is increased in the abducted joint, and that it may be consistent among subjects across a range of external rotation values.

When attempting to define joint positions for use in physical examinations for anterior-inferior capsule pathology, it is also critical that the remainder of the capsule does not provide stability to the joint in these positions, as pathology to the anterior-inferior capsule may then go unnoticed. The anterosuperior capsule has been shown to limit anterior humeral head translation when the joint is abducted and internally rotated [13], as well as limit inferior humeral head translation when the joint is adducted and externally rotated [38, 83-85]. The posterior capsule limits posterior humeral head translation when the joint is adducted and flexed [9, 86], especially when coupled with internal rotation [9, 87]. However, it has not been demonstrated that these regions contribute to anterior stability when the glenohumeral joint is abducted and externally rotated.

In order to quantify the distribution of load in the capsule, a means is required that can successfully measure the loads in specific regions of the capsule when the capsule is providing anterior stability to the joint. Loads in the capsule have been measured previously in clinically relevant joint positions using selective sectioning experiments to determine the load in the individual capsule regions [61]. However, more recent work has shown that the capsule functions as a sheet of tissue, and that loads are transferred between the capsule regions. Making incisions in the capsule tissue therefore affects the normal transfer of load in the capsule. The

use of load to measure stability provided by the capsule thus limits measurements to the whole capsule only, and prevents the measurement of the distribution of load in regions of the anterior-inferior capsule.

Surface strains in ligamentous tissue have been used to determine how load is distributed in the tissue [21, 32, 36, 88-101]. Surface strains can be measured in the capsule without modifying the tissue structure, allowing for measurement of the local distribution of load in the capsule without compromising the multi-directional stability provided by the capsule tissue. The distribution of strain on the surface of the anterior-inferior capsule therefore provides an effective means to answer the research question.

Obtaining quantitative measures of surface strain in a clinical setting is difficult, however, due to the presence of skin, musculature, and other soft tissue. Therefore, the use of multiple cadavers that have been dissected down to the capsule has been employed to measure distributions of strain on the capsules and evaluate the stability provided by the capsule. Previous authors have attempted to quantify the contribution of each capsule region to joint stability [14, 37, 56-59], however these techniques did not represent the capsule as a continuous sheet of tissue and thus failed to capture the multi-directional stability provided by the capsule.

More recently, strain analyses have been performed that treated the capsule as a composite sheet of tissue. A stereoradiogrammetric technique was used to determine the strain field in the anterior-inferior capsule during anterior subluxation in the abducted joint [36]. The use of a robotic manipulator has also been employed in our research group to evaluate the distribution of load in the anterior-inferior capsule in multiple joint positions [21], using an optical motion tracking system to record positions of capsule strain markers fixed to the capsule throughout joint motion in order to quantify distribution of strain in the capsule. While these

techniques have proven to be effective in providing quantitative measurements of the distribution of load in the anterior-inferior capsule, significant challenges remain in using these techniques for the proposed research. Extensive exposure of the capsule tissue to the environment that would occur from evaluation of multiple positions may result in tissue degradation and a change in material properties. Furthermore, the use of cadavers requires the use of a mechanical fixture or joint positioning apparatus, which inherently places limitations on joint ranges of motion. The ability to evaluate the distribution of load in multiple joint positions with cadavers is therefore limited by both overexposure to the capsule and the positioning devices.

These experimental challenges can be avoided with the use of finite element models, which provide a powerful tool for evaluating the stability provided by the capsule. By allowing for subject-specific inputs of joint geometry, capsule material properties, and joint kinematics during motion, finite element models can be developed that are subject-specific to cadaveric specimens. This allows for analyses to be made with multiple subject-specific models that can capture variations in the distribution of load in the capsule among subjects. Surface strains in the capsule tissue can be outputted by the models, allowing for a means of quantifying the local multi-directional distribution of load in the capsule in clinically relevant joint positions. Of significant importance is that these strains can be used to validate the models. Experimental surface strains can be recorded on cadavers in targeted clinically relevant joint positions, and predicted strains in the subject-specific finite element models can be computed in the equivalent joint positions. The predicted and experimental surface strains can then be compared at the equivalent joint positions, for one-to-one validation of the finite element model with the experimental data. The true power of the finite element models comes in that once validated at selected positions, they can be used to analyze the distribution of load in the capsule in infinite

positions, without regard to overexposure of the capsule to the environment or limitation of joint range of motion posed by the experimental setup.

The use of finite element modeling to analyze the distribution of load in the capsule has been performed previously within our research group [90, 102, 103], however these models did not treat the capsule as a continuous sheet of tissue. More recently, our research group developed and validated a subject-specific finite element model of the glenohumeral joint that treated the capsule as a continuous sheet of tissue [41] (Figure 1.5). This model, referred to as FE Model 1, and the previous models created within our research group were created using the nonlinear finite element solver NIKE3D [104], which has been used previously for analysis of the distribution of stress and strain in ligaments [90, 95, 102, 103, 105-110].

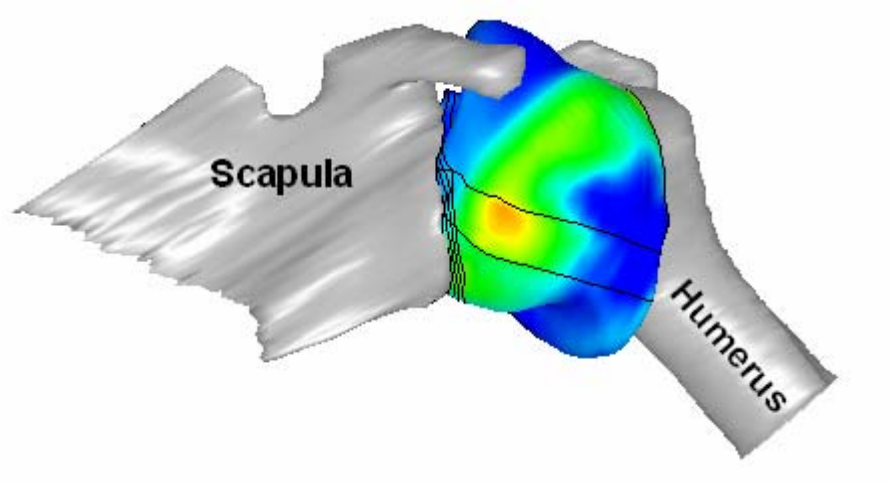

Figure 1.5 FE Model 1: Left shoulder, anterior view

The use of NIKE3D, however, prevented modeling the isotropic hyperelastic nature of the glenohumeral capsule tissue due to the lack of a built-in isotropic hyperelastic constitutive model. Instead, an isotropic hypoelastic constitutive model was used to represent the capsule. This type of constitutive model assumes a linear stiffening response of the tissue in response to stretching, and therefore does not represent the non-linear manner in which the capsule transfers load (Figure 1.6). FE Model 1 was validated at a joint position with 25 N anterior load applied at

60° of glenohumeral abduction and maximum external rotation, however it could not be validated at joint positions with 0° and 30° of external rotation. The predictive capability of this model is therefore limited when using the isotropic hypoelastic constitutive model to represent the tissue, and validation must first be performed with an isotropic hyperelastic model at additional clinically relevant joint positions before the finite element model can be used for the current work.

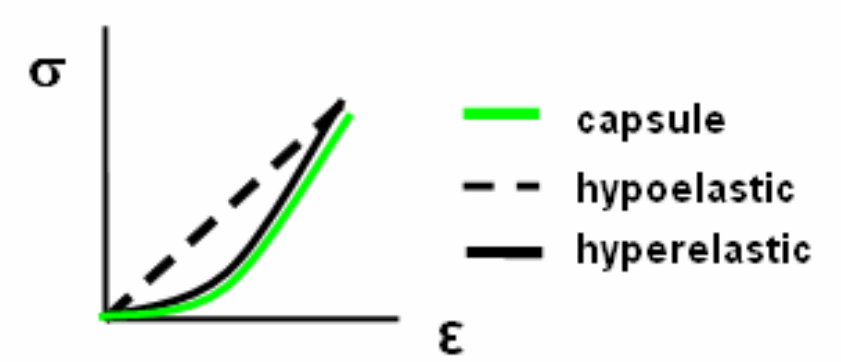

Figure 1.6 Material response of capsule tissue, a hypoelastic constitutive model, and a hyperelastic constitutive model

More recently, our research group has developed the non-linear finite element solver FEBio © (Maas and Weiss, Salt Lake City, UT, 2008), which contains a built-in isotropic hyperelastic constitutive model that has been used to represent the capsule's non-linear stiffening response to elongation [40]. In order to answer the research question, multiple subject-specific finite element models must be developed that use an isotropic hyperelastic constitutive model to represent the capsule. Therefore, FE Model 1 must be modified to run in FEBio using an isotropic hyperelastic constitutive model to represent the capsule so that it can be used to help answer the research question.

To identify joint positions with consistent distribution of load in the anterior-inferior capsule among multiple subjects, the development and validation of multiple subject-specific finite element models of the glenohumeral joint is required. Preliminary work suggested that

seven or more models would be required to successfully capture variation in the population, and for the current work one additional subject-specific finite element model of the glenohumeral joint that treats the capsule as a continuous sheet of ligamentous tissue will be developed, using an isotropic hyperelastic constitutive model to represent the capsule. Both this model (to be referred to as FE Model 2) and FE Model 1 can then be used to analyze the distribution of load in the anterior-inferior capsule in clinically relevant joint positions of abduction and external rotation. Specifically, the joint positions involving 60° of glenohumeral abduction (90° of humerothoracic abduction) and external rotations ranging from 0° to maximum external rotation will be evaluated, since it has been demonstrated that the anterior stability provided by the anterior-inferior capsule changes with external rotation. It has been shown that a load of approximately 25 N is a non-injurious load applied to the capsule by clinicians during clinical examinations, and has thus been used to simulate application of a load from a clinician during a clinical exam [19-21, 41, 86] Therefore, an anterior load of 25 N will be used in the analyses.

1.8 SPECIFIC AIMS

The research question in Section 1.6 will be answered by achieving the following Specific Aims:

Specific Aim #1a – Validate FE Model 1 using an isotropic hyperelastic constitutive model for the capsule tissue

Specific Aim #1b – Develop and validate one additional subject-specific finite element model of the glenohumeral joint (FE Model 2), with inputs of subject specific joint geometry, isotropic hyperelastic material coefficients, and kinematics, and with outputs of capsule strain

Specific Aim #2 – Use FE Model 1 and FE Model 2 to suggest external rotation angles in the abducted joint where the distribution of load in the anterior-inferior capsule is consistent among subjects in response to anterior loading, and further determine if the distribution of load is localized to regions of the anterior-inferior capsule. Specifically, evaluate the distribution of strains in the anterior-inferior capsule of each model in response to a 25 N anterior load applied at 60° of glenohumeral abduction and 10° increments of external rotation from 0° to maximum external rotation

2.0 DEVELOPMENT AND VALIDATION OF FE MODEL 1

2.1 INTRODUCTION

The development and validation of subject-specific finite element models of the glenohumeral capsule requires an elaborate experimental and computational procedure (Figure 2.1). For each finite element model, experimental inputs that are subject-specific to a respective cadaver must be collected, including a reference position for use in determining the reference configuration of capsule strain markers, geometry of the bones, capsule, and humeral head cartilage when the joint is in the reference position, the joint kinematics from the reference position to the clinically relevant joint positions, and material coefficients of the capsule tissue from an isotropic hyperelastic constitutive model. When collecting these experimental inputs, the strains on the surface of the cadaver, or *experimental strains*, are obtained at the clinically relevant joint positions. The geometry and material coefficients are then used to generate a 3-dimensional, scale finite element model of the cadaver. The joint kinematics are used to drive motion of the humerus with respect to the scapula within the finite element model, after which the strains on the surface of the capsule tissue within the model, or *predicted strains*, can be computed. Validation of the model is then performed by comparing the *experimental strains* with the *predicted strains* at equivalent joint positions, and ensuring that differences in strain are less than the experimental strain repeatability. Once validated in the joint positions, the model can be used to analyze the distribution of load in the capsule at any joint position by analyzing the

distribution of strain in the capsule after motions to additional joint positions have been simulated.

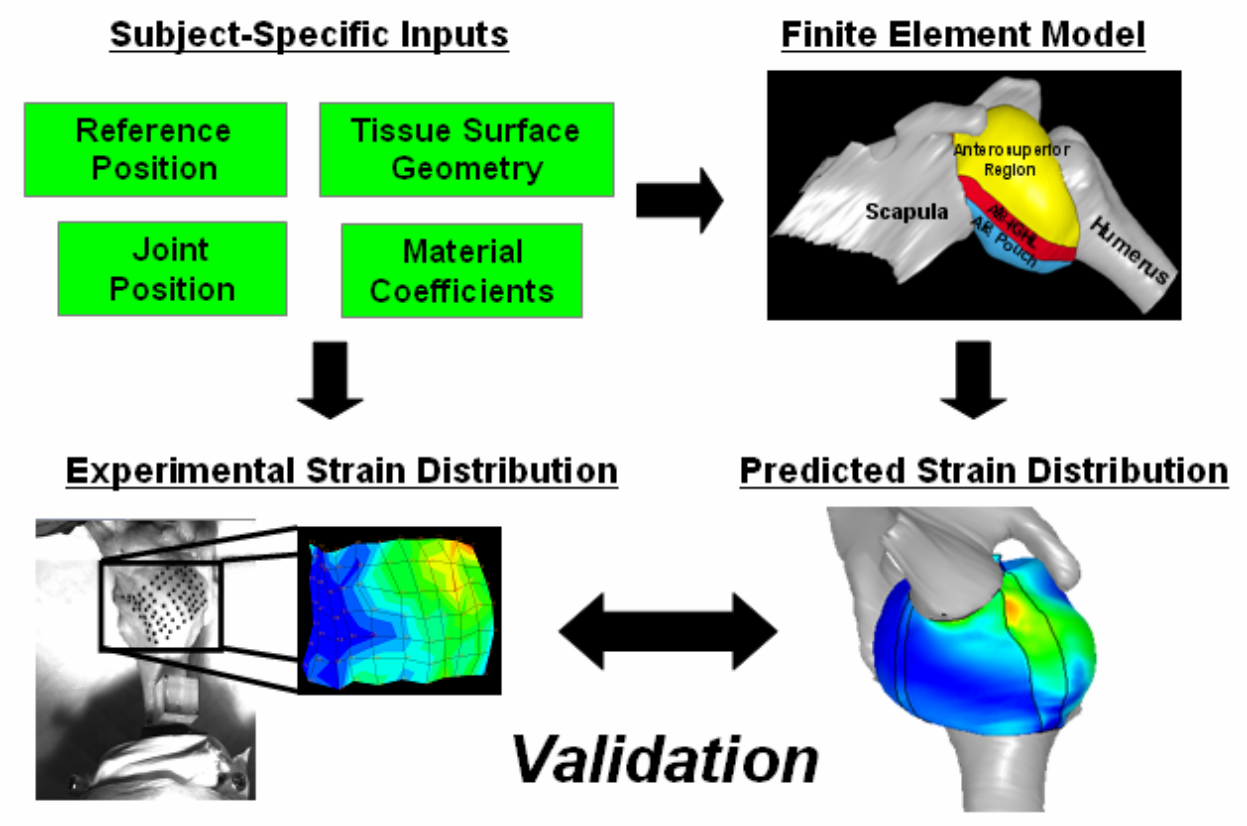

Figure 2.1 Overview of finite element model development and validation process

For FE Model 1, the subject-specific inputs and experimental surface strains were previously collected in our research group, although the material coefficients were for an isotropic hypoelastic constitutive model. FE Model 1 was developed and validated at a joint position with a 25 N anterior load applied at 60° of glenohumeral abduction and maximum external rotation [41], and inclusion of a glenoid labrum was simulated via computational modification of the capsule's thickness at the glenoid insertion site [111]. The complete description of the FE Model 1 development and validation process will therefore not be addressed in this section but will rather be explained in detail in Section 3.0 .

In order to address Specific Aim 1a, subject-specific material coefficients to an isotropic hyperelastic constitutive model needed to be obtained and incorporated into FE Model 1. In order to incorporate these material coefficients into FE Model 1, the finite element code also needed to be modified from a form suitable for the NIKE3D finite element solver to a form suitable for the FEBio finite element solver. Once these necessary steps were performed, motion could be simulated to the clinically relevant joint positions resulting from a 25 N anterior load applied to the joint at 60° of glenohumeral abduction and 0°, 30°, and 60°/maximum external rotation. At this point validation of FE Model 1 could be performed, with the use of an isotropic hyperelastic constitutive model to represent the capsule.

2.2 MATERIAL COEFFICIENTS

Subject-specific and region-specific material coefficients are needed in order to accurately predict distribution of strain throughout the glenohumeral capsule [112]. Therefore, an elaborate experimental and computational procedure is used to obtain material coefficients for each of the five capsule regions in each cadaver used for development of subject-specific finite element models. The complete experimental and computational procedure is provided in Section 3.2.4, therefore brief highlights of the procedure will be presented in this section. For each capsule region uni-directional elongations are applied, and the resulting load is measured to obtain an experimental load-elongation curve. This curve and the tissue sample geometry are used to generate a computational simulation of the uni-directional elongation using finite element modeling techniques. After a constitutive model has been selected to represent the tissue sample, an optimization algorithm is used to produce material coefficients that minimize differences

between the predicted load-elongation curve and the experimental load-elongation curve. This process is then repeated for each of the five capsule regions, generating five sets of optimized material coefficients for the selected constitutive model that are used to represent the capsule regions in the finite element model. The experimental load-elongation data for the capsule regions was previously obtained [41], therefore modifying the material coefficients for FE Model 1 only required generating the optimized material coefficients for each capsule region using an isotropic hyperelastic constitutive model to represent the capsule instead of an isotropic hypoelastic constitutive model.

A non-linear isotropic hyperelastic constitutive model has been recently employed within our research group to successfully model the loading response of capsule tissue to applied elongations [40] (Section 3.2.4). Developed by Veronda and Westmann [113] and later expanded by Weiss et al. [108], this constitutive model requires two material coefficients (C_1 and C_2) to model the non-linear stiffening response of the capsule tissue in response to applied elongation. C_1 and C_2 are interrelated, with both C_1 and C_2 scaling the magnitude of the stress-strain curve, and C_2 additionally governing the non-linearity of the stress-strain curve.

2.2.1 Available Data

Tissue samples collected from the anterosuperior region, anterior band of the inferior glenohumeral ligament, and posterior band of the inferior glenohumeral ligament were approximately 5 mm x 15 mm (longer in the longitudinal direction), therefore uni-directional elongations were applied in the longitudinal direction of the tissue samples. Tissue samples collected from the axillary pouch and the posterior region were approximately 25 mm x 25 mm. This allowed for uni-directional elongations to be applied in both the longitudinal and transverse

directions for these tissue samples, so that material coefficients could be obtained for each loading direction and be used to generate one set of material coefficients for each tissue sample. Therefore, a total of seven uni-directional elongations were used to generate the material coefficients for FE Model 1. The load-elongation data and tissue sample geometry for each of the seven uni-directional elongations were collected previously [41], using custom clamps, a tensile testing setup, and an optical motion tracking system (Section 3.2.4.2).

2.2.2 Computational Generation of Optimized Material Coefficients

Simulation of the experimental uni-directional elongations was then performed using the finite element method [108]. Using images recorded from the camera system and the tissue sample dimensional measurements, a finite element mesh was created for each capsule region. The clamped edges of the tissue were given rigid body properties, with one end fixed and the other allowed to move based on the non-destructive uni-directional elongations applied experimentally. The unclamped tissue was assigned a Veronda-Westmann isotropic hyperelastic constitutive model, and initial guesses of C1 and C2 were assigned so that the predicted load-elongation data matched the experimental load-elongation data with an R^2 value greater than 0.97. A non-linear optimization program that minimized the sum of the squared error between the predicted and experimental load-elongation data was then used to produce optimal C1 and C2 values for each capsule region.

For the anterosuperior region and the anterior and posterior bands of the inferior glenohumeral ligament, the optimized C1 and C2 values were used as input into FE Model 1. For the axillary pouch and posterior region, however, two sets of optimized material coefficients were produced, one each for the longitudinal and transverse uni-directional elongations. Due to

the non-linearity in the Veronda-Westmann constitutive model, for each region a single set of C1 and C2 values were obtained from the Cauchy stress-stretch curve that represented the average of the Cauchy stress-stretch curves in the longitudinal and transverse loading directions (Section 3.2.4.4). A total of five sets of optimized material coefficients to the Veronda-Westmann isotropic hyperelastic constitutive model were thus obtained for FE Model 1, with one set for each capsule region.

In addition to the values of C1 and C2, the Veronda-Westmann isotropic hyperelastic constitutive model required input of a bulk modulus value. Based on preliminary work a bulk modulus value of 75 was assigned, for all of the capsule elements.

2.3 FINITE ELEMENT MODEL DEVELOPMENT AND VALIDATION

2.3.1 Model Development

FE Model 1 was previously developed [41], and modifications were made to the capsule's glenoid insertion site to simulate the presence of a glenoid labrum [111]. For a complete description of the finite element model development process, please refer to Section 3.3.

2.3.1.1 Mesh Development

Quadrilateral YASE shell elements were used to mesh the glenohumeral capsule within the finite element pre-processor TrueGrid (XYZ Scientific, Livermore, CA), due to their accuracy during in-plane bending motions [114]. Specifically, the quadrilateral shell element mesh was created with a total of 80 nodes and 79 elements along the longitudinal direction of the capsule from the glenoid insertion to the humeral insertion, and with 144 nodes and 143 elements along the

circumferential direction of the capsule. The distribution of elements within the capsule regions of FE Model 1 are provided in Table 2.1.

Table 2.1 Distribution of shell elements within the five capsule regions of FE Model 1

	Elements		
	Circumferential	**Glenoid-Humerus**	**Total**
AB-IGHL	11	79	869
Axillary Pouch	33	79	2607
PB-IGHL	10	79	790
Posterior	55	79	4345
Anterosuperior	34	79	2686
Total	143	395	11297

The thicknesses of the capsule regions were measured during the material testing procedure. The quadrilateral shell elements were assigned a uniform capsule thickness that represented the average thickness (rounded to the nearest 0.5 mm) in the capsule regions of the anterior-inferior capsule. This resulted in a uniform capsule thickness of 2.0 mm for FE Model 1.

2.3.2 Insertion Site Modification

The insertion site of FE Model 1 was initially modeled with the capsule inserting directly into the glenoid, which resulted in extremely high strain in the insertion elements (Section 3.3.2). It was believed that these strains were due to the absence of a glenoid labrum at the insertion, since the labrum acts to stiffen the glenoid insertion of the capsule and distribute load from the capsule to the glenoid. Since it was unknown whether the high insertion site strains were affecting strain throughout the capsule and thus affecting model validation, it was determined that incorporation

of a glenoid labrum into FE Model 1 was necessary. Please see Section 3.3.2 for additional details.

2.3.2.1 Labrum Inclusion

It was decided to include the presence of a labrum within FE Model 1 as a computational modification to the quadrilateral shell elements at the glenoid insertion, as opposed to including the labrum as a physical structure within the model (Section 3.3.2.1.1). This was chosen based on the increased thickness of the insertion site relative to the capsule that is seen anatomically, the difficulties encountered when attempting to identify the labrum in the computed tomography scans, and the changes in the capsule boundary conditions that would have resulted from a physical change in shape of the insertion site. A sensitivity study was performed that evaluated the effect of modifying the shell element thickness and material properties at the insertion site, and based on the results it was decided to simulate the presence of a glenoid labrum by modifying the radial thickness of the insertion site shell elements (Section 3.3.2.2). The radial thickness of the labrum elements at the insertion site were thus tapered from 3.0 mm at the interface of the labrum with the glenoid down to 2.0 mm at the interface of the labrum with the capsule.

2.3.3 Finite Element Solution Procedure

The non-linear finite element solver FEBio was used for all analyses. The finite element pre-processor TrueGrid that was used to initially create the finite element input deck for NIKE3D did not have the capability to produce an input deck for FEBio. However, the finite element pre-processor PreView could be used to convert a NIKE3D input deck into a FEBio input deck.

Therefore, a NIKE3D input deck was outputted by TrueGrid, using an isotropic hypoelastic constitutive model to represent the capsule and labrum elements. This input deck was then imported into PreView, and converted to a FEBio input deck. The constitutive model of the capsule and labrum elements was changed to the Veronda-Westmann isotropic hyperelastic constitutive model, using the material coefficients obtained in Section 2.2.2. A sliding interface contact was prescribed between the humeral head cartilage and the articular surface of the capsule, with the humeral head cartilage as the master and the capsule as the slave. Specifically, the interface was initially assigned a tolerance value of 0.05 and a penalty value of 1.0, based on preliminary work.

The motion of the humerus from the reference position to each of the clinically relevant joint positions was then simulated using FEBio. Specifically, these joint positions involved a 25 N anterior load applied at 60° of glenohumeral abduction and 0°, 25.1°, and 51.8° of external rotation. An incremental-iterative solution strategy was employed, with iterations based on a quasi-Newton method [115] and convergence based on the L_2 displacement and energy norms [116]. The motions of the humerus with respect to the scapula were applied incrementally over quasi-time with the time step size being adjusted via an automatic procedure. Run time was approximately 1-2 hours for each clinically relevant joint position.

2.3.4 Model Validation

2.3.4.1 Predicted Strain Distribution

After full convergence of the finite element solution procedure, the results were visualized using the finite element post-processor LSPost (Livermore Software Technology Corporation, Livermore, CA). Green-Lagrange maximum principal strains were computed at the nodes in

each quadrilateral shell element. Groups of elements in the anterior-inferior capsule in FE Model 1 had previously been identified that matched the size and location of the experimental elements used to compute the experimental surface strains, therefore the average nodal strains were computed within the groups of shell elements in order for one-to-one comparison of predicted and experimental strains for validation.

2.3.4.2 Finite Element Model Validation

Validation of subject-specific finite element models is performed by comparing the surface strains predicted by the computational model with those obtained experimentally. Since there were 60 total validation elements from the experimental procedure, a total of 60 element-by-element comparisons could be made between the predicted and experimental strains. However, regions of the anterior-inferior capsule whose experimental strain measured at or below the experimental strain repeatability in any of the three clinically relevant joint positions were excluded from the analyses, since meaningful comparisons of predicted and experimental strains would be unable to be performed. Specifically, the repeatability of the entire procedure to obtain experimental strains was previously determined to be ±3.5% strain [41]. This additional criterion significantly lowered the number of available elements for validation. It was found that only the anterior band of the inferior glenohumeral ligament had validation elements with experimental strains that were above the experimental strain repeatability at each of the three clinically relevant joint positions. Therefore, only these elements were used for validation of FE Model 1.

The criteria for validation is that the average difference between the predicted and experimental strains in the validation elements of the anterior band of the inferior glenohumeral ligament was less than the experimental strain repeatability of ±3.5% strain. In addition, the

predicted shape of the capsule tissue in each clinically relevant joint position was compared to the experimental shape to further validate the predictive capabilities of FE Model 1.

3.0 DEVELOPMENT AND VALIDATION OF FE MODEL 2

3.1 INTRODUCTION

In order to address Specific Aim 1b, an additional subject-specific finite element model of the glenohumeral joint needed to be developed and validated (FE Model 2). This required performing all aspects of the experimental and computational approach outlined in Section 2.1 (Figure 2.1). Therefore, subject-specific inputs were collected, including a reference position for use in determining the reference configuration of capsule strain markers, geometry of the bones, capsule, and humeral head cartilage when the joint is in the reference position, the joint kinematics from the reference position to the clinically relevant joint positions, and material coefficients of the capsule tissue from an isotropic hyperelastic constitutive model. The *experimental strains* were obtained at the clinically relevant joint positions while obtaining the subject-specific inputs, and the *predicted strains* were computed within FE Model 2 after its generation with the subject-specific inputs and motion to the clinically relevant joint positions. Validation of FE Model 2 was then performed by comparing the *experimental strains* with the *predicted strains* at equivalent joint positions, and ensuring that differences in strain were less than the experimental strain repeatability. Once validated, FE Model 2 could then be used with FE Model 1 to analyze the distribution of load in the capsule at multiple clinically relevant joint positions.

3.2 SUBJECT-SPECIFIC EXPERIMENTAL INPUTS

3.2.1 Reference Configuration

Obtaining a reference configuration for the capsule is an essential process of the development of subject-specific finite element models. The reference configuration is defined as the 3-dimensional positions of capsule strain markers fixed to the anterior-inferior capsule when the joint is placed in its reference position, i.e. the joint position where slack in the tissue has been completely removed when the capsule is inflated with compressed air. Determining a 3-dimensional reference position for the capsule is similar to applying a pre-load to remove slack during uni-directional tensile testing of 2-dimensional ligaments such as the anterior cruciate ligament and medial collateral ligament. Motions of the capsule strain markers as the joint is moved from the reference position to the clinically relevant joint positions are then used to calculate the experimental surface strains at the clinically relevant joint positions. Methodology for obtaining a reference configuration for the capsule has been developed by Malicky et al. [117], however additional modifications have been made within our research group [21, 41] to produce the following methodology.

3.2.1.1 Specimen Preparation

A fresh-frozen specimen from the right shoulder of a 66 year old male that had been stored at -20° C was allowed to thaw overnight. The specimen was dissected down to the glenohumeral capsule so that all skin, fascia, fatty tissue, and musculature were removed, after which an experienced orthopaedic surgeon verified that there was no pathology to the joint in the form of rotator cuff tears, osteoarthritis, or soft-tissue lesions. The humerus was potted in a cylinder of epoxy putty so that the humeral shaft was concentric with the cylinder, and the scapula was

potted in a rectangular block of epoxy putty so that the scapular plane was approximated by the walls of the epoxy putty [10, 11, 118] (Figure 3.1). Radiographs were then taken of the joint from an anterior view, to verify that the scapula and humerus were potted correctly. Specifically, it was verified that the humeral shaft and humeral epoxy putty were concentric with each other, and that the angle of inclination of the glenoid with respect to the superior-inferior axis of the scapular epoxy putty was approximately 5-15°.

Figure 3.1 Anterior view of the cadaver for FE Model 2 (right shoulder), after dissection down to the capsule and after the humerus and scapula were potted in epoxy putty

The anterior and posterior bands of the inferior glenohumeral ligament and the axillary pouch were identified, and a clinician carefully marked the margins of these capsule regions using 5-0 suture (Davis & Geck, Manati, Puerto Rico). A 7 x 11 grid of black delrin strain markers (1.58 mm diameter) was glued to the surface of the anterior-inferior capsule using cyanoacrylate. The first column of capsule strain markers was placed at the superior margin of

the anterior band of the inferior glenohumeral ligament, so that the first and last capsule strain markers were 1 cm from the capsule insertion into either the humerus or glenoid, and approximately 5 mm apart (Figure 3.2). The remaining capsule strain markers were then fixed to the anterior-inferior capsule so that columns of capsule strain markers were approximately 5 mm apart and so that the 11th column terminated at the superior margin of the posterior band of the inferior glenohumeral ligament Throughout the entire experimental protocol, the capsule tissue was kept hydrated with 0.9% physiologic saline solution applied through a spray bottle.

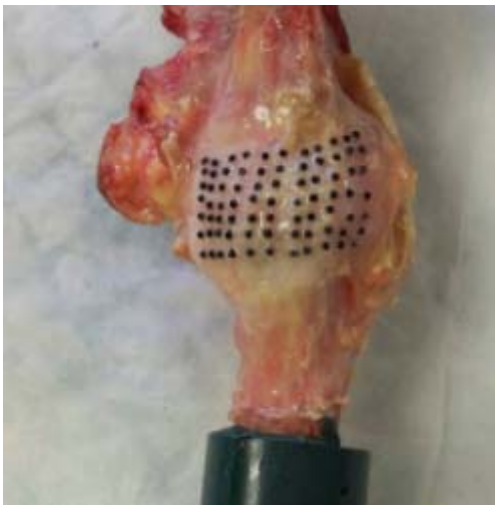

Figure 3.2 Inferior view of the 77 capsule strain markers applied to the anterior-inferior glenohumeral capsule for determination of the reference configuration

3.2.1.2 Experimental Setup

The joint was mounted in a custom-designed 6-degree of freedom plastic jig at 60° of glenohumeral abduction and neutral horizontal abduction and internal/external rotation (Figure 3.3). A small amount of joint distraction was then applied, and neutral rotation was determined by verifying that there was an equal amount of humeral head cartilage on the anterior and posterior sides of the glenoid.

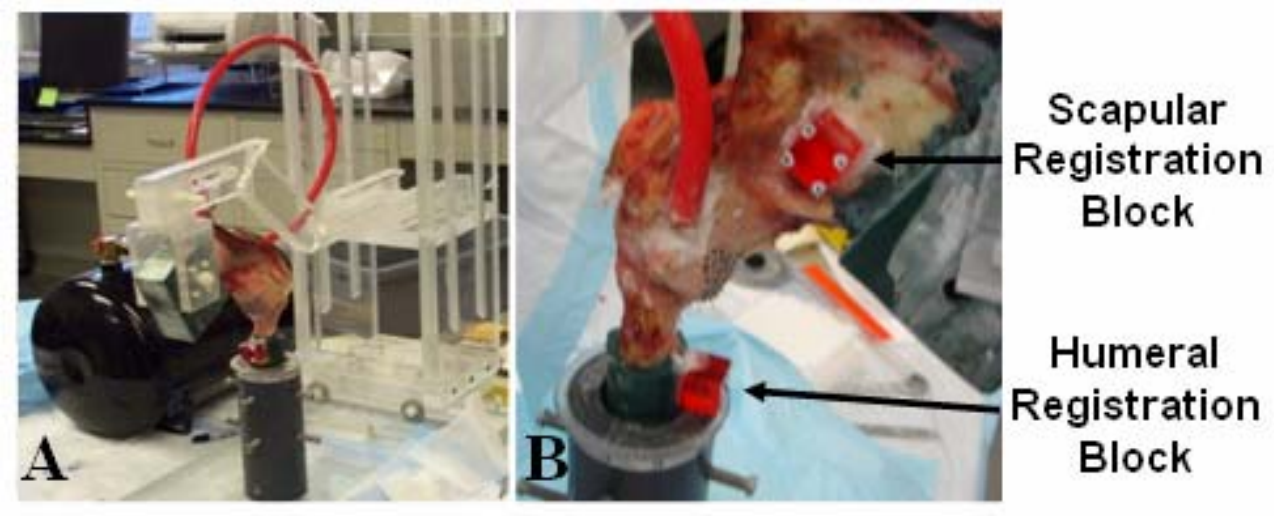

Figure 3.3 A) Joint mounted into custom fixture, with the air tank used for inflation shown B) Inflation via rubber hose inserted into rotator interval

Since the reference position and clinically relevant joint positions are determined using separate fixtures, a common coordinate system needed to be established between the reference position and clinically relevant joint positions so that 3-dimensional capsule strain marker motion from the reference position to the clinically relevant joint positions could be computed, for determination of experimental strains. For establishment of a common coordinate system between the reference position and the clinically relevant joint position, four strain markers were fixed to the corners of a registration block (20mm x 20mm x 20mm), which was then affixed to the humeral epoxy putty just distal to the humeral head using a cyanoacrylate/baking soda compound (Figure 3.3). The positions of the registration block strain markers in the reference position and clinically relevant joint positions were used to define local coordinate systems for the capsule strain markers placed on the anterior-inferior capsule, and thus allowed for computation of capsule strain marker motion from the reference position to the clinically relevant joint positions. The humeral registration block was mounted on the medial surface of

the humeral epoxy putty at neutral internal/external rotation, with the strain markers glued to the medial face of the registration block for visualization with the optical motion tracking system.

A scapular registration block was then fixed to the anterior face of the scapular plane (Figure 3.3), to be used with the humeral registration block when determining joint kinematics during motion as outlined in Section 3.2.3.2. The medial face of the scapular registration block was mounted perpendicular to the medial/lateral axis of the epoxy putty, for determination of a scapular anatomical coordinate system (Section 4.2.1.1). An attempt was made so that each of the three orthogonal faces of the scapular registration block were parallel to the faces of the scapular epoxy putty, however topological variations in the plane of the scapula made this challenging for the anterior and superior faces. Lastly, strain markers were attached to the scapular registration block with cyanoacrylate on the anterior face of the registration block, for visualization with the optical motion tracking system.

A pressure regulator (resolution: 0.1 psi or 0.7 kPa) was instrumented on an air tank, to be used to inflate the capsule. A plastic needle attached to the end of a rubber hose was inserted into the intra-articular joint space through the rotator interval, to inflate the capsule (Figure 3.3). A custom-built 3-camera (Adimec, Boston MA) optical motion tracking system with motion tracking software (DMAS, Olathe KS) was set into place, so that each capsule strain marker on the anterior-inferior capsule and the strain markers on the humeral registration block could be seen by at least two cameras. The specimen was removed from the custom fixture, and the motion tracking system was calibrated with the use of a custom-built calibration frame placed in the volume occupied by the joint. This motion tracking system was determined to be accurate to within ±0.08 mm. After calibration, the specimen was re-mounted into the fixture.

3.2.1.3 Data Collection

The capsule was inflated to 4.8 kPa, 5.2 kPa, and 6.2 kPa pressures as the humerus was positioned at 60° of glenohumeral abduction and 0°, ±5°, ±10°, and ±15° of internal/external rotation, in a randomly generated order. At each joint position, the locations of the capsule strain markers were recorded for the 4.8 kPa, 5.2 kPa, and 6.2 kPa inflation pressures using snapshots taken with the optical motion tracking system.

3.2.1.4 Determination of the Reference Configuration

At each joint position the two snapshots taken with 4.8 kPa and 6.2 kPa inflation pressures were overlaid on each other using image analysis software (MS Office Picture Manager), and differences in capsule strain marker positions were qualitatively measured (Figure 3.4). Joint positions where slack in the capsule is removed will have relatively low capsule strain marker motion between the 4.8 kPa and 6.2 kPa inflation pressures, as capsule strain markers will be more prone to move with increasing inflation pressure at joint positions where the slack is not removed at the 4.8 kPa inflation pressure. The three joint positions with the least amount of visual capsule strain marker motion were identified, and the 3-dimensional capsule strain marker positions during application of the 4.8 kPa and 6.2 kPa pressures were processed computationally for each of the three joint positions. The average and peak 3-dimensional capsule strain marker motion was computed for all 77 capsule strain markers. The joint position with the lowest average capsule strain marker motion between the two pressures and a peak marker motion less than 1.25 mm was defined as the reference position. The *reference configuration* for the capsule strain markers was then obtained by recording the capsule strain marker locations in the reference position when the joint was inflated to 5.2 kPa.

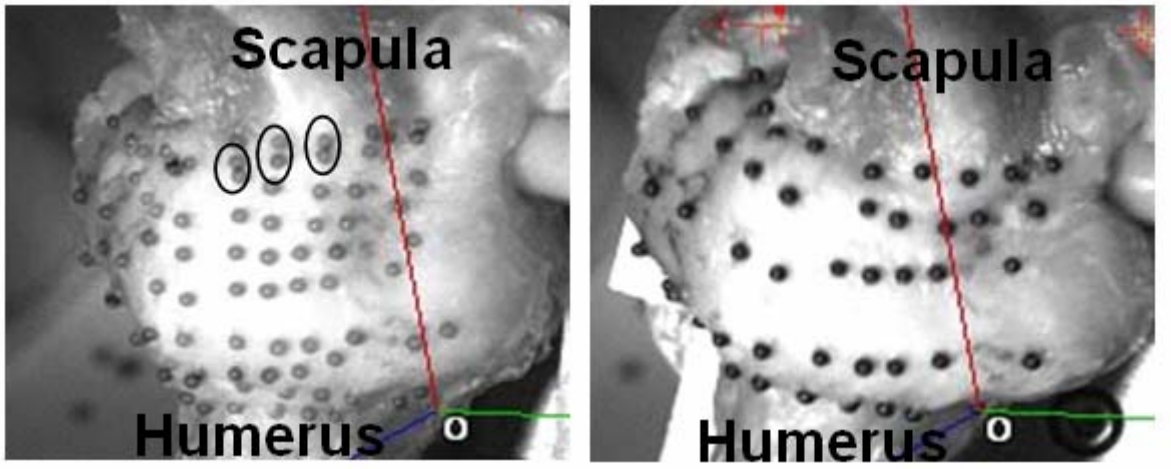

Figure 3.4 Overlaid snapshots at two different joint positions showing relatively large (left) and small (right) capsule strain marker motion between the 4.8 kPa and 6.2 kPa pressures. Black ovals enclose the same capsule strain marker at the two different pressures

3.2.2 Surface Geometry of Relevant Structures

In order to develop subject-specific finite element models, the 3-dimensional surface geometries of the bone and soft tissue structures must be obtained when the cadaver is in its reference position. Computed tomography (CT) and magnetic resonance imaging (MRI) have been used previously to obtain subject-specific geometry of bones and/or soft tissues for computational analyses [95, 110, 119-121]. The output from these medical imaging modalities is stacked 2-dimensional cross-sectional images of the body region of interest. Image segmentation software can then be used to generate 3-dimensional surfaces of the bones and/or soft tissues after their identification in each 2-dimensional slice. CT scans allow for relatively easy visualization of the bony geometry, although identifying boundaries of neighboring soft tissue structures can be challenging. MRI scans allow for relatively easy visualization of both bony geometry and soft tissue structures neighboring other soft tissues, however at a much higher cost than with CT imaging. Previous researchers have removed all soft tissues except those of interest prior to

scanning specimens with CT [95, 110, 121], which allows for improved visualization of the soft tissue structures of interest. The soft tissues of interest for the subject-specific finite element models of the glenohumeral joint include the capsule and humeral head cartilage. Since all other soft tissues have been previously removed to obtain the reference configuration (Section 3.2.1), the use of CT scans will be employed to obtain the subject-specific bone and soft-tissue geometry.

3.2.2.1 Structures of Interest

The anatomical structures of interest include the humerus, scapula, glenohumeral capsule, and humeral head cartilage. During glenohumeral joint motion, contact occurs between the humeral head cartilage and the articular surface of the capsule. Failure to include the cartilage in the finite element model would result in contact with the capsule and bony humerus, which may significantly change the distribution of stress and strain in the capsule. The glenoid labrum was not included as a structure of interest, due to the inability to differentiate the labrum from the capsule at the insertion of the capsule into the glenoid.

In addition to the anatomical structures, additional structures of the registration blocks, capsule strain markers, and margins of the capsule regions must be identified. Kinematics are prescribed within the finite element model through motion of the registration blocks from the reference position to the clinically relevant joint positions. Since the surfaces of the registration blocks must also be reconstructed and included in the finite element model, both the humeral and scapular registration blocks must also be visualized in the CT scans.

In order to perform one-to-one strain comparisons between predicted and experimental strains for FE Model 2 validation, the location of the experimental strain elements must be incorporated into the finite element model. This is done via segmentation of the capsule strain

markers, as the location of the capsule strain markers can be used to identify the identical elements within the computational model. Therefore, the capsule strain markers must also be visualized in the CT scans.

Rainis [40] demonstrated that the axillary pouch and posterior capsule region have similar material coefficients for an isotropic hyperelastic constitutive model, however this may not be true for the remaining capsule regions. It has been shown that differences exist between the data collected from various capsule regions [32, 34, 100, 122], therefore it is necessary to obtain the geometry of each separate capsule region during the CT scan so that region-specific properties can be incorporated into the model. Since the margins of the capsule regions are unidentifiable in the CT scan, rubber tubing (2.4 mm diameter, Danco, Concordville PA) was attached to the capsule using cyanoacrylate directly over the 5-0 suture applied in Section 3.2.1.1 to delineate the margins of the capsule regions. Additional materials such as copper wire, plastic coated wire, and beaded plastic cable were considered, however the rubber tubing was the only easily visible material that did not create artifacts in the images [41].

Therefore, a total of eight structures must be visualized in the CT scan for generation of surfaces to be input into the finite element model: the humerus, scapula, glenohumeral capsule, humeral head cartilage, humeral registration block, scapular registration block, capsule strain markers, and rubber tubing delineating the capsule margins.

3.2.2.2 CT Data Acquisition

Following determination of the reference configuration (Section 3.2.1.4), rubber tubing was affixed to the capsule using cyanoacrylate, directly over the 5-0 suture delineating the margins of the capsule regions. Care was taken so that the ends of the rubber tubes approximated the insertions of the capsule into the glenoid and humerus. The specimen was positioned within the

custom-built fixture (Section 3.2.1.2) at the reference position, with the air tank still connected to the specimen via the rubber hose through the rotator interval. The air tank, fixture, and specimen were then transported to a local hospital for the CT scan. The fixture was laid on its side such that it fit within the scanning area of the CT scanner (GE Lightspeed, Milwaukee, WI), with the slicing axis oriented parallel to the humeral shaft (Figure 3.5). The air tank was also placed near the CT scanner so that the joint could be inflated during the CT scan.

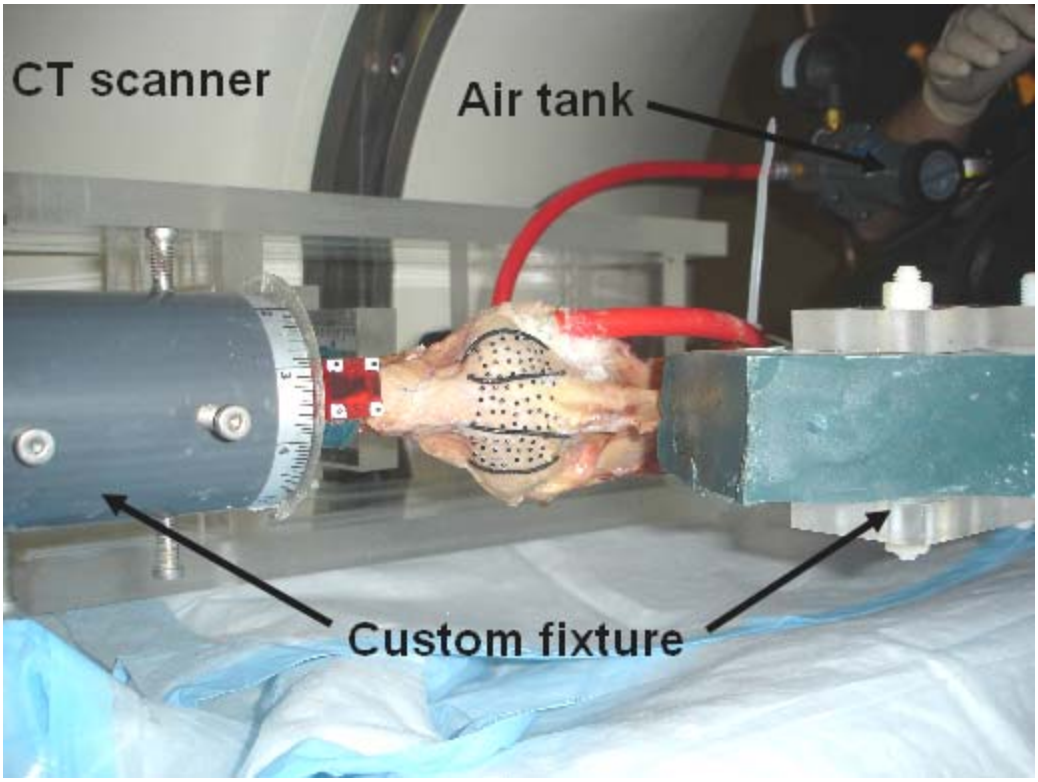

Figure 3.5 Joint, custom fixture, and air tank positioned in CT scanner

A 180 mm x 180 mm field of view was selected so that all structures of interest were within the viewing environment. The capsule was inflated to 5.2 kPa at the reference position, and a CT scan was taken (100 kV, 120 mA) with a slice increment of 1.25 mm. A total of 172 slices were obtained, starting from the humeral shaft distal to the registration block and ending proximal to the medial border of the scapula.

3.2.2.3 Surface Reconstruction and Development

All 172 2-dimensional slices from the CT dataset were loaded into Amira (v 4.1.1, Mercury Computer Systems, Inc, Chelmsford MA), and the geometry of the humerus, scapula, glenohumeral capsule, humeral head cartilage, registration blocks, capsule strain markers, and rubber tubes were manually segmented on each slice (Figure 3.6). The thickness of the capsule was made artificially large by defining the articular surface to be far from the anatomical articular surface in the 2-dimensional images. This was done to prevent TrueGrid from confusing the bursal and articular surfaces of the capsule when projecting the finite element mesh to the capsule during construction of the finite element model (Section 3.3.1.1). Since the mesh was fit to the capsule's bursal surface only, segmenting an increased capsule thickness had no effect on the capsule mesh but rather served as a useful tool to avoid mesh projection issues.

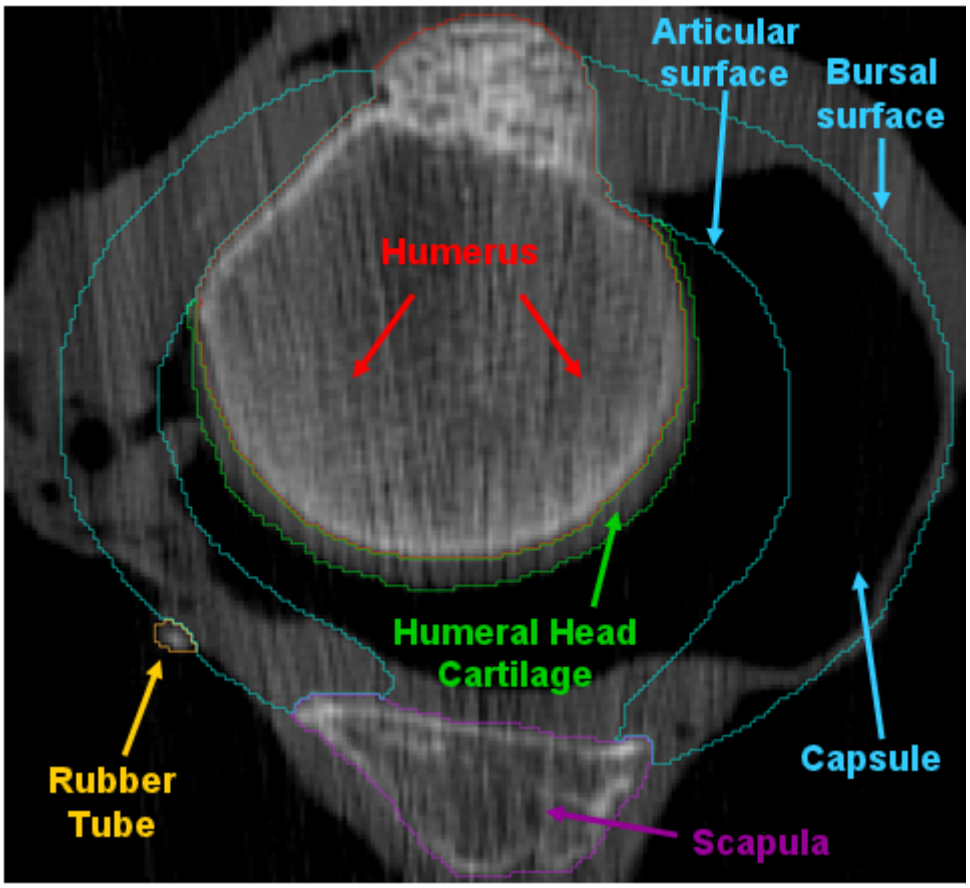

Figure 3.6 2-dimensional slice with the following structures segmented: humerus, humeral head cartilage, rubber tube, scapula, and capsule (capsule strain markers and registration blocks not shown)

3-dimensional surfaces were then created from the 2-dimensional images, as shown in Figure 3.7 .

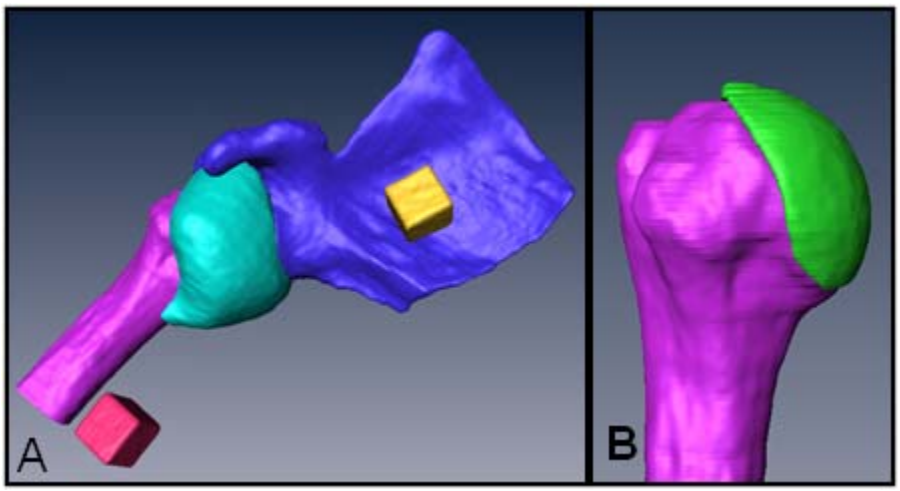

Figure 3.7 A) Anterior view of the 3-dimensional surfaces created in Amira for FE Model 2, right shoulder (capsule strain markers and rubber tubes not shown). B) Capsule removed to expose humeral head cartilage

Once the surfaces were generated, the rubber tubes were used to generate 3-dimensional spline curves that defined the margins of the capsule regions and the insertion of the capsule into the glenoid and humerus. It is worth noting that the capsule's glenoid insertion was modeled by a direct capsule insertion into the rigid glenoid. While this insertion is not typical of the anatomical glenoid insertions [48, 123], the presence of a labrum at the insertion site is simulated computationally (Section 3.3.2.2). After defining the curves for the capsule margins, the surfaces of all structures were discretized into triangulated surface elements and smoothed for input into TrueGrid.

Lastly, the 3-dimensional coordinates of the segmented capsule strain markers were obtained in order to define elements within the computational model that were identical to the experimental elements used to generate experimental strain distributions (Section 3.3.4).

3.2.3 Joint Positions for Validation

The majority of glenohumeral joint dislocations occur in the anterior direction, when the joint is abducted to approximately 90° of humerothoracic abduction and externally rotated. The anterior-inferior capsule provides anterior stability to the joint in positions of abduction and external rotation. Therefore, similar joint positions will be used to analyze the anterior stability provided by the anterior-inferior glenohumeral capsule in order to answer the research question and achieve the specific aims. Due to scapular elevation during humerothoracic abduction, the glenohumeral abduction angle in positions of dislocation is approximately 60° [124-126]. Since the distribution of load in the anterior-inferior capsule regions is variable with external rotation, it is necessary to evaluate a range of external rotation angles from neutral rotation to maximum external rotation, for identification of joint positions with consistent distribution of load in the

anterior-inferior capsule among a group of subjects. In order to use the models to confidently predict distribution of load in the anterior-inferior capsule throughout the range of external rotation, however, it is necessary to validate the model at multiple positions along the path of external rotation. Due to the variability among patients, however, not all cadavers can be externally rotated to the same maximum value, preventing comparisons of the distribution of load at a single maximum external rotation angle for all subjects. However, preliminary work has suggested that most cadavers can be rotated near to or beyond 60° of external rotation when a 3 N-m external rotation moment is applied. Therefore, the maximum external rotation used for the current work was chosen to be either the maximum external rotation angle or 60° of external rotation following application of a 3 N-m external rotation moment, whichever was lowest.

Since the ultimate goal of the proposed work is to suggest joint positions that may be used for more effective physical examinations, a clinically relevant load must be applied during the exam. A 50 N anterior load has been used previously for evaluation of the anterior stability provided by the capsule [10, 11, 118], however more recent work within our research group demonstrated that this load resulted in contact of the humerus with the coracoid process when applied to a cadaver dissected down to the glenohumeral capsule, at joint positions with abduction and low external rotation [41]. For the validation process it is essential that capsule surface strains exist, which may not occur if load is distributed between the bones and not the capsule. The work of additional researchers has suggested that 25 N may be an appropriate load to apply in order to simulate a physical examination of the glenohumeral joint with all soft-tissues removed except the capsule [11, 18-20]. Therefore, the joint positions resulting from the following condition will be used for validation; a 25 N anterior load applied to the joint at 60° of glenohumeral abduction in the scapular plane and 0°, 30°, and 60°/maximum external rotation.

3.2.3.1 Robotic Universal Force/Moment Sensor System

A 6-degree-of-freedom robotic/universal force-moment sensor (UFS) testing system developed and used extensively within our research center [10, 11, 118-120, 127-131] (Figure 3.8) has been used specifically to evaluate glenohumeral joint function, in order to position the joint in targeted joint orientations (i.e. abduction and external rotation) and to apply subsequent loads [10, 11, 21, 118]. The robotic technology allows for two user-controlled modes: force control mode, used to apply loads to the joint that result in paths of motion of the humerus with respect to the scapula at a targeted joint orientation, and position control mode, used to repeat the exact paths of motion obtained in force control mode. Once the joint is manipulated by the robot into targeted joint orientations, the force control mode can be used to apply loads to the joint. The subsequent joint motions are then stored as discretized positions along the path of joint motion. The position control mode can then be used to replay the path of motion at the discretized positions, in order to record experimental parameters such as glenohumeral joint kinematics and capsule strain at specific positions along the path of motion. The robotic manipulator has been previously determined to have an accuracy of 0.2 mm and 0.2°, and therefore was used to obtain the experimental joint positions for validation. The robot protocol used for the current work is provided in Appendix A.

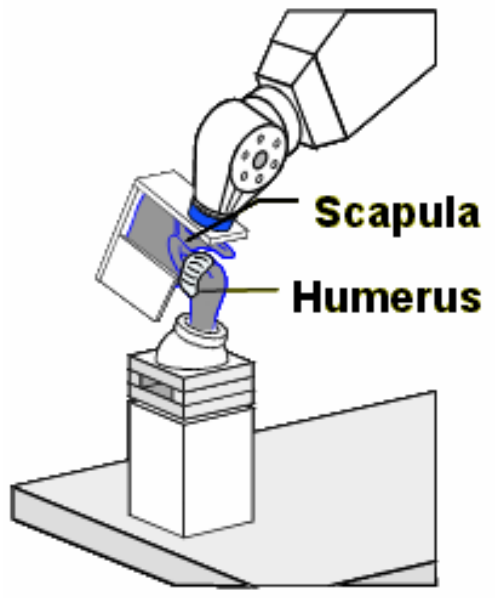

Figure 3.8 6-degree-of-freedom robotic/universal force-moment sensor testing system

3.2.3.1.1 Specimen Mounting

After the CT dataset has been obtained in Section 3.2.2.2, the joint was removed from the custom fixture and the rubber tubes were removed from the capsule tissue using a scalpel. Care was taken to preserve the attachment of the capsule strain markers to the capsule. The humerus and scapula were mounted into custom clamps attached to the base and end-effector of the robotic/UFS testing system, respectively. The scapula was mounted into the scapular clamp so that the anatomical coordinate system of the scapula was aligned with the Cartesian coordinate system of the robotic/UFS testing system, so that the anterior/posterior, medial/lateral, and superior/inferior axes of the scapula corresponded with the x, y, and z axes of the robot, respectively. Using the custom clamps, the humerus and scapula were mounted into the robotic manipulator with the joint in approximately 45° of glenohumeral abduction in the scapular plane, 0° of horizontal abduction, 0° of flexion, and 0° of external rotation.

The origin of the anatomical coordinate system of the scapula was located by identifying the midpoint between the most anterior aspect of the lesser tuberosity and the most posterior

aspect of the humeral ridge. The local, i.e. end-effector, coordinate system of the robotic/UFS testing system was then translated so that it was coincident with the anatomical coordinate system of the scapula, for force and moment calculations in the scapular anatomical coordinate system [10, 11, 118].

3.2.3.1.2 Application of Joint Motion

The passive path of glenohumeral abduction in the scapular plane was then determined, from 20° to 65° of abduction. A 22 N compressive (i.e. medially directed) load was applied and maintained throughout the path, ensuring that the humerus was centered within the glenoid cavity throughout the range of abduction. The joint was then manually abducted in 1° increments in the targeted range. The forces in the anterior/posterior and superior/inferior direction were minimized (~0 N), which was achieved by permitting joint translation along the three orthogonal axes. Once the passive path of abduction was obtained, radiographs were taken in the anterior-posterior plane at 30° and 60° of abduction, and an orthopaedic surgeon verified that the humerus was properly positioned within the glenoid cavity during the path of abduction.

The joint was then oriented at 60° of glenohumeral abduction, after which the path of internal/external rotation was established by applying a maximum internal/external rotation moment of 3 N-m to the scapula while maintaining the 22 N joint compressive force. The joint positions of 60° of glenohumeral abduction and 0°, 30°, and 60°/maximum (the smaller of the two values) of external rotation were then identified. The joint was then oriented in each of these positions, and using the robotic manipulator's force control mode a 25 N posterior load was applied to the scapula (simulating 25 N anterior load applied to the humerus) while maintaining the 22 N compressive force. During each of the three loading conditions the subsequent paths of motion were recorded using the robot program.

3.2.3.2 Measurement of Joint Kinematics and Capsule Strain

After the 25 N load was applied to the joint at 60° of glenohumeral abduction and 0°, 30°, and 60°/maximum external rotation, the position control mode of the robotic manipulator was used to position the joint at the exact points along the paths of motion where 25 N load was applied, at each of the three external rotations. At these positions, identified as the clinically relevant joint positions, an external digitizer (Microscribe © 2002, Immersion Corporation, San Jose, CA) was used to record the locations of the humeral and scapular registration blocks for future calculation of joint kinematics from the reference position to each of the clinically relevant joint positions (Section 3.3.3.1). The 3-dimensional positions of the strain markers on the humeral registration block were also recorded using the optical motion tracking system described in Section 3.2.1.2, so that experimental strains in the anterior-inferior capsule could be computed by determining the relative motion of the capsule strain markers from the reference position to each of the clinically relevant joint positions.

3.2.3.2.1 Experimental Setup

An overview of the experimental data collection setup is shown in Figure 3.9. The optical motion tracking system was set up as in Section 3.2.1.2, so that each capsule strain marker and the strain markers attached to the humeral registration block could be seen by at least two cameras at each of the three clinically relevant joint positions. The joint was removed from the robotic manipulator, and the volume enclosing the capsule was calibrated using the custom-built calibration frame. The joint was then remounted into the robotic manipulator. The external digitizer was set up so that three orthogonal faces on both the humeral and scapular registration blocks could be digitized at each of the three clinically relevant joint positions.

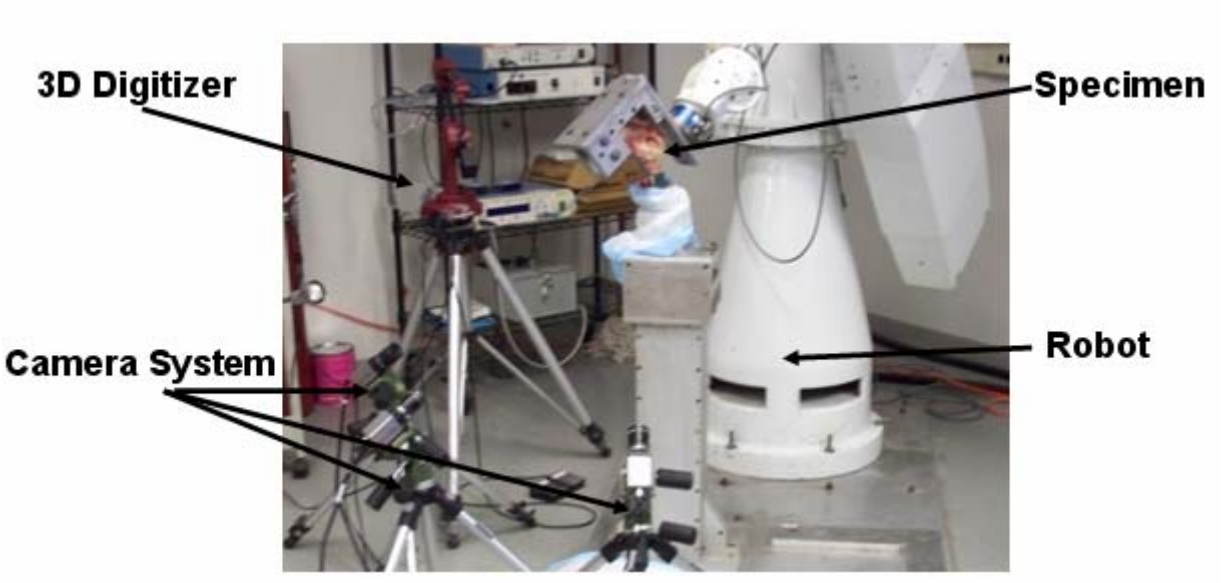

Figure 3.9 Experimental motion and strain tracking setup

3.2.3.2.2 Data Collection

After the force control mode was used to apply a 25 N anterior load (humerus with respect to the scapula) to the joint at 60° of glenohumeral abduction and 0°, 30°, and 60°/maximum external rotation, the joint was oriented at 60° of glenohumeral abduction and 0° of external rotation. Using the robotic manipulator's position control mode, the path of motion resulting from the applied 25 N anterior load was then repeated in incremental steps. At the position corresponding to 25 N of applied load, the 3-dimensional spatial locations of the humeral and scapular registration blocks were recorded using the external digitizer. Also at this position, the *strained configuration* of the capsule strain markers, i.e. the 3-dimensional positions of the strain markers attached to the anterior-inferior capsule with the joint in its clinically relevant joint position, was recorded using the optical motion tracking system. The 3-dimensional positions of the strain markers attached to the humeral registration block were also recorded at this position. This process was then repeated for the clinically relevant joint positions with 30° and 60°/maximum external rotation.

3.2.3.3 Determination of Experimental Capsule Strain

Using the *reference configuration, strained configurations*, and the 3-dimensional positions of the humeral registration block strain markers with the joint in its reference position (Section 3.2.1.4) and clinically relevant joint positions (Section 3.2.3.2.1), respectively, the relative motion of the capsule strain markers between the *reference configuration* and the s*trained configurations* was computed. A 6 x 10 arrangement of quadrilateral elements in the anterior-inferior capsule was identified from the 7 x 11 grid of capsule strain markers, for a total of 60 experimental strain elements. These 3-dimensional positions of the capsule strain markers in the reference position and the relative capsule strain marker motions between the *reference configuration* and *strained configuration* were then input into ABAQUS® (v 6.7-1, Dassault Systemes). The experimental strain in the anterior-inferior capsule at the clinically relevant joint positions was then determined by computing the Green-Lagrange maximum principal strain at the centroid of each element.

3.2.4 Material Coefficients to Constitutive Model

The glenohumeral capsule acts to distribute load in multiple directions, and unlike traditional uni-directional ligaments such as the cruciate and collateral knee ligaments that have a transversely isotropic material symmetry, the capsule tissue has isotropic material properties [13, 21, 35, 40, 41, 96].

Previously, sensitivity studies were performed within our research group to determine the effect that variances in material coefficients contributed to measures of the stability provided by the capsule [112]. The authors found that when using an isotropic hypoelastic constitutive model to represent the capsule, predictions of maximum principal strain and reaction forces were highly

sensitive to changes in material coefficients. Increasing or decreasing the tangent modulus by 50% resulted in changes in predicted maximum principal strain and reaction forces of 16% strain and 9N, respectively. These findings demonstrate the importance of using subject-specific material coefficients to represent the capsule within the finite element model. Furthermore, it has been shown that differences exist between the data collected from various capsule regions [32, 34, 100, 122] , suggesting it is appropriate to obtain region-specific material coefficients.

FE Model 1 was initially developed and validated using an isotropic hypoelastic constitutive model to represent the capsule [41]. However, validation was successfully performed only at the isolated joint position with a 25 N anterior load applied at 60° of glenohumeral abduction and maximum external rotation. At 0° and 30° of external rotation with the anterior load applied, differences in average predicted and experimental strains were beyond the experimental repeatability of ±3.5% strain, therefore the model was invalid at these positions. Ligamentous tissue has a non-linear load response to applied deformation, however, and the use of an isotropic hypoelastic constitutive model to represent the tissue may therefore decrease the predictive capability of finite element models of the glenohumeral joint.

A non-linear isotropic hyperelastic constitutive model has been recently employed within our research group to successfully model the loading response of capsule tissue to applied elongations [40]. Developed by Veronda and Westmann [113] and later expanded by Weiss et al. [108], this constitutive model allows for the material response of the capsule to be modeled with the strain energy function shown in in Figure 3.10.

$$W = C_1(e^{C_2(\tilde{I}_1-3)}-1)-\frac{C_1C_2}{2}(\tilde{I}_2-3)+U(J)$$

Figure 3.10 Veronda-Westmann isotropic hyperelastic strain energy function

This strain energy function groups the extracellular matrix and the collagen fibers into one material, and has been shown to predict physically reasonable behavior under tension, compression, and shear. The formulation allows for the uncoupling of the dilatational and deviatoric tissue behavior, however it provides an identical response to the formulation for a fully coupled strain energy in the limit of incompressibility or for an isochoric deformation, i.e. when J=1 [108]. Here I_1 and I_2 are the deviatoric invariants of the right deformation tensor, and U(J) governs the dilatational response of the tissue (where J is the volume ratio). C_1 and C_2 are the material coefficients that are to be incorporated into the subject-specific finite element model, with both C_1 and C_2 scaling the magnitude of the stress-strain curve, and C_2 additionally governing the non-linearity of the stress-strain curve.

In order to obtain these material coefficients, a combined experimental and computational approach was utilized, as developed by Weiss et al. [108] and furthered by Rainis [40]. Uni-directional elongations were applied to the capsule regions in the directions both parallel and perpendicular to the longitudinal (glenoid to humerus) direction of the capsule tissue, in order to obtain empirical load-elongation data. Using the finite element method the experiment was then simulated using the Veronda-Westmann isotropic hypoelastic constitutive model to represent the capsule tissue, and material coefficients were generated for the predicted curve. The predicted and experimental load-elongation curves were then compared, after which the material coefficients were optimized using an inverse finite element optimization routine until the predicted and experimental load-elongation curves matched. Based upon the work performed within our research group [40, 41] and on previously published work [108], the following experimental and computational protocol was used in order to obtain the subject-specific

material coefficients to a Veronda-Westmann isotropic hyperelastic constitutive model, for incorporation into the subject-specific finite element model.

3.2.4.1 Tissue Sample Procurement

After completion of the experimental protocol to obtain subject-specific joint kinematics in Section 3.2.3, the specimen was carefully removed from the robotic manipulator. The capsule strain markers were removed with a scalpel, and the entire glenohumeral capsule was excised from the joint by first cutting along the superior margins of the anterosuperior and posterior capsule regions, followed by cutting along the glenoid and humeral insertions. When cutting along the glenoid insertion, care was taken to preserve the glenoid labrum. After excision of the capsule tissue from the joint, digital calipers (Mitutoyo, Aurora IL) were used to take multiple measurements of the glenoid labrum radial thickness at various locations along the circumference of the labrum (Figure 3.11), for use in determining the computational insertion site modification described in Section 3.3.2.

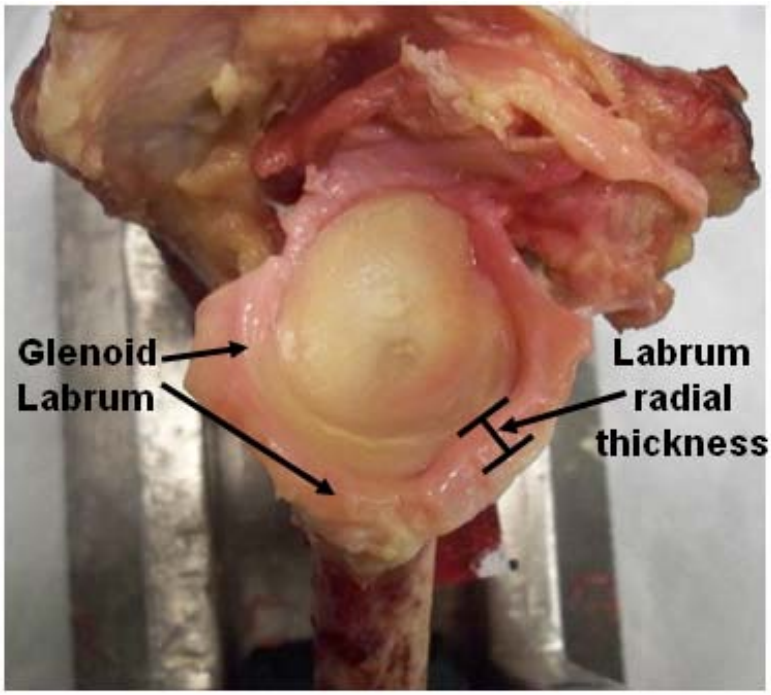

Figure 3.11 Lateral view of the glenoid labrum, with the labrum radial thickness indicated

In Section 3.2.1.1, 5-0 suture was used to delineate the margins of the capsule regions of the anterior-inferior capsule. After excision of the capsule from the joint a scalpel was used to isolate the capsule regions by cutting along the margins outlined by the sutures, resulting in five separate tissue samples corresponding to the five capsule regions. For the axillary pouch and posterior capsule, a 25 mm x 25 mm square tissue sample was obtained from the tissue mid-substance. Due to the dimensional limitations of the anterior and posterior bands of the inferior glenohumeral ligament and the anterosuperior region, 5 mm x 15 mm tissue samples were obtained from the tissue mid-substance in these capsule regions.

3.2.4.2 Experimental Setup

Each capsule region was placed in custom clamps and mounted into a tensile testing apparatus (Enduratec Elf 3200, BOSE Corporation, Minnetonka MN), so that uni-directional elongations

could be applied along the longitudinal direction of the capsule regions (Figure 3.12). A load cell (Sensotec, Columbus, OH; Model 31; Capacity 10 lbs.) was used to measure the load along the axis of motion of the tensile testing apparatus. The optical motion tracking system described in Section 3.2.1.2 was set up in order to record the 2-dimensional geometry of the tissue sample for incorporation into the computational simulation of the experiment (Section 3.2.4.4), however only one camera was necessary for the 2-dimensional image. For the axillary pouch and posterior capsule region, uni-directional elongations were also applied in the transverse direction of the tissue, i.e. the direction perpendicular to the longitudinal direction. After the longitudinal uni-directional elongations were applied to the axillary pouch and posterior capsule region, these capsule regions were removed from the custom clamps. The previously clamped tissue was excised using a scalpel, after which the tissue samples were re-clamped and remounted into the tensile testing apparatus so that uni-directional elongations could be applied in the transverse direction of the tissue.

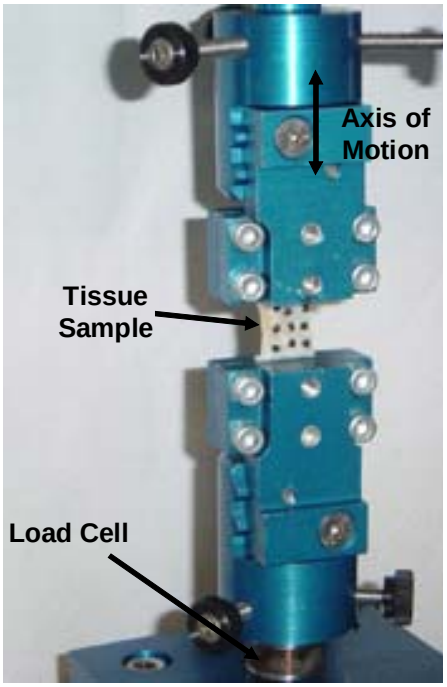

Figure 3.12 Material tensile testing apparatus setup

3.2.4.3 Data Collection

After mounting the specimens in the tensile testing apparatus for application of longitudinal uni-directional elongations, a pre-load was applied to remove slack in the tissue. The pre-load was 0.5 N for the anterior and posterior bands of the inferior glenohumeral ligament, the axillary pouch, and the posterior capsule region, and 0.3 N for the anterosuperior region. After application of the pre-load, a ruler and digital calipers were used to measure the clamp-to-clamp distance of the tissue sample as well as the tissue width and thickness near both clamps and at the mid-substance. Three thickness measurements were taken at each location near the clamps and at the mid-substance, and averaged to report a single value at each location. Following the dimensional measurements, the tissue samples were pre-conditioned by applying a cyclic elongation for 10 cycles at 10 mm/min, from 0-1.5 mm for all capsule regions. Preliminary experiments performed in our research group demonstrated that this elongation would load the capsule just beyond the transition into the linear region of the load-elongation curve (Figure 3.13). The pre-load was then re-applied, after which non-destructive uni-directional elongations were applied in the longitudinal direction of the tissue. The non-destructive elongation was 2.25 mm for the anterior and posterior bands of the inferior glenohumeral ligament, the axillary pouch, and the posterior capsule region, and 2.0 mm for the anterosuperior region. Preliminary experiments performed in our research group indicated that these elongations would load the capsule regions well into their linear region, without approaching the yield point of the tissue and damage the specimen. During the application of the non-destructive uni-directional elongations, the load cell recorded the force within the capsule tissue, and the optical motion tracking system was used to record the motion of the tissue.

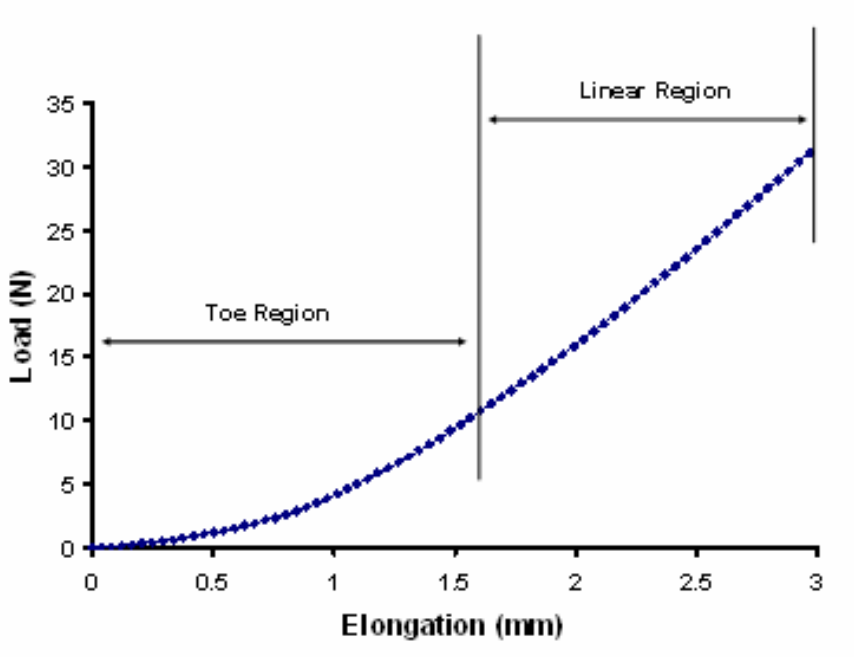

Figure 3.13 Typical load-elongation curve for tensile loading applied to capsule tissue, demonstrating toe and linear regions

For the anterior and posterior bands of the inferior glenohumeral ligament and the anterosuperior region, the tissue samples were immediately removed from the tensile testing apparatus following the longitudinal elongation. For the axillary pouch and posterior capsule regions the tissue samples were returned to their pre-load elongation, wrapped in saline-soaked gauze, and allowed to recover for 30 minutes, as this time duration has been shown to be the minimum time necessary for complete tissue recovery [40]. Following the recovery period the tissue samples were removed from the tensile testing apparatus, and the previously clamped tissue was excised with a scalpel. The samples were then re-clamped and re-mounted for application of the transverse uni-directional elongations. The pre-loads, pre-conditioning, tissue dimensional measurements, non-destructive elongations, and motion tracking were all repeated using the methodology for the longitudinal uni-directional elongations,, and following the non-

destructive transverse elongations the tissue samples were removed from the tensile testing apparatus.

3.2.4.4 Computational Generation of Optimized Coefficients

Simulation of the experimental uni-directional elongations was then performed using the finite element method [108]. Using images recorded from the optical motion tracking system and the tissue sample dimensional measurements, a finite element mesh was then created for each capsule region. The clamped edges of the tissue were given rigid body properties, with one end fixed and the other allowed to move based on the non-destructive uni-directional elongations applied experimentally. The unclamped tissue was assigned a Veronda-Westmann isotropic hyperelastic constitutive model, and initial guesses of C1 and C2 were assigned so that the predicted load-elongation data matched the experimental load-elongation data with an R^2 value greater than 0.97. A non-linear optimization program that minimized the sum of the squared error between the predicted and experimental load-elongation data was then used to produce optimal C1 and C2 values for each capsule region.

For the anterior and posterior bands of the inferior glenohumeral ligament and the anterosuperior region, the optimized C1 and C2 values were used as inputs into the subject-specific finite element model. For the axillary pouch and posterior capsule region, however, two sets of optimized material coefficients were produced; one each for the longitudinal and transverse uni-directional elongation simulations. Due to the non-linearity in the Veronda-Westmann constitutive model, averaging the two sets of C1 and C2 values for each region is inappropriate. Rather, the predicted longitudinal and transverse curves were used to create an average curve to be used to generate appropriate material coefficients. Specifically, the C1 and C2 values for the longitudinal and transverse elongations were used to generate two Cauchy

stress-stretch curves, as outlined in the work of Rainis [40]. The Cauchy stress values on the curves were then averaged together at each stretch increment (n=11 total increments), to generate an average Cauchy stress-stretch curve. This curve was then used to generate C1 and C2 values, which served as the inputs to the subject-specific finite element model (Figure 3.14). Therefore, the C1 and C2 material coefficients for the axillary pouch and posterior capsule regions represented the material coefficients of the average Cauchy stress-stretch curve, and not the average of the material coefficients from the longitudinal and transverse curves.

In addition to the values of C1 and C2, the Veronda-Westmann isotropic hyperelastic constitutive model required input of a bulk modulus value. Based on preliminary work a bulk modulus value of 75 was assigned, for all of the capsule elements.

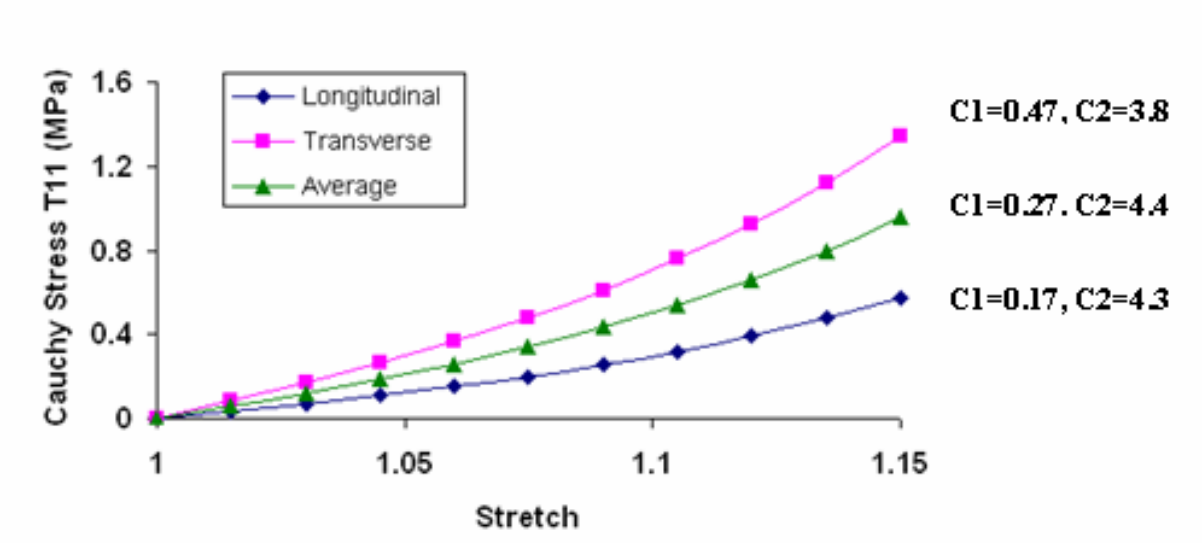

Figure 3.14 Sample Cauchy stress-stretch plot of the posterior capsule region, demonstrating how the longitudinal and transverse curves were used to generate material coefficients from an average curve

3.3 FINITE ELEMENT MODEL DEVELOPMENT AND VALIDATION

3.3.1 Model Development

The subject-specific bone and soft-tissue geometry collected in Section 3.2.2, as well as the subject-specific material coefficients to an isotropic hyperelastic constitutive model collected in Section 3.2.4, were used to create a 3-dimensional, scale, subject-specific finite element model of the glenohumeral joint that treated the capsule as a composite sheet of ligamentous tissue. The capsule's glenoid insertion was then modified computationally to simulate the presence of the glenoid labrum. Subject-specific joint kinematics were computed using the positions of the humeral and scapular registration blocks in the reference position and clinically relevant joint positions, and used to prescribe motion of the joint to the clinically relevant positions where experimental strains were collected. At each of these clinically relevant joint positions the predicted strains were recorded in the model, and compared with the experimental strains for model validation.

3.3.1.1 Mesh Development

The surfaces created for the humerus, scapula, glenohumeral capsule, humeral head cartilage, and registration blocks created in Section 3.2.2.3 were converted into a form suitable for incorporation into TrueGrid, and then imported into TrueGrid. The triangulated surfaces of the humerus, scapula, humeral head cartilage, and registration blocks were converted to rigid body triangular shell elements [112, 116]. The 3-dimensional spline curves delineating the capsule regions and marking the capsule's glenoid and humeral insertions were then projected to the bursal surface of the capsule.

A 2-dimensional rectangular sheet of quadrilateral YASE shell elements [114] was then created, with four intermediate partitions running widthwise along the sheet. The choice of YASE shell elements was selected due to their accuracy during in-plane bending motions. The edges and partitions were manually moved within TrueGrid so that the 2-dimensional sheet of elements became a 3-dimensional, tube-like structure that surrounded the capsule, with the lengthwise edges running along the insertions of the capsule into the glenoid and humerus, and the widthwise edges and partitions running along the margins of the capsule regions. The two widthwise edges of the mesh were projected to the spline curve delineating the margin between the anterior band of the inferior glenohumeral ligament and the anterosuperior region, and the lengthwise edges of the mesh were projected to the spline curves representing the glenoid and humeral insertions. The four partitions were then projected to the spline curves on the capsule's bursal surface that delineated the four remaining margins of the capsule regions, after which the sheet of quadrilateral shell elements was projected to the capsule's bursal surface (Figure 3.15). Due to the curvature of the capsule and the distance between partitions of the sheet, TrueGrid at times projected the shell elements to the capsule's articular surface as opposed to the outer bursal surface. In order to account for this, additional widthwise partitions were added to the quadrilateral sheet of elements, and projected to the bursal surface before projecting the sheet of quadrilateral shell elements. This allowed for smaller regions of the sheet to be projected to the capsule at once, thus minimizing the projections to the articular surface.

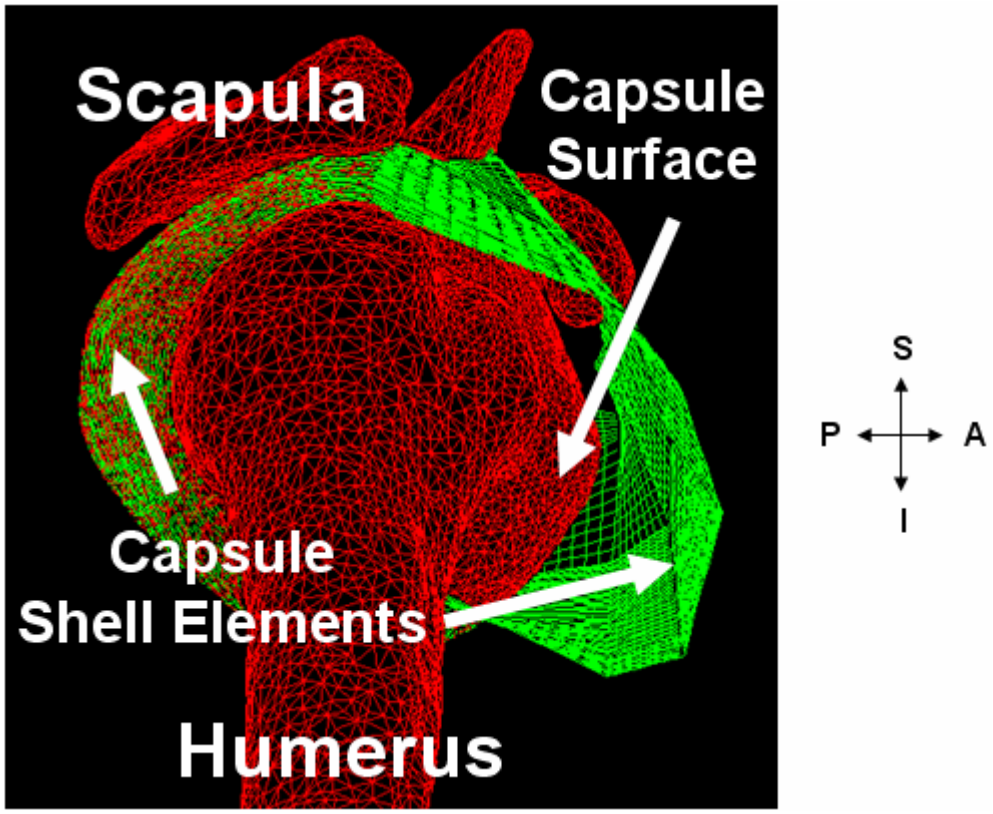

Figure 3.15 Lateral view of FE Model 2 (right shoulder), indicating the projection of the green mesh of capsule quadrilateral shell elements to the red surface of the capsule. The posterior half of the mesh has already been projected to the capsule surface. Also shown are the humeral and scapular surfaces in red

The quadrilateral shell element density within the capsule was assigned similar to FE Model 1 (Section 2.3.1.1). Specifically, the quadrilateral shell element mesh was created with a total of 80 nodes and 79 elements along the longitudinal direction of the capsule from the glenoid insertion to the humeral insertion, and with 144 nodes and 143 elements along the circumferential direction of the capsule. The distribution of elements within the capsule regions of FE Model 2 are provided in Table 3.1.

Table 3.1 Distribution of shell elements within the five capsule regions of FE Model 2

	Elements		
	Circumferential	**Glenoid-Humerus**	**Total**
AB-IGHL	11	79	869
Axillary Pouch	33	79	2607
PB-IGHL	11	79	869
Posterior	40	79	3160
Anterosuperior	48	79	3792
Total	143	395	11297

Within a capsule region, element dimensions were prescribed so that the elements were equally spaced from margin to margin, however from the glenoid insertion to the humeral insertion the spacing was unequal. When moving in a distal direction from the glenoid insertion to the mid-capsule, the element length was decreased so that each element was 96% the length of its proximal neighboring element. When continuing distally from the mid-capsule to the humeral insertion, the element length was decreased so that each element was 99% the length of its proximal neighboring element. Therefore, the capsule elements near the glenoid were greatest in length, and the capsule elements near the humerus were smallest in length. Preliminary work indicated that this element density was optimal for model convergence and accuracy of the predicted capsule strains. Lastly, the nodes at the widthwise edges of the mesh at the margin of the anterior band of the inferior glenohumeral ligament and the anterosuperior region were merged together, so that the quadrilateral shell element mesh was truly a continuous sheet of finite elements. Anterior, inferior, and posterior views of the mesh are provided in Figure 3.16.

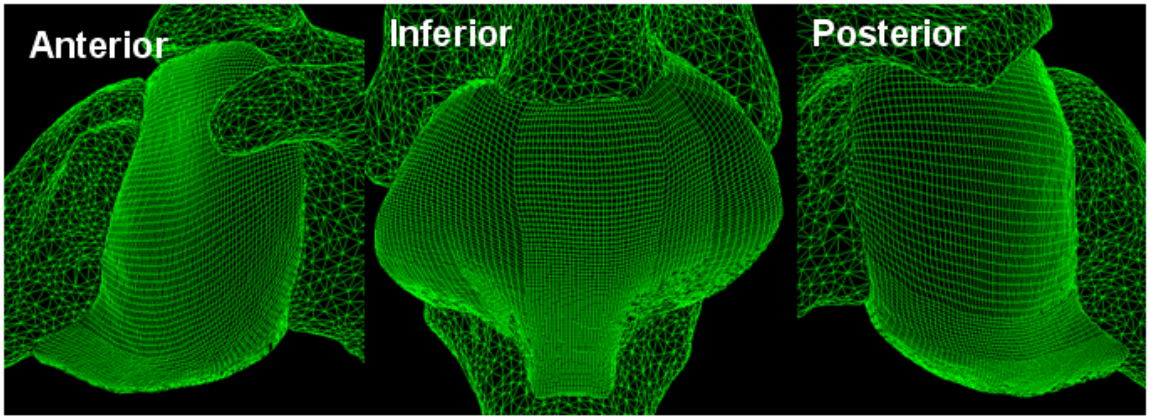

Figure 3.16 Anterior, inferior, and posterior views of FE Model 2 capsule mesh (right shoulder)

After generating the appropriate mesh density, elements within a capsule region were assigned material coefficients unique to that capsule region. Due to the inability of TrueGrid to generate a FEBio input deck using an isotropic hyperelastic constitutive model to represent the capsule, a NIKE3D input deck was generated that used an isotropic hypoelastic constitutive model to represent the capsule tissue. The finite element pre-processor PreView was then used to convert a NIKE3D input deck into a FEBio input deck (Section 3.3.3.3), at which point the material coefficients to the Veronda-Westmann isotropic hyperelastic constitutive model obtained in Section 3.2.4 were assigned to the appropriate capsule regions.

The thicknesses of the capsule regions were measured during the material testing procedure in Section 3.2.4.3, and are provided in Table 3.2. The quadrilateral shell elements were assigned a uniform capsule thickness that represented the average thickness in the capsule regions of the anterior-inferior capsule, rounded to the nearest 0.5 mm. Since the average thickness in the anterior and posterior bands of the inferior glenohumeral ligament and the axillary pouch was 2.8 mm, the capsule was assigned a uniform thickness of 3.0 mm.

Table 3.2 Capsule region thicknesses obtained experimentally in the cadaver for FE Model 2

Capsule Region	Thickness (mm)
AB-IGHL	2.8
Axillary Pouch	4.3
PB-IGHL	1.3
Anterosuperior	2.8
Posterior	1.5
Anterior-inferior capsule average	**2.8**

3.3.2 Insertion Site Modification

3.3.2.1 Preliminary Study

FE Model 1 did not initially contain a glenoid labrum, but rather modeled the capsule's glenoid insertion with the deformable capsule inserting directly into the rigid glenoid. Due to the difficulties encountered when trying to record experimental strain at the capsule's insertion site, validation could only be performed at the mid-substance of the capsule tissue where experimental strains were recorded. The model was validated using the non-linear finite element solver NIKE3D with an isotropic hypoelastic constitutive model, however irregular strain concentrations at the insertion site were predicted by the model. It can be seen in Figure 3.17 that maximum principal strains in the insertion site were above 60% strain, reaching as high as 87% strain in the axillary pouch's glenoid insertion.

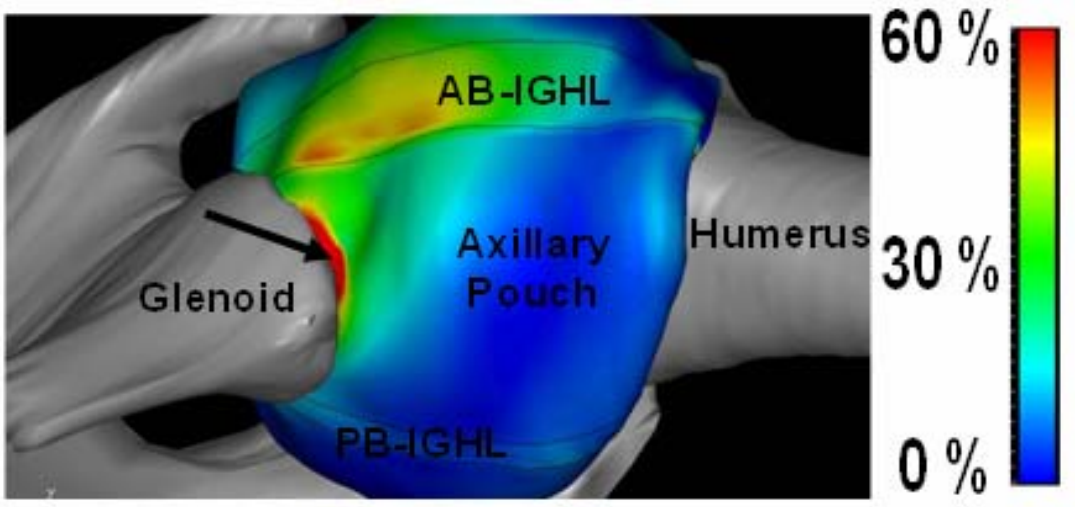

Figure 3.17 Inferior view of maximum principal strains in capsule of FE Model 1 (left shoulder) at 60° of abduction and maximum external rotation. Black arrow indicates irregular strain concentration at glenoid insertion of axillary pouch

Without experimental strain data for comparison the high strains at the insertion site could not be validated, however it was assumed that they were inaccurate. The strain magnitudes were well beyond previously published data for insertion site failure strains in the anterior-inferior capsule [32], and were further questionable since they occurred when the joint was placed in a clinically relevant joint position where injury does not occur.

The inaccuracies of the insertion site strains were cause for concern, in that they could have affected model validation. Since the capsule was modeled as a continuous sheet, high strains in one region may have had an affect on strains in neighboring regions, and model validation may have thus resulted from the inaccurate insertion site strains. The high strains were most likely due to the modeling of the insertion site with a deformable soft-tissue inserting directly into a rigid bone structure. This is physiologically inaccurate, however, as the insertion of the glenohumeral capsule into the glenoid contains a fibrocartilagenous transition from the ligamentous capsule to the osseous glenoid. An integral component of the capsule's glenoid insertion site is the glenoid labrum, a vascularized, pear-shaped ring of dense, predominantly

fibrous tissue that extends laterally from the articular cartilage of the glenoid and helps to stiffen the capsule's glenoid insertion [24, 42-48]. Furthermore, FE Model 1 experienced difficulty converging within the finite element solver when motions were simulated, which may have resulted from the lack of a transition in stiffness from the capsule to the glenoid. It was therefore decided to include the labrum into FE Model 1, to determine whether model validation was dependent on the incorrect modeling of the insertion site, to make the insertion site more physiologically accurate, and to aid in model convergence.

3.3.2.1.1 Labrum Inclusion

Consideration was initially given toward including the glenoid labrum into FE Model 1 as an anatomical structure, in addition to the humerus, scapula, capsule, and humeral head cartilage. Difficulties in identifying the labrum from the computed tomography images were encountered, however, as the fibrocartilagenous transition between capsule, labrum, and cartilage at the glenoid insertion site made identification of the separate soft-tissue structures challenging. In addition, adding another structure to the glenoid rim would have changed the geometric surface boundaries of the capsule near its glenoid insertion, thus preventing one-to-one comparisons of capsule strains before and after labrum inclusion. As a result, computational modification of the capsule shell element thickness and modulus at the glenoid insertion site was performed, which allowed for inclusion of a labrum and stiffening of the insertion without compromising the mid-substance surfaces.

In the preliminary study FE Model 1 was modified so that the collection of capsule elements inserting into the glenoid was redefined explicitly as labrum elements (Figure 3.18). Since there are five capsule regions, this allowed for creation of five new labrum regions. The insertion site was thus modeled with the capsule inserting directly into a labrum that was rigidly

fixed at its glenoid end, representing a common capsule-labrum interface that has been described previously [48]. The labrum elements were defined so that the labrum depth (dimension normal to the glenoid) was comparable to the 2 – 4 mm labrum depth reported by Howell and Galinat [42]. The labrum was assigned quadrilateral YASE shell elements similar to the capsule, and since the analyses were performed using the NIKE3D finite element solver, the isotropic hypoelastic constitutive model used to represent the capsule was also used to represent the labrum. The labrum elements were initially given the identical geometrical and material coefficient values of the capsule elements they replaced at the insertion site. Therefore, the labrum element radial thicknesses were a constant 2.0 mm throughout the labrum circumference, and the labrum element moduli were equivalent to the moduli of the neighboring capsule elements and thus not equivalent throughout the labrum circumference [132]. Specifically, the modulus of the labrum regions for the anterior band of the inferior glenohumeral ligament, posterior band of the inferior glenohumeral ligament, axillary pouch, anterosuperior, and posterior regions was 2.05, 3.73, 4.92, 2.12, and 5.83 MPa, respectively. This model was defined as the nominal model, and the modifications were such that the labrum and capsule strains were left unchanged relative to the original state of FE Model 1. Note that the nominal model essentially represents a joint without a labrum, as the labrum elements have geometrical and material properties of capsule tissue.

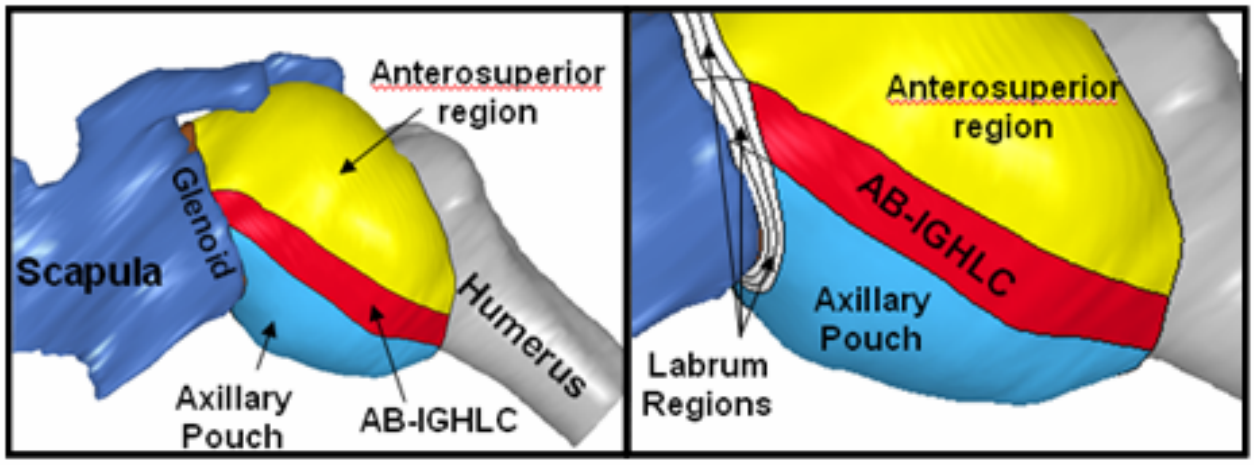

Figure 3.18 Left) Anterior view of FE Model 1 (left shoulder) Right) Newly added labrum regions

3.3.2.1.2 Sensitivity Study

A sensitivity study was designed in order to evaluate the effect that changes in labrum thickness and modulus had on the strains in both the insertion site and the mid-substance of the capsule, since increasing the labrum thickness and modulus will result in a stiffening of the elements and thus a change in strain. Results from the study could then be used to determine whether the high insertion site strains in FE Model 1 influenced model validation, as well as to determine the efficacy of including the labrum in finite element models of the glenohumeral joint as a computational modification of the capsule's insertion into the glenoid.

Physical measurements of the labrum thickness and modulus could not be taken from the labrum of the cadaver for FE Model 1, as the labrum was damaged during the excision of the capsule for material testing. In order to determine labrum thickness and modulus modifications for incorporation into the model, values were taken from the literature and from inspection of additional cadavers. Carey et al. [43] measured the radial thickness of six labrum specimens throughout their circumferences, reporting a thickness range of 2.4 – 11.2 mm. The inferior circumferential half of the labrum, however, had a thickness range of only 2.4 – 4.5 mm, and these values were given added consideration due to the overall objective of studying the anterior-

inferior capsule. Physical measurements were performed on selected cadavers with digital calipers, and it was found that the labrum thickness in the inferior circumferential half of the labrum ranged from 2.8 – 4.4 mm. It is worth noting that the cadavers examined and those in the referenced study were all over 49 years of age, thus labrum thicknesses in younger individuals may be greater due to the labrum thinning that occurs with age [133, 134]. In addition to thickness, the shape of the labrum was also examined. The labrum shape is not constant throughout its periphery, as it has been described as having radial cross-sections of both triangular and rounded appearance [24, 46]. Cadaveric inspection confirmed these descriptions, however it was determined that regardless of the shape, the radial thickness of the labrum decreased when moving laterally out of the glenoid. Thus it was decided that the labrum thickness modifications would include a linear taper from a maximum radial thickness at the interface of the labrum with the glenoid rim to a minimum radial thickness of 2.0 mm at the interface of the labrum with the capsule, giving the labrum a wedge-shaped radial cross-section. Two thickness models were created for analysis with the nominal model, containing a linear radial thickness taper of 4.0 mm (T_4mm model) and 6.0 mm (T_6mm model), respectively, down to the capsule thickness of 2.0 mm.

The labrum tensile modulus has been shown to vary throughout its circumference in animals [132], and it was decided that the labrum modulus would be varied with respect to the corresponding capsule region modulus. Smith et al. [135] reported the average human labrum tensile modulus to be 22.8 MPa, which is approximately five times higher than the average of the capsule region moduli in the model. The average acetabular labrum tensile modulus has been reported as 66.4 MPa [136], which may be an overestimate of the glenoid labrum tensile modulus since the hip is a weight-bearing joint. The labrum compressive properties have been

reported as similar to those of the meniscus [43, 137], a tissue with histological similarity to the labrum [24]. Based on the values discussed above and meniscal modulus data reported in the literature [138-140], two modulus modification models were created for analysis with the nominal model, with the labrum modulus two times (M_2X model) or five times (M_5X model) higher, respectively, than the modulus of the corresponding capsule region.

To evaluate the effects of labrum thickness modification the T_6mm, T_4mm, and nominal models were subjected to the kinematics of a physical examination for anterior instability, i.e. a 25 N anterior load applied at 60° of abduction and 60°/maximum external rotation. In each model, Green-Lagrange maximum principal strains were calculated at the nodes in labrum region elements of the anterior band of the inferior glenohumeral ligament, the axillary pouch, and the posterior band of the inferior glenohumeral ligament. Average nodal strains were also calculated in pre-defined elements of the mid-substance of the anterior band of the inferior glenohumeral ligament used for validation. The nodal strains were then averaged within each labrum region and among the capsule elements for analysis, in each model. Friedman tests were used to determine statistically significant strain differences ($p<0.05$) between a given labrum region or the capsule in the three thickness modification models, and Wilcoxon Signed Rank Tests with a Bonferroni correction were used for post-hoc pairwise comparisons ($p<0.017$). SPSS (Apache Software, 2000) was used for all analyses. Significant pairwise differences in strain (*) were qualified *a priori* with the requirement that they be statistically significant, but also greater than the previously determined experimental strain repeatability of ±3.5% strain.

To evaluate the effects of labrum modulus modification the M_5X, M_2X, and nominal models were then subjected to the same kinematics for the physical examination for anterior

instability. The methods for computation of strains and the statistical analyses used with the labrum thickness analyses were repeated with the labrum modulus analyses, so that the effect of labrum modulus modification could also be determined in the labrum regions and anterior-inferior capsule.

3.3.2.1.3 Sensitivity Study: Results

Strain increased in the labrum regions as the labrum thickness was decreased, however capsule strain decreased only as the labrum thickness was decreased from the T_6mm model to the nominal model (Figure 3.19). As the labrum thickness taper was decreased from the T_6mm model to the T_4mm model to the nominal model, strain significantly increased in the labrum regions of the anterior band of the inferior glenohumeral ligament (12.3% to 16.1% to 23.6% strain) and axillary pouch (16.2% to 20.1% to 30.6% strain). Significant changes in strain occurred in all regions when comparing the T_6mm model to the nominal model, as strains increased in the labrum region of the posterior band of the inferior glenohumeral ligament (8.4% to 12.3% strain) and decreased in the capsule (26.2% to 22.7% strain). The greatest changes occurred in the labrum regions of the anterior band of the inferior glenohumeral ligament and axillary pouch as the labrum thickness taper was decreased from the T_4mm model to the nominal model (an increase of 7.5% and 10.5% strain, respectively).

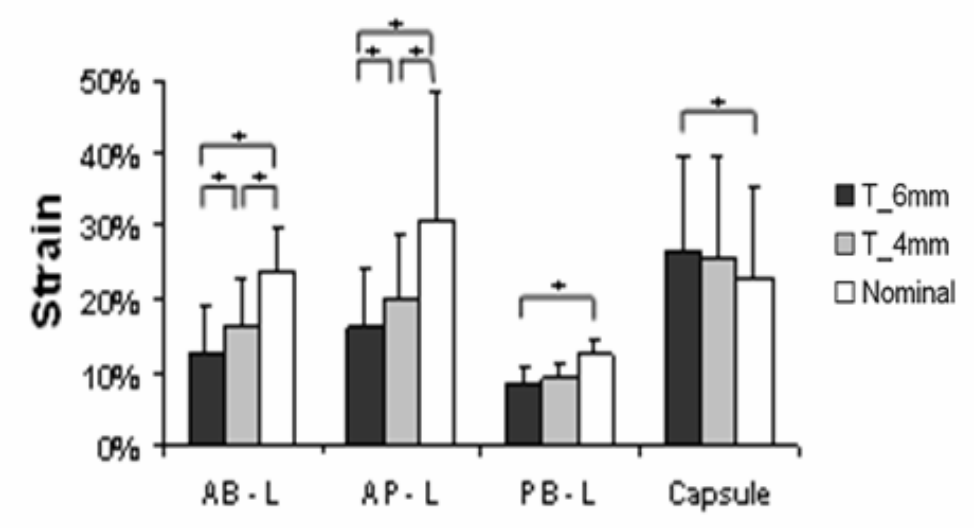

Figure 3.19 Labrum thickness modification comparisons. AB-L, AP-L, PB-L = labrum regions of the anterior band of the inferior glenohumeral ligament, the axillary pouch, and the posterior band of the inferior glenohumeral ligament. Capsule = mid-substance elements of the anterior band of the inferior glenohumeral ligament used for validation

Strain increased in the labrum regions and decreased in the capsule as the labrum modulus was decreased (Figure 3.20). As the labrum modulus was decreased from the M_5X model to the M_2X model, strain significantly increased in the labrum regions of the anterior band of the inferior glenohumeral ligament (6.6% to 13.3% strain) and axillary pouch (8.2% to 15.1% strain). As the labrum modulus was further decreased to that of the nominal model, strain significantly increased in the labrum regions of the anterior band of the inferior glenohumeral ligament (13.3% to 23.6% strain), axillary pouch (15.1% to 30.6% strain) and the posterior band of the inferior glenohumeral ligament (7.7% to 12.3% strain), and significantly decreased in the capsule (26.5% to 22.7% strain). Significant changes in strain occurred in all regions when comparing the M_5X model to the nominal model, as strain increased in the posterior band of the inferior glenohumeral ligament (4.4% to 12.3% strain) and decreased in the capsule (28.0% to 22.7% strain). The greatest changes in strain occurred in the labrum regions of the anterior band of the inferior glenohumeral ligament and axillary pouch as the modulus was

decreased from the M_2X model to the nominal model (an increase of 10.4% and 15.5%, respectively strain).

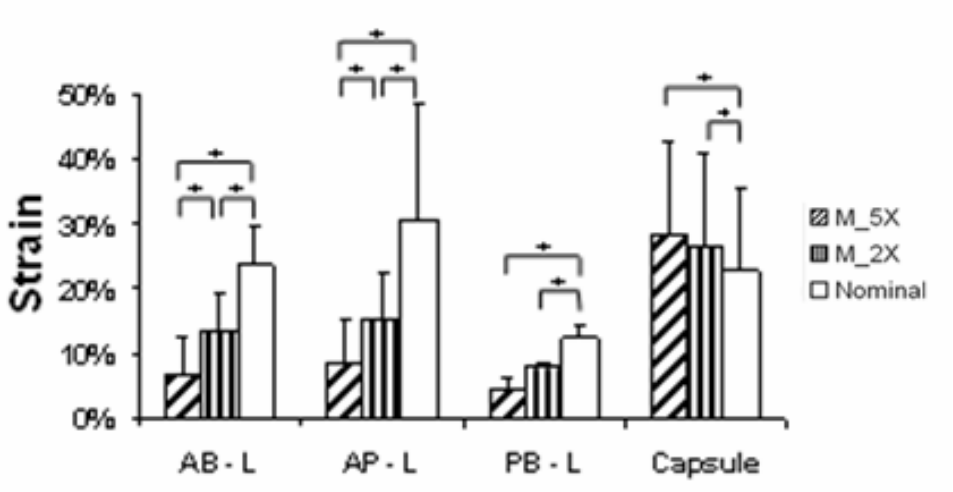

Figure 3.20 Labrum modulus modification comparisons. AB-L, AP-L, PB-L = labrum regions of the anterior band of the inferior glenohumeral ligament, the axillary pouch, and the posterior band of the inferior glenohumeral ligament. Capsule = mid-substance elements of the anterior band of the inferior glenohumeral ligament used for validation

The results of the labrum thickness analyses suggested that increases in labrum thickness to 4.0 mm or less from the initial thickness of 2.0 mm resulted in decreased insertion site strain without an increase in capsule strain. Increases in labrum thickness above 4mm, however, resulted in significant increases in capsule strain. The results of the labrum modulus analyses suggested that increases in labrum modulus of a factor of two relative to the initial modulus resulted in decreased insertion site strains, however with significant increases in capsule strains.

Since the T_4mm model significantly lowered insertion site strains without significantly increasing capsule strains, it was decided that the high insertion site strains in the initial state of FE Model 1 were not affecting model validation. To make the models more physiologically correct and to aid in model convergence, it was therefore decided to simulate the presence of a glenoid labrum in FE Model 1 and additional finite element models of the glenohumeral joint by increasing the thickness at the capsule's glenoid insertion.

3.3.2.2 Labrum Inclusion in FE Model 2

The mesh of quadrilateral capsule shell elements created in Section 3.3.1.1 was then modified to simulate inclusion of the glenoid labrum. The three circumferential columns of elements at the capsule's glenoid insertion were selected in TrueGrid and divided into five sections based on capsule region for a total of fifteen labrum regions. The elements within each labrum region were recorded. After generating a finite element input deck, the elements of a given labrum region were located within the input deck and the nodal thicknesses were modified so that a linear thickness taper was created in the labrum from the nodes at the interface of the labrum with the glenoid to the nodes at the interface of the labrum with the capsule regions. The exact values used in the labrum thickness taper are subject-specific and dependent upon experimental measurements of labrum and capsule thickness. However, the sensitivity study in Section 3.3.2.1 using FE Model 1 demonstrated that the labrum thickness taper for a joint with a capsule thickness of 2.0 mm should be approximately 3.0 – 4.0 mm at the interface of the labrum with the glenoid down to 2.0 mm at the interface of the labrum with the capsule.

In the cadaver for FE Model 2, the labrum was much thicker than in the previously measured cadavers and from published data [43], with physical measurements taken with the cadaver reporting an average labrum thickness of 7.6 mm in the anterior-inferior capsule. The capsule thickness of 3.0 mm for FE Model 2 (Section 3.3.1.1) was also thicker than the capsule thickness of 2.0 mm for FE Model 1. Preliminary work with FE Model 2 showed that using a labrum thickness taper from greater than 6.0 mm at the interface of the labrum with the glenoid down to 3.0 mm at the interface of the labrum with the capsule resulted in labrum element inversion and an inability to achieve model convergence. Therefore, a linear labrum thickness taper from 6.0 mm at the interface of the labrum with the glenoid down to 3.0 mm at the interface of the labrum with the capsule was prescribed.

3.3.3 Finite Element Solution Procedure

3.3.3.1 Joint Kinematics

In Section 3.2.3.2, three orthogonal faces on both the humeral and scapular registration blocks were digitized with the joint in its clinically relevant joint position. A plane-fitting procedure was used to create local coordinate systems for the humeral and scapular registration blocks with respect to the global coordinate system of the 3D Microscribe digitizer in the clinically relevant joint positions, after which the transformation matrix of the humeral registration block with respect to the scapular registration block was calculated.

The surfaces of the humeral and scapular registration blocks generated from the CT dataset with the joint in its reference position were input into TrueGrid. In order to prescribe motion of the humeral registration block with respect to the scapular registration block (and thus the humerus with respect to the scapula) within the model from the reference position to the clinically relevant joint positions, the registration blocks needed to be "digitized" within TrueGrid while the joint was in its reference position. This was performed by first selecting nodes on the equivalent orthogonal faces of the registration blocks within TrueGrid, and outputting the 3-dimensional nodal coordinates to a text file. The same plane-fitting procedure was then used to create local coordinate systems of the humeral and scapular registration blocks with respect to the global coordinate system of TrueGrid. All of the surfaces were then translated and rotated such that the humeral registration block coordinate system was aligned with the global coordinate system of TrueGrid. In addition, the transformation matrix of the humeral registration block with respect to the scapular registration block was calculated with the joint in its reference position.

Using the transformation matrices of the humeral registration block with respect to the scapular registration block in both the reference position and the clinically relevant joint positions, the relative motions of the humeral registration block with respect to the scapular registration block from the reference position to the clinically relevant joint positions were computed [141] (Figure 3.21). These motions were then incorporated into the finite element model with a method described by Simo and Qu-Voc [142], whereby transformation matrices are converted into quaternions that act as "load curves" [102]. Since the registration blocks were fixed rigidly to the bones, the load curves could be assigned to the humerus to prescribe motion of the humerus with respect to the scapula from the reference position to the clinically relevant joint positions.

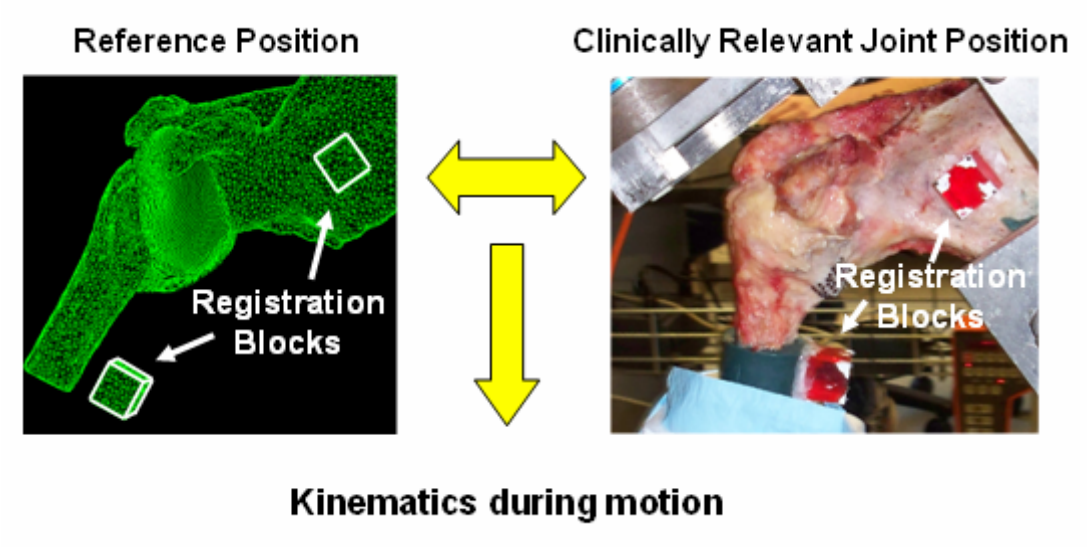

Figure 3.21 Overview of the process to obtain joint kinematics. Registration blocks were digitized in the reference position and in the clinically relevant joint positions, and the joint kinematics were obtained by computing relative motion of the registration blocks from the reference position to the clinically relevant joint positions

3.3.3.2 Boundary Conditions

The nodes of the mesh at the interface with the glenoid and the humerus were then prescribed to move with the bones. When the joint was positioned in its clinically relevant joint positions,

contact occurred between the capsule and the humeral head cartilage, as well as between the capsule and the humerus. No contact was observed between the capsule regions and the glenoid, therefore no contact was prescribed. Thus, for the humerus, a frictionless sliding surface was defined and contact was enforced using the penalty method [102-104].

3.3.3.3 Finite Element Solution Procedure

The non-linear finite element solver FEBio was used for all analyses. TrueGrid did not have the capability to produce an input deck for FEBio, however it could create an input deck for the non-linear finite element solver NIKE3D. The finite element pre-processor PreView could then be used to convert a NIKE3D input deck into a FEBio input deck. Therefore, a NIKE3D input deck was outputted by TrueGrid, using an isotropic hypoelastic constitutive model to represent the capsule and labrum elements (Appendix B). This input deck was then imported into PreView, and converted to a FEBio input deck (Appendix C). The capsule regions and corresponding labrum regions were assigned the material coefficients to the Veronda-Westmann isotropic hyperelastic constitutive model obtained in Section 3.2.4.4. A sliding interface contact was prescribed between the humeral head cartilage and the articular surface of the capsule, with the humeral head cartilage as the master and the capsule as the slave. Specifically, the interface was assigned a tolerance value of 0.1 and a penalty value of 0.5, based on the successful convergence of FE Model 1 with these values (Section 5.1.2).

The motion of the humerus from the reference position to each of the clinically relevant joint positions was then simulated using FEBio. An incremental-iterative solution strategy was employed, with iterations based on a quasi-Newton method [115] and convergence based on the L_2 displacement and energy norms [116]. The motions of the humerus with respect to the scapula were applied incrementally over quasi-time with the time step size being adjusted via an

automatic procedure. Run time was approximately 30 minutes for each clinically relevant joint position.

3.3.4 Model Validation

3.3.4.1 Predicted Strain Distribution

After full convergence of the finite element solution procedure, the results were visualized within the finite element post-processor LSPost (Livermore Software Technology Corporation, Livermore, CA). The 3-dimensional coordinate positions of the capsule strain markers segmented with the joint in its reference position in Section 3.2.2.3 were incorporated into LSPost as discrete points in space, for identification of the experimental strain elements. Since all surfaces in LSPost had been previously shifted by the relationship of the humeral registration block with respect to the global coordinate system of TrueGrid, the coordinates of the points were similarly transformed before being visualized within LSPost. This allowed for the visualization of the points on the surface of the capsule that represented the locations of the 7 x 11 grid of capsule strain markers with the joint in its reference position. In Section 3.2.3.3 the 7 x 11 grid of capsule strain markers was used to identify a 6 x 10 arrangement of quadrilateral elements on the surface of the capsule, in which strains were reported for each element. For notation purposes, these elements will be referred to as validation elements. The points representing the capsule strain markers within LSPost were similarly used to identify corresponding validation elements in the anterior-inferior capsule of FE Model 2. Since each validation element within FE Model 2 was composed of multiple quadrilateral shell elements, the quadrilateral shell elements that fell within a validation element were grouped together for

analysis (Figure 3.22). Typically, each validation element was composed of approximately 10-20 shell elements.

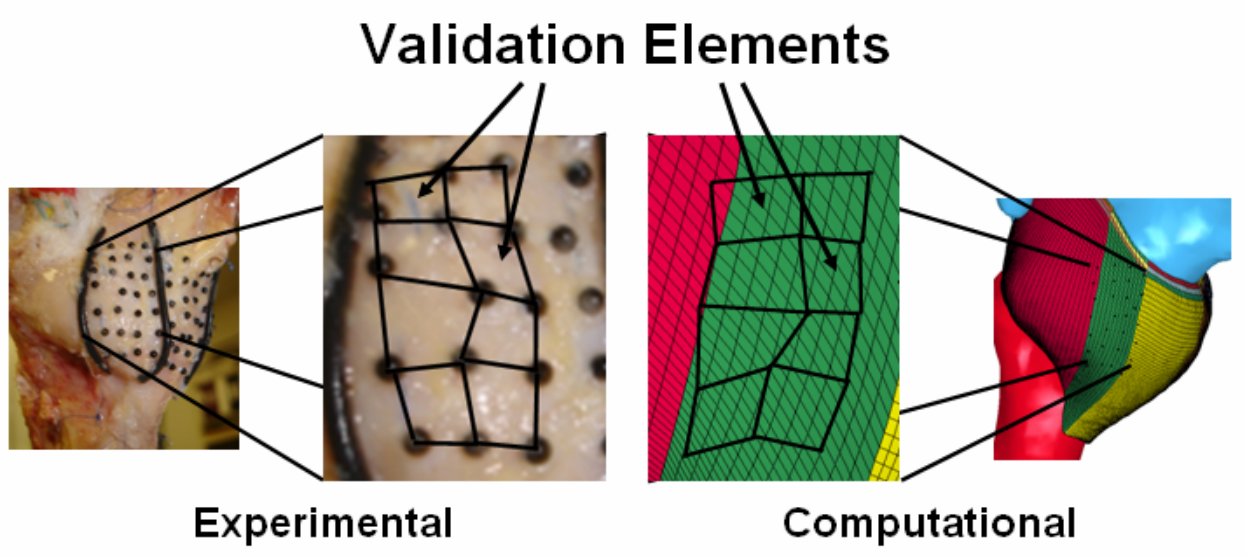

Figure 3.22 Anterior-inferior views of experimental and computational validation elements for FE Model 2 (right shoulder), determined from the positions of the capsule strain markers

Green-Lagrange maximum principal strains were computed at the nodes in each quadrilateral shell element in FE Model 2, and averaged within the validation elements to generate the predicted strains.

3.3.4.2 Finite Element Model Validation

Validation of subject-specific finite element models is performed by comparing the surface strains predicted by the computational model with those obtained experimentally. Since there are 60 validation elements formed from the 7 x 11 grid of capsule strain markers, a total of 60 element-by-element comparisons can be made between the predicted and experimental strains. However, regions of the anterior-inferior capsule whose experimental strains measured at or below the experimental strain repeatability in any of the three clinically relevant joint positions were excluded from the analyses, since meaningful comparisons of predicted and experimental

strains would be unable to be performed Specifically, the repeatability of the entire procedure to obtain experimental strains was previously determined to be ± 3.5% strain [41]. This additional criterion significantly lowered the number of available elements for validation. It was found that only the anterior band of the inferior glenohumeral ligament had validation elements with strains that were above the experimental strain repeatability at each of the three positions. Therefore, only these validation elements were used for validation of FE Model 2.

The criteria for validation is that the average difference between the predicted and experimental strains in the validation elements of the anterior band of the inferior glenohumeral ligament was less than the experimental strain repeatability of ±3.5% strain. In addition, the predicted shape of the capsule tissue in each clinically relevant joint position was compared to the experimental shape to further validate the predictive capabilities of FE Model 2.

4.0 ANALYSIS OF JOINT POSITIONS

4.1 INTRODUCTION

In order to use the validated, subject-specific finite element models to predict the clinically relevant joint positions in which the distribution of strain in the anterior-inferior capsule is consistent among subjects in response to anterior loading, the distribution of strain in the capsule needed to be evaluated in clinically relevant joint positions involving application of anterior load at abduction and multiple external rotation angles. Specific Aim 2 established that the distribution of strain in the anterior-inferior capsule would be measured when a 25 N anterior load was applied to the joint at 60° of glenohumeral abduction and at external rotation angles from 0° to 60°/maximum external rotation, in 10° increments. The clinically relevant joint positions with 0°, 30°, and 60°/maximum external rotation were experimentally obtained and used for model validation, however the intermediate clinically relevant joint positions with external rotation angles of 10°, 20°, 40°, etc, were not obtained experimentally.

The finite element models provide a means for simulating motion of the glenohumeral joint from the reference position to the intermediate clinically relevant joint positions. Anatomical coordinate systems of the humerus and scapula with respect to the global coordinate system of TrueGrid were created in both FE Model 1 and FE Model 2. In each model, rotations and translations of the humeral anatomical coordinate system with respect to the scapular anatomical coordinate system were computed that moved the joint to the desired intermediate

clinically relevant joint positions. These motions were then transformed to motions of the humeral registration block with respect to the scapular registration block, so that load curves could be computed that moved the humerus from the reference position to the intermediate clinically relevant joint positions. This methodology allows for evaluation of the distribution of strain in the capsule in an infinite number of joint positions, and was used to evaluate the distribution of strain in the anterior-inferior capsule when an anterior load was applied to the abducted joint throughout the range of external rotation.

Once all clinically relevant joint positions resulting from application of a 25 N anterior load at 60° of glenohumeral abduction and 0° to maximum external rotation in 10° increments were identified for both FE Model 1 and FE Model 2, the motions from the reference position to the clinically relevant joint positions were simulated using the finite element solver. Predicted strains in the anterior-inferior capsule were then computed in each model. When validating FE Model 1 and FE Model 2 in Section 2.3.4 and Section 3.3.4, respectively, only the predicted and experimental strains in the anterior band of the inferior glenohumeral ligament were used. To answer the research question and achieve the specific aims of the proposed work, however, the distribution of strain throughout the entire anterior-inferior capsule needed to be evaluated. Both previous work examining the stability provided by the capsule in clinically relevant joint positions and clinical outcomes following anterior dislocation suggest that the distribution of load throughout the anterior-inferior capsule may be localized to the glenoid side of the capsule tissue during joint positions associated with anterior instability [21, 52, 53, 55, 96]. These data suggest the need to localize evaluations of the distribution of strain in the anterior-inferior capsule to the glenoid and humeral sides of the anterior-inferior capsule.

Furthermore, previously published data suggests that the distribution of load within the anterior-inferior capsule may be localized to certain regions of the anterior-inferior capsule. Bigliani et al. [32] measured capsule strains at failure in response to uniaxial tensile tests to isolated bone-capsule region-bone complexes of the anterior-inferior capsule. The authors found significant differences in failure strains among the three regions, as well as region-specific capsule thicknesses, suggesting that the three regions of the anterior-inferior capsule may have different roles in providing stability to the joint. This conclusion is further supported by the work of Itoi et al. [34] and Ticker et al. [100], who reported that significant differences in tensile properties occurred throughout the regions of the capsule. The results of these studies demonstrate the need to compute the strains within each region of the anterior-inferior capsule.

In light of the aforementioned studies suggesting that the distribution of load in the anterior-inferior capsule may be localized to the glenoid and humeral sides of the anterior-inferior capsule as well as within the different regions of the anterior-inferior capsule, the distribution of strain in the anterior-inferior capsule in the current work was evaluated by dividing the anterior-inferior capsule into glenoid and humeral sides of the anterior and posterior bands of the inferior glenohumeral ligament and the axillary pouch. Evaluations were then performed using the strains in these six newly created “sub-regions”.

Once computed, strains in the sub-regions were used to determine joint positions with consistent distribution of strain and thus consistent distribution of load among subjects. Moore et al. [21] computed the distribution of strain in the anterior-inferior capsule in multiple subjects at three clinically relevant joint positions. The authors found high variability in capsule strain magnitudes among subjects at each joint position, suggesting that capsule strain magnitudes are subject-specific at joint positions where the capsule is providing stability to the joint. Therefore,

comparing strain magnitudes in the capsule regions among different models may not be appropriate. However, the data presented by the authors suggests that there are similar patterns in the distribution of strain in the anterior-inferior capsule among subjects, as strains became highest in the glenoid side of the anterior band of the inferior glenohumeral ligament and the axillary pouch in each specimen. Furthermore, previous work using a subject-specific finite element model indicated that the strains in the anterior-inferior capsule are highest in the glenoid side of the anterior band of the inferior glenohumeral ligament at joint positions with increasing external rotation [55]. Therefore, for each model the highest sub-region strain among all clinically relevant joint positions was identified. The strains in each sub-region at each clinically relevant joint position were then normalized to this value. Comparisons were then made between FE Model 1 and FE Model 2 to suggest clinically relevant joint positions where the distribution of strain and thus distribution of load in the anterior-inferior capsule is most consistent among patients. Analyses were then performed at these positions to determine if strain in a sub-region was higher than strains in the other sub-regions, in order to localize the stability provided by the anterior-inferior capsule at the clinically relevant joint positions with consistent distribution of load among subjects.

4.2 KINEMATICS FOR INTERMEDIATE JOINT POSITIONS

4.2.1 Development of Anatomical Coordinate Systems

The anatomical coordinate systems were defined within each finite element model when the joint was in its reference position, in a manner consistent with the coordinate systems defined on the robotic/UFS testing system [10, 11, 118] (Section 3.2.3.1). In Section 3.2.1.1, the scapular

anatomical coordinate system was defined using the block of epoxy putty in which the scapula was potted, so that the anterior/posterior axis was approximated as being perpendicular to the scapular plane, the superior/inferior axis was approximated by the medial border, and the medial/lateral axis was orthogonal to the anterior/posterior and superior/inferior axes. The humeral anatomical coordinate system was defined using the cylinder of epoxy putty in which the humeral shaft was potted, so that the axis of internal/external rotation was parallel to the humeral shaft. The origin of the scapular and humeral coordinate systems was marked as the midpoint between the most anterior aspect of the lesser tuberosity and the most posterior aspect of the humeral ridge.

4.2.1.1 Scapular Anatomical Coordinate System

The joint was placed in the reference position within TrueGrid. Due to the difficulties in segmenting the scapular epoxy putty in the CT images, an attempt was made in Section 3.2.1.2 to fix the scapular registration block to the scapula so that the anterior, medial, and superior faces of the registration block were parallel to the anterior, medial, and superior faces of the scapular epoxy putty, respectively. This was done so that the three orthogonal faces of the scapular registration block, which could easily be visualized in the CT images, could be used to approximate the scapular anatomical coordinate system. Furthermore, this method would allow for use of the coordinate system of the scapular registration block with respect to the global coordinate system of TrueGrid (Section 3.3.3.1) as the scapular anatomical coordinate system with respect to the global coordinate system of TrueGrid.

The medial face of the scapular registration block was determined to be parallel to the medial face of the epoxy putty, thus a unit vector normal to the medial face of the scapular registration block was created for the medial/lateral axis of the scapular anatomical coordinate

system (Figure 4.1). This was performed by determining the 3-dimensional coordinates of nodes in the global coordinate system of TrueGrid on the medial face of the scapular registration block, generating two vectors in the plane of the medial face using these coordinates, and computing the normalized cross-product of the two vectors.

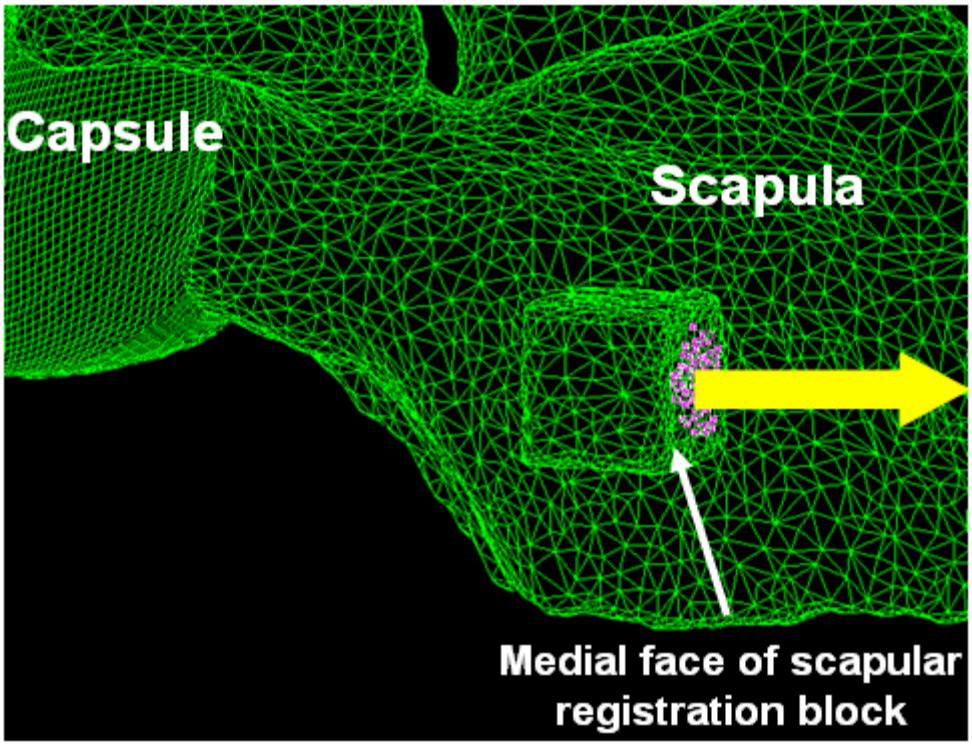

Figure 4.1 Anterior-medial view of FE Model 2 (right shoulder). Yellow arrow indicates medial axis of anatomical coordinate system, determined from the coordinates of the nodes on the medial face of the scapular registration block

Topological variations in the plane of the scapula made alignment of the anterior and superior faces of the scapular registration block and epoxy putty difficult. Therefore, means were needed to define the remaining axes of the scapular anatomical coordinate system. For the anterior/posterior axis, a region of nodes on the surface of the scapula was identified that collectively formed a plane parallel to the scapular plane. A unit normal vector of the plane was

then computed using the 3-dimensional coordinates of the nodes to generate two vectors in the scapular plane, and computing the normalized cross-product of two vectors Figure 4.2.

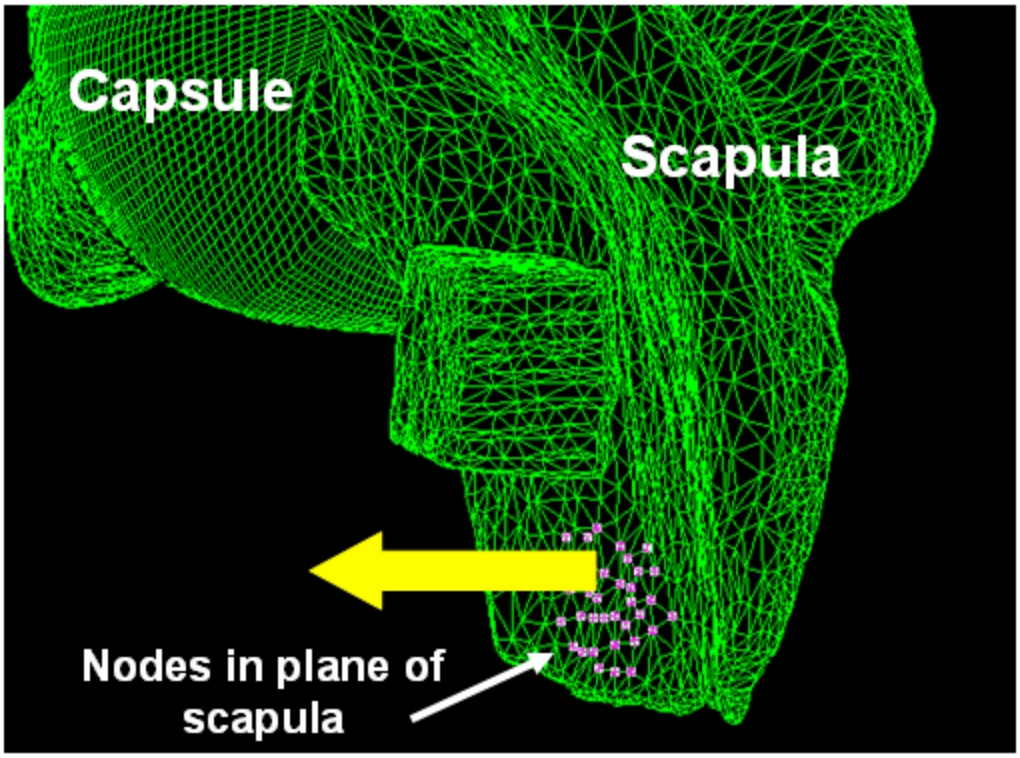

Figure 4.2 Medial view of FE Model 2 (right shoulder). Yellow arrow indicates anterior axis of anatomical coordinate system, determined from the coordinates of the nodes located in the plane of the scapula

The unit normal vectors of the medial and anterior axes were then used to create an orthonormal coordinate system of the scapula with respect to the global coordinate system of TrueGrid.

To determine the origin of the scapular anatomical coordinate system, groups of nodes were identified on the most anterior aspect of the lesser tuberosity and the most posterior aspect of the humeral ridge (Figure 4.3). The 3-dimensional coordinates of the nodes were then obtained for each group, and averaged at both locations to produce one point at each location. The coordinates of these two points were then averaged together, providing the midpoint of the

most anterior aspect of the lesser tuberosity and the most posterior aspect of the humeral ridge. The coordinates at the midpoint were used as the origin of the scapular anatomical coordinate system.

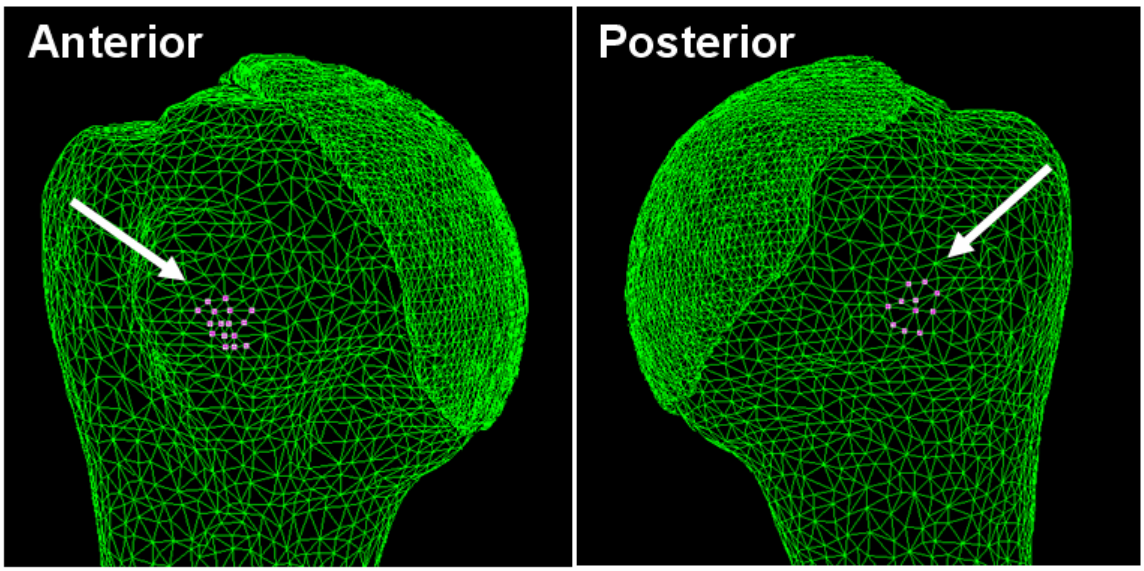

Figure 4.3 Nodes approximating the most anterior aspect of the lesser tuberosity (Anterior side) and most posterior aspect of the humeral ridge (Posterior side)

4.2.1.2 Humeral Anatomical Coordinate System

With the joint still in its reference position in TrueGrid, a vector representing the longitudinal axis of the humeral shaft was created. A circumferential ring of nodes was digitized on the surface of the humeral shaft at two separate locations along the shaft, approximately 5 cm apart. The coordinates of the nodes were then obtained, and averaged for each ring to obtain coordinates of two points at the center of the humeral shaft. The vector connecting these two points was then obtained, and used as the longitudinal axis of the humerus for internal/external rotation (Figure 4.4).

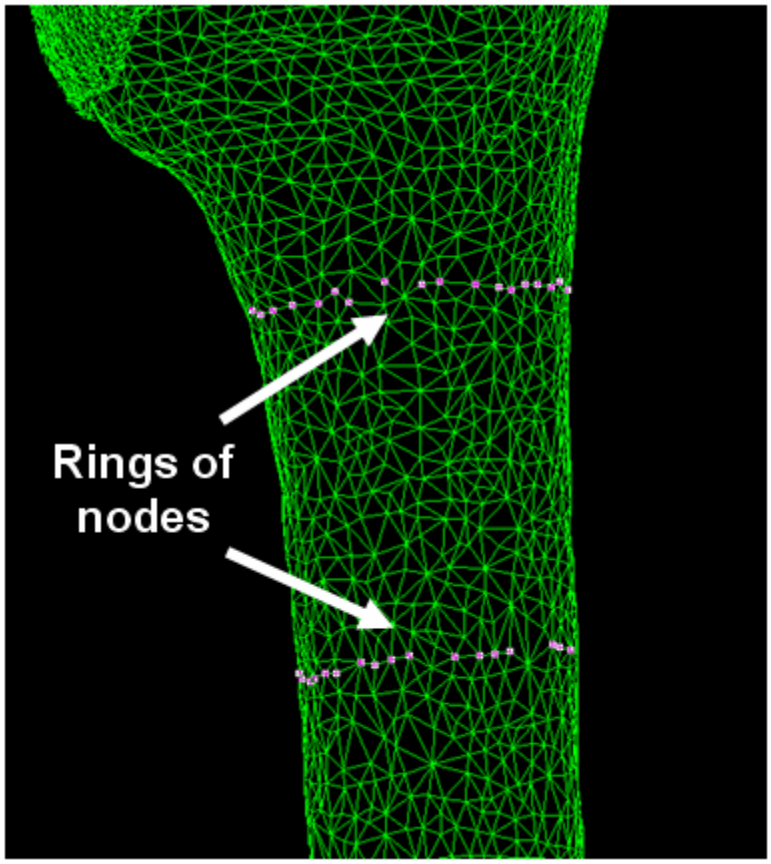

Figure 4.4 Posterior view of humerus (right shoulder) with circumferential rings of nodes identified, for use in determining the humeral axis of internal/external rotation

The coordinates at the points of the most anterior aspect of the lesser tuberosity and the most posterior aspect of the humeral ridge were used to create a vector joining the two locations, that approximated the anterior/posterior axis of the humeral anatomical coordinate system. This vector was then used with the vector of the axis of internal/external rotation to define an orthonormal humeral anatomical coordinate system with respect to the global coordinate system of TrueGrid. The origin of this coordinate system was defined as in Section 4.2.1.1, so that the scapular and humeral anatomical coordinate systems shared the same origin with the joint in its reference position.

4.2.2 Joint Motions Using Anatomical Coordinate Systems

In order to simulate motion of the joint from the reference position to the intermediate clinically relevant joint positions, the humerus needed to be rotated and translated within the finite element model. A custom code was developed within Matlab® (version 7.0.1, The MathWorks, Inc., Natick MA) that allowed for rotation of the humeral anatomical coordinate system about the axes of the scapular anatomical coordinate system as well as about the axis of rotation of the humerus (Appendix D). A total of three glenohumeral joint rotations could be simulated: 1) abduction about the anterior/posterior scapular axis, 2) flexion about the medial/lateral scapular axis, and 3) internal/external rotation about the longitudinal axis of rotation. Additionally, the custom code allowed for translation of the humerus with respect to the scapular anatomical coordinate system, so that 6-degree-of-freedom glenohumeral motion could be simulated similar to the experimental setup with the robotic manipulator. Since the joint was initially in its reference position, the initial glenohumeral abduction angle was offset to 60° and the initial external rotation angle was offset to the value determined in Section 3.2.1.4.

Once the desired rotations and translations of the intermediate clinically relevant joint positions were input into the code, the newly computed position of the humeral anatomical coordinate system with respect to the scapular anatomical coordinate system was transformed into the position of the humeral registration block with respect to the global coordinate system of TrueGrid. The motion of the humeral registration block from the reference position to the intermediate clinically relevant joint positions were then determined as in Section 3.3.3.1, so that load curves could be created that would move the model from the reference position to the intermediate clinically relevant joint positions.

4.2.3 Rotations and Translations for Intermediate Joint Positions

The rotations for the intermediate clinically relevant joint positions were defined as glenohumeral abduction of 60° and external rotation in 10° increments, i.e. 10°, 20°, 40°, etc. up to the maximum external rotation angle. Motion to the intermediate clinically relevant joint positions, however, required application of a 25 N anterior load after abduction and external rotation of the joint. Motion within the finite element models is driven by prescribing displacements and not by applying loads, therefore translations approximating those that would result from application of a 25 N load were needed to simulate full motion from the reference position to the intermediate clinically relevant joint positions.

Therefore, the translations at the intermediate clinically relevant joint positions were approximated by the translations resulting from application of a 25 N anterior load at the clinically relevant joint positions with 0°, 30°, and 60°/maximum external rotation. This required the transformation of the joint motion to the clinically relevant joint positions with 0°, 30°, and 60°/maximum external rotation (Section 3.3.3.1) into the anatomical coordinate systems defined within the finite element model. The Matlab code developed in Section 4.2.2 used inputs of abduction angle, external rotation angle, and humeral translation with respect to the scapular anatomical coordinate system to output motion of the humeral registration block from the reference position to a clinically relevant joint position. The code was modified so that inputs of abduction angle, external rotation angle, and motion of the humeral registration block from the reference position to a clinically relevant joint position could be used to output humeral translation with respect to the scapular anatomical coordinate system that resulted from application of the 25 N anterior load.

For each of the clinically relevant joint positions with 0°, 30°, and 60°/maximum external rotation, an abduction angle of 60°, external rotations of 0°, 30°, or 60°/maximum external rotation, respectively, and the motion of the humeral registration block from the reference position to the clinically relevant joint position obtained in Section 3.3.3.1 were input into the Matlab code. The output was the motion of the humerus with respect to the scapular anatomical coordinate system, which corresponded to the translation resulting from application of a 25 N anterior load.

The translations of the humerus with respect to the scapular anatomical coordinate system at the intermediate clinically relevant joint positions were then approximated by the translations of the humerus with respect to the scapular anatomical coordinate system at the clinically relevant joint positions with 0°, 30°, and 60°/maximum external rotation, through linear interpolation. This methodology operates under the assumption that a linear relationship exists between external rotation angle and humeral translation resulting from application of a 25 N anterior load.

4.2.3.1 Translations for Intermediate Joint Positions: FE Model 1

For FE Model 1, the abduction angle measured 60° and the external rotation angle measured 0.0°, 31.1°, and 51.8° for the clinically relevant joint positions with 0°, 30°, and 60°/maximum external rotation, respectively. Using these angles and the motion of the humeral registration block from the reference position to the clinically relevant joint position, the humeral translations with respect to the scapular coordinate system that resulted from application of the 25 N anterior load were computed at the three clinically relevant joint positions (Table 4.1). The humeral translations with respect to the scapular coordinate system resulting from application of the 25 N anterior load were then approximated for the intermediate clinically relevant joint positions with

10°, 20°, and 40° of external rotation, by linearly interpolating the humeral translations from the experimentally obtained positions with 0°, 31.1°, and 51.8° of external rotation (Table 4.1).

Table 4.1 Humeral translations with respect to the scapular anatomical coordinate system for FE Model 1, resulting from application of a 25 N anterior load after the joint was abducted and externally rotated. Highlighted rows are for experimental joint positions

FE Model 1			
External Rotation (°)	Humeral Translation (mm)		
	Anterior	Medial	Inferior
0	25.4	12.0	-8.3
10	21.3	12.0	-9.0
20	17.2	12.1	-9.8
31.1	12.6	12.1	-10.7
40	7.0	12.7	-11.2
51.8 (max)	-0.3	13.5	-11.8

It is worth noting that in FE Model 1 at the maximum rotation angle, the anterior translation of the humerus in the scapular coordinate system was measured to be -0.3 mm. The humerus did not necessary move in the posterior direction, however this value is negative due to the transformations involved with rotating the humerus about its axis before translation.

The humeral translations in the scapular coordinate system at positions with 10°, 20°, and 40° of external rotation were then input into the Matlab code developed in Section 4.2.2 along with an abduction angle of 60° and the respective external rotation angles in order to generate transformation matrices of motion of the humeral registration block from the reference position to the intermediate clinically relevant joint position. The transformation matrices were then used to generate load curves that could be implemented into the finite element solver as in Section 3.3.3.1.

Before analyzing the strains in the anterior-inferior capsule at all clinically relevant joint positions, the load curves were used to simulate motions of the bones from the reference position to the clinically relevant joint positions. The positions of the humerus with respect to the scapula were then qualitatively compared among the clinically relevant joint positions, to verify that the motions to the intermediate clinically relevant joint positions appeared reasonable. It was verified that the positions of the humerus in the intermediate clinically relevant joint positions fit within the positions of the humerus in the clinically relevant joint positions with 0°, 31.1°, and 51.8° of external rotation (Figure 4.5).

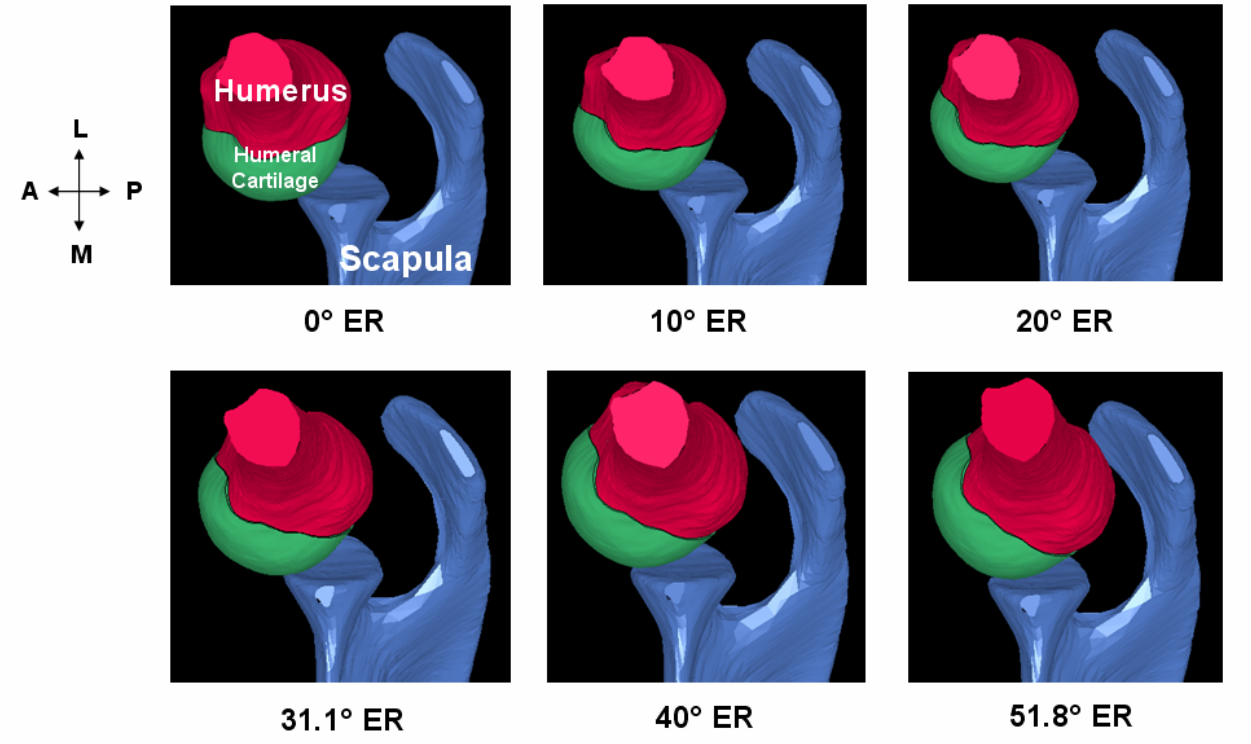

Figure 4.5 Inferior view of FE Model 1 (left shoulder) at six clinically relevant joint positions. The capsule is removed to show the positions of the humerus with respect to the scapula at each clinically relevant joint position. The intermediate joint positions with 10°, 20°, and 40° of external rotation appear to be interpolated between the joint positions with 0°, 31.1°, and 51.8° of external rotation

4.2.3.2 Translations for Intermediate Joint Positions: FE Model 2

For FE Model 2, the abduction angle measured 60° and the external rotation angle measured 0.0°, 25.5°, and 57.3° for the clinically relevant joint positions with 0°, 30°, and 60°/maximum external rotation, respectively. Using these angles and the motion of the humeral registration block from the reference position to the clinically relevant joint position, the humeral translations with respect to the scapular coordinate system that resulted from application of the 25 N anterior load were computed at the three clinically relevant joint positions (Table 4.2). The humeral translations with respect to the scapular coordinate system resulting from application of the 25 N anterior load were then approximated for the intermediate clinically relevant joint positions with 10°, 20°, 40°, and 50° of external rotation, by linearly interpolating the humeral translations at the experimentally obtained positions with 0°, 25.5°, and 57.3° of external rotation (Table 4.2).

Table 4.2 Humeral translations with respect to the scapular anatomical coordinate system for FE Model 2, resulting from application of a 25 N anterior load after the joint was abducted and externally rotated. Highlighted rows are for experimental joint positions

FE Model 2			
External Rotation (°)	Humeral Translation (mm)		
	Anterior	Medial	Superior
0	13.6	2.9	5.5
10	9.0	2.8	5.1
20	4.4	2.8	4.7
25.1	2.1	2.8	4.5
40	-2.9	3.6	1.9
50	-6.3	4.2	0.1
57.3 (max)	-8.7	4.6	-1.2

The humeral translations in the scapular coordinate system at joint positions with 10°, 20°, 40°, and 50° of external rotation were then input into the Matlab code developed in Section

4.2.2 along with an abduction angle of 60° and the respective external rotation angles in order to generate transformation matrices of motion of the humeral registration block from the reference position to the intermediate clinically relevant joint position. The transformation matrices were then used to generate load curves that could be implemented into the finite element solver as in Section 3.3.3.

As with FE Model 1, the load curves were used to simulate motions of the humerus with respect to the scapula in FE Model 2 from the reference position to the clinically relevant joint positions without the capsule, for qualitative verification that the motions to the intermediate clinically relevant joint positions appeared reasonable. It was verified that the positions of the humerus with respect to the scapula in the intermediate clinically relevant joint positions with 10°, 20°, 40°, and 50° fit within the positions of the humerus with respect to the scapula in the clinically relevant joint positions with 0°, 25.1°, and 57.3° of external rotation (Figure 4.6).

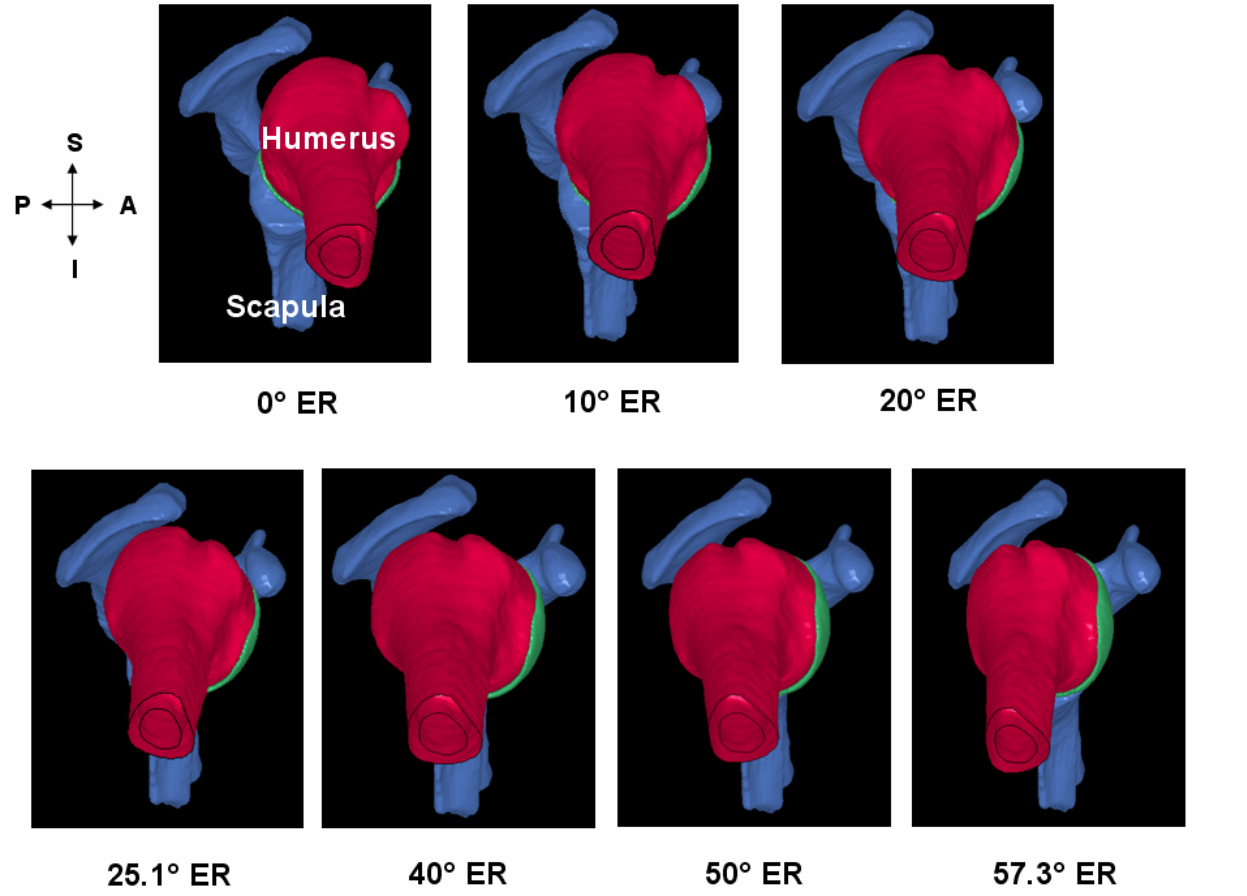

Figure 4.6 Lateral view of FE Model 2 (right shoulder) at six clinically relevant joint positions. The capsule is removed to show the positions of the humerus with respect to the scapula at each clinically relevant joint position. The intermediate joint positions with 10°, 20°, 40°, and 50° of external rotation appear to be interpolated between the joint positions with 0°, 25.1°, and 57.3° of external rotation

4.3 ANTERIOR-INFERIOR CAPSULE STRAIN

4.3.1 Finite Element Model Output

Predicted distributions of strain in the capsule were obtained by computing the Green-Lagrange maximum principal strain in the nodes of the shell elements in the capsule, at each clinically relevant joint position. Element nodes of the anterior-inferior capsule were then grouped into six sub-regions, corresponding to the glenoid and humeral sides of the anterior band of the inferior

glenohumeral ligament, the axillary pouch, and the posterior band of the inferior glenohumeral ligament (Figure 4.7). The glenoid and humeral sub-regions were created by assigning elements to the glenoid or humeral side of a circumferential ring of nodes halfway between the glenoid and humeral insertions of the capsule.

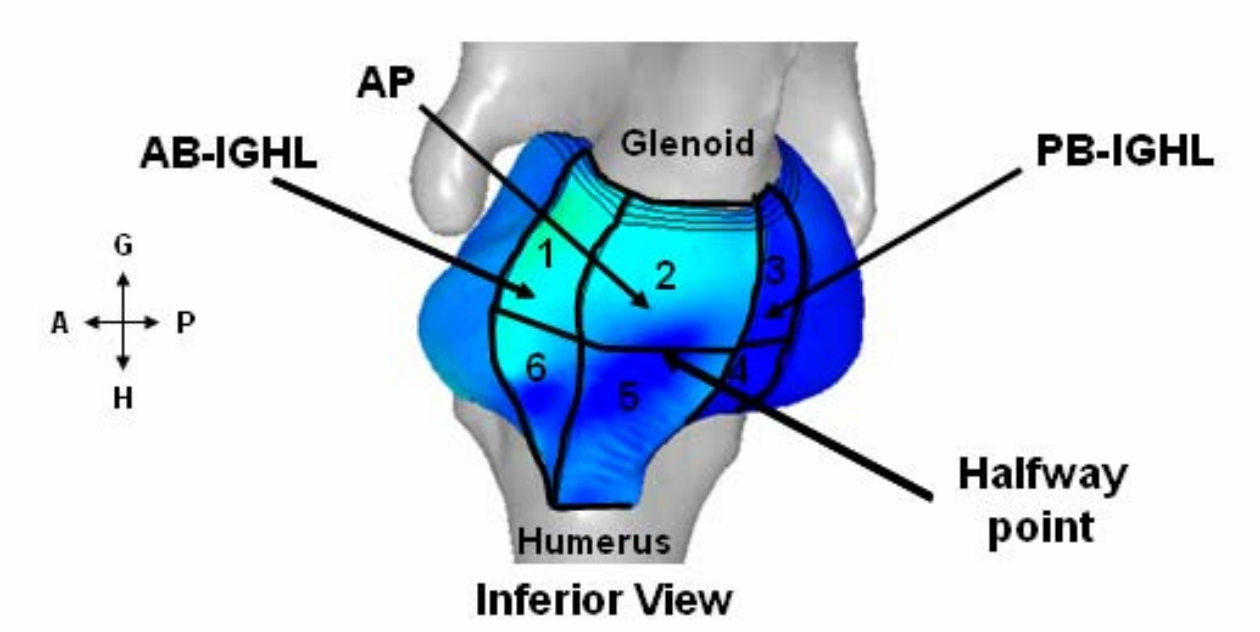

Figure 4.7 Inferior view of FE Model 2 (right shoulder), indicating six sub-regions of the anterior-inferior capsule formed by the anterior-inferior capsule halfway point. AB-IGHL = anterior band of the inferior glenohumeral ligament, AP = axillary pouch, PB-IGHL = posterior band of the inferior glenohumeral ligament

The number of shell elements and nodes varied among the sub-regions in each model. Since the shell element length in the glenoid-to-humerus direction was not constant and decreased when moving from the glenoid to the humerus, there was a greater number of elements in the humeral sub-regions than in the glenoid sub-regions. In addition, the elements that were modified to represent the presence of a labrum were not included in the glenoid sub-regions, further decreasing the number of elements in the glenoid sub-regions. The glenoid and humeral sub-regions of the anterior band of the inferior glenohumeral ligament and axillary pouch contained the same number of elements in both FE Model 1 and FE Model 2, however the

different geometric sizes of the posterior-bands of the inferior glenohumeral ligament in FE Models 1 and 2 resulted in a greater number of elements in the glenoid and humeral sub-regions of the posterior band of the inferior glenohumeral ligament in FE Model 2. The discrepancy in elements was small relative to the total number of elements in the sub-regions, therefore it was decided that comparing strains in the sub-regions of FE Model 1 with those in FE Model 2 was appropriate. The distribution of elements in the sub-regions for FE Model 1 and FE Model 2 are shown in Table 4.3 and Table 4.4, respectively.

Table 4.3 Distribution of elements in the sub-regions of FE Model 1

FE Model 1		
Sub-Region		# Elements
AB-IGHL	glenoid	252
	humerus	684
Axillary Pouch	glenoid	714
	humerus	1938
PB-IGHL	glenoid	231
	humerus	627

Table 4.4 Distribution of elements in the sub-regions of FE Model 2

FE Model 2		
Sub-Region		# Elements
AB-IGHL	glenoid	252
	humerus	684
Axillary Pouch	glenoid	714
	humerus	1938
PB-IGHL	glenoid	252
	humerus	684

For each model the nodal strains in the anterior-inferior capsule were then averaged within each of the six sub-regions, at each clinically relevant joint position.

4.3.2 Statistical Analyses

4.3.2.1 Joint Positions with Consistent Distribution of Strain

In order to determine clinically relevant joint positions with consistent distribution of strain and thus consistent distribution of load in the anterior-inferior capsule among subjects, comparisons between the distribution of strain in the sub-regions of the anterior-inferior capsule in FE Model 1 and FE Model 2 were made. Due to the subject-specificity of capsule strains resulting from variability in joint size and capsule stiffness, comparing magnitudes of strain in the sub-regions among models may be problematic, since the stability provided by the anterior-inferior capsules of two separate shoulders may be similar even though strain magnitudes are much different.

Instead, for each model the highest average sub-region strain among all clinically relevant joint positions was identified, and the average strains in the six sub-regions at each clinically relevant joint position were then normalized to this value. For example, in FE Model 1 the highest average sub-region strain was found in the glenoid side of the anterior band of the inferior glenohumeral ligament at the clinically relevant joint position with 51.8° of external rotation. The average strains in each of the six sub-regions at the clinically relevant joint positions with 0°, 10°, 20°, 31.1°, 40°, and 51.8° of external rotation were then normalized to this value. The process was then repeated for FE Model 2.

This provided six ratios ranging from 0 to 1 at each of the clinically relevant joint position for both FE Model 1 and FE Model 2. At each clinically relevant joint position the groups of six ratios in the two models were compared by determining a Pearson correlation

coefficient, or *r* value, between the two groups using SPSS. A total of six correlation tests were therefore performed, based on the available shared joint positions of FE Model 1 and FE Model 2 (Table 4.5). It was determined that squared correlation coefficients above 0.7 were reflective of high correlation [143]. Therefore, joint positions with a squared correlation coefficient value above 0.7 were defined as having consistent distribution of strain and thus consistent distribution of load in the anterior-inferior capsule among the two models.

Table 4.5 Joint positions in FE Model 1 and FE Model 2 where correlation tests were performed

	Joint Position (external rotation angle)	
Correlation Test	**FE Model 1**	**FE Model 2**
1	**0°**	**0°**
2	**10°**	**10°**
3	**20°**	**20°**
4	**31.1°**	**25.1°**
5	**40°**	**40°**
6	**51.8°**	**50°**

Using the methodology of determining correlation between ratios in FE Model 1 and FE Model 2, it is possible that the clinically relevant joint positions have high correlation in the distributions of strain in the anterior-inferior capsules of both models, however the strain magnitudes at the joint positions may be relatively low with respect to the strain magnitudes in other joint positions for each model. For effective physical examinations of the stability provided by the anterior-inferior capsule, it is crucial that the joint positions used result in a transfer of load in the capsule between the humerus and scapula. Joint positions with relatively

low transfer of load in the capsule are therefore unhelpful for diagnoses, regardless of whether the distribution of load was consistent among subjects at these joint positions. The experimental strain repeatability of the current work is ±3.5% strain, and it was therefore decided that joint positions would be excluded from consideration if either model did not have at least one sub-region with an average strain of 7% or more at the joint position, a value that is double the experimental strain repeatability.

4.3.2.2 Localization of Stability Provided by Anterior Capsule

In order to address Specific Aim 2 and expand the clinical relevance of the work, the distribution of strain in the anterior-inferior capsules of both FE Model 1 and FE Model 2 were analyzed to determine if the stability provided by the anterior-inferior capsule was localized to a sub-region in the clinically relevant joint positions identified in Section 4.3.2.1.

At each of the clinically relevant joint positions with r^2 values of 0.7 or greater when correlating the distribution of strain between FE Model 1 and FE Model 2, as well as with at least one sub-region in which average strain was greater than 7%, the sub-region strains were analyzed to determine if strain in the anterior-inferior capsule was highest in a particular sub-region or group of sub-regions. Specifically, in each model the values of strain in the six sub-regions were compared at each joint position using a Kruskal-Wallis test ($p<0.05$) with Bonferroni-corrected Mann-Whitney tests for post-hoc analysis. SPSS was used for all analyses. Due to the large number of nodes in each sub-region, statistical differences were present even when average strain differences were less than the experimental repeatability of ±3.5% strain. Therefore, differences in strain among the sub-regions were defined to be significant only if they were statistically significant and on average greater than the experimental strain repeatability of ±3.5% strain. Clinically relevant joint positions were then identified in which strain in a sub-

region was significantly higher than strain in the remaining five sub-regions, for both FE Model 1 and FE Model 2, in order to suggest clinically relevant joint positions where the stability provided by the anterior-inferior capsule could be localized to a specific sub-region.

5.0 RESULTS

5.1 DEVELOPMENT OF FE MODEL 1

FE Model 1 was previously validated at a clinically relevant joint position with 25 N of anterior load applied at 60° of glenohumeral abduction and 51.8° of external rotation, using the NIKE3D finite element solver with an isotropic hypoelastic constitutive model used to represent the capsule [41]. However, the model was unable to be validated at joint positions with a 25 N anterior load applied at 60° of glenohumeral abduction and 0° or 31.1° of external rotation. For the current work, FE Model 1 was modified to use an isotropic hyperelastic constitutive model to represent the capsule. Since its initial publication [41], the model's mesh density was changed and the insertion site elements were modified to simulate the presence of a glenoid labrum. However the remaining subject-specific inputs of reference position, bone and soft-tissue surface geometry, and joint kinematics were unaltered.

5.1.1 Computational Modifications

5.1.1.1 Material Coefficients

In order to evaluate the distribution of strain in the anterior-inferior capsule in FE Model 1 using an isotropic hyperelastic constitutive model to represent the capsule, material coefficients to the Veronda-Westmann isotropic hyperelastic constitutive model were generated for each capsule

region (Table 5.1). For the axillary pouch and posterior region, there were optimized material coefficients for the uni-directional elongations in both the longitudinal and transverse directions of the capsule. Therefore, the procedure outlined in Section 3.2.4.4 to generate material coefficients from the average Cauchy stress-stretch curve of the longitudinal and transverse Cauchy stress-stretch curves was used to compute a single set of material coefficients for the axillary pouch and posterior capsule.

Table 5.1 Material coefficients for the five capsule regions. For the axillary pouch and posterior region, the longitudinal and transverse Cauchy stress-stretch curves were used to create an average Cauchy stress-stretch curve to which material coefficients were generated

		Material Coefficients	
Capsule Region	**Direction**	**C1**	**C2**
Anterosuperior	Longitudinal	**0.45**	**3.6**
AB-IGHL	Longitudinal	**0.30**	**3.4**
PB-IGHL	Longitudinal	**0.84**	**3.2**
Axillary Pouch	Longitudinal	0.02	17.6
	Transverse	0.06	8.6
	Average	**0.03**	**13.1**
Posterior	Longitudinal	0.51	3.0
	Transverse	0.11	3.4
	Average	**0.24**	**3.7**

The material coefficients for each capsule region fit well within the ranges of C1 and C2 values determined by Rainis [40] and in preliminary work performed within our research group (Table 5.2), and it was therefore decided to proceed with their implementation into the finite element model.

Table 5.2 Ranges of values for C1 and C2 in selected capsule regions obtained by Rainis [40] and during preliminary experiments in our research group

	Material Coefficients			
	C1		C2	
Capsule Region	min	max	min	max
Anterosuperior	0.02	0.25	6.8	22.4
Axillary Pouch	0.04	1.36	2.2	16.7
Posterior	0.04	1.93	2.2	10.9
AB-IGHL	0.12	0.64	2.3	9.4

5.1.2 Finite Element Solution Procedure

The NIKE3D input deck was converted to a FEBio input deck as described in Section 3.3.3.3. When running the FEBio input deck with the FEBio solver at each of the three clinically relevant joint positions, full convergence of the solution was unable to be obtained due to inversion of elements during the path of motion. This was due to the contact at the sliding interface between the humeral head cartilage and the articular surface of the capsule tissue. These convergence issues were not seen when the model was run in NIKE3D due to a more robust contact algorithm that was not available in FEBio. Therefore, a brief sensitivity study was performed in which model convergence was evaluated when modifications were made to the penalty factor and tolerance of the sliding interface between the humeral head cartilage and the articular surface of the capsule.

Since element inversion occurred as a result of the sliding interface being too stiff, modifications were explored that increased the tolerance and decreased the penalty. Decreasing the stiffness of the interface, however, could possibly lead to penetration of the humeral head cartilage through the capsule tissue, thus altering predictions of capsule surface strain. When

modifying the tolerance and penalty, care was taken to confirm that penetration of the humeral head cartilage through the capsule did not occur. The sensitivity study was first performed at the clinically relevant joint position with 31.1° of external rotation, after which optimal tolerance and penalty values were explored at the clinically relevant joint positions with 0° and 51.8° of external rotation.

Table 5.3 shows the results of modifications to the tolerance and penalty parameters at the clinically relevant joint position with 31.1° of external rotation. Initially, the tolerance value was set at 0.05 and the penalty value was set at 1.0. Full convergence was obtained with a tolerance of 0.1 and a penalty of 0.5, as well as with a tolerance of 0.3 and a penalty of 0.25. Predicted capsule strains were computed with all modifications, and compared at equivalent converged states (Figure 5.1). It was found that the predicted strains in the anterior-inferior capsule were not sensitive to the changes in tolerance and penalty values, and that only the model's ability to fully converge was affected.

Table 5.3 Contact parameter modification at the joint position with 31.1° of external rotation

	Initial	Modifications at 31.1° ER						
Tolerance	**0.05**	**0.05**	**0.05**	**0.1**	**0.1**	**0.1**	**0.1**	**0.3**
Penalty	**1.0**	**0.5**	**1.5**	**1.0**	**0.5**	**1.5**	**2.0**	**0.25**
% convergence	77%	56%	45%	56%	100%	57%	77%	100%

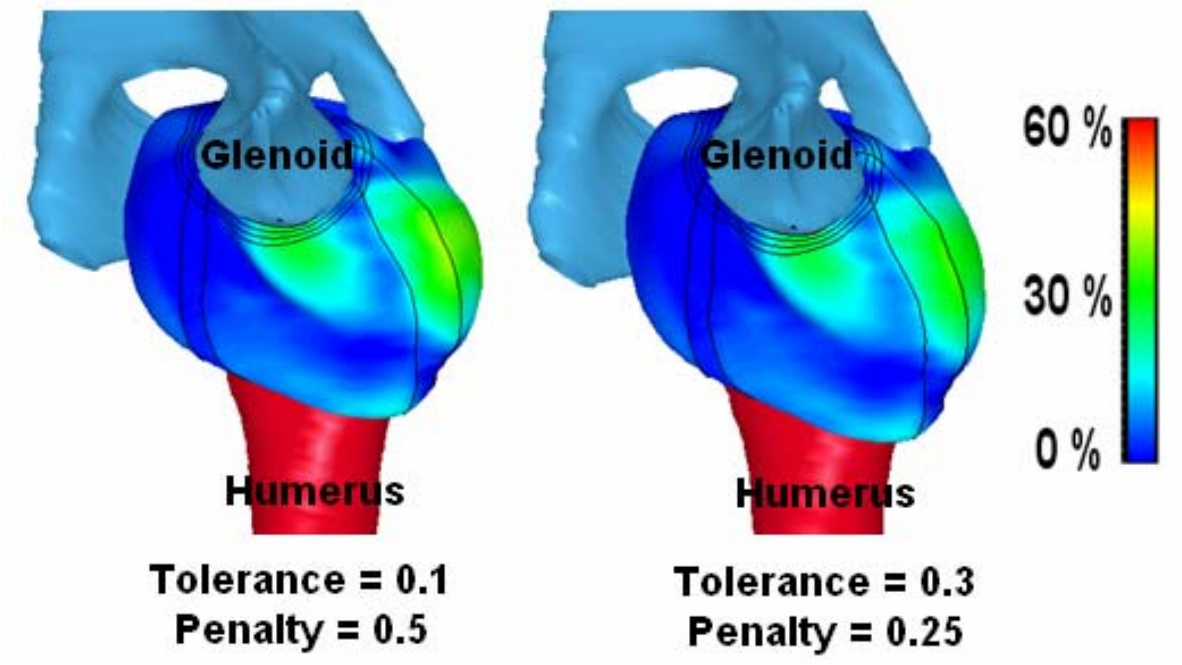

Figure 5.1 Inferior view of FE Model 1 (left shoulder) at the clinically relevant joint position with 31.1° of external rotation. The magnitude and distribution of strain in the anterior-inferior capsule was almost identical when either set of contact parameters was used that resulted in 100% convergence of the model

The tolerance and penalty values that resulted in full convergence at the clinically relevant joint position with 31.1° of external rotation were then evaluated when the joint motions were simulated to the clinically relevant joint positions with 51.8° and 0° of external rotation. At the clinically relevant joint position with 51.8° of external rotation, using a tolerance of 0.1 and a penalty of 0.5 resulted in full convergence, however using a tolerance of 0.3 and a penalty of 0.25 resulted in only 46% convergence. At the clinically relevant joint position with 0° of external rotation, neither of these parameter combinations resulted in full convergence, as a tolerance of 0.1 and a penalty of 0.5 resulted in 46% convergence and a tolerance of 0.3 and a penalty of 0.25 resulted in 47% convergence. It was decided to create a dynamic tolerance, i.e. a tolerance that changed as the simulated motion progressed. Keeping the penalty fixed at 0.5, the tolerance was set to 0.1 from 0-45% of the solution procedure, and then changed to 0.2 from

45%-100% of the solution procedure. This resulted in full convergence of the model at the clinically relevant joint position with 0° of external rotation.

It was therefore decided that the tolerance and penalty values for all clinically relevant joint positions for FE Model 1 would be assigned a penalty value of 0.5 and a dynamic tolerance value fluctuating between 0.1 and 0.2 depending on model convergence at a given clinically relevant joint position.

5.2 VALIDATION OF FE MODEL 1

The predicted and experimental strain patterns and magnitudes in the anterior band of the inferior glenohumeral ligament were relatively similar at the clinically relevant joint positions with 31.1° and 51.8° of external rotation, however this was not the case at the clinically relevant joint position with 0° of external rotation (Figure 5.2). These observations were confirmed quantitatively with the average predicted and experimental strain magnitudes in the anterior band of the inferior glenohumeral ligament, shown in Table 5.4. The average difference between the predicted and experimental strains at the clinically relevant joint positions with 0°, 31.1°, and 51.8° of external rotation was -13.1%, 1.2%, and 1.9% strain, respectively. Since the criteria for validation is that the average difference in predicted and experimental strain in the anterior band of the inferior glenohumeral ligament must be less than or equal to ±3.5% strain, FE Model 1 was validated at the joint positions with 31.1° and 51.8° of external rotation, but was unable to be validated at the joint position with 0° of external rotation.

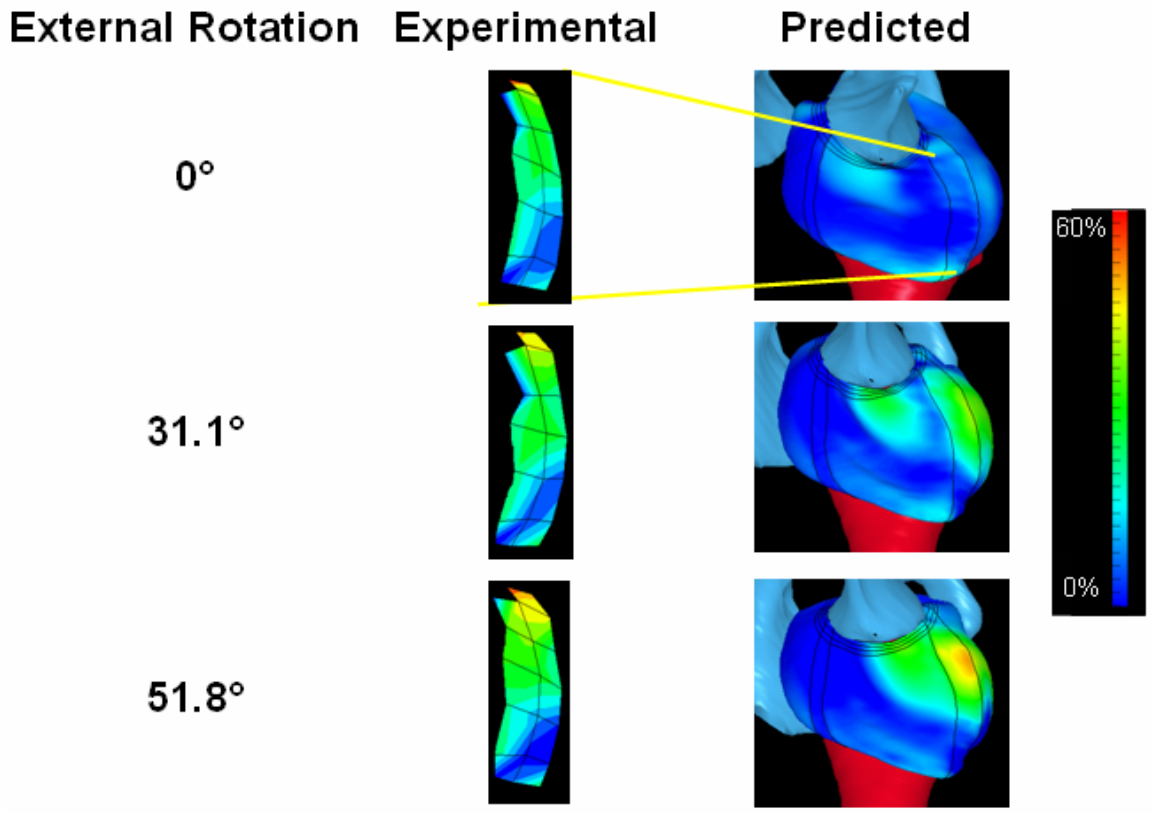

Figure 5.2 Inferior views of experimental and predicted strains in the anterior band of the inferior glenohumeral ligament for FE Model 1 (left shoulder), at the three clinically relevant joint positions for validation

Table 5.4 FE Model 1 experimental and predicted strains in the anterior band of the inferior glenohumeral ligament, at the three clinically relevant joint positions for validation

Experimental and Predicted AB-IGHL Strains (%)									
	0° ER			31.1° ER			51.8° ER		
Element	Exp.	Pred.	Diff.	Exp.	Pred.	Diff.	Exp.	Pred.	Diff.
1	15	4	-11	18	6	-12	11	2	-10
2	9	3	-6	9	17	8	7	7	0
3	10	5	-5	8	26	18	8	18	10
4	29	8	-21	27	34	6	28	35	7
5	36	9	-27	36	34	-2	36	44	8
6	35	8	-27	34	24	-10	38	37	-1
7	0	7	7	0	4	4	0	3	3
8	14	0	-13	12	12	0	12	10	-2
9	22	1	-21	26	21	-5	24	24	0
10	21	6	-15	19	23	4	41	36	-5
11	12	7	-6	19	20	1	28	40	12
AVE	**18.5**	**5.4**	**-13.1**	**18.9**	**20.1**	**1.2**	**21.1**	**23.0**	**1.9**
SD	**11.4**	**2.9**	**10.5**	**11.3**	**9.9**	**8.4**	**14.0**	**15.8**	**6.6**

The predicted shape of the capsule was also compared with the shape of the capsule seen experimentally at the equivalent clinically relevant joint position. For each of the three clinically relevant joint positions with 0°, 31.1°, and 51.8° of external rotation, the predicted and experimental shape of the deformed capsule tissue appeared similar, in that the anterior-inferior capsule wrapped around the humeral head during motion of the joint (Figure 5.3).

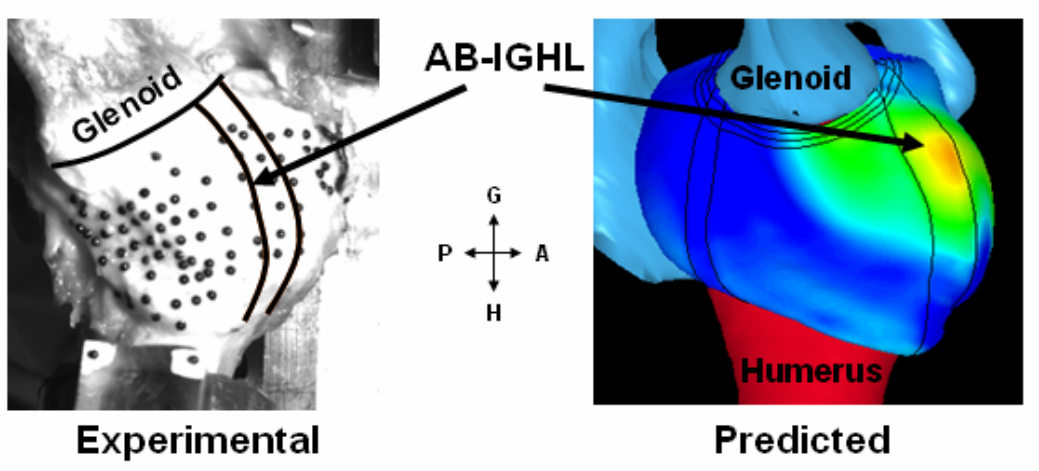

Figure 5.3 Comparisons of experimental and predicted shape of the capsule for FE Model 1 (left shoulder), at the clinically relevant joint position with 51.8° of external rotation. The anterior band of the inferior glenohumeral ligament is outlined in black. Note that the capsule wraps around the humeral head during the joint motion

When using an isotropic hypoelastic constitutive model to represent the capsule, FE Model 1 was able to be validated only at the clinically relevant joint position with 51.8° of external rotation. Therefore, the use of the Veronda-Westmann isotropic hyperelastic constitutive model to represent the capsule resulted in an improvement in the model's predictive capability, in that validation was able to be performed at clinically relevant joint positions with both 31.1° and 51.8° of external rotation.

5.3 DEVELOPMENT OF FE MODEL 2

5.3.1 Reference Position

5.3.1.1 Scapular and Humeral Potting

The anterior radiograph taken of the cadaver for FE Model 2 after potting the humerus and scapula in the epoxy putty is shown in Figure 5.4 It was verified that the humeral shaft was concentric with the humeral epoxy putty cylinder and that the angle of inclination of the glenoid with respect to the superior-inferior axis of the scapular epoxy putty block was ~10°. Therefore, the potting procedure was determined to be appropriate.

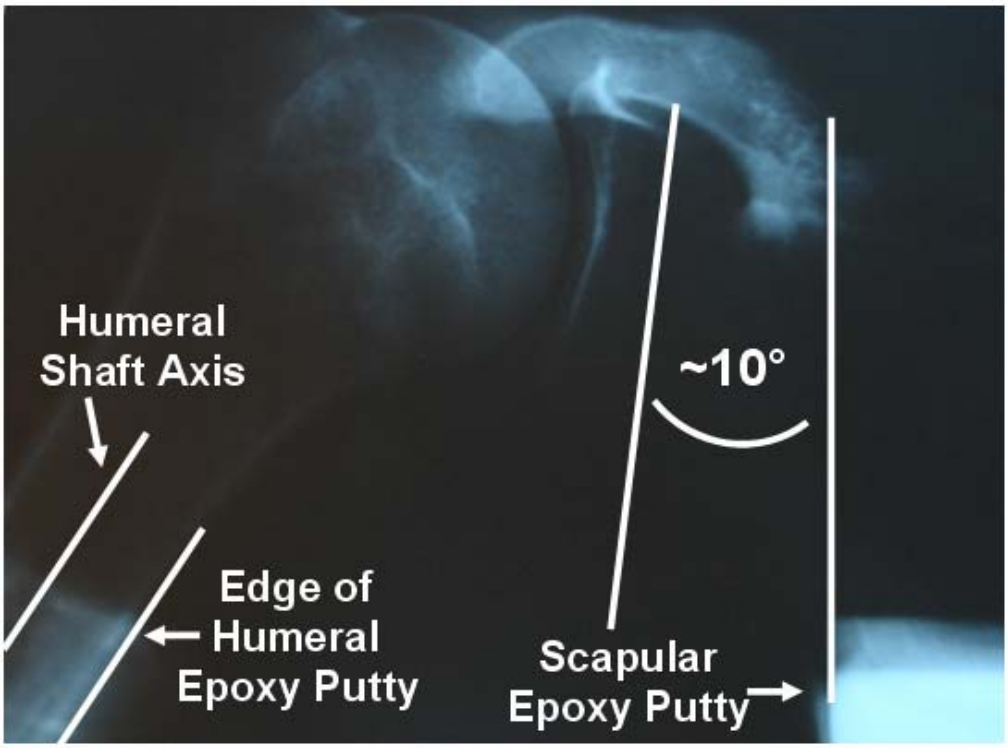

Figure 5.4 Radiograph with anterior view of joint (right shoulder) after potting procedure, demonstrating adequate potting

5.3.1.2 Reference Position

The three joint positions for FE Model 2 with the least amount of visual capsule strain marker motion were identified to be 60° of glenohumeral abduction with 5° of external rotation, 5° of internal rotation, and 10° of internal rotation. The average and peak 3-dimensional capsule strain marker motions for all 77 capsule strain markers attached to the anterior-inferior capsule are shown in Table 5.5. The joint position with 5° of external rotation was determined to be the reference position, based on its lowest average capsule strain marker motion and its peak capsule strain marker motion below 1.25 mm.

Table 5.5 Quantitative 3-dimensional capsule strain marker motion at the three joint positions identified to have the lowest visual capsule strain marker motion. ER=external rotation, IR=internal rotation

Joint Position	Marker Motion (mm)	
	Ave ± stdev	Peak
5° ER	0.38 ± 0.16	1.12
5° IR	0.48 ± 0.21	1.77
10° IR	0.43 ± 0.24	1.17

5.3.2 Application of Joint Motion

5.3.2.1 Joint Kinematics

The specimen was mounted into the robotic/UFS testing system at 41° of glenohumeral abduction, and the path of passive glenohumeral abduction was obtained from 25° to 65°. Radiographs taken at 30° and 60° of glenohumeral abduction with neutral rotation are shown in Figure 5.5 After consulting with an experienced orthopaedic surgeon it was decided that the humerus articulated appropriately with the glenoid at both abduction angles and that the specimen was mounted properly.

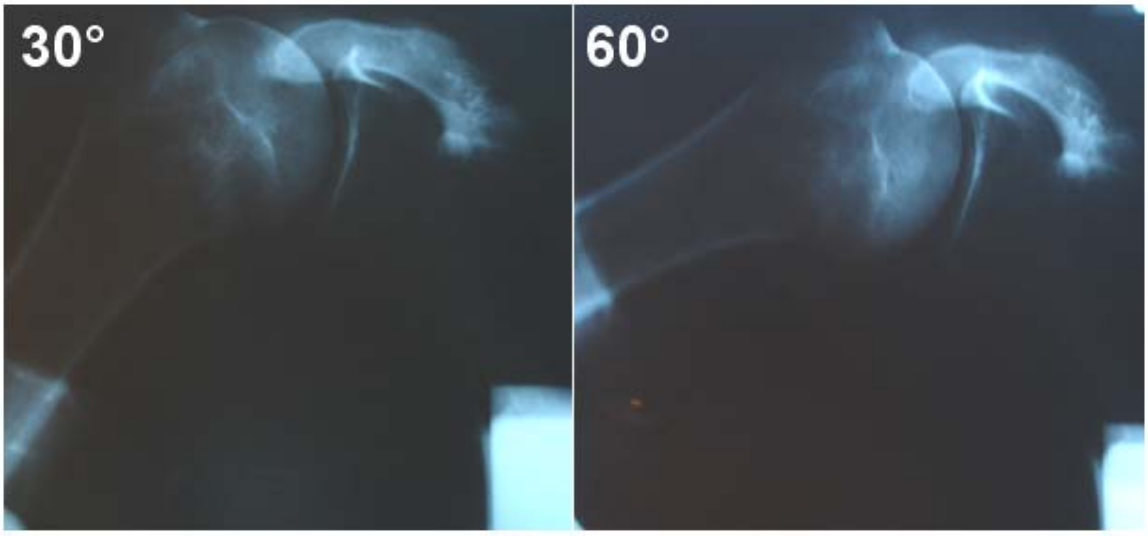

Figure 5.5 Anterior radiographs of joint (right shoulder) when mounted on robot, at 30° and 60° of glenohumeral abduction

The external rotation moment applied to the joint at 60° of glenohumeral abduction resulted in a maximum of 64.5° of external rotation. The incremental rotation values closest to 30° and 60°/maximum external rotation were identified as 25.1° and 57.3°, respectively. Therefore, a 25 N anterior load was applied to the humerus at 0°, 25.1°, and 57.3° of external rotation. The anterior-posterior motion of the humerus with respect to the scapula in response to the loading condition is shown in Figure 5.6 at each of the three joint positions. The anterior translations of the humerus with respect to the scapula at 0°, 25.1°, and 57.3° were found specifically to be 15.7 mm, 14.2 mm, and 3.5 mm, respectively, which agreed with previous work demonstrating that anterior joint translations decrease with external rotation when the joint is abducted to 60° [19, 20]. During the posterior motion of the humerus with respect to the scapula at 0° of external rotation, the load appeared to fluctuate as posterior humeral translation neared 20 mm. It was decided to proceed with the analyses since the focus of the current work

involved motion resulting from application of anterior load to the humerus with respect to the scapula, and these motions did not have such fluctuations at any of the three joint positions.

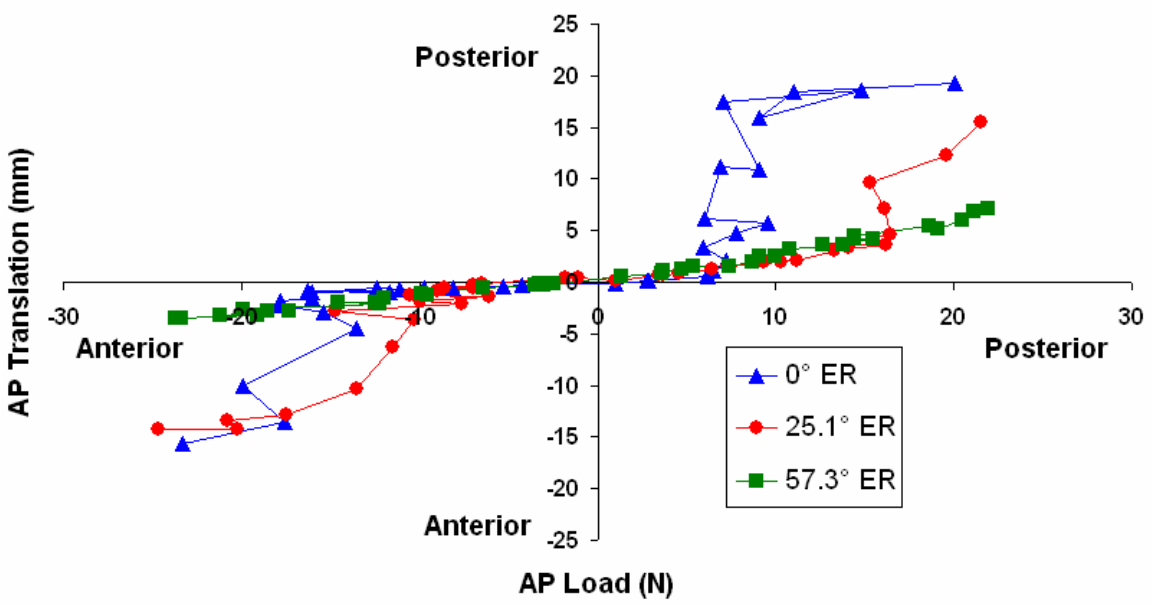

Figure 5.6 Anterior-posterior humeral translation in response to 25 N anterior-posterior load, at the three clinically relevant joint positions with 0°, 25.1°, and 57.3° of external rotation

When the anterior-posterior 25 N load was applied with the joint in 0°, 25.1°, or 57.3° of external rotation, coupled superior-inferior and medial-lateral translations were also observed due to the shape of the glenoid and obligate translations caused by the tightening of the capsule structure. The inferior translations of the humerus with respect the scapula at joint positions with 0°, 25.1°, and 57.3° of external rotation were found specifically to be 1.1 mm, -0.6 mm, and -1.1 mm, respectively (Figure 5.7). The lateral translations of the humerus with respect the scapula at joint positions with 0°, 25.1°, and 57.3° of external rotation were found specifically to be 5.0 mm, 3.9 mm, and 0.7 mm, respectively (Figure 5.8).

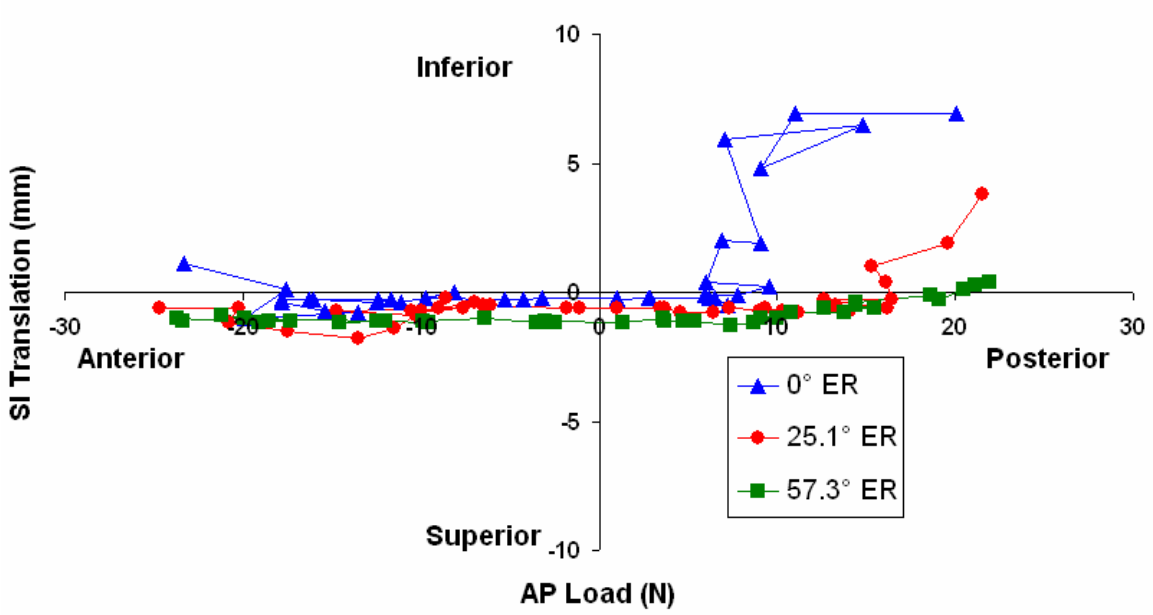

Figure 5.7 Superior-inferior humeral translation in response to 25 N anterior-posterior load, at the three clinically relevant joint positions with 0°, 25.1°, and 57.3° of external rotation

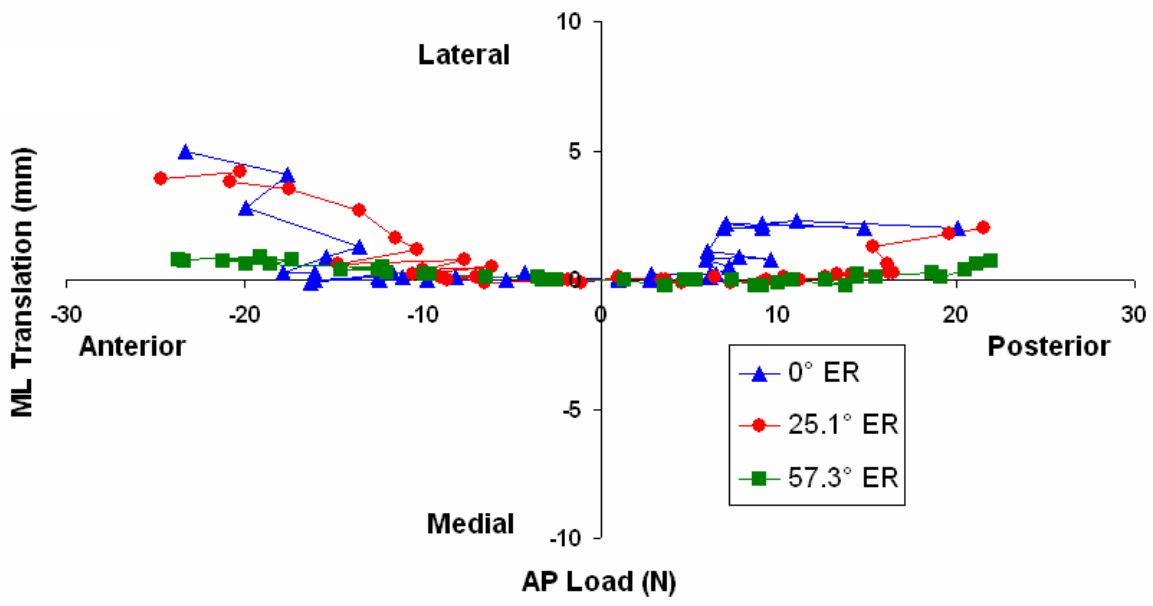

Figure 5.8 Medial-lateral humeral translation in response to 25 N anterior-posterior load, at the three clinically relevant joint positions with 0°, 25.1°, and 57.3° of external rotation

5.3.2.2 Experimental Strains

At the clinically relevant joint positions with 0°, 25.1°, and 57.3° of external rotation, the anterior-inferior capsule became increasingly lax in the axillary pouch and posterior band of the inferior glenohumeral ligament. The capsule tissue became extremely folded in these regions, resulting in an inability to visualize all capsule strain markers with at least two cameras from the optical motion tracking system. Therefore, the number of experimental strain elements in the anterior-inferior capsule was reduced from a maximum of 60 possible elements to 56 elements, 42 elements, and 28 elements at the clinically relevant joint positions with 0°, 25.1°, and 57.3° of external rotation, respectively.

Fringe plots of the magnitude and direction of the maximum principal strain in the anterior-inferior capsule at the three clinically relevant joint position are shown in Figure 5.9**.** The average, standard deviation, and peak strains at each joint position are shown in Table 5.6.

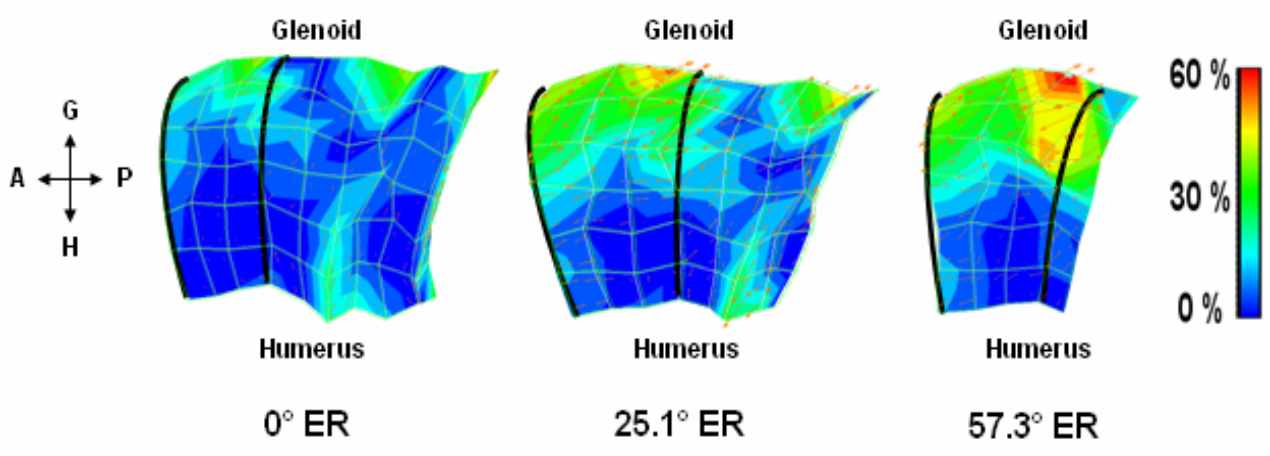

Figure 5.9 Inferior view of the magnitude and direction of maximum principal strains at the clinically relevant joint positions with 0°, 25.1°, and 57.3° of external rotation (right shoulder). Black lines indicate margins of the anterior band of the inferior glenohumeral ligament

Table 5.6 Average, standard deviation (SD), and peak maximum principal strains in the anterior-inferior capsule at the 3 clinically relevant joint positions with 0°, 25.1°, and 57.3° of external rotation

	External Rotation		
	0°	25.1°	57.3°
Average (%)	7.6	11.6	17.1
SD	9.0	12.3	14.9
Peak	31.6	39.5	41.5

The average strain magnitudes at each position are well within the ranges of anterior-inferior capsule strain in similar joint positions found by Moore et al. [21], as well as the directions of maximum principal strain. The average strain magnitude and direction further compare well with a previous study that reported average maximum principal strain in the glenoid and humeral halves of the anterior-inferior capsule to be 14.4±4% and 15.6±6%, respectively, when 18 mm anterior humeral translation was applied with the joint at 60° of glenohumeral abduction and minimal external rotation [96].

5.3.3 Material Coefficients

The optimized load-elongation curves using the Veronda-Westmann isotropic hyperelastic constitutive model closely matched the experimental load-elongation curves obtained from application of the uni-directional elongations to each capsule region (Section 3.2.4). In Figure 5.10 it can be seen that the optimized load-elongation curves predict slightly higher toe-region loads with respect to the experimental load-elongation curves, for the anterosuperior region, anterior band of the inferior glenohumeral ligament, and posterior band of the inferior

glenohumeral ligament. This pattern is also seen in the optimized longitudinal and transverse load-elongation curves for the axillary pouch and posterior capsule in Figure 5.11 and Figure 5.12, respectively. The systematic difference in the optimized and experimental load-elongation curves in the toe region suggests that the Veronda-Westmann isotropic hypoelastic constitutive model may overestimate the stiffening response of each capsule region when loaded into the toe region. This may explain why FE Model 1 was unable to be validated at the clinically relevant joint position with 0° of external rotation. If the clinically relevant joint position with 0° of external rotation resulted in loading of the tissue into the toe-region only, then the overestimation of the stiffness of the anterior-inferior capsule would result in relatively low predicted strains, as was the case.

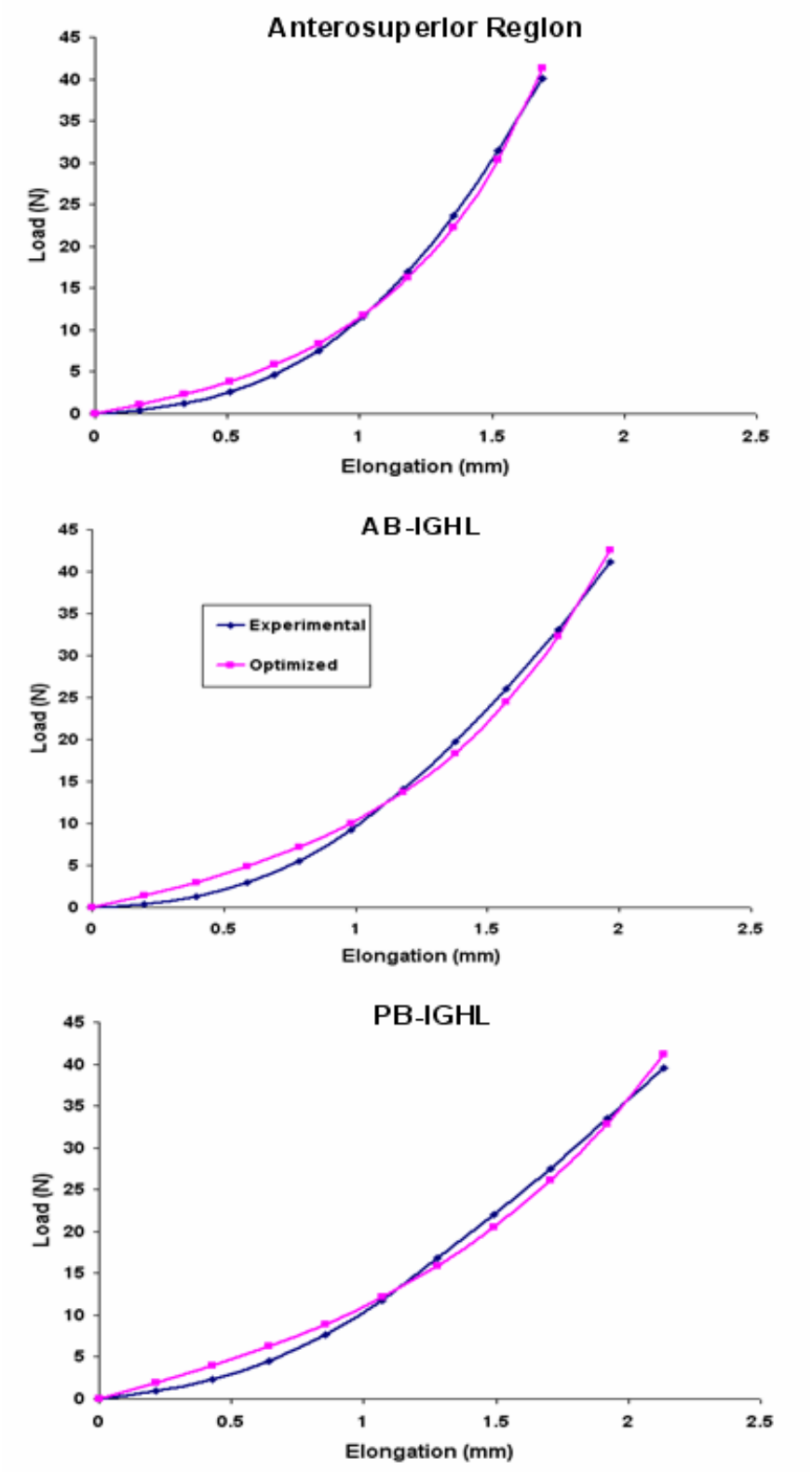

Figure 5.10 Experimental and optimized load-elongation curves for the anterosuperior region, anterior band of the inferior glenohumeral ligament (AB-IGHL), and posterior band of the inferior glenohumeral ligament (PB-IGHL)

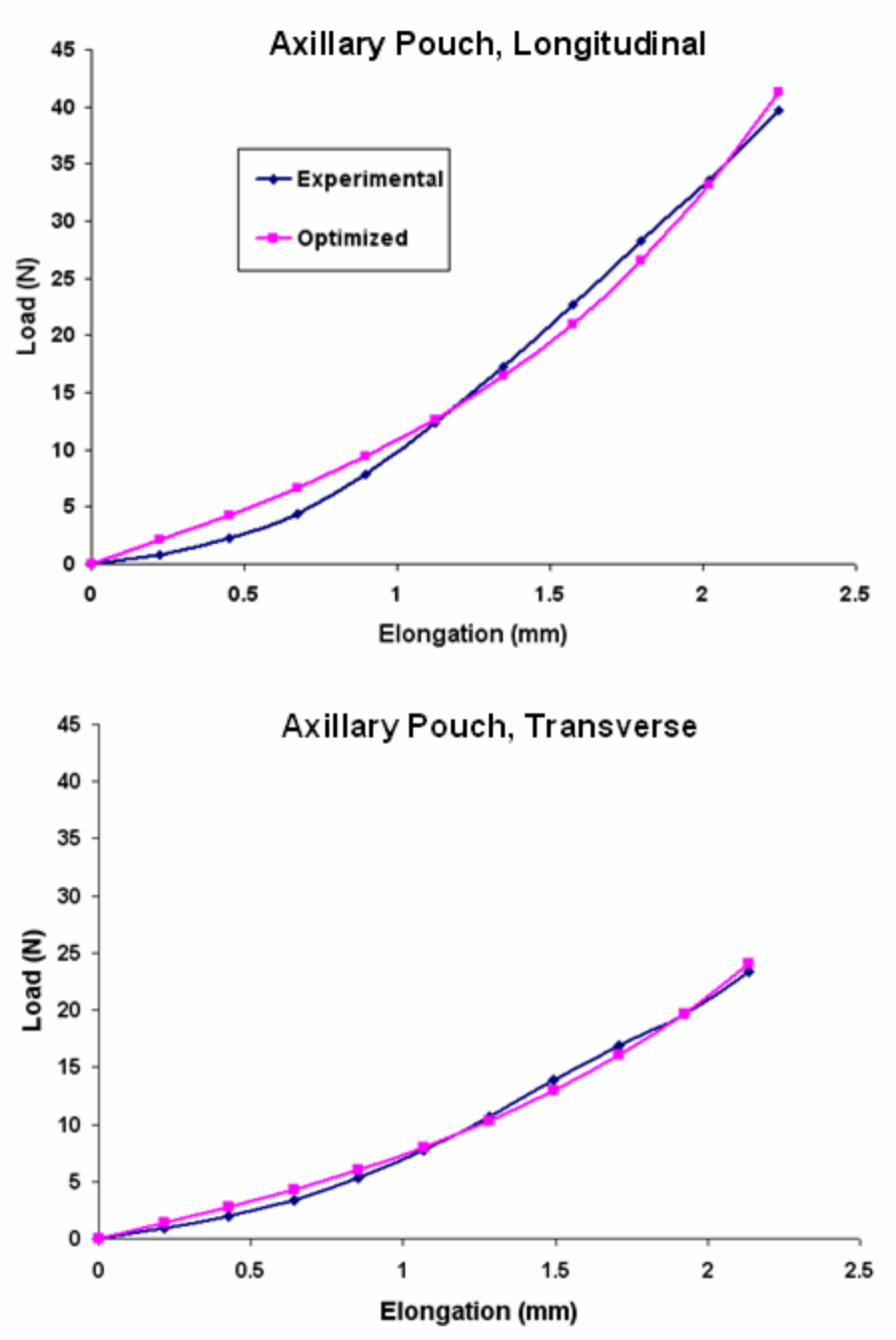

Figure 5.11 Experimental and optimized load-elongation curves for the axillary pouch, with elongations in the longitudinal and transverse directions

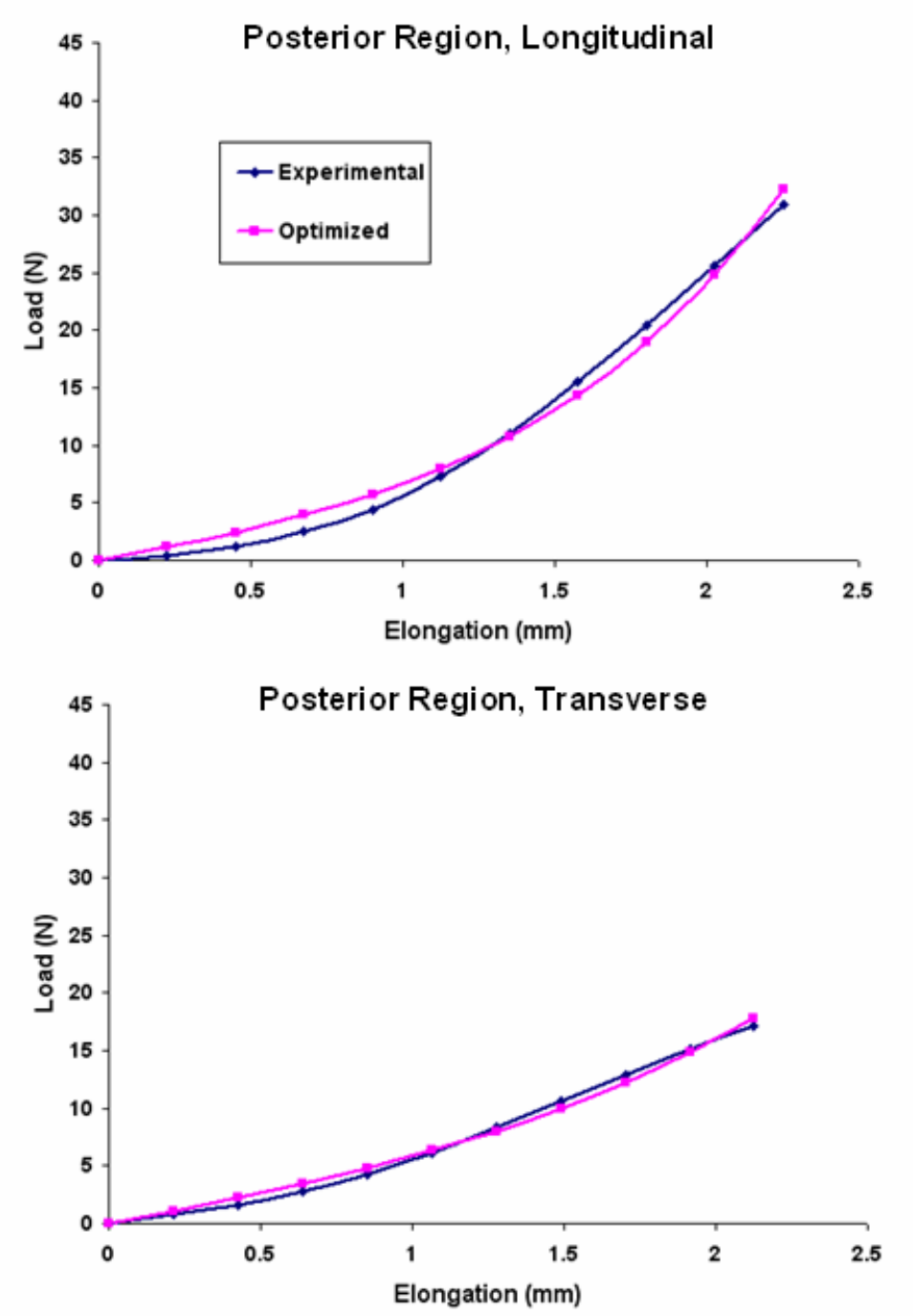

Figure 5.12 Experimental and optimized load-elongation curves for the posterior region, with elongations in the longitudinal and transverse directions

For the anterosuperior region, anterior band of the inferior glenohumeral ligament, and the posterior band of the inferior glenohumeral ligament, optimized material coefficients were obtained for uni-directional elongations in the longitudinal direction of the capsule (Table 5.7). For the axillary pouch and posterior region, optimized material coefficients were obtained for uni-directional elongations in both the longitudinal and transverse directions of the capsule. Therefore, the procedure outlined in Section 3.2.4.4 to generate material coefficients from the average Cauchy stress-stretch curve of the longitudinal and transverse Cauchy stress-stretch curves was used to compute a single set of material coefficients for the axillary pouch and posterior capsule.

Table 5.7 Material coefficients for the five capsule regions. For the axillary pouch and posterior region, the longitudinal and transverse Cauchy stress-stretch curves were used to create an average Cauchy stress-stretch curve to which material coefficients were generated

		Material Coefficients	
Capsule Region	**Direction**	**C1**	**C2**
Anterosuperior	Longitudinal	**0.07**	**6.8**
AB-IGHL	Longitudinal	**0.12**	**5.4**
PB-IGHL	Longitudinal	**0.91**	**3.1**
Axillary Pouch	Longitudinal	0.16	4.4
	Transverse	0.08	6.6
	Average	**0.11**	**5.4**
Posterior	Longitudinal	0.17	4.3
	Transverse	0.47	3.8
	Average	**0.27**	**4.4**

The material coefficients for each capsule region fit well within the ranges of C1 and C2 values determined by Rainis [40] and in preliminary work performed within our research group (Table 5.2), and it was therefore decided to proceed with their implementation into the finite element model.

5.3.4 Finite Element Solution Procedure

The NIKE3D input deck was converted to a FEBio input deck as described in Section 3.3.3.3. Based on the convergence results of FE Model 1 in Section 5.1.2, the tolerance and penalty values at the sliding interface between the humeral head cartilage and the articular surface of the capsule were set to constant values of 0.1 and 0.5, respectively. The humeral head cartilage was again assigned to be the master and the capsule assigned to be the slave. Due to the shape of the anterior-inferior capsule near its humeral insertion, contact also occurred between the humerus and the articular surface of the capsule, resulting in penetration of the humerus through the capsule (Figure 5.13). Therefore, an additional sliding interface was assigned with the humerus as the master and the capsule as the slave. The tolerance and penalty values of this interface were set to constant values of 0.1 and 0.5, respectively.

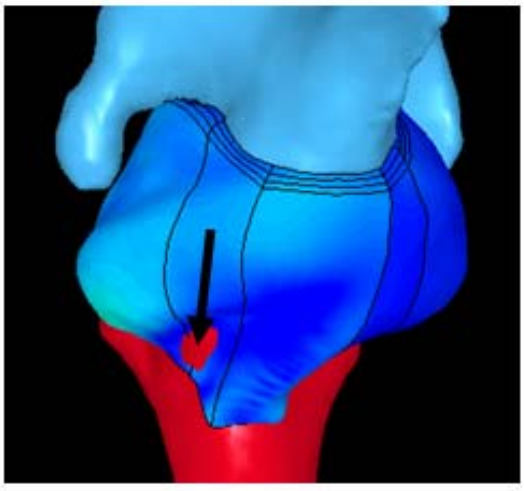

Figure 5.13 Inferior view of FE Model 2 (right shoulder) at the clinically relevant joint position with 30° of external rotation. Black arrow indicates penetration of humerus through the capsule

Full convergence of the solution was obtained when running the FEBio input deck with the FEBio solver, at each of the three clinically relevant joint positions with 0°, 25.1°, and 57.3° of external rotation.

5.4 VALIDATION OF FE MODEL 2

5.4.1 Initial Validation Attempt

Using the subject-specific inputs produced from the methodology in Section 3.2 and the model development methodology in Section 3.3, motions of the joint were simulated in FE Model 2 from the reference position to the clinically relevant joint positions with a 25 N anterior load applied at 60° of glenohumeral abduction and 0°, 25.1°, and 57.3° of external rotation. Fringe plots of the experimental strains in the anterior band of the inferior glenohumeral ligament and the predicted strains in the entire capsule are shown in Figure 5.14. While the predicted and experimental strain patterns appeared relatively similar, the magnitudes of the experimental strains were much higher than the magnitudes of the predicted strains in the anterior band of the inferior glenohumeral ligament. This is further confirmed quantitatively with the average experimental and predicted strain magnitudes in the anterior band of the inferior glenohumeral ligament (Table 5.8). The average difference between the predicted and experimental strains at the clinically relevant joint positions with 0°, 25.1°, and 57.3° external rotation was -4.9%, -6.0%, and -9.9% strain, respectively, all beyond the validation criteria of an average strain difference less than or equal to ±3.5% strain. Therefore, FE Model 2 was unable to be validated at the three clinically relevant joint positions using the subject-specific inputs obtained from Section 3.2.

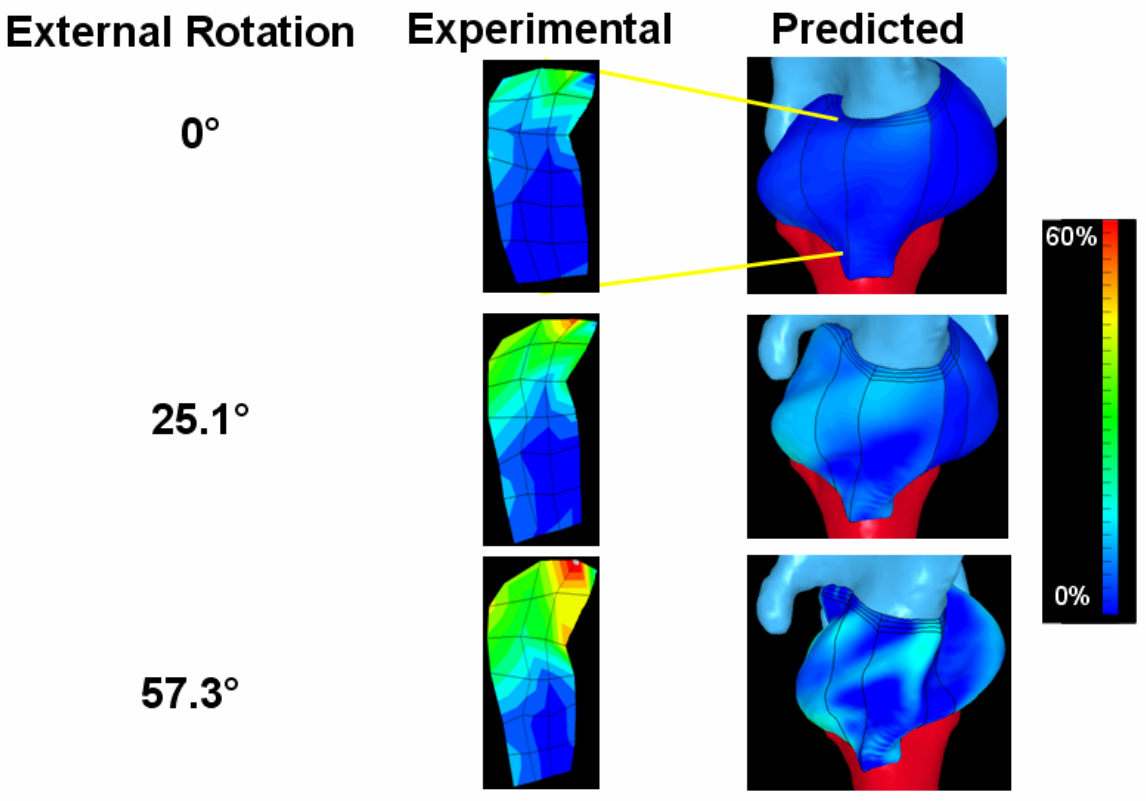

Figure 5.14 Inferior views of experimental and predicted strains in the anterior band of the inferior glenohumeral ligament (right shoulder), at the three clinically relevant joint positions for validation

Table 5.8 FE Model 2 experimental and predicted strains in the anterior band of the inferior glenohumeral ligament, at the three clinically relevant joint positions for validation

	Experimental and Predicted AB-IGHL Strains (%)								
	0° ER			25.1° ER			57.3° ER		
Element	Exp.	Pred.	Diff.	Exp.	Pred.	Diff.	Exp.	Pred.	Diff.
1	19	3	-16	36	10	-26	38	9	-29
2	17	3	-14	38	10	-27	40	6	-34
3	7	3	-4	26	10	-16	29	7	-22
4	9	3	-6	11	9	-1	15	9	-6
5	5	3	-2	11	8	-3	13	7	-6
6	1	2	2	10	5	-4	12	8	-4
7	22	3	-19	30	9	-21	33	7	-26
8	7	3	-3	11	10	-1	14	4	-10
9	0	4	4	2	10	8	5	7	2
10	0	4	4	0	9	9	2	9	7
11	0	3	3	0	7	7	3	6	3
12	0	3	3	0	5	5	0	2	2
13	26	3	-23	40	10	-30	39	3	-36
14	22	4	-18	30	10	-20	35	4	-31
15	5	4	-1	11	10	-1	5	8	4
16	0	4	4	5	9	4	3	10	8
17	0	3	3	0	6	6	4	4	1
18	5	2	-3	0	4	4	0	0	0
AVE	**8.0**	**3.2**	**-4.9**	**14.4**	**8.4**	**-6.0**	**16.1**	**6.2**	**-9.9**
SD	**9.0**	**0.5**	**9.0**	**14.6**	**2.1**	**13.3**	**15.2**	**2.8**	**15.3**

5.4.2 FE Model 2 Modification

In order to validate FE Model 2, a sensitivity study was performed involving evaluation of the magnitude and distribution of strain in the capsule after a series of modifications were made to the model, focusing on modifications of the labrum thickness taper, the thickness of the capsule, and the material coefficients of the capsule regions. For simplification of the sensitivity study, the modifications were initially evaluated at the clinically relevant joint position with 25.1° of external rotation. Modifications were then evaluated at the clinically relevant joint positions

with 0° and 57.3° of external rotation only if changes in the magnitude and distribution of strain in the capsule were found at the clinically relevant join position with 25.1° of external rotation.

When developing FE Model 2, the presence of a glenoid labrum was simulated by tapering the shell element thickness from 6.0 mm at the interface of the labrum with the glenoid down to 3.0 mm at the interface of the labrum with the capsule. The labrum thickness sensitivity study performed in Section 3.3.2.1 with FE Model 1 demonstrated that lowering the thickness of the labrum elements resulted in increased strain in the capsule. Since FE Model 1 was able to be validated with a labrum thickness taper from 3.0 mm at the interface of the labrum with the glenoid down to 2.0 mm at the interface of the labrum with the capsule, the labrum taper in FE Model 2 was changed to 4.0 mm at the interface of the labrum with the glenoid down to 3.0 mm at the interface of the labrum with the capsule. This had essentially no effect on the magnitude and distribution of strain in the capsule at the clinically relevant joint position with 25.1° of external rotation (Figure 5.15). Attempts were then made with labrum tapers from 7.0 mm and 9.0 mm at the glenoid down to 3.0 mm at the capsule, however the model was unable to run due to inversion of the insertion site elements. Therefore, it was decided to proceed with additional model modifications to achieve validation.

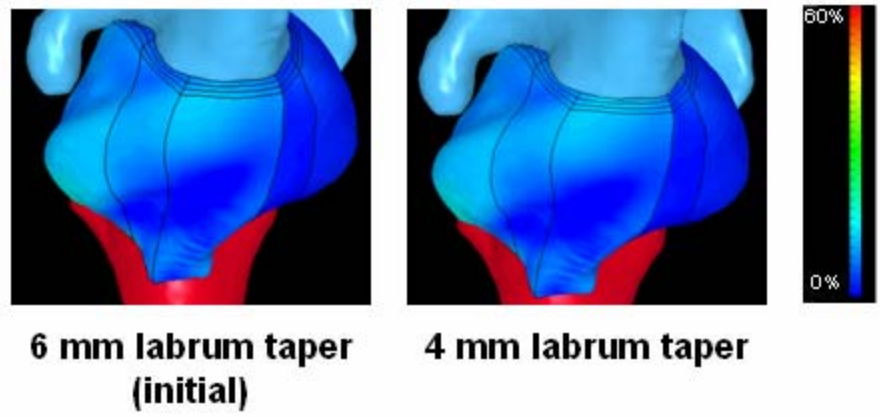

Figure 5.15 Inferior views of FE Model 2 (right shoulder) at the clinically relevant joint position with 25.1° of external rotation with modification of the simulated labrum. There were little if any qualitative differences when the labrum taper was decreased from 6.0 mm to 4.0 mm at the interface with the glenoid

The capsule shell element thickness was then modified. Since FE Model 1 was successfully validated with a uniform capsule thickness of 2.0 mm, the capsule thickness in FE Model 2 was decreased from 3.0 mm to 2.5 mm. This had essentially no effect on the magnitude and distribution of strain in the capsule at the clinically relevant joint position with 25.1° of external rotation (Figure 5.16). Attempts were then made to increase the capsule thickness to 3.5 mm, however the model was unable to converge due to inversion of capsule elements. Therefore, it was decided to proceed with additional model modifications to achieve validation.

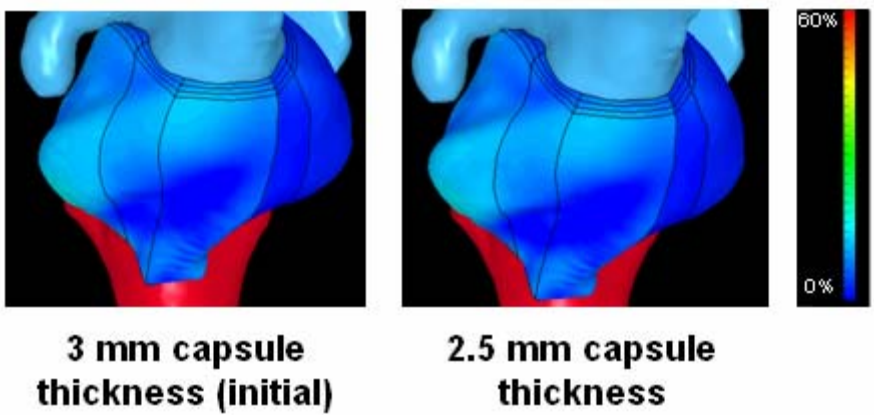

Figure 5.16 Inferior views of FE Model 2 (right shoulder) at the clinically relevant joint position with 25.1° of external rotation with modification of the capsule thickness. There were little if any qualitative differences when the capsule thickness was decreased from 3.0 mm to 2.0 mm

The capsule material coefficients were then modified. A study performed within our research group [112] demonstrated that predictions of strain in the anterior-inferior capsule were highly sensitive to changes in bulk/shear ratio in the capsule tissue. The finite element model in this previous study used an isotropic hypoelastic constitutive model to represent the capsule, however it was decided to determine the effects of modifying the bulk modulus in FE Model 2 when using an isotropic hyperelastic constitutive model to represent the capsule. A bulk

modulus value of 75 was initially used for each capsule region, however the bulk modulus used to generate the optimized load-elongation curves in Section 5.3.3 was often an order of magnitude greater than this value. Modifications were therefore made that involved changing the bulk modulus to 150, 500, or 1000 in each capsule region. These modifications had essentially no effect on the magnitude and distribution of strain in the capsule at the clinically relevant joint position with 25.1° of external rotation (Figure 5.17), which may have been a result of the constitutive model used to represent the tissue. Therefore, it was decided to proceed with additional model modifications to achieve validation.

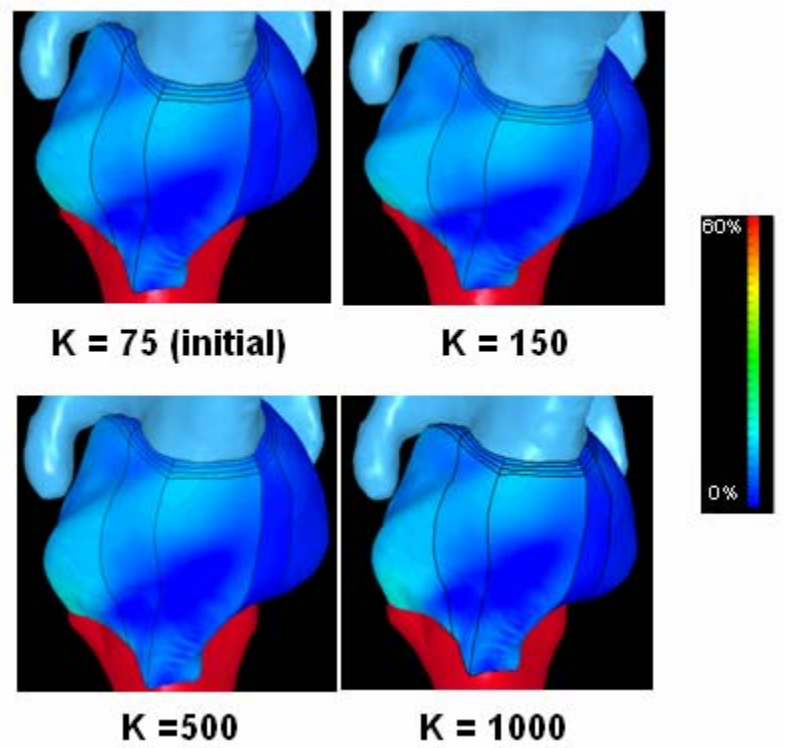

Figure 5.17 Inferior views of FE Model 2 (right shoulder) at the clinically relevant joint position with 25.1° of external rotation with modification of the capsule bulk modulus. There were little if any qualitative differences when the bulk modulus was changed to 150, 500, or 1000

The material coefficient values of C1 and C2 for the capsule regions were then modified. The goal of the material coefficient modification was to change the stiffening response of the capsule in order to change the magnitude and distribution of strain in the capsule. It was found through a brief sensitivity study that scaling the values of C1 and C2 was sufficient to change the stiffening response of the Cauchy stress-stretch curve, without compromising the non-linearity of the Cauchy stress-stretch curve. The latter finding was significant since before the brief sensitivity study was performed, it was unclear whether scaling the C1 and C2 values for each region would result in an increase or decrease in the non-linear stiffening response of the Veronda-Westmann isotropic hyperelastic constitutive model.

The optimized load-elongation curves in Section 5.3.3 suggested that the predicted stiffening response for the capsule regions may be overestimated in the toe-regions of the

optimized load-elongation curves, thus causing a potential underestimate of capsule strain when the capsule regions were loaded into their toe-regions. Therefore, a modification was made to scale the values of C1 and C2 in each capsule region by a factor of 0.5X. For additional evaluation modifications were also made to scale the values of C1 and C2 in each capsule region by a factor of 1.5X and 2X. These modifications had essentially no effect on the magnitude and distribution of strain in the capsule at the clinically relevant joint position with 25.1° of external rotation (Figure 5.18). Stress in the capsule was found to change by an order of magnitude with the variations in material coefficients, which was to be expected with the changes in the material coefficients. The magnitude and distribution of strain in the capsule, however, was relatively unchanged, which may be due to the displacement-driven nature of the joint motions. Without changing the relative magnitudes of the material coefficients in a capsule region with respect to the material coefficients in neighboring capsule regions, the magnitude and distribution of strains in the capsule may be unaffected when driving motions with displacement of the humerus with respect to the scapula.

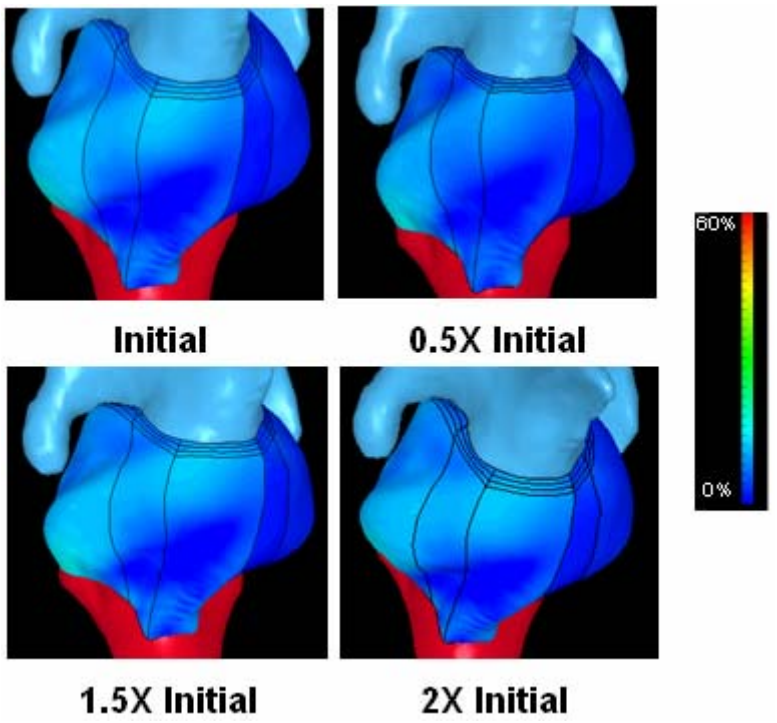

Figure 5.18 Inferior views of FE Model 2 (right shoulder) at the clinically relevant joint position with 25.1° of external rotation with modification of the capsule material coefficients. There were little if any qualitative differences in the magnitude and distribution of strain in the capsule when the values of C1 and C2 were scaled by 0.5X, 1.5X, or 2X of the initial values of C1 and C2

Since uniform modification of the material coefficients proved ineffective, the material coefficients were then modified on a region-specific basis. As a proof-of-concept, the values of C1 and C2 in the anterosuperior region and the axillary pouch were increased from their initial values (Section 5.3.3) to 1 and 15, respectively, while the values in the anterior band of the inferior glenohumeral ligament were decreased from their initial values to 0.05 and 0.5, respectively. It was found that this modification resulted in a drastic change in the magnitude and distribution of strain in the anterior-inferior capsule, as well as the shape of the anterior-inferior capsule (Figure 5.19). It was thus concluded that decreasing the material coefficients in a capsule region with respect to its neighboring capsule regions may result in an increase in strain in that capsule region.

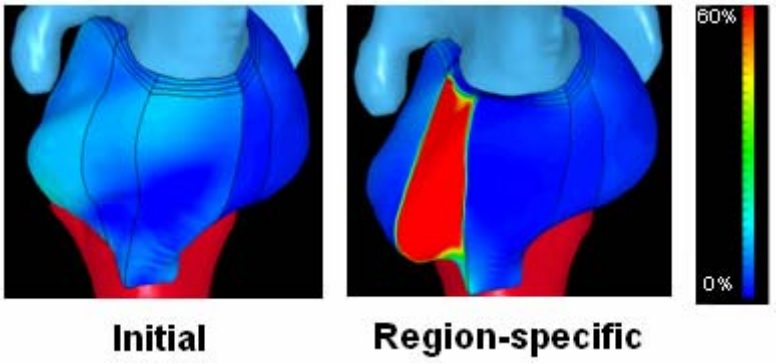

Figure 5.19 Inferior views of FE Model 2 (right shoulder) at the clinically relevant joint position with 25.1° of external rotation with region-specific modification of the capsule material coefficients. There was significant change in the magnitude and distribution of strain in the anterior-inferior capsule following the modification

A series of region-specific material coefficient modifications was then made in which manual adjustments to the C1 and C2 values in the capsule regions was performed until validation was achieved in each of the three clinically relevant joint positions with 0°, 25.1°, and 57.3° of external rotation. Attempts were made to modify as few capsule regions as possible so as to maintain as much subject-specificity in the model as possible. Furthermore, changes in the capsule regions were kept to an order of magnitude or less with respect to the initial material coefficients, in an additional attempt to maintain subject-specificity in the model. Modifications involved decreasing the material coefficients in certain capsule regions, in light of the overestimation of the toe-region stiffening response in the optimized load-elongation curves using the Veronda-Westmann isotropic hyperelastic constitutive model (Section 5.3.3). Using these criteria, an optimal modification of the capsule region material coefficients was determined that involved changing the material coefficients of the anterior band of the inferior glenohumeral ligament and the axillary pouch only, decreasing the values of C1 and C2 by a factor of 2 so that their new values were 0.06 and 2.7, respectively. The material coefficients in the remaining capsule regions were left unchanged. This modification resulted in a significant change in strain in the anterior-inferior capsule in each of the three clinically relevant joint positions with 0°,

25.1°, and 57.3° of external rotation (Figure 5.20). At each of the three clinically relevant joint positions the magnitude of strain in the anterior-inferior capsule increased. It appeared that the relative distribution of strain in the anterior-inferior capsule did not change, as when using either the initial material coefficients or the optimal region-specific material coefficients strains were highest in the anterior band of the inferior glenohumeral ligament and the axillary pouch. The shape of the capsule remained unchanged in the clinically relevant joint positions with 0° and 25.1° of external rotation, however for the clinically relevant joint position with 57.3° of external rotation the use of optimal region-specific material coefficients appeared to increase folding of the axillary pouch and posterior band of the inferior glenohumeral ligament

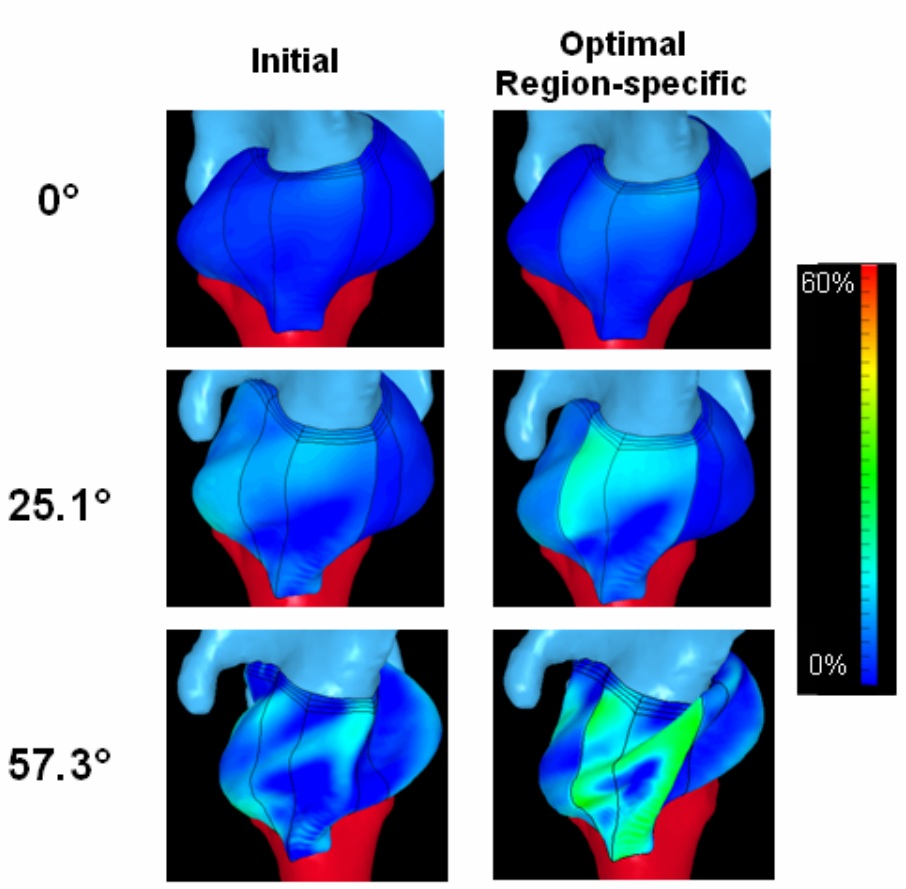

Figure 5.20 Inferior views of FE Model 2 (right shoulder) at the clinically relevant joint positions with 0°, 25.1°, and 57.3° of external rotation, using initial material coefficients and the optimal region-specific material coefficients

5.4.3 FE Model 2 Validation

Predicted strains in FE Model 2 using the optimal region-specific material coefficient modification from Section 5.4.2 were then compared to the experimental strains at the clinically relevant joint positions with 0°, 25.1°, and 57.3° of external rotation, for validation of FE Model 2. Relative to the fringe plot comparisons in Section 5.4.1, the predicted strains more closely approximated the experimental strains in the anterior band of the inferior glenohumeral ligament (Figure 5.21). This is additionally confirmed quantitatively when comparing the average predicted and experimental strain magnitudes in the anterior band of the inferior glenohumeral ligament (Table 5.9). The average difference between the predicted and experimental strains at the clinically relevant joint positions with 0°, 25.1°, and 57.3° of external rotation was -2.8%, 0.5%, and 0.6% strain, respectively, all within the validation criteria of an average strain difference less than or equal to ±3.5% strain. Therefore, FE Model 2 was determined to be validated at the three clinically relevant joint positions using the slight modification to the material coefficients in the anterior band of the inferior glenohumeral ligament and the axillary pouch. It is worth noting that while differences in the average predicted and experimental strain magnitudes in the anterior band of the inferior glenohumeral ligament were within the validation threshold of ±3.5% strain, differences in predicted and experimental strain magnitudes within the 18 individual validation elements were rarely within the validation threshold of ±3.5% strain (Table 5.9). This would indicate that the predictive capability of FE Model 2 is suitable when analyzing predicted strain over regions of the anterior-inferior capsule, but not suitable if attempting to perform point-by-point analyses of predicted strain in the anterior-inferior capsule. The implications of this limitation are discussed further in the Discussion section (Section 6.0).

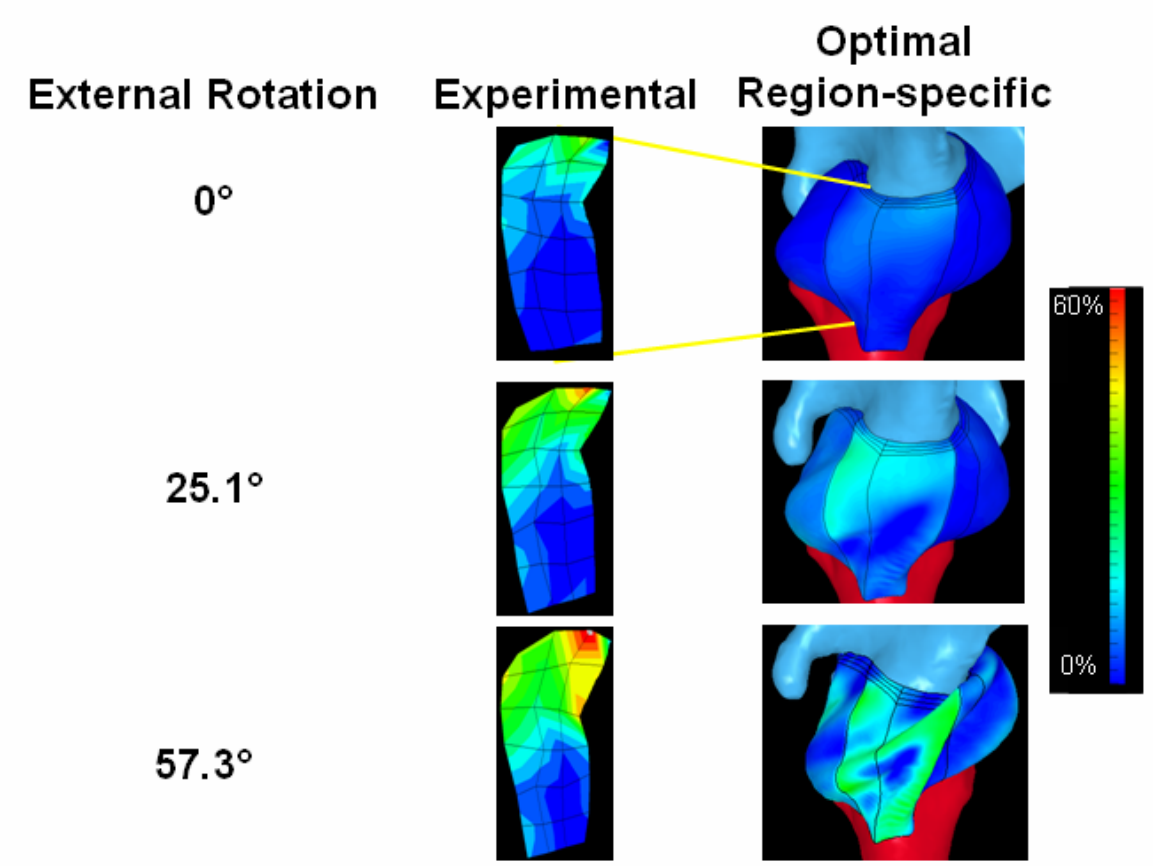

Figure 5.21 Inferior views of experimental and predicted strains in the anterior band of the inferior glenohumeral ligament (right shoulder), at the clinically relevant joint positions with 0°, 25.1°, and 57.3° of external rotation

Table 5.9 FE Model 2 experimental and predicted strains in the anterior band of the inferior glenohumeral ligament, at the three clinically relevant joint positions for validation

Experimental and Predicted AB-IGHL Strains (%)									
	0° ER			25.1° ER			57.3° ER		
Element	Exp.	Pred.	Diff.	Exp.	Pred.	Diff.	Exp.	Pred.	Diff.
1	19	2	-17	36	16	-20	38	16	-22
2	17	4	-14	38	16	-21	40	12	-28
3	7	5	-2	26	16	-10	29	13	-16
4	9	5	-4	11	16	5	15	20	5
5	5	5	0	11	16	5	13	23	9
6	1	4	4	10	12	3	12	25	13
7	22	5	-17	30	19	-11	33	19	-14
8	7	6	-1	11	17	6	14	14	1
9	0	6	6	2	16	14	5	13	7
10	0	6	6	0	15	15	2	19	17
11	0	6	6	0	14	14	3	20	17
12	0	5	5	0	11	11	0	16	16
13	26	7	-19	40	17	-22	39	16	-24
14	22	7	-15	30	16	-14	35	14	-21
15	5	7	2	11	15	4	5	15	10
16	0	6	6	5	13	8	3	20	17
17	0	5	5	0	11	11	4	19	15
18	5	4	-1	0	9	9	0	9	9
AVE	**8.0**	**5.3**	**-2.8**	**14.4**	**14.8**	**0.5**	**16.1**	**16.7**	**0.6**
SD	**9.0**	**1.3**	**9.2**	**14.6**	**2.5**	**13.0**	**15.2**	**4.1**	**16.4**

The predicted shape of the capsule was also compared with the shape of the capsule seen experimentally at the equivalent clinically relevant joint position. For the clinically relevant joint positions with 0° and 31.1° of external rotation, the predicted and experimental shape of the deformed capsule tissue appeared similar. For the clinically relevant joint position with 51.8° of external rotation, however, the predicted and experimental shape of the deformed capsule tissue did not appear similar in the axillary pouch (Figure 5.22). The predicted shape of the axillary pouch appeared to project outwards away from the humerus, whereas the experimental shape of the axillary pouch collapsed inwards. This may have resulted from the lack of a gravity boundary condition applied in FE Model 2, which may have changed the folding patterns and thus the distribution of strain in the axillary pouch. While FE Model 2 was validated at the

clinically relevant joint positions with 0°, 25.1°, and 57.3° of external rotation, it may be important to note that the strains in the axillary pouch at joint positions with relatively high external rotation may be overestimates of the experimental strain in the axillary pouch.

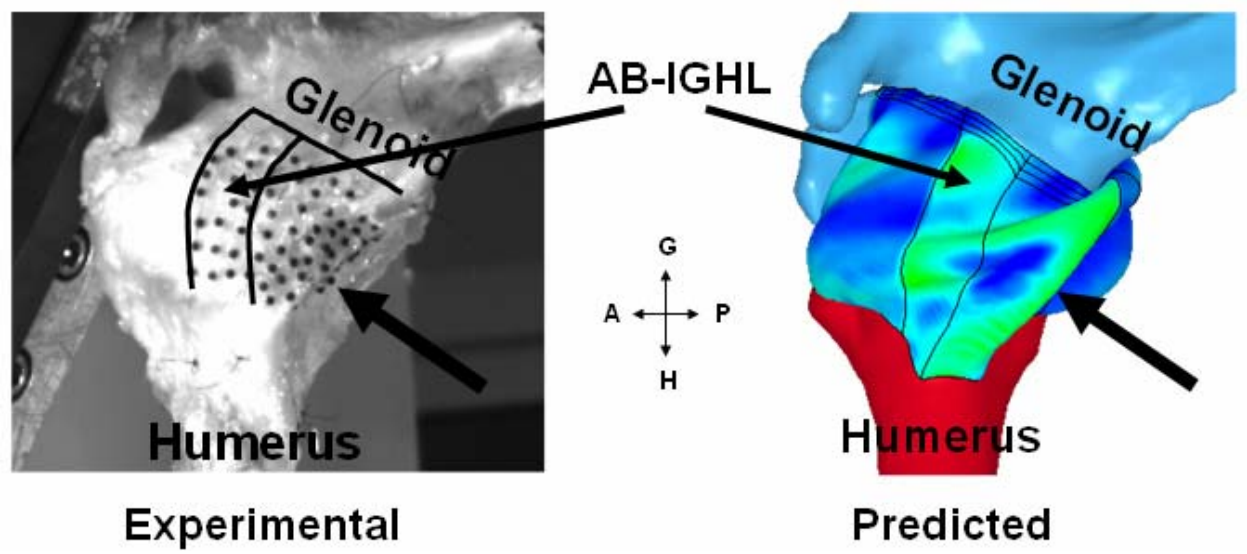

Figure 5.22 Comparisons of experimental and predicted shape of the capsule for FE Model 2 (right shoulder), at the clinically relevant joint position with 57.3° of external rotation. The anterior band of the inferior glenohumeral ligament is outlined in black. The large black arrows indicate discrepancies in the predicted and experimental shape of the axillary pouch

5.5 ANALYSIS OF JOINT POSITIONS

5.5.1 Joint Positions with Consistent Strain Distributions

Qualitative analysis of the distribution of strain in the anterior-inferior capsules of FE Model 1 and FE Model 2 at the six clinically relevant joint positions evaluated (Table 4.5) suggests that the distribution of strain in the anterior-inferior capsule is most consistent at the clinically relevant joint positions with 10°, 20°, and 30° of external rotation relative to the clinically

relevant joint positions with 0°, 40°, and 50° of external rotation (Figure 5.23). Quantitative analysis of the strain ratios in the sub-regions of FE Model 1 and FE Model 2 indicate that the clinically relevant joint positions with 10°, 20°, 30°, and 40° of external rotation all had r^2 values greater than 0.7, indicating high correlation of the distribution of strain in the anterior-inferior capsule in FE Model 1 and FE Model 2 (Figure 5.24).

The maximum sub-region strain in FE Model 1 occurred in the glenoid side of the anterior band of the inferior glenohumeral ligament at the joint position with 50° of external rotation, measuring 36.6% strain. The maximum sub-region strain in FE Model 2 also occurred in the glenoid side of the anterior band of the inferior glenohumeral ligament at the joint position with 50° of external rotation, measuring 21.7% strain. A value of 7% strain corresponded to ratio values of 0.19 and 0.32 for FE Model 1 and FE Model 2, respectively. When examining the ratios in the sub-regions of each model at these joint positions, it was found that both FE Model 1 and FE Model 2 had at least one sub-region with a strain ratio value above 0.19 and 0.32, respectively, at each of the four joint positions (Table 5.10 and Table 5.11, respectively). Therefore, it was determined that the clinically relevant joint positions with 10°, 20°, 30°, and 40° of external rotation had consistent distribution of strain among the anterior-inferior capsules of FE Model 1 and FE Model 2, and resulted in at least one sub-region having average strain more than double the experimental strain repeatability of ±3.5% strain.

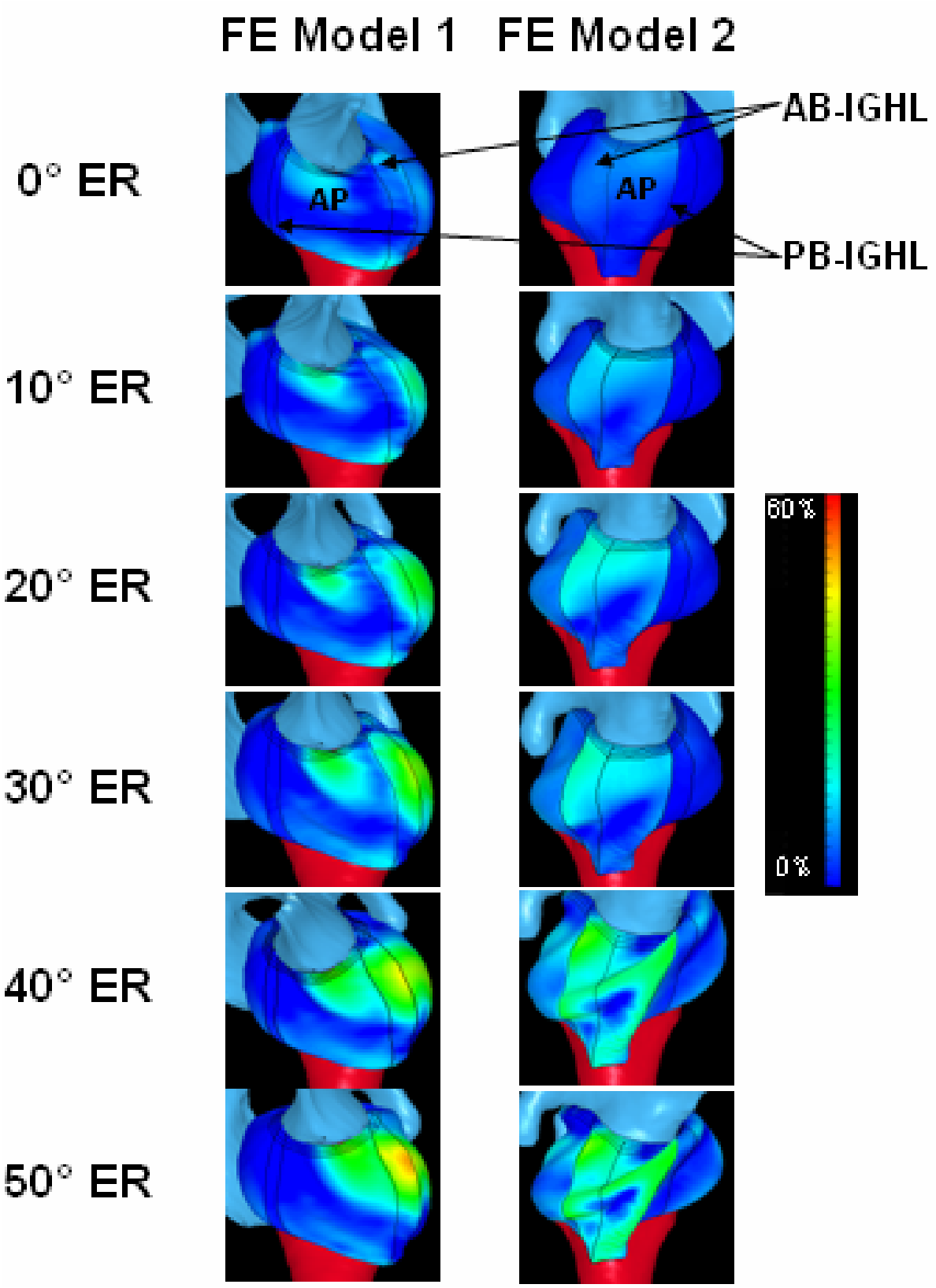

Figure 5.23 Inferior views of the distribution of strain in the anterior-inferior capsule in FE Model 1 (left) and FE Model 2 (right) at the six clinically relevant joint positions

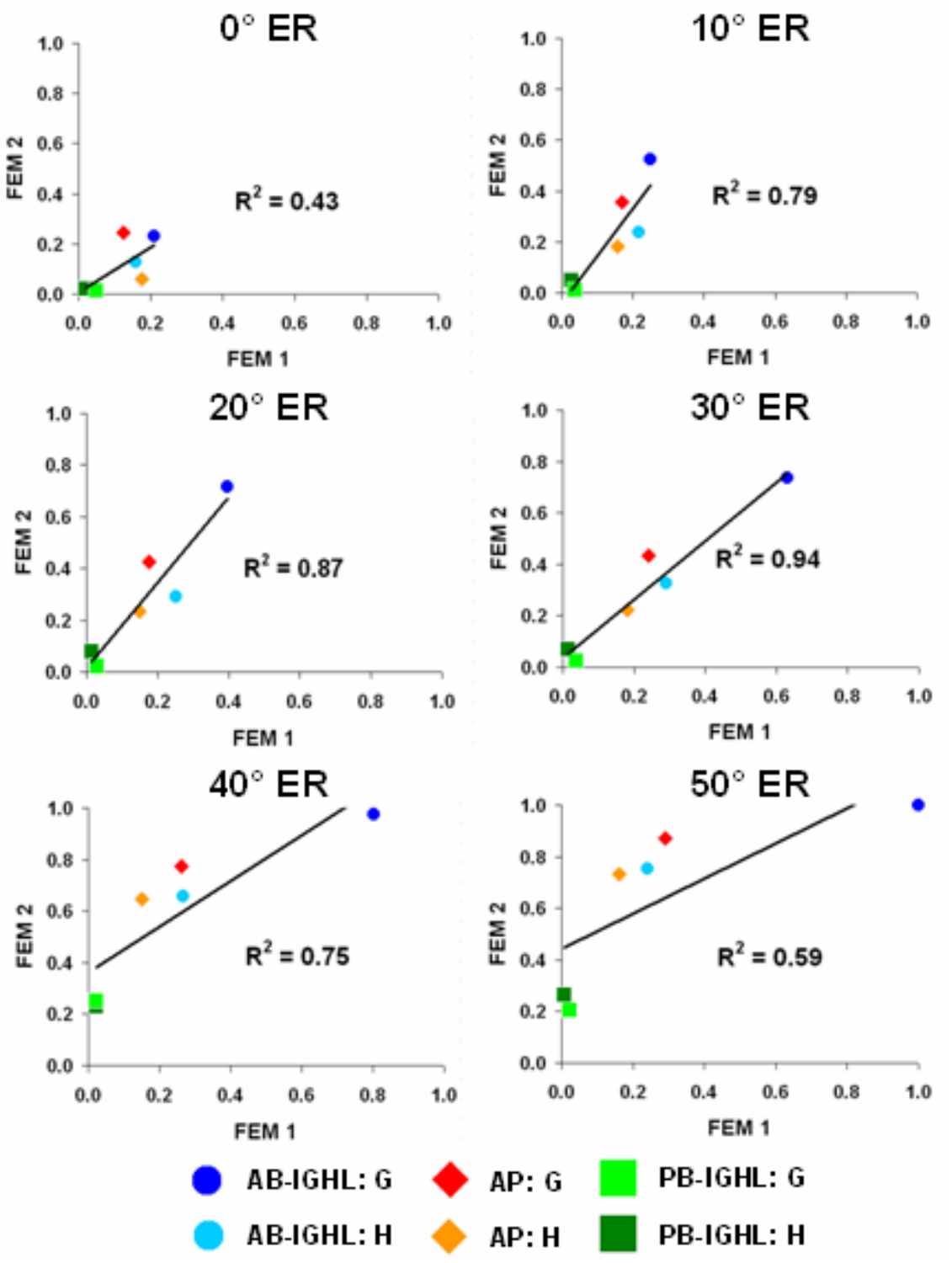

Figure 5.24 Correlation of strain ratios in the sub-regions of the anterior-inferior capsule of FE Model 2 vs. FE Model 1, at each of the six clinically relevant joint positions. r2 > 0.7 indicates high correlation between the distribution of strain in the anterior-inferior capsule in FE Model 1 and FE Model 2. AB-IGHL: G, AB-IGHL: H = glenoid and humeral sides of the anterior band of the inferior glenohumeral ligament. AP: G, AP: H = glenoid and humeral sides of the axillary pouch. PB-IGHL: G, PB-IGHL: H = glenoid and humeral sides of the posterior band of the inferior glenohumeral ligament

Table 5.10 FE Model 1 strain ratios in the six sub-regions, at the four clinically relevant joint positions with an r^2 value greater than 0.7

	Ratio at Joint Positions, FE Model 1			
	10° ER	20° ER	30° ER	40° ER
AB-IGHL: G	0.25	0.40	0.63	0.80
AB-IGHL: H	0.22	0.25	0.29	0.27
AP: G	0.17	0.18	0.24	0.26
AP: H	0.16	0.15	0.18	0.15
PB-IGHL: G	0.03	0.02	0.01	0.02
PB-IGHL: H	0.04	0.03	0.04	0.02

Table 5.11 FE Model 2 strain ratios in the six sub-regions, at the four clinically relevant joint positions with an r^2 value greater than 0.7

	Ratio at Joint Positions, FE Model 2			
	10° ER	20° ER	30° ER	40° ER
AB-IGHL: G	0.52	0.72	0.74	0.98
AB-IGHL: H	0.24	0.29	0.33	0.66
AP: G	0.36	0.43	0.43	0.77
AP: H	0.18	0.23	0.22	0.65
PB-IGHL: G	0.05	0.08	0.07	0.23
PB-IGHL: H	0.01	0.02	0.02	0.25

5.5.2 Localization of Stability at Clinically Relevant Joint Positions

The strains in the six sub-regions of FE Model 1 and FE Model 2 were determined at the clinically relevant joint positions with 10°, 20°, 30°, and 40° of external rotation (Figure 5.25, Figure 5.26, Figure 5.27, and Figure 5.28, respectively).

5.5.2.1 Joint position with 10° of external rotation

In FE Model 1, strains in the glenoid and humeral sides of the anterior band of the inferior glenohumeral ligament and the axillary pouch were significantly higher than strains in the glenoid and humeral sides of the posterior band of the inferior glenohumeral ligament. However, there were no other significant differences among the sub-regions.

In FE Model 2, strain in the glenoid side of the anterior band of the inferior glenohumeral ligament was significantly higher than strains in the remaining five sub-regions, by at least 3.6% strain. Strain in the humeral side of the anterior band of the inferior glenohumeral ligament was significantly higher than strains in the glenoid and humeral sides of the posterior band of the inferior glenohumeral ligament. Strain in the glenoid side of the axillary pouch was significantly higher than strains in the humeral side of the axillary pouch and the glenoid and humeral sides of the posterior band of the inferior glenohumeral ligament. Strain in the humeral side of the axillary pouch was significantly higher than strain in the humeral side of the posterior band of the inferior glenohumeral ligament.

While significant differences in strain were present among sub-regions in both models at the clinically relevant joint position with 10° of external rotation, there was not a single sub-region that in both FE Model 1 and FE Model 2 had significantly higher strain than the five other sub-regions. Therefore, the clinically relevant joint position with 25 N of anterior load applied at 60° of glenohumeral abduction and 10° of external rotation may not allow clinicians to localize pathology within the anterior-inferior capsule among patients.

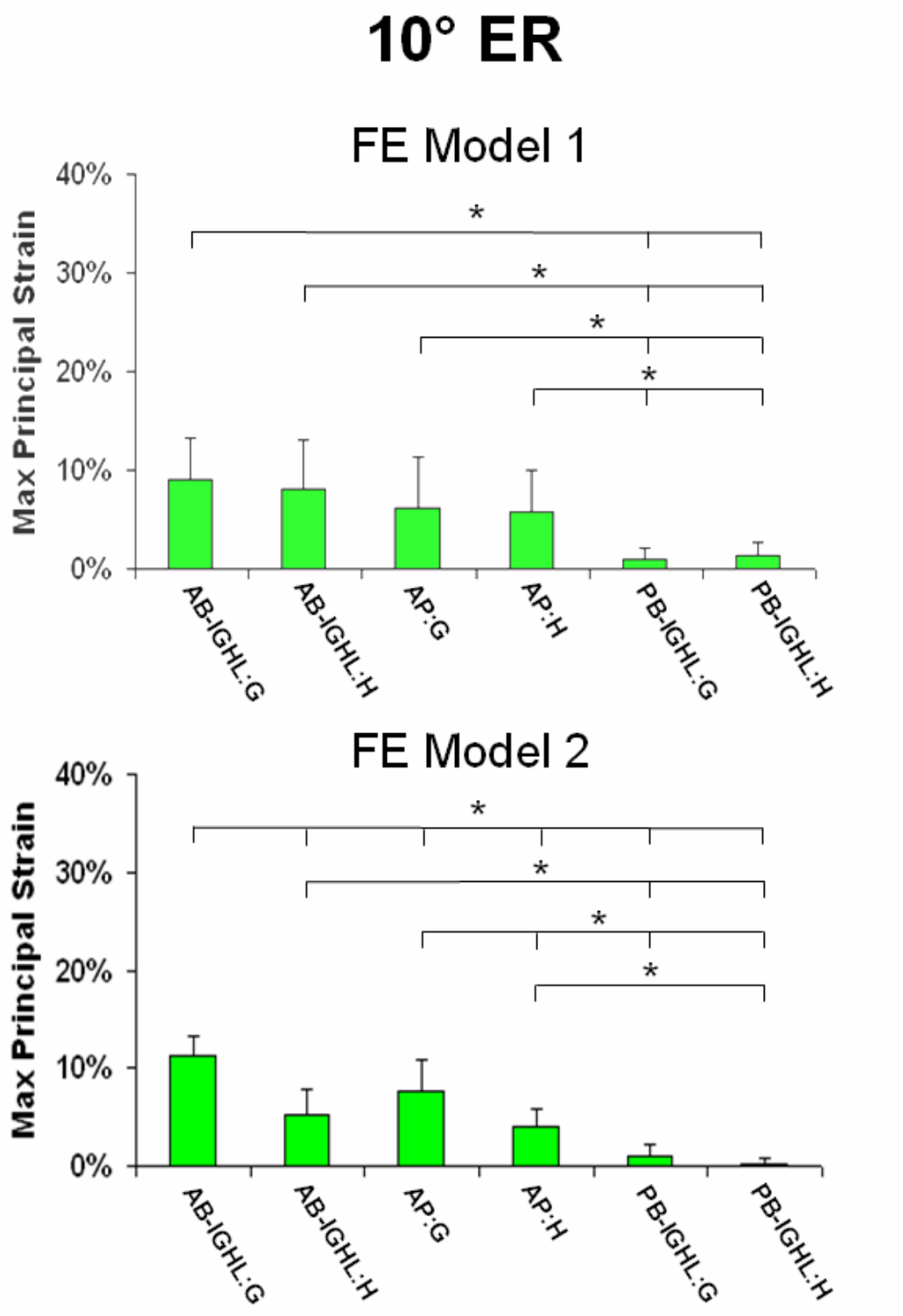

Figure 5.25 Strains in the six sub-regions of FE Model 1 and FE Model 2, at the clinically relevant joint position with 10° of external rotation. AB-IGHL: G, AB-IGHL: H = glenoid and humeral sides of the anterior band of the inferior glenohumeral ligament, AP: G, AP: H = glenoid and humeral sides of the axillary pouch, PB-IGHL: G, PB-IGHL: H = glenoid and humeral sides of the posterior band of the inferior glenohumeral ligament

5.5.2.2 Joint position with 20° of external rotation

In FE Model 1, strain in the glenoid side of the anterior band of the inferior glenohumeral ligament was significantly higher than strains in the remaining five sub-regions, by at least 5.3% strain. Strain in the humeral side of the anterior band of the inferior glenohumeral ligament was significantly higher than strains in the humeral side of the axillary pouch and the glenoid and humeral sides of the posterior band of the inferior glenohumeral ligament. Strains in the glenoid and humeral sides of the axillary pouch were significantly higher than strains in the glenoid and humeral sides of the posterior band of the inferior glenohumeral ligament.

In FE Model 2, strain in the glenoid side of the anterior band of the inferior glenohumeral ligament was significantly higher than strains in the remaining five sub-regions, by at least 6.3% strain. Strain in the humeral side of the anterior band of the inferior glenohumeral ligament was significantly higher than strains in the glenoid and humeral sides of the posterior band of the inferior glenohumeral ligament. Strain in the glenoid side of the axillary pouch was significantly higher than strains in the humeral side of the axillary pouch and the glenoid and humeral sides of the posterior band of the inferior glenohumeral ligament. Strain in the humeral side of the axillary pouch was significantly higher than strain in the humeral side of the posterior band of the inferior glenohumeral ligament.

The glenoid side of the anterior band of the inferior glenohumeral ligament had significantly higher strain than the remaining five sub-regions in both FE Model 1 and FE Model 2. Therefore, the clinically relevant joint position with 25 N of anterior load applied at 60° of glenohumeral abduction and 20° of external rotation may allow clinicians to localize pathology within the anterior-inferior capsule to the glenoid side of the anterior band of the inferior glenohumeral ligament among patients.

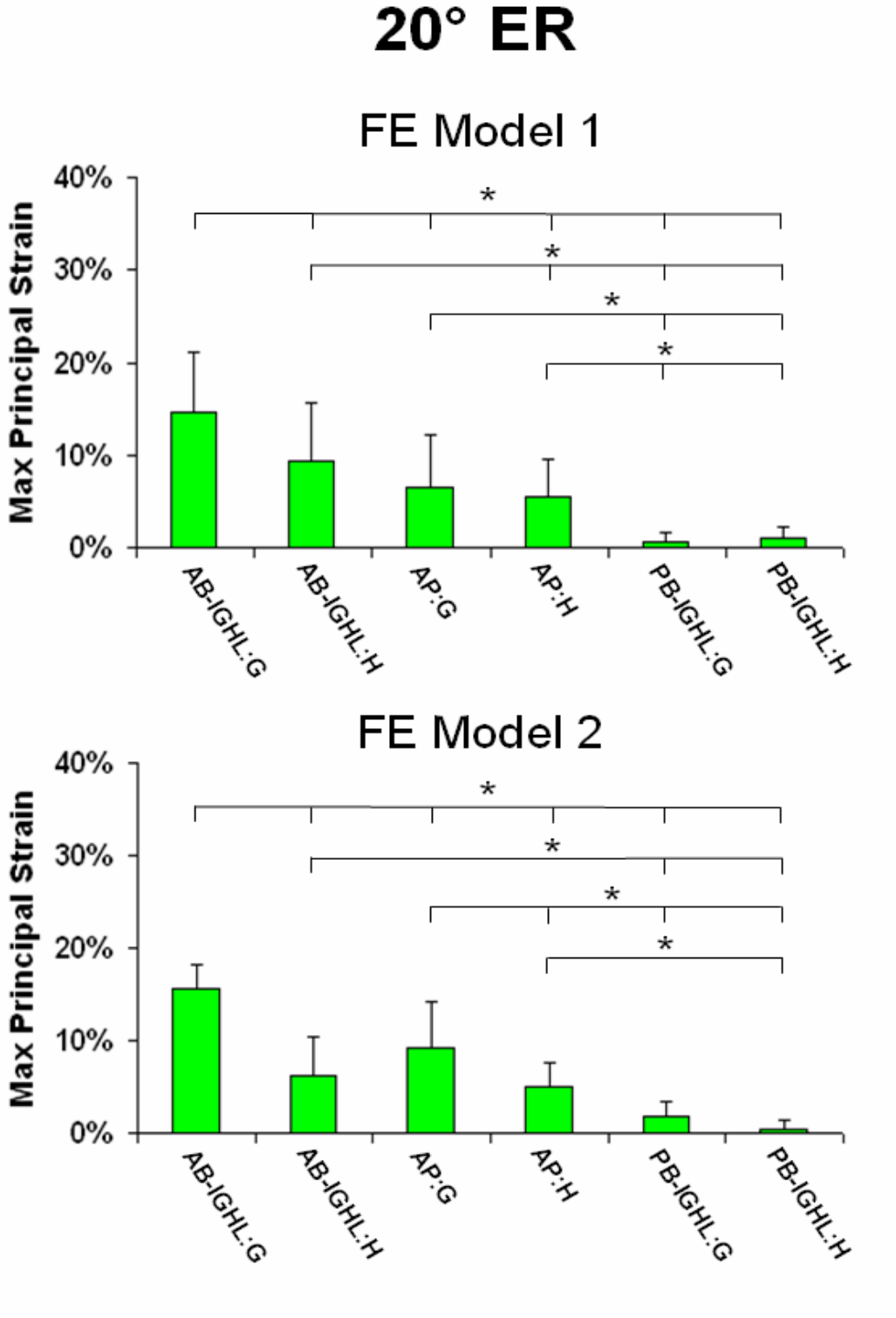

Figure 5.26 Strains in the six sub-regions of FE Model 1 and FE Model 2, at the clinically relevant joint position with 20° of external rotation. AB-IGHL: G, AB-IGHL: H = glenoid and humeral sides of the anterior band of the inferior glenohumeral ligament, AP: G, AP: H = glenoid and humeral sides of the axillary pouch, PB-IGHL: G, PB-IGHL: H = glenoid and humeral sides of the posterior band of the inferior glenohumeral ligament

5.5.2.3 Joint position with 30° of external rotation

In FE Model 1, strain in the glenoid side of the anterior band of the inferior glenohumeral ligament was significantly higher than strains in the remaining five sub-regions, by at least 12.5% strain. Strains in the humeral side of the anterior band of the inferior glenohumeral ligament and the glenoid and humeral sides of the axillary pouch were significantly higher than strains in the glenoid and humeral sides of the posterior band of the inferior glenohumeral ligament.

In FE Model 2, strain in the glenoid side of the anterior band of the inferior glenohumeral ligament was significantly higher than strains in the remaining five sub-regions, by at least 6.6% strain. Strain in the humeral side of the anterior band of the inferior glenohumeral ligament was significantly higher than strains in the glenoid and humeral sides of the posterior band of the inferior glenohumeral ligament. Strain in the glenoid side of the axillary pouch was significantly higher than strains in the humeral side of the axillary pouch and the glenoid and humeral sides of the posterior band of the inferior glenohumeral ligament. Strain in the humeral side of the axillary pouch was significantly higher than strains in the glenoid and humeral sides of the posterior band of the inferior glenohumeral ligament.

The glenoid side of the anterior band of the inferior glenohumeral ligament had significantly higher strain than the remaining five sub-regions in both FE Model 1 and FE Model 2. Therefore, the clinically relevant joint position with 25 N of anterior load applied at 60° of glenohumeral abduction and 30° of external rotation may allow clinicians to localize pathology within the anterior-inferior capsule to the glenoid side of the anterior band of the inferior glenohumeral ligament among patients.

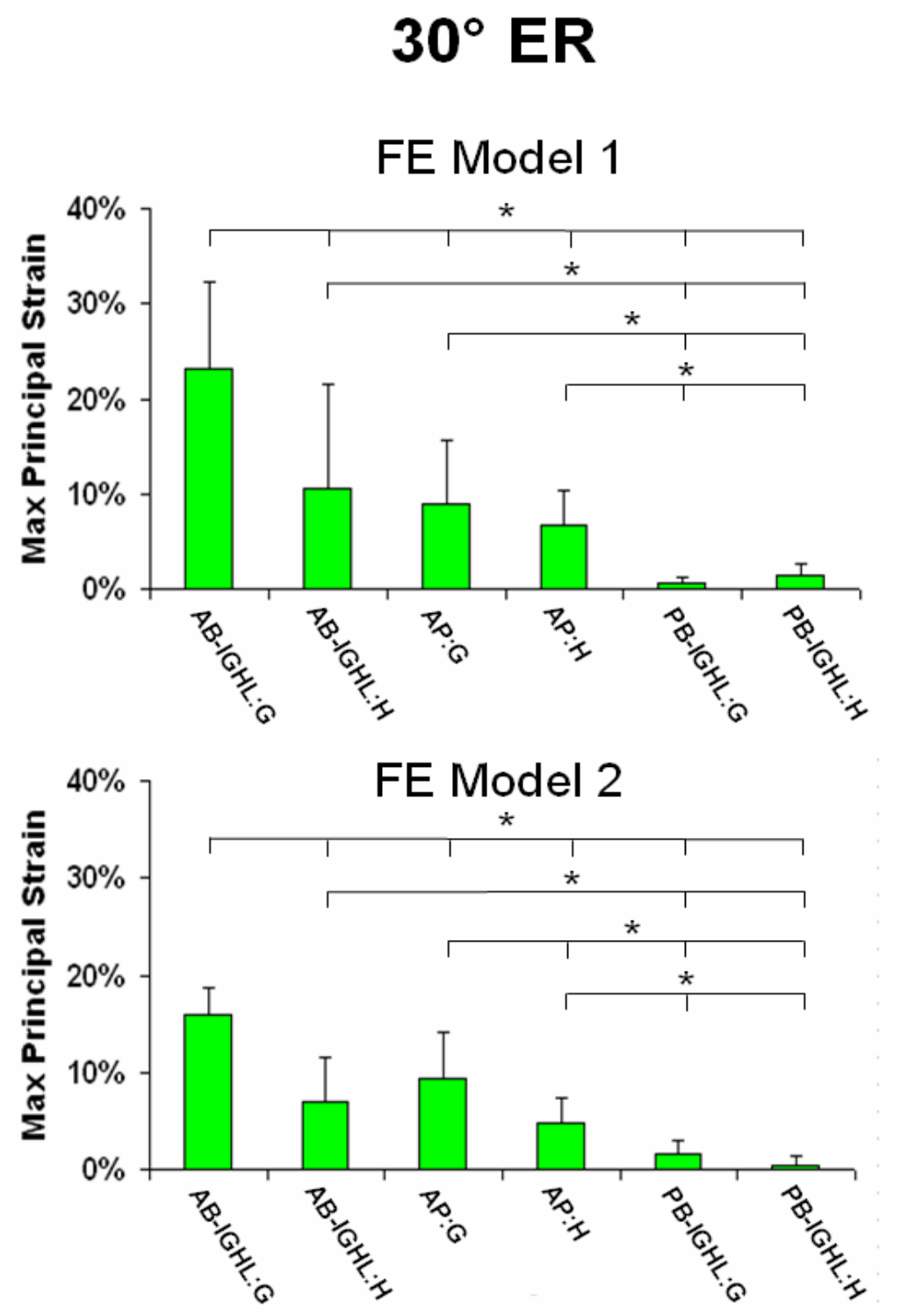

Figure 5.27 Strains in the six sub-regions of FE Model 1 and FE Model 2, at the clinically relevant joint position with 30° of external rotation. AB-IGHL: G, AB-IGHL: H = glenoid and humeral sides of the anterior band of the inferior glenohumeral ligament, AP: G, AP: H = glenoid and humeral sides of the axillary pouch, PB-IGHL: G, PB-IGHL: H = glenoid and humeral sides of the posterior band of the inferior glenohumeral ligament

5.5.2.4 Joint position with 40° of external rotation

In FE Model 1, strain in the glenoid side of the anterior band of the inferior glenohumeral ligament was significantly higher than strains in the remaining five sub-regions, by at least 19.6% strain. Strains in the humeral side of the anterior band of the inferior glenohumeral ligament and the glenoid side of the axillary pouch were significantly higher than strains in the glenoid and humeral sides of the posterior band of the inferior glenohumeral ligament. Strain in the humeral side of the axillary pouch was significantly higher than strains in the glenoid and humeral sides of the posterior band of the inferior glenohumeral ligament.

In FE Model 2, strain in the glenoid side of the anterior band of the inferior glenohumeral ligament was significantly higher than strains in the remaining five sub-regions, by at least 4.4% strain. Strains in the humeral side of the anterior band of the inferior glenohumeral ligament and the glenoid and humeral sides of the axillary pouch were significantly higher than strains in the glenoid and humeral sides of the posterior band of the inferior glenohumeral ligament.

The glenoid side of the anterior band of the inferior glenohumeral ligament had significantly higher strain than the remaining five sub-regions in both FE Model 1 and FE Model 2. Therefore, the clinically relevant joint position with 25 N of anterior load applied at 60° of glenohumeral abduction and 40° of external rotation may allow clinicians to localize pathology within the anterior-inferior capsule to the glenoid side of the anterior band of the inferior glenohumeral ligament among patients.

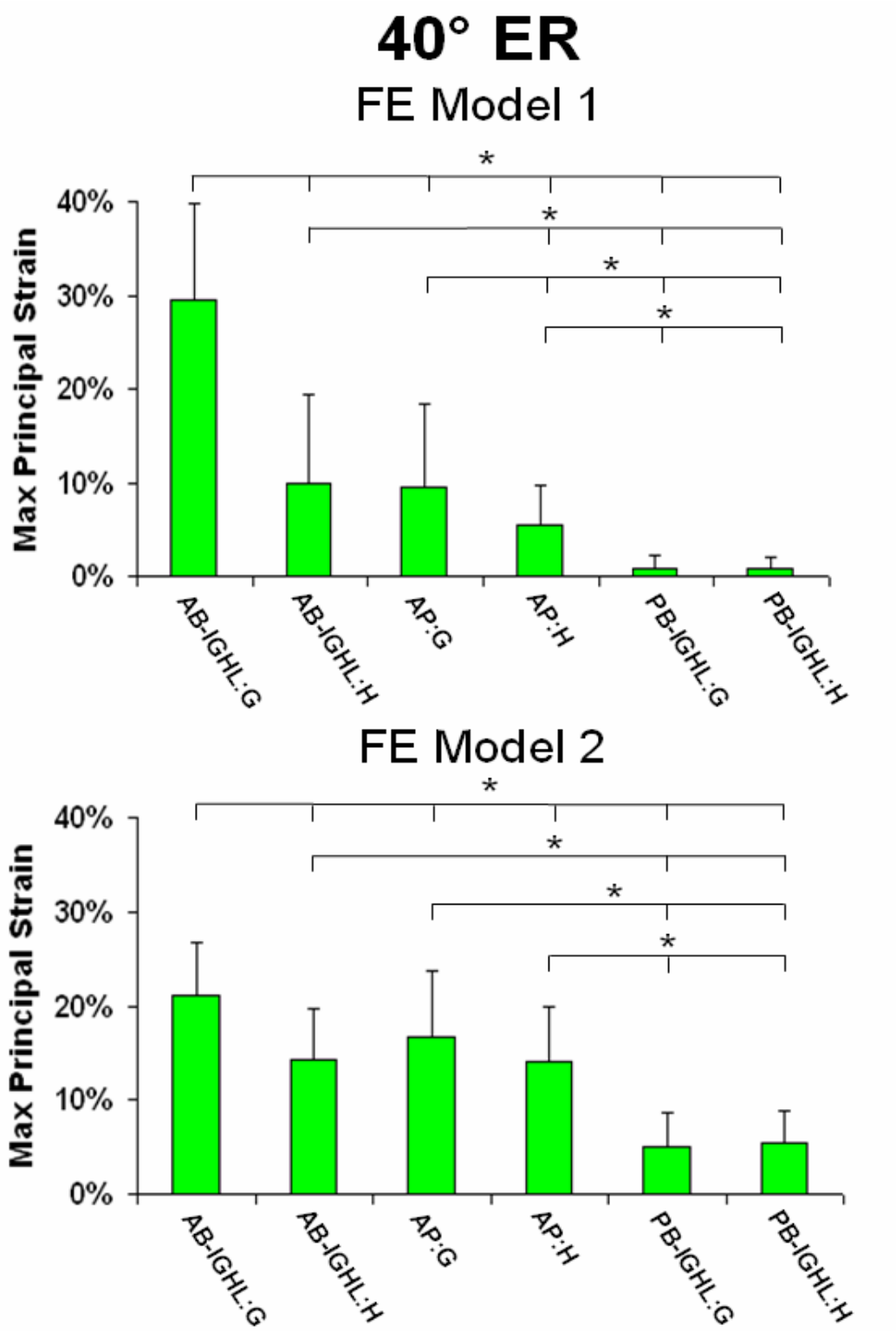

Figure 5.28 Strains in the six sub-regions of FE Model 1 and FE Model 2, at the clinically relevant joint position with 40° of external rotation. AB-IGHL: G, AB-IGHL: H = glenoid and humeral sides of the anterior band of the inferior glenohumeral ligament, AP: G, AP: H = glenoid and humeral sides of the axillary pouch, PB-IGHL: G, PB-IGHL: H = glenoid and humeral sides of the posterior band of the inferior glenohumeral ligament

5.5.2.5 Summary: Localization of Stability

In the clinically relevant joint positions with 20°, 30°, and 40° of external rotation, strain in the glenoid side of the anterior band of the inferior glenohumeral ligament was significantly higher than strains in the remaining five sub-regions of the anterior-inferior capsule, in both FE Model 1 and FE Model 2. Strain in the glenoid side of the anterior band of the inferior glenohumeral ligament was 14.5%, 23.1%, and 29.4% strain in FE Model 1 and 15.5%, 15.9%, and 21.2% strain in FE Model 2 at the clinically relevant joint positions with 20°, 30°, and 40° of external rotation, respectively (Table 5.12). This indicates that the stability provided by the glenoid side of the anterior band of the inferior glenohumeral ligament increases with external rotation in these clinically relevant joint positions. Furthermore, the minimum difference in strain between the glenoid side of the anterior band of the inferior glenohumeral ligament and the remaining five sub-regions generally increased with external rotation in these clinically relevant joint positions. This suggests that the relative contribution of the glenoid side of the anterior band of the inferior glenohumeral ligament to the stability provided by the anterior-inferior capsule increases with external rotation in these clinically relevant joint positions, with respect to the remaining five sub-regions of the anterior-inferior capsule.

Table 5.12 Magnitude (Ave ± SD) of strain in the glenoid side of the anterior band of the inferior glenohumeral ligament, as well as the minimum differences in strain when compared to the remaining five sub-regions, at the clinically relevant joint positions with 20°, 30°, and 40° of external rotation

	FE Model 1		FE Model 2	
	Magnitude (Ave ± SD)	Min. differerence from sub-regions	Magnitude (Ave ± SD)	Min. differerence from sub-regions
20° ER	14.5 ± 6.5%	5.3%	15.5 ± 2.7%	6.4%
30° ER	23.1 ± 9.2%	12.5%	15.9 ± 2.7%	6.6%
40° ER	29.4 ± 10.3%	19.6%	21.2 ± 5.7%	4.4%

6.0 DISCUSSION

Two validated, subject-specific finite element models of the glenohumeral joint were used to suggest clinically relevant joint positions where the distribution of load in the anterior-inferior capsule is consistent among subjects in response to anterior loading. An isotropic hyperelastic constitutive model was used to represent the capsule in each model, and distribution of strains on the surface of the anterior-inferior capsule was used as a measure of the distribution of load in the anterior-inferior capsule. The correlation of the distribution of strain between the two models was highest at joint positions with 10° - 40° of external rotation, with r^2 values greater than 0.7 in each position. In the joint positions with 20° - 40° of external rotation, however, strains were significantly higher in the glenoid side of the anterior band of the inferior glenohumeral ligament than in all other regions of the anterior-inferior capsule, suggesting that clinicians may be able to use these joint positions for effective diagnosis of pathology to the anterior-inferior capsule. The current work provides advancements in the areas of both validation and analysis of subject-specific finite element models of the glenohumeral joint, and contains significant engineering and clinical relevance. While the current work provides an excellent foundation for the development, validation, and analysis of multiple subject-specific finite element models of the glenohumeral joint, several assumptions and limitations also raised issues for future development.

6.1 FE MODEL VALIDATION

6.1.1 Advancements

The current work marked an advancement in the validation procedure for subject-specific finite element models of the glenohumeral joint, since a constitutive model was used to represent the capsule that resulted in closer prediction of strains on the surface of the anterior-inferior capsule with those obtained experimentally. Previous validation of FE Model 1 was performed using an isotropic hypoelastic constitutive model to represent the capsule [41], however the model was only able to be validated at the clinically relevant joint position with 51.8° of external rotation. In the current work, a Veronda-Westmann isotropic hyperelastic constitutive model was used to represent the capsule, and validation of FE Model 1 was able to be performed at the clinically relevant joint position with 51.8° of external rotation as well as at the clinically relevant joint position with 31.1° of external rotation. Furthermore, FE Model 2 was able to be validated at the clinically relevant joint positions with 0°, 25.1°, and 57.3° of external rotation. Therefore, the use of the Veronda-Westmann isotropic hyperelastic constitutive model to represent the capsule marked a significant advancement in the validation of finite element models of the glenohumeral joint, in that the predictive capability of the models was increased.

In addition, the current work marked advancement in model validation by simulating the presence of a glenoid labrum via increase of the radial thickness of the capsule elements near the capsule's glenoid insertion. Validation of the finite element models in the current work involved comparing predicted and experimental strains in the mid-substance of the anterior band of the inferior glenohumeral ligament, and validation was able to be performed when a labrum was included even though strains significantly decreased in the insertion site regions. The current

work therefore demonstrated that modifications can be performed at the insertion site that affect the predictive capability of the models in the insertion site without affecting the predictive capability in the mid-substance of the capsule. This marks a significant advancement in the development and validation of finite element models of the glenohumeral joint, since it was demonstrated that modifications could be made that allowed for more robust convergence of the models without affecting model validation. It can also be stated that that the predictive capability of the models increased from the insertion site modification, since the modification resulted in the removal of unreasonable strain concentrations at the capsule's insertion into the glenoid. Since enhancement of model convergence and predictive capability provided the initial motivation to evaluate inclusion of a labrum in the models, it was decided to include the labrum in both FE Model 1 and FE Model 2 as a computational modification to the insertion site. Based on the successful results it is suggested that the labrum be similarly included in all future developed finite element models of the glenohumeral joint.

6.1.2 Assumptions

Experimental strains were computed in 60 validation elements in the anterior-inferior capsule by measuring motions of the 7 x 11 grid of capsule strain markers from the reference position to each clinically relevant joint position. Care was taken to attach the capsule strain markers to the capsule with cyanoacrylate (Section 3.2.1.1), however the application of 0.9% saline solution to the capsule resulted in isolated capsule strain markers becoming unattached from the capsule throughout the experimental procedure. These capsule strain markers were carefully replaced on the capsule in their original positions using cyanoacrylate and photographs of the 7 x 11 grid of capsule strain markers taken immediately after their initial attachment to the capsule (Figure

3.2), however it is possible that the capsule strain markers were not replaced in their exact initial positions on the capsule. It was decided that any errors in capsule strain marker replacement were negligible relative to the displacement of the capsule strain markers during joint motion, and it was therefore assumed that any capsule strain marker motion used to calculate experimental strains in the anterior-inferior capsule was the result of stretching of the capsule tissue and not from a failure to replace the capsule strain markers to their original positions.

During the clinically relevant joint motions, folding of the capsule tissue occurred that prevented measurement of the 3-dimensional positions of each capsule strain marker using the optical motion tracking system. Since ligamentous tissue only carries load in tension, it was assumed that folding of a capsule region indicated that the region was not transferring load between the humerus and scapula, and that the tissue would be unstrained relative to the reference position. Therefore, these elements were not included in the validation process.

Validation of FE Model 1 and FE Model 2 was performed by comparing predicted and experimental strains in validation elements of the anterior band of the inferior glenohumeral ligament. The predicted strain value in each validation element was reported as the average value of the maximum principal strains at the nodes composing each validation element. The experimental strain value in each validation element was reported as the maximum principal strain at the centroid of each validation element, which was calculated by using the positions of the four capsule strain markers composing each validation element in the reference position and in the clinically relevant joint positions. It was decided that these two different means of calculating strain for a validation element were comparable, and the validation procedure therefore operated under this assumption.

In addition, there may have been slight differences in the shapes of the predicted and experimental validation elements. The shape of the predicted validation elements was determined by identifying areas of the capsule surface in the finite element model that were enclosed within points representing the locations of the capsule strain markers on the surface of the capsule (Section 3.3.4.1). Therefore, the shape of each predicted validation element contained the curvature of the capsule surface. The shape of the experimental validation elements, however, was created in ABAQUS and approximated as a plane formed between the locations of the four capsule strain markers used to create each experimental validation element (Section 3.2.3.3). Therefore, the shape of each experimental validation element did not contain the curvature of the capsule surface. This may have allowed for a greater surface area in each predicted validation element relative to its corresponding experimental validation element, however it was assumed that differences in strain resulting from this discrepancy would not affect model validation.

The use of the Veronda-Westmann isotropic hyperelastic constitutive model to represent the capsule required the assumption that the capsule is homogeneous in its entirety and that it has purely isotropic material properties. Debski et al. [35], however, reported that while the global function of the capsule is isotropic, there are local regions of the capsule where the material symmetry is transversely isotropic. This may have contributed to an ability to validate FE Model 1 and FE Model 2 when comparing average predicted and experimental strains in the validation elements of the anterior band of the inferior glenohumeral ligament, but an inability to validate individual validation elements (Section 5.2 and Section 5.4.3, respectively). Furthermore, in order to validate FE Model 2 the values of the material coefficients in the anterior band of the inferior glenohumeral ligament and the axillary pouch were decreased by a factor of two. It was

assumed that these modifications, which were less than an order of magnitude and similar to the values of C1 and C2 reported by Rainis [40] and performed in preliminary work within our research group (Section 5.1.1.1), were appropriate.

The assumptions listed above were necessary in order to perform the validation procedure required for the current work. The glenohumeral capsule is a complex tissue that poses significant challenges for validation that previously developed finite element models of soft tissues throughout the body did not encounter. Song et al. [121] used measures of predicted and experimental force in the anterior cruciate ligament in clinically relevant joint positions to validate a finite element model of the anterior cruciate ligament. For the current work, however, the multi-directional transfer of load that occurs across the margins of the capsule regions prevented the use of force as a means for validation in the anterior-inferior capsule, thereby requiring the use of the capsule strain markers to calculate experimental distributions of strain in the anterior-inferior capsule for validation. The force in the entire capsule could be obtained computationally and experimentally and thus be used as an additional means for validation, however to answer the research question and achieve the specific aims of the current work it was decided to concentrate efforts on measuring the predicted and experimental distributions of strain in the anterior-inferior capsule. Gardiner et al. [144] and Ellis et al. [145] used strain markers to calculate distributions of strain on the surface of the medial collateral ligament in clinically relevant joint positions for validation of finite element models of the medial collateral ligament, however measurement of marker motion was facilitated by the relatively little folding or buckling of the tissue in the clinically relevant joint positions. With the glenohumeral capsule, however, considerable folding occurs in regions of the capsule that are not transferring load, thus

preventing measurement of strain in the folded regions of the capsule and requiring the assumption that these regions were unstrained.

Furthermore, finite element modeling of the collateral ligaments is facilitated by the material symmetry of the ligaments. The collagen fibers of the medial collateral ligament are aligned predominantly in the longitudinal direction of the ligament, with clearly evident transversely isotropic material symmetry. Previous authors have therefore performed validation of finite element models of the medial collateral ligament using a transversely isotropic hyperelastic constitutive model to represent the tissue [144, 145]. The glenohumeral capsule, however, contains collagen fibers that are randomly aligned in such a manner that provides localized regions of transversely isotropic material symmetry, but overall isotropy in the entire capsule [35]. This provides significant challenges for finite element modeling of the glenohumeral joint, in that using an isotropic or transversely isotropic constitutive model to represent the capsule will result in difficulties predicting regional or global distribution of load in the capsule, respectively. This, along with the requirement for the use of capsule strain markers and the folding of the capsule that occurs with joint motion, combine to make validation of finite element models of the glenohumeral joint a complicated and complex task.

6.1.3 Limitations

FE Model 1 was unable to be validated at the clinically relevant joint position with 0° of external rotation, thus limiting conclusions drawn in the comparisons between FE Model 1 and FE Model 2 at the clinically relevant joint positions with low external rotation. However, the results from Section 5.5 indicate that the clinically relevant joint positions with 20° - 40° of external rotation may be most beneficial for physical examinations to diagnose pathology to the anterior-inferior

capsule, therefore an inability to draw conclusions from the comparisons of FE Model 1 and FE Model 2 at low external rotations may not be problematic. It is worth noting that the experimental strains in the anterior band of the inferior glenohumeral ligament for FE Model 1 at the clinically relevant joint position with 0° of external rotation were relatively high when compared to experimental strains in the anterior band of the inferior glenohumeral ligament for FE Model 2 and in five specimens used in our research group for another study [21] (Table 6.1). A clear pattern emerged with the experimental data for FE Model 2 and the five specimens, in which the strain magnitude in the anterior band of the inferior glenohumeral ligament increased from the clinically relevant joint position with 0° of external rotation to the clinically relevant joint position with 30° of external rotation, by at least 1.9% strain and as high as 13.2% strain. For FE Model 1, however, the strain only increased by 0.4% from the clinically relevant joint position with 0° of external rotation to the clinically relevant joint position with 30° of external rotation, and it can be seen in Table 6.1 that experimental strains in FE Model 1 are relatively high at the clinically relevant joint position with 0° of external rotation. Therefore, the inability to validate FE Model 1 at the clinically relevant joint position with 0° of external rotation may have resulted from relatively high experimental strains at this joint position. These high strains could be the result of subject-specific variability in the stability provided by the capsule among subjects, suggesting that validation of finite element models of the glenohumeral joint may be difficult when experimental strains are relatively high at clinically relevant joint positions with low external rotation. This could be confirmed with future development and validation of additional subject-specific finite element models of the glenohumeral joint that have similar experimental strains at clinically relevant joint positions with low external rotation.

Table 6.1 Average strains in the anterior band of the inferior glenohumeral ligament at the clinically relevant joint positions with 0°, 30°, and maximum external rotation. Specimen 1 – Specimen 5 = specimens used within our research group for an additional study [21]

AB-IGHL Experimental Strains Mean (SD)							
External Rotation	Specimen 1	Specimen 2	Specimen 3	Specimen 4	Specimen 5	FE Model 1	FE Model 2
0°	7.8% (6.5)	15.9% (14.0)	19.1% (6.4)	3.9% (8.0)	8.9% (12.2)	18.5% (11.4)	8.0% (9.0)
30°	11.6% (7.4)	17.8% (13.4)	25.6% (8.0)	17.1% (18.5)	18.7% (17.0)	18.9% (11.3)	14.4% (14.6)
max	15.8% (8.0)	19.2% (14.0)	26.5% (7.2)	24.5% (17.2)	20.3% (18.3)	21.1% (14.0)	16.1% (15.2)

The experimental strains in FE Model 1 at the clinically relevant joint position with 0° of external rotation are also high relative to the work of Malicky et al. [36]. In this previous study the authors measured strain in the entire anterior-inferior capsule, when the glenohumeral joints of eight cadavers were subjected to similar kinematics as those for FE Model 1 at the clinically relevant joint position with 0° of external rotation. It was found that the average strains in the glenoid and humeral sides of the anterior-inferior capsule were 13±5% and 9±4%, respectively, and that peak strains in the glenoid and humeral sides were 25±8% and 18±9%, respectively. For the current work, average strains in the glenoid and humeral sides of the anterior-inferior capsule of FE Model 1 at the clinically relevant joint position with 0° of external rotation measured 16% and 14%, respectively, and the peak strains in the glenoid and humeral sides measured 51% and 45%, respectively. This again confirms the relatively high experimental strains in FE Model 1 at the clinically relevant joint position with 0° of external rotation, which may have contributed to the inability to validate FE Model 1 at this joint position.

It is also possible that the use of the Veronda-Westmann isotropic hyperelastic constitutive model hindered validation of FE Model 1 at the clinically relevant joint position with 0° of external rotation. In Section 5.3.3 it was found that the use of Veronda-Westmann

isotropic hyperelastic constitutive model to represent the capsule may result in an underestimation of strains in the capsule tissue when the capsule is loaded into its toe region, which may help explain why the predicted strains in FE Model 1 were lower than the experimental strains at the clinically relevant join position with 0° of external rotation. However, this constitutive model was used to successfully validate FE Model 2 at the clinically relevant joint position with 0° of external rotation. It may therefore be possible that the inability to validate FE Model 1 may have been an exception to model validation, which could also be confirmed with the future development and validation of additional subject-specific finite element models of the glenohumeral joint.

Validation of subject-specific finite element models of the glenohumeral joint requires that differences in average predicted and experimental strains within the anterior band of the inferior glenohumeral ligament are less than the experimental strain repeatability of ±3.5% strain. Table 5.4 for FE Model 1 and Table 5.9 for FE Model 2 demonstrate that while average differences in predicted and experimental strains were less than ±3.5% strain at multiple clinically relevant joint positions, differences in predicted and experimental strains within the individual validation elements were often much greater than ±3.5% strain. This may be due to the nature of finite element models to distribute high strains concentrated within a capsule region over larger areas of the capsule, while the experimental strains are calculated solely from the positions of the capsule strain markers. For example, Figure 6.1 shows that the experimental strains in the anterior band of the inferior glenohumeral ligament in FE Model 2 at 30° of external rotation have relatively high strain on the glenoid side of the tissue and relatively low strain on the humeral side of the tissue. The predicted strain in the anterior band of the inferior glenohumeral ligament, however, is more evenly distributed between the glenoid and humeral

sides of the tissue. The average predicted and experimental strains, however, differ by only 1.2% strain.

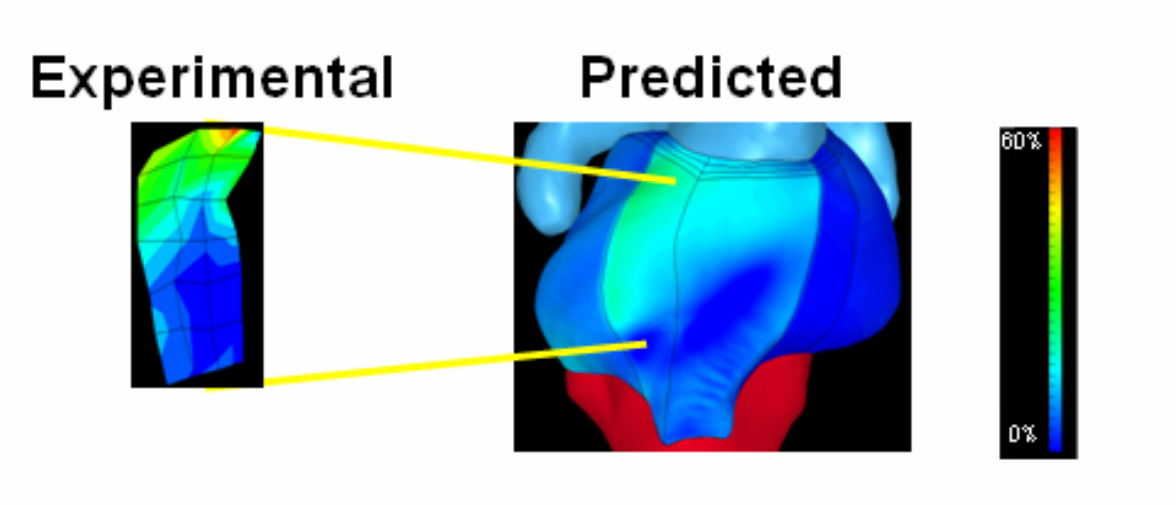

Figure 6.1 Inferior views of experimental and predicted strains in the anterior band of the inferior glenohumeral ligament of FE Model 2 (right shoulder), at the clinically relevant joint position with 30° of external rotation

Therefore, while the finite element models were able to predict average strains in a capsule region, they were unable to predict strains on a point-by-point basis in the capsule. In addition to possibly resulting from the tendency of finite element models to distribute strain concentrations over a larger area of tissue, this may have resulted from the use of the Veronda-Westmann isotropic hyperelastic constitutive model to represent the capsule. Using this constitutive model allowed the finite element models to accurately represent the global isotropic nature of the capsule, but not accurately represent the local transversely isotropic nature of the capsule. To answer the research question and achieve the specific aims, however, the models did not need to predict the stability provided by localized points of the capsule, but rather needed to be able to predict the stability provided by localized regions of the capsule. This was possible with both FE Model 1 and FE Model 2, as indicated by the validation at multiple clinically relevant joint positions and by the localization of the distribution of strain to the glenoid side of

the anterior band of the inferior glenohumeral ligament at the clinically relevant joint positions with 20 – 40° of external rotation. Therefore, the validation procedure was consistent with the types of analyses performed using the finite element models, in that both validation and analyses were performed by computing average strain within regions of the capsule. While it is possible that the models could be used for more refined point-by-point validation and analyses of the stability provided by the capsule, performing such analyses may not provide any additional benefit to clinicians, since current surgical procedures address regions of capsule tissue and not isolated points in the capsule. There may still be merit in refining the validation procedure so that validation is performed in smaller regions of the capsule than in the entire anterior band of the inferior glenohumeral ligament, however, since doing so would provide an ability to more specifically identify regions of the capsule where validation was unable to be performed.

The predicted shape of FE Model 2 was unable to match the experimental shape seen at the clinically relevant joint position with 57.3° of external rotation (Figure 5.22). This may have resulted from the lack of an applied gravity boundary condition within the finite element models, as application of gravity may have affected the predicted shape of the unloaded tissue in the posterior half of the anterior-inferior capsule. Therefore, a sensitivity study should be performed that evaluates the effects of gravity on the predicted shape of the capsule and strain in the anterior-inferior capsule at the clinically relevant joint positions.

Lastly, the material coefficients in FE Model 2 for the anterior band of the inferior glenohumeral ligament and the axillary pouch required modification in order for validation to occur. This may therefore prevent complete subject-specificity of FE Model 2. However, the modifications were such that the material coefficients used in the model were in close approximation to those obtained experimentally, therefore a degree of subject-specificity

remained in these two regions. It may be possible, however, that these modifications will result in inaccurate strain predictions in the capsule when the joint is moved to other clinically relevant joint positions.

6.1.4 Future Directions

In light of the assumptions and limitations that exist with the current work, future directions are suggested that may improve the validation procedure for subject-specific finite element models. The inability to validate FE Model 1 at the clinically relevant joint position with 0° of external rotation, as well as the inability for point-by-point validation of the models at multiple clinically relevant joint positions, may have resulted from the use of the Veronda-Westmann isotropic hyperelastic constitutive model to represent the capsule. This model combines the ground substance and collagen fibers into one isotropic material that is homogeneous throughout the capsule. It may be beneficial to use a constitutive model that allows for separate contributions of the fibers and ground substance to the capsule's response to application of load, and that can also represent the non-homogeneity throughout the capsule tissue. An example of this would be a transversely isotropic Mooney-Rivlin constitutive model [98, 107, 146], which represents the capsule with transversely isotropic collagen fibers imbedded in an isotropic ground substance. The global isotropic / local transversely isotropic nature of the capsule could be represented by assigning this constitutive model to each element within the finite element models, and randomly assigning the preferred collagen fiber alignment in each element. This constitutive model may allow for more accurate representation of the capsule tissue, and may lead to more accurate predictions of local capsule strains. Therefore, future use of the transversely isotropic Mooney-

Rivlin constitutive model to represent the capsule in finite element models of the glenohumeral joint should be evaluated.

An additional future direction involves changing the regions of validation elements in which average predicted and experimental strains are reported. Currently, the predicted and experimental strains in the validation elements of the anterior-inferior capsule are averaged within the region of the anterior band of the inferior glenohumeral ligament. This resulted in averaging predicted and experimental strains in eleven and eighteen validation elements for FE Model 1 and FE Model 2, respectively. It is suggested that in the future, predicted and experimental strains in the validation elements of the anterior-inferior capsule are averaged within more refined regions of the capsule (Figure 6.2), so that predicted and experimental strains are averaged together in four validation elements, in multiple locations throughout the anterior-inferior capsule. This would result in comparing predicted and experimental strains in up to fifteen regions throughout the anterior-inferior capsule, as opposed to just one region as is done currently. This refinement in the validation process would still allow for regional evaluation of validation as is done currently, but also allow for "validation mapping" throughout the anterior-inferior capsule so that specific areas can be identified where discrepancies in predicted and experimental strains may occur.

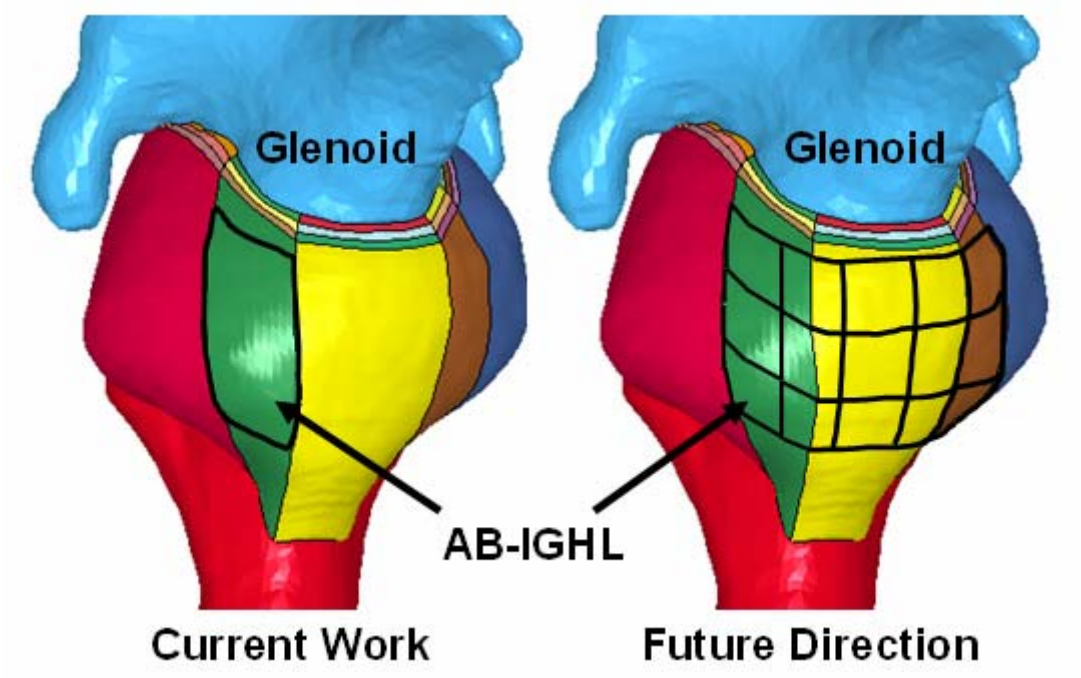

Figure 6.2 Inferior views of FE Model 2 (right shoulder). For the current work, the strains in the validation elements were averaged within the region of the AB-IGHL. It is suggested for future direction that the strains in the validation elements are averaged within more refined regions of the anterior-inferior capsule

Lastly, it is suggested that a sensitivity study be performed that evaluates how application of a gravity boundary condition in the finite element models affects predicted shape and distribution of strain in the capsule. Furthermore, it is suggested that sensitivity studies be performed to determine how predicted strains in the finite element models are affected by changes in contact parameters, labrum dimensions, mesh density, capsule thickness, and even material coefficients. Similar analyses were previously performed in a finite element model of the glenohumeral joint [112], however conclusions drawn from this previous study may not be applicable to the current work due to the use of an isotropic hypoelastic constitutive model to represent the tissue. In addition to providing valuable information on the predictive capability of the models using constant parameters, the proposed sensitivity studies would allow for determination of whether average parameters could be used, which would limit the number of subject-specific inputs and simplify the finite element model development process.

6.2 ANALYSIS OF JOINT POSITIONS

6.2.1 Advancements

FE Model 1 and FE Model 2 were used to evaluate the distribution of load in the anterior-inferior glenohumeral capsule in multiple clinically relevant joint positions, in order to suggest joint positions that could become standardized in physical examinations for more effective diagnoses of pathology to the anterior-inferior capsule. A total of six clinically relevant joint positions were evaluated, involving application of a 25 N anterior load at 60° of glenohumeral abduction and 0°, 10°, 20°, 30°, 40°, and 50° of external rotation. In order to perform the evaluations, a methodology was designed and implemented to simulate motion within the finite element models to the clinically relevant joint positions without the use of experimentally-obtained kinematics. The methods involved determining anatomical coordinate systems of the humerus and scapula within the finite element model, and assigning joint motion based on coordinate system transformations. Previously, finite element model motion has been simulated through the use of experimentally obtained kinematics [41, 95, 110, 112, 120], limiting analyses to those positions obtained with the experimental tools. The methodology developed in the current work, however, can be used to simulate motion to infinite joint positions, thus increasing the capability to contribute to the existing knowledge of the stability provided by the capsule throughout the joint range of motion.

In addition, the analyses performed allowed for localizing the distribution of strain in the anterior-inferior capsule to “sub-regions”, corresponding to the glenoid and humeral sides of the anterior band of the inferior glenohumeral ligament, the axillary pouch, and the posterior band of the inferior glenohumeral ligament. This provided important clinical significance to the

analyses, since capsule pathology can often occur to localized regions of the capsule. The size of the sub-regions is optimal for the analyses, since they are small enough in size to allow for localization of the distribution of load in the anterior-inferior capsule, but large enough that clinicians could identify the sub-regions during operative procedures.

6.2.2 Assumptions

Using the methodology developed in Section 4.2.3, motion of FE Model 1 and FE Model 2 from the reference position to the intermediate clinically relevant joint positions was performed. The desired glenohumeral abduction angle and external rotation angle were input into the Matlab code to generate load curves for motion from the reference position to the intermediate clinically relevant joint positions, and the analyses performed in the current work operated under the assumption that these motions were correct and representative of the inputs. In order to validate the developed Matlab code, a brief preliminary study was performed using FE Model 1. In Section 2.3.4.1 the predicted strains in the anterior band of the inferior glenohumeral ligament were obtained at the clinically relevant joint position with 51.8° of external rotation, with joint motion to this position prescribed with the use of experimentally obtained kinematics. To validate the Matlab code, the predicted strains in the anterior band of the inferior glenohumeral ligament were obtained after joint motion to this position was prescribed using the Matlab code and the procedure outlined in Section 4.2.3. It was found that the average difference in predicted strain in the anterior band of the inferior glenohumeral ligament when using the experimental kinematics or computationally-derived kinematics was 0.6% strain. Therefore, it was assumed that the methodology to simulate motion to the intermediate clinically relevant joint positions was valid.

In the current work, application of a 25 N anterior load at the intermediate clinically relevant joint positions was simulated by applying translations of the humerus with respect to the scapula that were interpolated from the translations resulting from application of a 25 N anterior load at the clinically relevant joint positions with 0°, 30°, and 60°/maximum external rotation. It was therefore assumed that there was a linear relationship between the translation of the humerus with respect to the scapula resulting from application of a 25 N anterior load and the external rotation angle when the joint is abducted to 60°. This assumption was necessary since the finite element solution procedure was driven by displacements of the humerus with respect to the scapula, and not by loads applied to the humerus.

6.2.3 Limitations

For the current work, it was suggested that the clinically relevant joint positions with a 25 N anterior load applied at 60° of glenohumeral abduction and 20° - 40° of external rotation result in a consistent distribution of load in the anterior-inferior capsule among patients, where the distribution of load can be localized to the glenoid side of the anterior band of the inferior glenohumeral ligament. However, only two validated, subject-specific finite element models were used to identify these joint positions, with each being subject-specific to male cadavers over the age of 45. In order for more widespread clinical acceptance of the conclusions, a population of subject-specific finite element models needs to be developed and validated that are subject-specific to a wider demographic base, including expansion of age, gender, and race. Preliminary calculations suggested that seven subject-specific finite element models of the glenohumeral joint would be needed to capture the patient variability in the population. In spite of the small sample size in the current work, the techniques performed provide an excellent

foundation for the future development, validation, and analysis of subject-specific finite element models of the glenohumeral joint.

6.2.4 Future Directions

The development, validation, and analysis of multiple subject-specific finite element models of the glenohumeral joint are required to solidify the conclusions made in the current work. Therefore, future directions require that the techniques and procedures outlined in the current work be used to develop a population of at least seven subject-specific finite element models that are subject-specific to cadavers with variable age, gender, and race. Once these models have been developed, validated, and used for analysis of the distribution of load in the anterior-inferior capsule in clinically relevant joint positions, power analyses should be performed in order to determine whether additional models are needed to draw conclusions. Once an adequate number of models have been developed and validated, they can be used to identify clinically relevant joint positions where the distribution of load in the anterior-inferior capsule is consistent among patients in response to anterior loading. These joint positions can then be suggested for use in physical examinations of the capsule following anterior dislocation, to allow for more effective diagnoses of anterior-inferior capsule pathology and an ultimate improvement in surgical outcomes. It may be possible that a single joint position or range of joint positions cannot be identified that result in a consistent distribution of load in the capsule among all subjects. In the event that this occurs, the subject-specific finite element models could be used to determine if physical examinations need to be specific to certain demographics, i.e. specific to age, gender, or race. It may be possible that different clinically relevant joint positions could be used for effective diagnoses among different demographic groups, and a population of finite element

models that are subject-specific to a wide demographic base would be able to provide this information.

6.3 RELEVANCE OF FINDINGS

6.3.1 Engineering Relevance

The data presented in the current work have many implications for experimental and computational analyses, and thus have relevance for the field of Bioengineering. Validation of multiple subject-specific finite element models of the glenohumeral joint was able to be performed using a Veronda-Westmann isotropic hyperelastic constitutive model to represent the capsule, at clinically relevant joint positions where validation was unable to be performed using an isotropic hypoelastic constitutive model to represent the capsule [41]. Therefore, when developing and validating subject-specific finite element models of the glenohumeral joint, using an isotropic hyperelastic constitutive model to represent the capsule is more appropriate than using an isotropic hypoelastic constitutive model to represent the capsule.

In the current work, both model convergence and predictive capability was enhanced by simulating the presence of a glenoid labrum via increase of the radial thickness of the capsule elements near the capsule's glenoid insertion. Future development and validation of subject-specific finite element models of the glenohumeral joint should therefore modify the thickness of the capsule elements at the glenoid insertion to represent the presence of the glenoid labrum. Furthermore, subject-specific finite element models of additional joints in the human body such as the hip may be able to simulate complex soft-tissue insertions into bone using computational modification of the soft-tissue element thickness near the bony insertion.

Furthermore, the current work marked the first attempt at using the non-linear finite element solver FEBio for development, validation, and analysis of multiple subject-specific finite element models of the glenohumeral joint. The successful validation performed on both FE Model 1 and FE Model 2, and the ensuing analyses using the distribution of strain in the anterior-inferior capsule, indicate that FEBio is a suitable finite element tool for development, validation, and analysis of finite element models of the glenohumeral joint.

Additionally, methodology was developed using transformations of anatomical coordinate systems within the finite element model to simulate motion of the humerus with respect to the scapula, so that strains in the anterior-inferior capsule could be evaluated in clinically relevant joint positions that did not have experimentally-obtained kinematics. This methodology can be used to simulate motion to any glenohumeral joint position, and thus provides an important foundation for future work evaluating the distribution of load in the glenohumeral capsule at additional joint positions.

6.3.2 Clinical Relevance

The results of the current work have significant clinical implications. Currently, physical examinations for pathology to the anterior-inferior capsule are not standardized for joint position among subjects, leading to misdiagnoses of capsule function that may lead to post-operative redislocation, joint pain, limited motion, and osteoarthritis. The distribution of strain in the anterior-inferior capsules of two validated, subject-specific finite element models suggest that the distribution of load in the anterior-inferior capsule in response to application of anterior load may be consistent across patients in clinically relevant joint positions with 60° of glenohumeral abduction and 10° – 40° of external rotation. Therefore, clinicians may be able to use these joint

positions to make diagnoses of pathology to the anterior-inferior capsule that are independent of patient age, size, gender, race, and other demographic factors.

Furthermore, the current work demonstrated that at joint positions with an anterior load applied at 60° of glenohumeral abduction and 20° - 40° external rotations, strains were significantly higher in the glenoid side of the anterior band of the inferior glenohumeral ligament than in all other regions of the anterior-inferior capsule. Therefore, clinicians may be able to use these joint positions to diagnose pathology to the glenoid side of the anterior band of the inferior glenohumeral ligament, regardless of patient demographics. Furthermore, it was found that strain in the glenoid side of the anterior band of the inferior glenohumeral ligament increased with external rotation in these clinically relevant joint positions, and that the minimum difference in strain between the glenoid side of the anterior band of the inferior glenohumeral ligament and the remaining sub-regions generally increased with external rotation in these clinically relevant joint positions. Therefore, clinicians may have greater capability to diagnose instability and thus pathology to the glenoid side of the anterior band of the inferior glenohumeral ligament at joint positions with 25 N of anterior load applied to the glenohumeral joint at 60° of glenohumeral abduction and 30° – 40° of external rotation.

These findings provide significant contribution to clinical understanding of the stability provided by the glenohumeral capsule. The glenoid side of the anterior band of the inferior glenohumeral ligament is frequently injured following anterior glenohumeral joint dislocation, indicated by the presence of Bankart lesions to this region of the anterior-inferior capsule [52, 53]. Providing clinicians with specific joint positions to test for pathology to the glenoid side of the anterior band of the inferior glenohumeral ligament that are independent of patient demographics may allow for more accurate diagnoses of pathology to a clinically relevant region

of the capsule. When performing surgical procedures to restore the stability provided by the capsule, clinicians can then use these diagnoses to localize repair procedures to a specific region of the glenohumeral capsule, and thus limit post-operative failure from surgically altering regions of the capsule that are non-pathologic.

In addition to evaluating the distribution of load in the anterior-inferior capsule in response to application of anterior load in joint positions of abduction and external rotation, the validated, subject-specific finite element models can be used to analyze the distribution of load in additional regions of the capsule at different joint positions. While the joint positions evaluated for the current work involve those where the majority of glenohumeral joint dislocations occur, dislocation and instability can also occur in posterior and inferior directions in joint positions where stability is provided by other regions of the capsule. The models can therefore be used to identify specific joint positions where more effective diagnoses of pathology to other regions of the capsule can be made, in addition to those evaluated in the current work.

A significant application of these models is that a series of joint positions can be identified in which clinicians can diagnose pathology to multiple areas of the glenohumeral capsule. Currently, clinician misdiagnosis of the type of instability, i.e. uni-directional or multi-directional instability, is responsible for 38% of redislocations following surgery [23]. Using a series of standardized joint positions that allow for diagnosis of anterior instability, inferior stability, and/or posterior instability, clinicians could more effectively diagnose the type of instability and limit post-operative failures from surgical procedures that do not address the specific type of instability. It has been shown recently using FE Model 1 that the anterior-inferior capsule provides inferior stability to the glenohumeral joint when an inferior load is applied at positions with abduction and external rotation [64]. Therefore, it may be possible for

clinicians to use this joint position to diagnose inferior capsule instability and the joint positions identified in the current work to diagnose anterior capsule instability, in order to make more effective diagnoses of uni-directional or multi-directional instability.

In addition, a collection of validated, subject-specific finite element models could be used to examine the effects of capsule degradation or diminished material properties that occur with aging [7], disease, or surgical repair procedures that change the material properties of the capsule such as thermocapsular shrinkage [147, 148]. Furthermore, the models can be used by both clinicians and engineers to design and evaluate novel surgical procedures without risk to patients.

6.4 SUMMARY

Physical examinations for pathology to the anterior-inferior capsule following anterior dislocation are not standardized for joint position among patients, which affects the ability of clinicians to diagnose the location, extent, and type of pathology to the anterior-inferior capsule. This is a clinically significant issue since the misdiagnoses often lead to post-operative redislocation, pain, osteoarthritis, and limited range of motion. Therefore, the objective of the current work was to suggest joint positions where the distribution of load in the anterior-inferior capsule is consistent among patients in response to application of an anterior load.

Two validated, subject-specific finite element models of the glenohumeral joint were used to evaluate the distribution of load in the anterior-inferior capsule when positioned in clinically relevant joint positions. Specifically, the distributions of strain in the anterior-inferior capsule were evaluated when the models were subjected to a 25 N anterior load applied at 60° of glenohumeral abduction and 0° - maximum external rotation in 10° increments. Methodologies

were developed in order to use an isotropic hyperelastic constitutive model to represent the capsule, to include the glenoid labrum within the finite element models, and to simulate motion of the humerus with respect to the scapula to joint positions without experimentally obtained kinematics. It was found that the distribution of strain in the anterior-inferior capsule was consistent among the two models at the clinically relevant joint positions with 10° - 40° of external rotation, with r^2 values greater than 0.7. Specifically, it was found that the strain became highest in the glenoid side of the anterior band of the inferior glenohumeral ligament in the clinically relevant joint positions with 20° - 40° of external rotation.

Based on the findings in the current work, it may be possible to establish standard joint positions for physical examinations that clinicians can use to diagnose pathology to the anterior-inferior capsule. Before the conclusions of the current work can be applied clinically, however, additional finite element models of the glenohumeral joint need to be developed and validated that are subject-specific to a more diverse population. Therefore, future direction includes using the methodology described in the current work to develop and validate multiple subject-specific finite element models of the glenohumeral joint, and use the models to suggest clinically relevant joint positions where the distribution of load in the anterior-inferior capsule is consistent among patients. This may allow for more accurate diagnoses of anterior-inferior capsule pathology during physical examinations that use these clinically relevant joint positions, which may ultimately lead to an improve in surgical outcomes.

APPENDIX A

APPENDIX A. EXPERIMENTAL ROBOT PROTOCOL

1. Flip rear switch on Unimate to On. Make sure to have the console's key switch set to LOCAL and Motion Control to RUN
2. Open RP Talker, Supervisor (aka Ddcmp), and HyperTerminal on desktop of robot computer
   - Select Emulate in RP Talker
3. Check load cell (ON/OFF). If off, turn on power to UFS at least 30 minutes before calibration.
4. Turn power key on Unimate to ON position (|)
5. Puma HyperTerminal commands:
   Load VAL-II from floppy (Y/N)? **Y**
   Language for VAL-II error messages? **0** (English)
   Robot serial #? **234**
   -Go to RP Talker, and press and hold the space bar down until the numbers stop in HyperTerminal
   Initialize (Y/N)? **Y**
   Are you sure (Y/N)? **Y**
   -Hit space bar in RP Talker
   Enter **.en net** in HyperTerminal
   Enter **.en sup** in HyperTerminal
6. In Supervisor
   en disk *enables disk communication
   Press black button (|) on Unimate to turn arm power on
   load safe.pg *****loads predefined joint positions for robot motion
   do ready
   -when prompted that "not calibrated", hit "y"
   *aligns robot joint at midrange position to visually verify proper alignment, check to make sure joints of robot calibrated correctly, i.e. aligned as follows

Joint	1	2	3	4	5	6	
Position		0	-90	90	0	0	aligned w/ white Y-axis label

cal (if the position values do not match up as above)
do ready (now the joints should be calibrated correctly)
comm safe * loads robot's self-awareness program
* first movement in robot occurs here
do speed 30 ***** changes speed from default so that a slower motion will result
do move #scapclamp ***** moves to a position for easy mounting of scapular clamp

7. Attach potting block (smaller of the 2 potting blocks made of BONDO) to scapular clamp for calibration with metal bolts.
8. Attach clamp-block unit to UFS endplate of robot to determine center of gravity
   do speed 10 *****change speed to a slow setting
   do move #pp1 * moves joints back to position for execution of calibration protocol
   ex calib * to calibrate UFS
9. In the HyperTerminal:
   a. Choose *Branch Code* option **3** = *Keyboard Entry of Fixture Parameter(s)*
      i. Choose *Change Above*: **1** = *new mass*
      ii. *Fixture Parameters (with mounting plate): mass* **5068**
      * note: 5068 g= mass of scapular clamp + smaller potting block (2788 g) + mass of cylinder and endplate (2280 g)
   b. Choose *Branch Code* option **1** = *Perform The Tare*, record values in lab notebook
   c. Choose *Branch Code* option **1** = *Perform The Tare* again, record values in lab notebook. Ensure that the six New Digital Tares are each within ± 50 of those in Step 9.c. If so, record *New Digital Tare* values in *cal2.xls* worksheet
   d. Choose *Branch Code* option **2** = *Automatic Measure of Fixture Parameters (Assumes Above Tares)*
   e. Press <Enter> at *Combine Tibial-Cylinder* prompt
   f. Press <Enter> at *Continue Clamp* prompt
   g. Ensure that center of gravity values are reasonable based on the distribution of weight of the block-clamp complex, and record center of gravity values in lab notebook.
   h. Check calibration values with previous *cal2.xls* worksheets in the Calibration & Tare History binder, to make sure they seem reasonable
10. Calibrate UFS
    a. Remove clamp-block unit from robot's UFS plate
    b. Attach calibration plate to UFS plate
    c. Choose *Branch Code* option **4** = *Take a Measurement Set*
       i. Collect measurements for Null no external loads
       ii. Record data in *cal2.xls* for Null no external loads
       * StDev must be <1.0
    d. Choose *Branch Code* option 4 and record in EXCEL. Repeat for appropriate applied 5000 g loads applied in the 8 directions specified on the calibration plate (refer to diagram in *cal2.xls*):
       - StDev <1.0 for each of 8 loadings
       - % Difference for each of 6 directions (3 Forces, 3 Moments) <10.0 %, preferably <5%

e. Print 2 copies of completed EXCEL file—one for robot log (folder beside robot terminal), one for experimental records
f. Save file appropriately
g. Close file
h. Record the center of gravity (average of measurements)
i. Remove all attachments from robot UFS (clamps and specimens will not clear the ceiling during movement to starting position)
j. Type **999** in HyperTerminal to go back to Supervisor, then hit the <enter> key
k. **do speed 20** in Supervisor
l. Without having anything mounted in the pedestal, type **do move #ghstart2** in the Supervisor
m. Use the teach pendant to manually move UFS to approximately 0° GH abduction, neutral IE position (need to turn motion control to "Teach" on Unimate console)

11. Mount the specimen:
    a. Set ball on base pedestal, aligned with screws; secure with single screw from underside of pedestal
    b. Insert potted specimen into humeral/femoral clamp; tighten side screws around the clamp. Secure potted scapula in scapular clamp
    c. Insert humeral/femoral clamp into ball and adjust humerus to desired height and tighten the ball with single side screw
        i. NOTE: you will need to tilt the humeral shaft away from the robot (almost parallel to the wall with the air tanks on it)
    d. Secure scapula-clamp unit to UFS
    e. Align humerus to neutral horizontal abduction
    f. Align humerus to neutral internal/external rotation
        i. Equal amount of cartilage on anterior and posterior side of glenoid (0° ER)
        ii. Tighten screws on plate of ball plate
12. Program execution:
    a. Turn the robot controller back to the "Run" position
    b. **load gh5.v5**, the robot's program for glenohumeral abduction, in the Supervisor
    c. Open protocol and enter date, test number
    d. Measure the center of the scapular coordinate system using the most anterior point of the lesser tuberosity and the most posterior point of the humeral ridge as reference landmarks. Take all measurements from the marks located on the endplate. Note that for the "specimen's left," the x-value will be negative (need to move in the negative x direction to get from endplate to point on humeral head). Measure the angle of abduction using a goniometer.
    e. Record all geometric measurements in data sheet
    f. Digitize anatomic coordinate system and registration blocks with Microscribe
    g. **ex gh** in the Supervisor to execute the GH abduction program
    h. In the HyperTerminal:
        i. Choose subroutine **210**—*Review Parameters (center and fixture c.g.)*
            1. Input Geometric Center from Excel file (calculated from measured joint)
            2. Record COF in protocol (*C.G. of Fixture*)

ii. Choose subroutine **240**—*Find Passive ROA (force control)*
GHSide: [default=Right]\1=Left **1** or <enter>
* changes depending on specimen
Angles: Now, Abduct.min, Abduct.max ****,0,70**
* *Now* cannot be greater than *Abduct.max* or less than *Abduct min*
* These value vary depending on measured abduction angle of mounted specimen
Force targets? Left, Sup, Prox **0,0,-22**
- Negative value for compressive force

i. Type **60** in the Hyperterminal to move to 60° GH abduction along the passive path of abduction
j. Type **999** in Hyperterminal to exit the program
k. Type **here #start** in Supervisor to save spatial location of scapula (wrt fixed/mounted humerus) - hit <enter> when prompted if want to change
l. Path of passive glenohumeral abduction is now established. Supervisor Commands

storer H***La**
storer = stores real variables (will create a file H*****La.rv that contains each variable in the code, with the most updated value)
l = specifies left shoulder
m = model (a=animal, h=human, p=porcine)
***** = YearMonthDay (ex: 40524 = May 24, 2004)
a = passive path of abduction notation

storel H***La**
storel = stores locations, i.e. the 6 joint angles at all stored positions that were run previously

j. Have clinician and engineer verify equal distribution of humeral head on sides of glenoid rim by palpation
k. Take anterior/posterior radiographs at 30° and 60° of abduction to verify proper glenoid-humeral head alignment
l. Type **ex gh** in Supervisor to get back into GH abduction program
m. In Hyperterminal:
a. Choose subroutine **220—***Enter (add to) testing flexion angles*
Enter number of abduction angles, total: **1**
Enter the next test abduction angle value: **60**

<u>Camera Set-up for Strain Tracking</u>

13. With joint at 60° of GH abduction and neutral horizontal abduction and rotation, set up 3 cameras such that all markers on inferior capsule are visible by at least 2 of the cameras at all time
    a. Also check that markers on humeral and scapular registration blocks are visible by at least 2 cameras
14. Type **260** in the HyperTerminal to run the loading program
    a. *Apply load, at 1 Abduction (codes 601 to 603)* with code structure:

600, index, magnitude, constant (1)/ramp(0)

600 = change previous code

Index

0 = LR (left-right—anterior-posterior—index)
1 = SI (superior-inferior index)
2 = PD (proximal-distal—compression force—index)
3 = AB
4 = GHIE (glenohumeral internal/external rotation)
7 = Rate

15. Apply compressive force in HyperTerminal:
    600,2,-22,1 * i.e. 22 N compressive force, constant
16. 603 for application of pure IE – cannot do this with a 601 or a 602, must be 603.
    a. Apply external rotation with 3Nm of torque (negative degrees for ER on a left shoulder) with ramping (collects data for both ER and IR) and no other forces at 60° abduction:
       600,4,3,0 * i.e. 3 N-m IE torque, ramped
    b. Choose subroutine **603** to run loading condition
       i. *Are you sure? (0=NO, 1=YES)?* **1**
    c. Determine the number of steps to reach 30° and 60° ER (or maximum if 60° ER is not reached)

       *mGHIE = moment during IE loading; GHIE = angle of IE at loading

       * for a left shoulder, external rotation will be first performed. If looking at the output on the HyperTerminal screen, look at the % of motion obtained. When the ER value is ~60° (-60° for a left shoulder), count the number of steps on the screen to get to this value (n). Since the HyperTerminal does not output all steps, the total number of steps is N = 2(n)-1 steps. For example, if ~60° was at 100% of the path, corresponding to step 10 (n=10), the number of robot steps that correspond to 60° of ER would be 19, i.e. 2*10-1
17. Move to 60° ABD, 60° ER
    a. NOTE: Take a movie of the following path of external rotation
    b. Choose subroutine **609--** *Move to extremes (Position Control)*

       Step out to specific position? (0=YES, 1=NO) **0**
       Internal (0) or External (1) rotation ? **1**
       Number of steps to reach desired angle **##**
       -enter N for ~60° or maximum ER from step 16.c
       Stay(0) or Return(1)? **0**
18. Type **999** to exit 260 program
19. Type **999** to exit gh5.v5 program
20. Check that all markers on inferior capsule and both registration blocks are visible by at least 2 cameras (may need to make some minor adjustments)
21. Unscrew base of pedestal and unclamp scapula and remove shoulder from robot testing environment. **BE CAREFUL NOT TO BUMP THE CAMERAS**
22. Fix calibration cube to end of robot manipulator using zip-ties
23. Using teach pendant, move calibration cube such that EACH camera can see ALL the markers (will need to make sure in "teach" mode on Unimate console)

24. Calibrate cameras and record calibration data
25. Remove calibration cube and return manipulator to 60° ABD
    a. Ensure that in "run" mode on Unimate console
    b. Type **do move #start** in Supervisor (should move back to 60° abduction, neutral rotation)
26. Remount shoulder in robot testing environment (**BE CAREFUL NOT TO BUMP ANY CAMERAS!!!**)
    Take photos of entire setup

Intact Shoulder in Robotic Testing System

27. Type **ex gh** to get back into the gh5.v5 program
28. Type **260**
29. Make sure that the IE moment has been removed
    600,4,0,0
30. Apply compressive force:
    600,2,-22,1
31. 601 for application of AP loading at 60° GH Abduction, 0° ER
    a. Apply AP of 25N or other, with ramping and no other forces at 60°:
       600,0,25,0
    b. Type **601** to run the 601 subroutine loading condition
    c. Determine number of steps to reach 15 and 25N anterior and posterior loads
       * since 25 N load applied, should be at ~100% of load, i.e. step 19
       * for a left shoulder, the first motion will be posterior translation of the humeral head with respect to the scapula (scapula is moving anterior)
       * for a right shoulder, the first motion will be anterior translation of the humeral head with respect to the scapula (scapula is moving posterior)
    d. Record data in EXCEL spreadsheet and data sheet
32. 602 for application of AP load at 60° GH Abduction, 30° ER
    a. Choose subroutine **609**-- *Move to extremes (Position Control)*
       Step out to specific position? (0=YES, 1=NO) **0**
       Internal (0) or External (1) rotation ? **1**
       Number of steps to reach desired angle **##**
       - enter N for ~30° ER from step 16.c
       Stay(0) or Return(1)? **0**
    b. Type **602** to run 602 subroutine loading condition at 30°ER
    c. Determine number of steps to reach 15 and 25N anterior and posterior loads
    d. Prompt: *Stay at extreme (0) or return to PPA (1)?* **1**
       * will move back to 60° abduction, 0° rotation
    e. Record data in EXCEL spreadsheet and data sheet
33. Type **999** to exit 260 program
34. Type **999** to exit gh5.v5 program
35. Store data appropriately in Supervisor
    storer H***Lb**
    storel H***Lb**

→ PROCESS DATA←

36. Type **ex gh** in Supervisor to open gh5.v5 program
37. Type **260**
38. 601 for application of AP load at 60° GH Abduction, and 60° ER
    a. Choose subroutine **609--** *Move to extremes (Position Control)*
        Step out to specific position? (0=YES, 1=NO) **0**
        Internal (0) or External (1) rotation ? **1**
        Number of steps to reach desired angle **##**
            - enter N for ~60° or maximum ER from step 16.c
        Stay(0) or Return(1)? **0**
    b. Type **601** to run 601 subroutine loading condition at 60° ER
    c. Determine the number of steps to reach 15 and 25N anterior and posterior loads
    d. Prompt: *Stay at extreme (0) or return to PPA (1)?* **1**
        * will move back to 60° abduction, 0° rotation
    e. Record data in EXCEL spreadsheet and data sheet
39. Type **999** to exit 260 program
40. Type **999** to exit gh5.v5 program
41. Store data appropriately.
    storer H***Lc**
    storel H***Lc**

→ PROCESS DATA←

42. Type **ex gh**
43. Type **260**

Strain Measurements

* Digitize Registration blocks (for 60° GH Abduction, neutral rotation position)

44. Load data file for loads applied at 60° GH Abduction, and 0° and 30°ER
    a. Load **H*****Lb.rv**
    b. Load **H*****Lb.lc**
45. Type **ex gh**
46. Type **260**
47. 607 for position control of AP loading at 0° ER (601 in step 31)
    a. Choose subroutine **607**—Step out to each position manually using position control ability at 0° ER, 60° ABD
    b. Prompt: *Step out to specific position (0=YES) or go in one step increments (1)* **1**
        # cycles, Hold extremes (1=NO)? [1,hold] **1**
    c. Strike ENTER key until you reach the number of steps that corresponds to the position where 15 and 25N of posterior (L) or anterior (R) load was applied (step 31.c)
        * Algorithm:
            - After pressing <enter> in step 53.b, prompts will be given to press Return to continue
                - i.e. “Positive / Negative, press Return to continue”

- Return
  - 1st -19th return: 19 steps in first direction of loading path
  - 20th return: same as 19th return
  - 21st -39th return: steps back to zero position
  - 40th – 58th return: 19 steps in second direction of loading path
  - 59th return: goes back to zero position
- Example: Left shoulder, 25N posterior load is at N = 17 steps (posterior hh motion wrt scapula), 25 N anterior load is at N = 15 steps (anterior hh motion wrt scapula)
  - Need to return 17x to get to 25 N posterior load, since posterior humeral head motion is first for a left shoulder
  - Need to return (39+15) = 44x to get to 25 N anterior load

d. Take strain measurement with camera system
e. Digitize registration blocks
f. Take multiple pictures (ant, post, inf views) of the capsule using a camera
g. Strike ENTER key until you reach the number of steps that corresponds to the position where 15 and 25N of anterior (L) or posterior (R) load was applied (step 31.c)
h. Take strain measurement with camera system
i. Digitize registration blocks
j. Take multiple pictures
k. Go back to neutral translation at 0°ER by pressing <enter> until you have returned a total of 59 times

48. 608 for position control of AP loading at 30° ER (602 in step 32)
    a. Digitize registration blocks (30 ER neutral position)
    b. Choose subroutine **609**-- *Move to extremes (Position Control)*
       Step out to specific position (0=YES) or go in one step increments (1) **0**
       Internal (0) or External (1) rotation ? **1**
       Number of steps to reach desired angle **##**
       - enter N for ~30° ER from step 16.c
       Stay(0) or Return(1)? **0**
    c. Choose subroutine **608**—Step out to each position manually using position control ability at 30° ER, 60° ABD
    d. Prompt: *Step out to specific position (0=YES) or go in one step increments (1)* **1**
       # cycles, Hold extremes (1=NO)? [1,hold] **1**
    e. Strike ENTER key until you reach the number of steps that corresponds to the position where 15 and 25N of posterior (L) or anterior (R) load was applied (step 32.e)
    f. Take strain measurement with camera system
    g. Digitize registration blocks
    h. Take multiple pictures

i. Strike ENTER key until you reach the number of steps that corresponds to the position where 15 and 25N of anterior (L) or posterior (R) load was applied (step 32.e)
j. Take strain measurement with camera system
k. Digitize registration blocks
l. Take multiple pictures
m. Go back to neutral translation at 30°ER by pressing <enter> until you have returned a total of 59 times

49. Return position to 0°ER
    a. Type in an angle value that is within the passive path of abduction (i.e. 60)
    b. Prompt: *At externally rotated position*
        Type '0' to Continue **0**
        (1) Return to PPA position **1**
50. Type **999** to exit 260
51. Type **999** to exit gh5.v5
52. Load data file for loads applied to AP load at 60° ER, 60° ABD
    a. Load **H*****Lc.rv**
    b. Load **H*****Lc.lc**
53. Type **ex gh** in Supervisor
54. Type **260** in Hyperterminal
55. 607 for position control of AP loading at 60°ER (601 in step 38)
    a. Choose subroutine **609--** *Move to extremes (Position Control)*
        Step out to specific position (0=YES) or go in one step increments (1) **0**
        Internal (0) or External (1) rotation ? **1**
        Number of steps to reach desired angle **##**
        - enter N for ~60° or maximum ER from step 16.c

        Stay(0) or Return(1)? **0**
    b. Digitize Registration Blocks (60 ER neutral position)
    c. Choose subroutine **607**—Step out to each position manually using position control ability at 60° ER, 60° ABD
    d. Prompt: *Step out to specific position (0=YES) or go in one step increments (1)* **1**
        # cycles, Hold extremes (1=NO)? [1,hold] **1**
    e. Strike ENTER key until you reach the number of steps that corresponds to the position where 15 and 25N of posterior (L) or anterior (R) load was applied (step 38.e)
    f. Take strain measurement with camera system
    g. Digitize registration blocks
    h. Take multiple pictures
    i. Strike ENTER key until you reach the number of steps that corresponds to the position where 15 and 25N of anterior (L) or posterior (R) load was applied (step 38.e)
    j. Take strain measurement with camera system
    k. Digitize registration blocks
    l. Tale multiple pictures

m. Go back to neutral translation at 60°ER by pressing <enter> until you have returned a total of 59 times

56. Return position to 0°ER
    a. Type in an angle value that is within the passive path of abduction (i.e. 60)
    b. Prompt: *At externally rotated position*

Type '0' to Continue	**0**	*(1)*
Return to PPA position	**1**	

Clean Up

57. Remove and clean all clamps, clean the work area, return the robot to the start position, and shut down robot

APPENDIX B

APPENDIX B. NIKE3D INPUT DECK FOR FE MODEL 2

TrueGridauto

```
*
* This file was created using TrueGrid by XYZ Scientific Applications, Inc.
* For further information, call (925) 373-0628 or write to:
*
*      XYZ Scientific Applications, Inc.
*      1324 Concannon Blvd.
*      Livermore, CA  94550
*
*  TrueGrid version  2.2.6   dated 08/25/06
*    generated on Jun  2 2008 at 07:57:35
*
*------------------------- CONTROL CARD #2 --------------------------*
*
* Input format [1]
* Number of materials [2]
* Number of node points [3]
* Number of brick elements [4]
* Number of beam elements [5]
* Number of shell elements [6]
* Number of 1D slide lines [7]
* Number of sliding interfaces [8]
* Number of rigid walls and symmetry planes [9]
* Discrete element input flag [10]
*
FL 22     28946        0        0     46297    0    0    0    0   72
*
*------------------------- CONTROL CARD #3 --------------------------*
*
* Number of time steps [1]
```

```
* Time step size [2]
* Automatic time step control flag [3]
* Maximum number of retries allowable per step [4]
* Optimal number of iterations per step [5]
* Minimum allowable step size [6]
* Maximum allowable step size [7]
* Size of the iteration window [8]
*
      20       0.1 auto    0   20    0.0001       -7.0    0
*
*------------------------- CONTROL CARD #4 --------------------------*
*
* Number of load curves [1]
* Maximum number of points defining any load curve [2]
* Number of concentrated nodal loads [3]
* Number of element surfaces having pressure loads applied [4]
* Number of displacement boundary condition cards [5]
* Number of beam elements with aerodynamic drag loads [6]
* Number of node constraint cards [7]
* Body force loads due to base acceleration in x-direction [8]
* Body force loads due to base acceleration in y-direction [9]
* Body force loads due to base acceleration in z-direction [10]
* Body force loads due to angular velocity about the x-direction [11]
* Body force loads due to angular velocity about the y-direction [12]
* Body force loads due to angular velocity about the z-direction [13]
*
   7    3    0    0    0    0    0    0    0    0    0    0    0    0    0
*
*------------------------- CONTROL CARD #5 --------------------------*
*
* Output print interval [1]
* Output plotting interval [2]
* Number of node printblocks [3]
* Number of brick printout blocks [4]
* Number of beam printout blocks [5]
* Number of shell printout blocks [6]
* Number of time steps between restart file generation [7]
* Shell surface strain dump flag [8]
* Initial sense switch toggles [9]
* Acceleration data dump flag [10]
*
  1    1   -1   -1   -1   -1    0    0    036000    0    0    1
*
*------------------------- CONTROL CARD #6 --------------------------*
*
* Method of iterating for equilibrium [1]
```

```
* Bandwidth minimization flag [2]
* Number of steps between stiffness reformations [3]
* Number of steps between equilibrium iterations [4]
* Maximum number of equilibrium iterations between stiffness matrix
*   reformations [5]
* Maximum number of stiffness matrix reformations per time step [6]
* Convergence tolerance on displacement [7]
* Convergence tolerance on energy [8]
* Convergence tolerance line search [9]
* Convergence tolerance for the augmented Lagrangian [10]
* Convergence tolerance on residuals [11]
*
   1    2        1        1    1   50     -0.01     0.001       0.0       0.0
*
*-------------------------- CONTROL CARD #7 --------------------------*
*
* Analysis type [1]
* Initial condition parameter [2]
* Thermal effects option [3]
* Temperature profile input flag [4]
* Number of eigenvalues and eigenvectors to be executed [5]
* Frequency shift, cycles per unit time [6]
* First Newmark integration parameter [7]
* Second Newmark integration parameter [8]
*
   0    0    0    0    0       0.0       0.5      0.25
*
*-------------------------- CONTROL CARD #8 --------------------------*
*
* Percent of memory option [1]
* Buffer size (words)element I/O [2]
* Stiffness matrix storage option [3]
* BFGS update vectors storage option [4]
* Brick element formulation [5]
* Brick element geometric stiffness flag [6]
* Shell element formulation [7]
* Hourglass control parameter (Belytschko-Tsay shell only) [8]
* Shell element geometric stiffness flag [9]
* Beam element formulation [10]
* Beam element geometric stiffness flag [11]
*
   0        0    1    2   10    2    2 0.000E+00    0    0    0
*
*-------------------------- CONTROL CARD #9 --------------------------*
*
* Number of unloading steps in modified arc length method (optional) [1]
```

```
* Solution method during arc length unloading [2]
* Node number for displacement arc length method [3]
* Direction of displacement at arc length controlling node [4]
* Desired arc length [5]
* Arc length constraint method [6]
* Arc length damping option [7]
* Number of user-specified integration rules for beams [8]
* Maximum number of user-specified integration points [9]
* Number of user-specified integration rules for shells [10]
* Maximum number of user-specified integration points [11]
*
   0    0    0    0      0.0    0    0    0    0    0    0
*
*------------------------- CONTROL CARD #10--------------------------*
*
* Linear equation solver option [1]
* Iteration limit for linear solver [2]
* Iteration convergence tolerance [3]
* Buffer size (element) for out-of-core iterative linear solver [4]
* Print-out option for linear iterative solver [5]
*
   0    0      0.0    0    0    0
*
*-------------------------- MATERIAL CARDS ---------------------------*
*
   1    1    0.0007    2      0.0      0.0      0.0
ABIGHL
     2.05       0.0       0.0       0.0       0.0       0.0       0.0       0.0
   0.4995       0.0       0.0       0.0       0.0       0.0       0.0       0.0
      0.0       0.0       0.0       0.0       0.0       0.0       0.0       0.0
      0.0       0.0       0.0       0.0       0.0       0.0       0.0       0.0
      0.0       0.0       0.0       0.0       0.0       0.0       0.0       0.0
      0.0       0.0       0.0       0.0       0.0       0.0       0.0       0.0
      0.0       0.0       0.0       0.0
      2.5       2.5       2.5       2.5       0.0
   2    1    0.0007    2      0.0      0.0      0.0
AxPouch
 4.9200001       0.0       0.0       0.0       0.0       0.0       0.0       0.0
   0.4995       0.0       0.0       0.0       0.0       0.0       0.0       0.0
      0.0       0.0       0.0       0.0       0.0       0.0       0.0       0.0
      0.0       0.0       0.0       0.0       0.0       0.0       0.0       0.0
      0.0       0.0       0.0       0.0       0.0       0.0       0.0       0.0
      0.0       0.0       0.0       0.0       0.0       0.0       0.0       0.0
      0.0       0.0       0.0       0.0
      2.5       2.5       2.5       2.5       0.0
   3    1    0.0007    2      0.0      0.0      0.0
```

```
PBIGHL
     3.73       0.0       0.0       0.0       0.0       0.0       0.0       0.0
   0.4995       0.0       0.0       0.0       0.0       0.0       0.0       0.0
      0.0       0.0       0.0       0.0       0.0       0.0       0.0       0.0
      0.0       0.0       0.0       0.0       0.0       0.0       0.0       0.0
      0.0       0.0       0.0       0.0       0.0       0.0       0.0       0.0
      0.0       0.0       0.0       0.0       0.0       0.0       0.0       0.0
      0.0       0.0       0.0       0.0
      2.5       2.5       2.5       2.5       0.0
   4    1    0.0007    2       0.0       0.0       0.0
AntSup
 2.1199999       0.0       0.0       0.0       0.0       0.0       0.0       0.0
   0.4995       0.0       0.0       0.0       0.0       0.0       0.0       0.0
      0.0       0.0       0.0       0.0       0.0       0.0       0.0       0.0
      0.0       0.0       0.0       0.0       0.0       0.0       0.0       0.0
      0.0       0.0       0.0       0.0       0.0       0.0       0.0       0.0
      0.0       0.0       0.0       0.0       0.0       0.0       0.0       0.0
      0.0       0.0       0.0       0.0
      2.5       2.5       2.5       2.5       0.0
   5    1    0.0007    2       0.0       0.0       0.0
PostCaps
 5.8299999       0.0       0.0       0.0       0.0       0.0       0.0       0.0
   0.4995       0.0       0.0       0.0       0.0       0.0       0.0       0.0
      0.0       0.0       0.0       0.0       0.0       0.0       0.0       0.0
      0.0       0.0       0.0       0.0       0.0       0.0       0.0       0.0
      0.0       0.0       0.0       0.0       0.0       0.0       0.0       0.0
      0.0       0.0       0.0       0.0       0.0       0.0       0.0       0.0
      0.0       0.0       0.0       0.0
      2.5       2.5       2.5       2.5       0.0
   6   20    1000.0    2       0.0       0.0       0.0
humerus material - rigid
   10000.0       0.0       0.0       0.0       0.0       0.0       0.0       0.0
      0.3       0.0       0.0       0.0       0.0       0.0       0.0       0.0
      1.0       2.0       3.0       4.0       5.0       6.0       0.0       0.0
      1.0       0.0       0.0       0.0       0.0       0.0       0.0       0.0
      0.0       0.0       0.0       0.0       0.0       0.0       0.0       0.0
      0.0       0.0       0.0       0.0       0.0       0.0       0.0       0.0
      0.0       0.0       0.0       0.0
      0.5       0.5       0.5       0.5       0.0
   7   20    1000.0    2       0.0       0.0       0.0
scapula material - rigid
   10000.0       0.0       0.0       0.0       0.0       0.0       0.0       0.0
      0.3       0.0       0.0       0.0       0.0       0.0       0.0       0.0
     -1.0      -1.0      -1.0      -1.0      -1.0      -1.0       0.0       0.0
      1.0 25.174601 141.10899  -13.3056       0.0       0.0       0.0       0.0
      0.0       0.0       0.0       0.0       0.0       0.0       0.0       0.0
```

0.0 0.0 0.0 0.0 0.0 0.0 0.0 0.0
0.0 0.0 0.0 0.0
0.5 0.5 0.5 0.5 0.0
8 1 0.0007 2 0.0 0.0 0.0
ABIGHL Labrum Deep
2.05 0.0 0.0 0.0 0.0 0.0 0.0 0.0
0.4995 0.0 0.0 0.0 0.0 0.0 0.0 0.0
0.0 0.0 0.0 0.0 0.0 0.0 0.0 0.0
0.0 0.0 0.0 0.0 0.0 0.0 0.0 0.0
0.0 0.0 0.0 0.0 0.0 0.0 0.0 0.0
0.0 0.0 0.0 0.0 0.0 0.0 0.0 0.0
0.0 0.0 0.0 0.0
3.5 4.0 4.0 3.5 0.0
9 1 0.0007 2 0.0 0.0 0.0
ABIGHL Labrum Middle
2.05 0.0 0.0 0.0 0.0 0.0 0.0 0.0
0.4995 0.0 0.0 0.0 0.0 0.0 0.0 0.0
0.0 0.0 0.0 0.0 0.0 0.0 0.0 0.0
0.0 0.0 0.0 0.0 0.0 0.0 0.0 0.0
0.0 0.0 0.0 0.0 0.0 0.0 0.0 0.0
0.0 0.0 0.0 0.0 0.0 0.0 0.0 0.0
0.0 0.0 0.0 0.0
3.0 3.5 3.5 3.0 0.0
10 1 0.0007 2 0.0 0.0 0.0
ABIGHL Labrum Art
2.05 0.0 0.0 0.0 0.0 0.0 0.0 0.0
0.4995 0.0 0.0 0.0 0.0 0.0 0.0 0.0
0.0 0.0 0.0 0.0 0.0 0.0 0.0 0.0
0.0 0.0 0.0 0.0 0.0 0.0 0.0 0.0
0.0 0.0 0.0 0.0 0.0 0.0 0.0 0.0
0.0 0.0 0.0 0.0 0.0 0.0 0.0 0.0
0.0 0.0 0.0 0.0
2.5 3.0 3.0 2.5 0.0
11 1 0.0007 2 0.0 0.0 0.0
AxPouch Labrum Deep
4.9200001 0.0 0.0 0.0 0.0 0.0 0.0 0.0
0.4995 0.0 0.0 0.0 0.0 0.0 0.0 0.0
0.0 0.0 0.0 0.0 0.0 0.0 0.0 0.0
0.0 0.0 0.0 0.0 0.0 0.0 0.0 0.0
0.0 0.0 0.0 0.0 0.0 0.0 0.0 0.0
0.0 0.0 0.0 0.0 0.0 0.0 0.0 0.0
0.0 0.0 0.0 0.0
3.5 4.0 4.0 3.5 0.0
12 1 0.0007 2 0.0 0.0 0.0
AxPouch Labrum Middle
4.9200001 0.0 0.0 0.0 0.0 0.0 0.0 0.0

0.4995 0.0 0.0 0.0 0.0 0.0 0.0 0.0
0.0 0.0 0.0 0.0 0.0 0.0 0.0 0.0
0.0 0.0 0.0 0.0 0.0 0.0 0.0 0.0
0.0 0.0 0.0 0.0 0.0 0.0 0.0 0.0
0.0 0.0 0.0 0.0 0.0 0.0 0.0 0.0
0.0 0.0 0.0 0.0
3.0 3.5 3.5 3.0 0.0
13 1 0.0007 2 0.0 0.0 0.0
AxPouch Labrum Art
4.9200001 0.0 0.0 0.0 0.0 0.0 0.0 0.0
0.4995 0.0 0.0 0.0 0.0 0.0 0.0 0.0
0.0 0.0 0.0 0.0 0.0 0.0 0.0 0.0
0.0 0.0 0.0 0.0 0.0 0.0 0.0 0.0
0.0 0.0 0.0 0.0 0.0 0.0 0.0 0.0
0.0 0.0 0.0 0.0 0.0 0.0 0.0 0.0
0.0 0.0 0.0 0.0
2.5 3.0 3.0 2.5 0.0
14 1 0.0007 2 0.0 0.0 0.0
PBIGHL Labrum Deep
3.73 0.0 0.0 0.0 0.0 0.0 0.0 0.0
0.4995 0.0 0.0 0.0 0.0 0.0 0.0 0.0
0.0 0.0 0.0 0.0 0.0 0.0 0.0 0.0
0.0 0.0 0.0 0.0 0.0 0.0 0.0 0.0
0.0 0.0 0.0 0.0 0.0 0.0 0.0 0.0
0.0 0.0 0.0 0.0 0.0 0.0 0.0 0.0
0.0 0.0 0.0 0.0
3.5 4.0 4.0 3.5 0.0
15 1 0.0007 2 0.0 0.0 0.0
PBIGHL Labrum Middle
3.73 0.0 0.0 0.0 0.0 0.0 0.0 0.0
0.4995 0.0 0.0 0.0 0.0 0.0 0.0 0.0
0.0 0.0 0.0 0.0 0.0 0.0 0.0 0.0
0.0 0.0 0.0 0.0 0.0 0.0 0.0 0.0
0.0 0.0 0.0 0.0 0.0 0.0 0.0 0.0
0.0 0.0 0.0 0.0 0.0 0.0 0.0 0.0
0.0 0.0 0.0 0.0
3.0 3.5 3.5 3.0 0.0
16 1 0.0007 2 0.0 0.0 0.0
PBIGHL Labrum Art
3.73 0.0 0.0 0.0 0.0 0.0 0.0 0.0
0.4995 0.0 0.0 0.0 0.0 0.0 0.0 0.0
0.0 0.0 0.0 0.0 0.0 0.0 0.0 0.0
0.0 0.0 0.0 0.0 0.0 0.0 0.0 0.0
0.0 0.0 0.0 0.0 0.0 0.0 0.0 0.0
0.0 0.0 0.0 0.0 0.0 0.0 0.0 0.0
0.0 0.0 0.0 0.0

2.5 3.0 3.0 2.5 0.0
17 1 0.0007 2 0.0 0.0 0.0
AntSup Labrum Deep
2.1199999 0.0 0.0 0.0 0.0 0.0 0.0 0.0
0.4995 0.0 0.0 0.0 0.0 0.0 0.0 0.0
0.0 0.0 0.0 0.0 0.0 0.0 0.0 0.0
0.0 0.0 0.0 0.0 0.0 0.0 0.0 0.0
0.0 0.0 0.0 0.0 0.0 0.0 0.0 0.0
0.0 0.0 0.0 0.0 0.0 0.0 0.0 0.0
0.0 0.0 0.0 0.0
3.5 4.0 4.0 3.5 0.0
18 1 0.0007 2 0.0 0.0 0.0
AntSup Labrum Middle
2.1199999 0.0 0.0 0.0 0.0 0.0 0.0 0.0
0.4995 0.0 0.0 0.0 0.0 0.0 0.0 0.0
0.0 0.0 0.0 0.0 0.0 0.0 0.0 0.0
0.0 0.0 0.0 0.0 0.0 0.0 0.0 0.0
0.0 0.0 0.0 0.0 0.0 0.0 0.0 0.0
0.0 0.0 0.0 0.0 0.0 0.0 0.0 0.0
0.0 0.0 0.0 0.0
3.0 3.5 3.5 3.0 0.0
19 1 0.0007 2 0.0 0.0 0.0
AntSup Labrum Art
2.1199999 0.0 0.0 0.0 0.0 0.0 0.0 0.0
0.4995 0.0 0.0 0.0 0.0 0.0 0.0 0.0
0.0 0.0 0.0 0.0 0.0 0.0 0.0 0.0
0.0 0.0 0.0 0.0 0.0 0.0 0.0 0.0
0.0 0.0 0.0 0.0 0.0 0.0 0.0 0.0
0.0 0.0 0.0 0.0 0.0 0.0 0.0 0.0
0.0 0.0 0.0 0.0
2.5 3.0 3.0 2.5 0.0
20 1 0.0007 2 0.0 0.0 0.0
PostCaps Labrum Deep
5.8299999 0.0 0.0 0.0 0.0 0.0 0.0 0.0
0.4995 0.0 0.0 0.0 0.0 0.0 0.0 0.0
0.0 0.0 0.0 0.0 0.0 0.0 0.0 0.0
0.0 0.0 0.0 0.0 0.0 0.0 0.0 0.0
0.0 0.0 0.0 0.0 0.0 0.0 0.0 0.0
0.0 0.0 0.0 0.0 0.0 0.0 0.0 0.0
0.0 0.0 0.0 0.0
3.5 4.0 4.0 3.5 0.0
21 1 0.0007 2 0.0 0.0 0.0
PostCaps Labrum Middle
5.8299999 0.0 0.0 0.0 0.0 0.0 0.0 0.0
0.4995 0.0 0.0 0.0 0.0 0.0 0.0 0.0
0.0 0.0 0.0 0.0 0.0 0.0 0.0 0.0

```
      0.0       0.0       0.0       0.0       0.0       0.0       0.0       0.0
      0.0       0.0       0.0       0.0       0.0       0.0       0.0       0.0
      0.0       0.0       0.0       0.0       0.0       0.0       0.0       0.0
      0.0       0.0       0.0       0.0
      3.0       3.5       3.5       3.0       0.0
  22    1    0.0007    2       0.0       0.0       0.0
PostCaps Labrum Art
 5.8299999       0.0       0.0       0.0       0.0       0.0       0.0       0.0
   0.4995        0.0       0.0       0.0       0.0       0.0       0.0       0.0
      0.0       0.0       0.0       0.0       0.0       0.0       0.0       0.0
      0.0       0.0       0.0       0.0       0.0       0.0       0.0       0.0
      0.0       0.0       0.0       0.0       0.0       0.0       0.0       0.0
      0.0       0.0       0.0       0.0       0.0       0.0       0.0       0.0
      0.0       0.0       0.0       0.0
      2.5       3.0       3.0       2.5       0.0
*
*--------------------------- NODE DEFINITIONS --------------------------*
*

(NODE DEFINITIONS, LEFT OFF FOR SPACE SAVING REASONS)

*
*----------------------- SHELL ELEMENT DECK ------------------------*
*

(SHELL ELEMENT DEFINITIONS)

*
*---------------------- RIGID NODES AND FACET DECK ----------------------*
*

(RIGID NODES AND FACET DEFINITIONS)

*
*-------------------------- LOAD CURVE DECK -------------------------*
*
  1    3
      0.0       0.0
      1.0   -0.9600
      2.0   -4.9600
   2    3
      0.0       0.0
      1.0    3.3076
      2.0    6.3076
   3    3
      0.0       0.0
```

```
  1.0   3.0601
  2.0   13.0601
4   3
  0.0       0.0
  1.0  0.031825
  2.0  0.031825
5   3
  0.0       0.0
  1.0 -0.106967
  2.0 -0.306967
6   3
  0.0       0.0
  1.0  0.065887
  2.0  0.065887
7   2
  0.0       0.0
  2.0       0.2
```

APPENDIX C

APPENDIX C. FEBIO INPUT DECK FOR FE MODEL 2

```
<?xml version="1.0" encoding="ISO-8859-1"?>
<febio_spec version="1.0">
	<Control>
		<title>TrueGridauto</title>
		<time_steps>20</time_steps>
		<step_size>0.1</step_size>
		<max_refs>50</max_refs>
		<max_ups>15</max_ups>
		<dtol>0.001</dtol>
		<etol>0.01</etol>
		<rtol>1e+010</rtol>
		<lstol>0.9</lstol>
		<time_stepper>
			<dtmin>0.01</dtmin>
			<dtmax lc="1"></dtmax>
			<max_retries>10</max_retries>
			<opt_iter>25</opt_iter>
			<aggressiveness>1</aggressiveness>
		</time_stepper>
		<plot_level>PLOT_MUST_POINTS</plot_level>
		<restart>1</restart>
	</Control>
	<Material>
		<material id="1" name="humerus material - rigid" type="rigid body">
			<density>1000</density>
			<center_of_mass>0,0,0</center_of_mass>
			<trans_x type="prescribed" lc="2">1</trans_x>
			<trans_y type="prescribed" lc="3">1</trans_y>
			<trans_z type="prescribed" lc="4">1</trans_z>
			<rot_x type="prescribed" lc="5">1</rot_x>
```

```
        <rot_y type="prescribed" lc="6">1</rot_y>
        <rot_z type="prescribed" lc="7">1</rot_z>
</material>
<material id="2" name="scapula material - rigid" type="rigid body">
        <density>1000</density>
        <center_of_mass>25.1746,141.109,-13.3056</center_of_mass>
        <trans_x type="fixed"></trans_x>
        <trans_y type="fixed"></trans_y>
        <trans_z type="fixed"></trans_z>
        <rot_x type="fixed"></rot_x>
        <rot_y type="fixed"></rot_y>
        <rot_z type="fixed"></rot_z>
</material>
<material id="3" name="AB-IGHL" type="Veronda-Westmann">
        <c1>0.06</c1>
        <c2>2.7</c2>
        <k>75</k>
</material>
<material id="4" name="Ax Pouch" type="Veronda-Westmann">
        <c1>0.06</c1>
        <c2>2.7</c2>
        <k>75</k>
</material>
<material id="5" name="PB-IGHL" type="Veronda-Westmann">
        <c1>0.91</c1>
        <c2>3.1</c2>
        <k>75</k>
</material>
<material id="6" name="AS" type="Veronda-Westmann">
        <c1>0.07</c1>
        <c2>6.8</c2>
        <k>75</k>
</material>
<material id="7" name="Post Caps" type="Veronda-Westmann">
        <c1>0.27</c1>
        <c2>4.4</c2>
        <k>75</k>
</material>
<material id="8" name="ABLab_glen" type="Veronda-Westmann">
        <c1>0.06</c1>
        <c2>2.7</c2>
        <k>75</k>
</material>
<material id="9" name="ABLab_mid" type="Veronda-Westmann">
        <c1>0.06</c1>
        <c2>2.7</c2>
```

```
        <k>75</k>
</material>
<material id="10" name="ABLab_art" type="Veronda-Westmann">
        <c1>0.06</c1>
        <c2>2.7</c2>
        <k>75</k>
</material>
<material id="11" name="APLab_glen" type="Veronda-Westmann">
        <c1>0.06</c1>
        <c2>2.7</c2>
        <k>75</k>
</material>
<material id="12" name="APLab_mid" type="Veronda-Westmann">
        <c1>0.06</c1>
        <c2>2.7</c2>
        <k>75</k>
</material>
<material id="13" name="APLab_art" type="Veronda-Westmann">
        <c1>0.06</c1>
        <c2>2.7</c2>
        <k>75</k>
</material>
<material id="14" name="PBLab_glen" type="Veronda-Westmann">
        <c1>0.91</c1>
        <c2>3.1</c2>
        <k>75</k>
</material>
<material id="15" name="PBLab_mid" type="Veronda-Westmann">
        <c1>0.91</c1>
        <c2>3.1</c2>
        <k>75</k>
</material>
<material id="16" name="PBLab_art" type="Veronda-Westmann">
        <c1>0.91</c1>
        <c2>3.1</c2>
        <k>75</k>
</material>
<material id="17" name="AntSupLab_glen" type="Veronda-Westmann">
        <c1>0.07</c1>
        <c2>6.8</c2>
        <k>75</k>
</material>
<material id="18" name="AntSupLab_mid" type="Veronda-Westmann">
        <c1>0.07</c1>
        <c2>6.8</c2>
        <k>75</k>
```

```
            </material>
            <material id="19" name="AntSupLab_art" type="Veronda-Westmann">
                  <c1>0.07</c1>
                  <c2>6.8</c2>
                  <k>75</k>
            </material>
            <material id="20" name="PostLab_glen" type="Veronda-Westmann">
                  <c1>0.27</c1>
                  <c2>4.4</c2>
                  <k>75</k>
            </material>
            <material id="21" name="PostLab_mid" type="Veronda-Westmann">
                  <c1>0.27</c1>
                  <c2>4.4</c2>
                  <k>75</k>
            </material>
            <material id="22" name="PostLab_art" type="Veronda-Westmann">
                  <c1>0.27</c1>
                  <c2>4.4</c2>
                  <k>75</k>
            </material>
      </Material>
      <Geometry>
            <Nodes>

(NODE DEFINITIONS – LEFT OFF FOR SPACE SAVING REASONS)

            </Nodes>
            <Elements>

(ELEMENT DEFINITIONS)

            </Elements>
            <ElementData>

(ELEMENT THICKNESS DEFINITIONS)

            </ElementData>
      </Geometry>
      <Boundary>
            <contact type="rigid">

(RIGID NODE DEFINITIONS)

            </contact>
            <contact type="sliding_with_gaps">
```

```
                    <tolerance lc="8">1</tolerance>
                    <penalty lc="9">1</penalty>
                    <two_pass>0</two_pass>
                    <surface type="master">

(CONTACT BETWEEN CARTILAGE AND CAPSULE: MASTER ELEMENTS)

                    </surface>
                    <surface type="slave">

(CONTACT BETWEEN CARTILAGE AND CAPSULE: SLAVE ELEMENTS)

                    </surface>
                </contact>
                <contact type="sliding_with_gaps">
                    <tolerance lc="10">1</tolerance>
                    <penalty lc="11">1</penalty>
                    <two_pass>0</two_pass>
                    <surface type="master">

(CONTACT BETWEEN HUMERUS AND CAPSULE: MASTER ELEMENTS)

                    </surface>
                    <surface type="slave">

(CONTACT BETWEEN HUMERUS AND CAPSULE: SLAVE ELEMENTS)

                    </surface>
                </contact>
            </Boundary>
            <LoadData>
                <loadcurve id="1">
                    <loadpoint>0,0</loadpoint>
                    <loadpoint>0.1,0.1</loadpoint>
                    <loadpoint>0.2,0.1</loadpoint>
                    <loadpoint>0.3,0.1</loadpoint>
                    <loadpoint>0.4,0.1</loadpoint>
                    <loadpoint>0.5,0.1</loadpoint>
                    <loadpoint>0.6,0.1</loadpoint>
                    <loadpoint>0.7,0.1</loadpoint>
                    <loadpoint>0.8,0.1</loadpoint>
                    <loadpoint>0.9,0.1</loadpoint>
                    <loadpoint>1.0,0.1</loadpoint>
                    <loadpoint>1.1,0.1</loadpoint>
                    <loadpoint>1.2,0.1</loadpoint>
                    <loadpoint>1.3,0.1</loadpoint>
```

```
        <loadpoint>1.4,0.1</loadpoint>
        <loadpoint>1.5,0.1</loadpoint>
        <loadpoint>1.6,0.1</loadpoint>
        <loadpoint>1.7,0.1</loadpoint>
        <loadpoint>1.8,0.1</loadpoint>
        <loadpoint>1.9,0.1</loadpoint>
        <loadpoint>2.0,0.1</loadpoint>
</loadcurve>
<loadcurve id="2">
        <loadpoint>0,0</loadpoint>
        <loadpoint>1,-0.9600</loadpoint>
        <loadpoint>2,-4.9600</loadpoint>
</loadcurve>
<loadcurve id="3">
        <loadpoint>0,0</loadpoint>
        <loadpoint>1,3.3076</loadpoint>
        <loadpoint>2,6.3076</loadpoint>
</loadcurve>
<loadcurve id="4">
        <loadpoint>0,0</loadpoint>
        <loadpoint>1,3.0601</loadpoint>
        <loadpoint>2,13.0601</loadpoint>
</loadcurve>
<loadcurve id="5">
        <loadpoint>0,0</loadpoint>
        <loadpoint>1,0.0318253</loadpoint>
        <loadpoint>2,0.0318253</loadpoint>
</loadcurve>
<loadcurve id="6">
        <loadpoint>0,0</loadpoint>
        <loadpoint>1,-0.106967</loadpoint>
        <loadpoint>2,-0.306967</loadpoint>
</loadcurve>
<loadcurve id="7">
        <loadpoint>0,0</loadpoint>
        <loadpoint>1,0.0658876</loadpoint>
        <loadpoint>2,0.0658876</loadpoint>
</loadcurve>
<loadcurve id="8">
        <loadpoint>0.0,0.1</loadpoint>
        <loadpoint>2.0,0.1</loadpoint>
</loadcurve>
<loadcurve id="9">
        <loadpoint>0.0,0.5</loadpoint>
        <loadpoint>2.0,0.5</loadpoint>
</loadcurve>
```

```
		<loadcurve id="10">
			<loadpoint>0.0,0.1</loadpoint>
			<loadpoint>2.0,0.1</loadpoint>
		</loadcurve>
		<loadcurve id="11">
			<loadpoint>0.0,0.5</loadpoint>
			<loadpoint>2.0,0.5</loadpoint>
		</loadcurve>
	</LoadData>
	<Output>
		<plotfile>
			<shell_strain>1</shell_strain>
		</plotfile>
	</Output>
</febio_spec>
```

APPENDIX D

APPENDIX D. MATLAB CODE FOR SIMULATION OF JOINT MOTION

```
%Nick Drury
%8/28/07
%This program uses inputs of abduction, flexion, external rotation, and
%translation of the humerus with respect to the scapular anatomical
%coordinate system to produce an output representing the transformation
%matrix of motion for the humeral registration block from the reference
%position to the intermediate clinically relevant joint positions for
%FE Model 1.  The transformation matrices of motion are then input into
%quat.m for generation of load curves for input into the finite element
%solver for FE Model 1.

%notation:
% CS=coordinate system
% ACS=anatomical coordinate system
% TG=TrueGrid
% HRB=humeral registration block
% SRB=scapular registration block

clear all
%obtain required inputs
```

```
abd_in=60; %GH abduction angle
flex_in=0; %GH flexion angle
er_in =40; %external rotation angle
trans = [5.86 12.84 -11.25]; %vector of translation representing motion of
                    %the humerus with respect to the scapular
                    %anatomical coordinate system
                    %[anterior medial inferior]

abd_ref = 60;   %abduction angle in reference position
er_ref = 10;    %ER angle in reference position
flex_ref=0;     %flexion angle in reference position

abd=(abd_in-abd_ref)*pi/180;   %convert to radians
er=(er_in-er_ref)*pi/180;      %convert to radians
flex=(flex_in-flex_ref)*pi/180;%convert to radians

%humeral and scapular ACS  with respect to TG CS
T_AH_TG = [-0.6044 0.7953 0.0337 -45.2128;0.7960 0.6042 0.0192 -15.0807;-0.0051 0.0384 -
0.9992 36.1248;0 0 0 1];
T_AS_TG = [-0.3293 0.7733 0.5299 -45.2128;0.9438 0.2533 0.2085 -15.0807;0.0274 0.5688 -
0.8133 36.1248; 0 0 0 1];

%HRB CS with respect to TG CS (previously all
%coordinates shifted so that HRB CS was identical to TG CS)
T_HRB_TG = eye(4);

%Compute transform of humeral ACS with respect to HRB CS
T_AH_HRB = T_HRB_TG^-1 * T_AH_TG;

%Compute humeral ACS with respect to scapular ACS
T_AH_AS= T_AS_TG^-1 * T_AH_TG;
```

```
%%%ABDUCTION%%%
%redefine T_AH_AS for abduction
T_AH_AS_rabd=T_AH_AS;

%redefine T_AH_AS to include the desired abduction angle (abduction is humeral ACS rotation about the x axis
%of the scapular ACS)
%rotate the X axis of the transformation about the scapular x axis
tXx=T_AH_AS(1,1); tXy=T_AH_AS(2,1); tXz=T_AH_AS(3,1);
thetaX_x=atan2(abs(tXz),abs(tXy));
if tXz>0 & tXy>0        %quadrant 1
   newthetaX_x=thetaX_x+abd;
elseif tXz>0 & tXy<0    %quadrant 2
   newthetaX_x=-thetaX_x+pi+abd;
elseif tXz<0 & tXy<0    %quadrant 3
   newthetaX_x=thetaX_x+pi+abd;
else
   newthetaX_x=-thetaX_x+2*pi+abd;
end
newtXz=sin(newthetaX_x)*sqrt(tXz^2+tXy^2);
newtXy=newtXz/tan(newthetaX_x);
T_AH_AS_rabd(1:3,1)=[T_AH_AS(1,1) newtXy newtXz]';

%rotate the Y axis of the transformation about the scapular x axis
tYx=T_AH_AS(1,2); tYy=T_AH_AS(2,2); tYz=T_AH_AS(3,2);
thetaY_x=atan2(abs(tYz),abs(tYy));
if tYz>0 & tYy>0        %quadrant 1
   newthetaY_x=thetaY_x+abd;
elseif tYz>0 & tYy<0    %quadrant 2
   newthetaY_x=-thetaY_x+pi+abd;
```

```
elseif tYz<0 & tYy<0    %quadrant 3
   newthetaY_x=thetaY_x+pi+abd;
else
   newthetaY_x=-thetaY_x+2*pi+abd;
end
newtYz=sin(newthetaY_x)*sqrt(tYz^2+tYy^2);
newtYy=newtYz/tan(newthetaY_x);
T_AH_AS_rabd(1:3,2)=[T_AH_AS(1,2) newtYy newtYz]';

%rotate the Z axis of the transformation about the scapular x axis
tZx=T_AH_AS(1,3); tZy=T_AH_AS(2,3); tZz=T_AH_AS(3,3);
thetaZ_x=atan2(abs(tZz),abs(tZy));
if tZz>0 & tZy>0        %quadrant 1
   newthetaZ_x=thetaZ_x+abd;
elseif tZz>0 & tZy<0    %quadrant 2
   newthetaZ_x=-thetaZ_x+pi+abd;
elseif tZz<0 & tZy<0    %quadrant 3
   newthetaZ_x=thetaZ_x+pi+abd;
else
   newthetaZ_x=-thetaZ_x+2*pi+abd;
end
newtZz=sin(newthetaZ_x)*sqrt(tZz^2+tZy^2);
newtZy=newtZz/tan(newthetaZ_x);
T_AH_AS_rabd(1:3,3)=[T_AH_AS(1,3) newtZy newtZz]'

%Compute new transform of humeral ACS wrt TG CS after abduction
T_AH_TG_rabd = T_AS_TG * T_AH_AS_rabd;


%%%FLEXION%%%
%redefine T_AH_AS_rabd for flexion
```

```
T_AH_AS_rabd_rflex=T_AH_AS_rabd;

%redefine T_AH_AS to include the desired flexion angle (flexion is humeral ACS rotation about the y axis
%of the scapular ACS)
%rotate the X axis of the transformation about the scapula y axis
tXx=T_AH_AS_rabd_rflex(1,1);
tXy=T_AH_AS_rabd_rflex(2,1);
tXz=T_AH_AS_rabd_rflex(3,1);
thetaX_y=atan2(abs(tXx),abs(tXz));
if tXx>0 & tXz>0        %quadrant 1
   newthetaX_y=thetaX_y+flex;
elseif tXx>0 & tXz<0    %quadrant 2
   newthetaX_y=-thetaX_y+pi+flex;
elseif tXx<0 & tXz<0    %quadrant 3
   newthetaX_y=thetaX_y+pi+flex;
else
   newthetaX_y=-thetaX_y+2*pi+flex;
end
newtXx=sin(newthetaX_y)*sqrt(tXx^2+tXz^2);
newtXz=newtXx/tan(newthetaX_y);
T_AH_AS_rabd_rflex(1:3,1)=[newtXx T_AH_AS_rabd_rflex(2,1) newtXz]';

%rotate the Y axis of the transformation about the scapula y axis
tYx=T_AH_AS_rabd_rflex(1,2);
tYy=T_AH_AS_rabd_rflex(2,2);
tYz=T_AH_AS_rabd_rflex(3,2);
thetaY_y=atan2(abs(tYx),abs(tYz));
if tYx>0 & tYz>0        %quadrant 1
   newthetaY_y=thetaY_y+flex;
elseif tYx>0 & tYz<0    %quadrant 2
```

```
   newthetaY_y=-thetaY_y+pi+flex;
elseif tYx<0 & tYz<0    %quadrant 3
   newthetaY_y=thetaY_y+pi+flex;
else
   newthetaY_y=-thetaY_y+2*pi+flex;
end
newtYx=sin(newthetaY_y)*sqrt(tYx^2+tYz^2);
newtYz=newtYx/tan(newthetaY_y);
T_AH_AS_rabd_rflex(1:3,2)=[newtYx T_AH_AS_rabd_rflex(2,2) newtYz]';

%rotate the Z axis of the transformation about the scapula y axis
tZx=T_AH_AS_rabd_rflex(1,3);
tZy=T_AH_AS_rabd_rflex(2,3);
tZz=T_AH_AS_rabd_rflex(3,3);
thetaZ_y=atan2(abs(tZx),abs(tZz));
if tZx>=0 & tZz>=0        %quadrant 1
   newthetaZ_y=thetaZ_y+flex;
elseif tZx>=0 & tZz<0    %quadrant 2
   newthetaZ_y=-thetaZ_y+pi+flex;
elseif tZx<0 & tZz<0    %quadrant 3
   newthetaZ_y=thetaZ_y+pi+flex;
else
   newthetaZ_y=-thetaZ_y+2*pi+flex;
end
newtZx=sin(newthetaZ_y)*sqrt(tZx^2+tZz^2);
newtZz=newtZx/tan(newthetaZ_y);
T_AH_AS_rabd_rflex(1:3,3)=[newtZx T_AH_AS_rabd_rflex(2,3) newtZz]'

%Compute new transform of humeral ACS with respect to TG CS
T_AH_TG_rabd_rflex = T_AS_TG * T_AH_AS_rabd_rflex;
```

```
%%%EXTERNAL ROTATION%%%
%Externally rotate humerus about its long axis (z axis)
%positive z-axis rotation = internal rotation, so need to negate angle
T_rer = [cos(-er) -sin(-er) 0 0;sin(-er) cos(-er) 0 0; 0 0 1 0; 0 0 0 1];
T_AH_TG_rabd_rflex_rer = T_AH_TG_rabd_rflex*T_rer;

%Recompute transform of humeral ACS wrt scapular ACS after external
%rotation (note that z axis should not change relative to T_AH_AS_rabd_rflex)
T_AH_AS_rabd_rflex_rer = T_AS_TG^-1 * T_AH_TG_rabd_rflex_rer;

%add translations of humerus in scapular ACS
T_AH_AS_rabd_rflex_rer_trans = T_AH_AS_rabd_rflex_rer + [0 0 0 trans(1);0 0 0 trans(2); 0 0
0 trans(3); 0 0 0 0];

%recompute transform of humeral ACS with respect to TG CS
T_AH_TG_rabd_rflex_rer_trans = T_AS_TG * T_AH_AS_rabd_rflex_rer_trans;

%compute new transform of HRB CS wrt TG CS
T_HRB_TG_rabd_rflex_rer_trans = T_AH_TG_rabd_rflex_rer_trans * T_AH_HRB^-1

%compute transform of HRB CS in clinically relevant joint position with
%respect to the HRB CS in the reference position, after abduction, flexion,
%external rotation, and translation
T_HRBcrjp_HRBref = T_HRB_TG^-1 * T_HRB_TG_rabd_rflex_rer_trans
```

BIBLIOGRAPHY

1. Cave, E., J. Burke, and R. Boyd, *Trauma Management*. 1974, Chicago, IL: Year Book Medical Publishers. 437.

2. Hawkins, R.J. and N.G. Mohtadi, *Controversy in anterior shoulder instability.* Clin Orthop Relat Res, 1991(272): p. 152-61.

3. Arciero, R.A., et al., *Arthroscopic Bankart repair versus nonoperative treatment for acute, initial anterior shoulder dislocations.* Am J Sports Med, 1994. **22**(5): p. 589-94.

4. Baker, C.L., J.W. Uribe, and C. Whitman, *Arthroscopic evaluation of acute initial anterior shoulder dislocations.* Am J Sports Med, 1990. **18**(1): p. 25-8.

5. Caspari, R.B., *Arthroscopic reconstruction for anterior shoulder instability.* Techniques in Orthopaedics, 1988. **3**: p. 59-66.

6. Field, L.D., D.J. Bokor, and F.H. Savoie, 3rd, *Humeral and glenoid detachment of the anterior inferior glenohumeral ligament: a cause of anterior shoulder instability.* J Shoulder Elbow Surg, 1997. **6**(1): p. 6-10.

7. Lee, T.Q., et al., *Age related biomechanical properties of the glenoid-anterior band of the inferior glenohumeral ligament-humerus complex.* Clin Biomech (Bristol, Avon), 1999. **14**(7): p. 471-6.

8. Morgan, C.D. and A.B. Bodenstab, *Arthroscopic Bankart suture repair: technique and early results.* Arthroscopy, 1987. **3**(2): p. 111-22.

9. Gerber, C. and R. Ganz, *Clinical assessment of instability of the shoulder. With special reference to anterior and posterior drawer tests.* J Bone Joint Surg Br, 1984. **66**(4): p. 551-6.

10. Burkart, A.C. and R.E. Debski, *Anatomy and function of the glenohumeral ligaments in anterior shoulder instability.* Clin Orthop, 2002(400): p. 32-9.

11. Debski, R.E., et al., *In situ force distribution in the glenohumeral joint capsule during anterior-posterior loading.* J Orthop Res, 1999. **17**(5): p. 769-76.

12. Moseley, H. and B. Overgaard, *The anterior capsular mechanism in recurrent anterior dislocation of the shoulder: Morphological and clinical studies with special reference to the glenoid labrum and glenohumeral ligaments.* J Bone Joint Surg Br, 1962. **44**: p. 913-27.

13. O'Brien, S.J., et al., *The anatomy and histology of the inferior glenohumeral ligament complex of the shoulder.* Am J Sports Med, 1990. **18**(5): p. 449-56.

14. Turkel, S.J., et al., *Stabilizing mechanisms preventing anterior dislocation of the glenohumeral joint.* J Bone Joint Surg Am, 1981. **63**(8): p. 1208-17.

15. Matsen, F.A., 3rd, D.T. Harryman, 2nd, and J.A. Sidles, *Mechanics of glenohumeral instability.* Clin Sports Med, 1991. **10**(4): p. 783-8.

16. Pollock, R.G. and L.U. Bigliani, *Recurrent posterior shoulder instability. Diagnosis and treatment.* Clin Orthop Relat Res, 1993(291): p. 85-96.

17. Brenneke, S.L., et al., *Glenohumeral kinematics and capsulo-ligamentous strain resulting from laxity exams.* Clin Biomech (Bristol, Avon), 2000. **15**(10): p. 735-42.

18. Harryman, D.T., 2nd, et al., *Laxity of the normal glenohumeral joint: A quantitative in vivo assessment.* J Shoulder Elbow Surg, 1992. **1**: p. 66-76.

19. Moore, S.M., et al., *Multidirectional kinematics of the glenohumeral joint during simulated simple translation tests: impact on clinical diagnoses.* J Orthop Res, 2004. **22**(4): p. 889-94.

20. Musahl, V., et al., *Orientation feedback during simulated simple translation tests has little clinical significance on the magnitude and precision of glenohumeral joint translations.* Knee Surg Sports Traumatol Arthrosc, 2006. **14**(11): p. 1194-9.

21. Moore, S.M., et al., *The current anatomical description of the inferior glenohumeral ligament does not correlate with its functional role in positions of external rotation.* J Orthop Res, 2008.

22. Tzannes, A., et al., *An assessment of the interexaminer reliability of tests for shoulder instability.* J Shoulder Elbow Surg, 2004. **13**(1): p. 18-23.

23. Hawkins, R.H. and R.J. Hawkins, *Failed anterior reconstruction for shoulder instability.* J Bone Joint Surg Br, 1985. **67**(5): p. 709-14.

24. Cooper, D.E., et al., *Anatomy, histology, and vascularity of the glenoid labrum. An anatomical study.* J Bone Joint Surg Am, 1992. **74**(1): p. 46-52.

25. Lusardi, D.A., et al., *Loss of external rotation following anterior capsulorrhaphy of the shoulder.* J Bone Joint Surg Am, 1993. **75**(8): p. 1185-92.

26. Hovelius, L., *Incidence of shoulder dislocation in Sweden.* Clin Orthop, 1982(166): p. 127-31.

27. *United States Census 2000*. 2000, United States Census Bureau.

28. Nelson, B.J. and R.A. Arciero, *Arthroscopic management of glenohumeral instability.* Am J Sports Med, 2000. **28**(4): p. 602-14.

29. Hovelius, L., *Shoulder dislocation in Swedish ice hockey players.* Am J Sports Med, 1978. **6**(6): p. 373-7.

30. Zebas, C.J., et al., *Musculoskeletal injuries in a college-age population during a 1-semester term.* J Am Coll Health, 1995. **44**(1): p. 32-4.

31. DePalma, A.F., G. Callery, and G.A. Bennett, *Variational anatomy and degenerative lesions of the shoulder joint.* American Academy of Orthopaedic Surgery Instructional Course Lecture Series, 1949. **6**: p. 225-81.

32. Bigliani, L.U., et al., *Tensile properties of the inferior glenohumeral ligament.* J Orthop Res, 1992. **10**(2): p. 187-97.

33. McMahon, P.J., et al., *Deformation and strain characteristics along the length of the anterior band of the inferior glenohumeral ligament.* J Shoulder Elbow Surg, 2001. **10**(5): p. 482-8.

34. Itoi, E., et al., *Capsular properties of the shoulder.* Tohoku J Exp Med, 1993. **171**(3): p. 203-10.

35. Debski, R.E., et al., *The collagen fibers of the anteroinferior capsulolabrum have multiaxial orientation to resist shoulder dislocation.* J Shoulder Elbow Surg, 2003. **12**(3): p. 247-52.

36. Malicky, D.L., et al., *Total and nonrecoverable strain fields of the glenohumeral joint capsule under shoulder subluxation.* Transcripts of the Orthopaedic Research Society, 1999. **40**: p. 94.

37. Warner, J.J.P., et al., *Dynamic capsuloligamentous anatomy of the glenohumeral joint.* J Shoulder Elbow Surg, 1993. **2**: p. 115-33.

38. Warner, J.J.P., et al., *Static capsuloligamentous restraints to superior-inferior translation of the glenohumeral joint.* Am J Sports Med, 1992. **20**(6): p. 675-85.

39. Schwartz, R.E., et al., *Capsular restraints to anterior-posterior motion of the abducted shoulder. A biomechanical study.* Orthopaedic Transactions, 1988. **12**: p. 727.

40. Rainis, E.J., *Characterizing the Mechanical Properties of the Glenohumeral Capsule: Implications for Finite Element Modeling.* Thesis Document, University of Pittsburgh, 2006.

41. Moore, S.M., *Glenohumeral Capsule Should Be Evaluated as a Sheet of Fibrous Tissue: A Study in Functional Anatomy.* Thesis Document, University of Pittsburgh, 2006.

42. Howell, S.M. and B.J. Galinat, *The glenoid-labral socket. A constrained articular surface.* Clin Orthop Relat Res, 1989(243): p. 122-5.

43. Carey, J., C.F. Small, and D.R. Pichora, *In situ compressive properties of the glenoid labrum.* J Biomed Mater Res, 2000. **51**(4): p. 711-6.

44. Hara, H., N. Ito, and K. Iwasaki, *Strength of the glenoid labrum and adjacent shoulder capsule.* J Shoulder Elbow Surg, 1996. **5**(4): p. 263-8.

45. Rao, A.G., et al., *Anatomical variants in the anterosuperior aspect of the glenoid labrum: a statistical analysis of seventy-three cases.* J Bone Joint Surg Am, 2003. **85-A**(4): p. 653-9.

46. Nishida, K., et al., *Histologic and scanning electron microscopic study of the glenoid labrum.* J Shoulder Elbow Surg, 1996. **5**(2 Pt 1): p. 132-8.

47. Lippitt, S. and F. Matsen, *Mechanisms of glenohumeral joint stability.* Clin Orthop Relat Res, 1993(291): p. 20-8.

48. Eberly, V.C., P.J. McMahon, and T.Q. Lee, *Variation in the glenoid origin of the anteroinferior glenohumeral capsulolabrum.* Clinical Orthopaedics & Related Research, 2002(400): p. 26-31.

49. Tamai, K., Okinaga, S, Ohtsuka, M, Inokuchi, A, *Fibrous architecture of the glenoid labrum. In: Takagishi N, Editor. The Shoulder. Professional Postgraduate Services, 1986: 27-9.* .

50. Steinbeck, J., U. Liljenqvist, and J. Jerosch, *The anatomy of the glenohumeral ligamentous complex and its contribution to anterior shoulder stability.* J Shoulder Elbow Surg, 1998. **7**(2): p. 122-6.

51. Uhthoff, H.K. and M. Piscopo, *Anterior capsular redundancy of the shoulder: congenital or traumatic? An embryological study.* J Bone Joint Surg Br, 1985. **67**(3): p. 363-6.

52. Bankart, A.S., *Recurrent or habitual dislocation of the shoulder-joint.* Br Med J, 1923. **2**: p. 1132-3.

53. Bankart, A.S., *The pathology and treatment of recurrent dislocation of the shoulder joint.* British Journal of Surgery, 1938. **26**: p. 23-9.

54. Ovesen, J. and S. Nielsen, *Stability of the shoulder joint. Cadaver study of stabilizing structures.* Acta Orthop Scand, 1985. **56**(2): p. 149-51.

55. Drury, N.J., et al., *Maximum Principal Strains in the Glenohumeral Capsule During a Clinical Exam: A Validated Finite Element Model.* ASME 2007 Summer Bioengineering Conference, SBC2007-175358. Keystone, CO, 2007.

56. Hoffmeyer, P., et al., *Stabilizing mechanism of the glenohumeral ligaments.* Biomed Sci Instrum, 1990. **26**: p. 49-52.

57. O'Connell, P.W., et al., *The contribution of the glenohumeral ligaments to anterior stability of the shoulder joint.* Am J Sports Med, 1990. **18**(6): p. 579-84.

58. Terry, G.C., et al., *The stabilizing function of passive shoulder restraints.* Am J Sports Med, 1991. **19**(1): p. 26-34.

59. Miller, M.C., et al., *A mathematical and experimental model of length change in the inferior glenohumeral ligament in the late cocking phase of pitching.* Transcripts of the Orthopaedic Research Society, 1991. **16**: p. 609.

60. Lew, W.D., J.L. Lewis, and E.V. Craig, *Stabilization by capsule, ligaments, and labrum: Stability at the extremes of motion*, in *The Shoulder: A Balance of Mobility and Stability*, F.A. Matsen, 3rd, F.H. Fu, and R.J. Hawkins, Editors. 1993, American Academy of Orthopaedic Surgeons: Rosemont, IL. p. 69-90.

61. Debski, R.E., et al., *An analytical approach to determine the in situ forces in the glenohumeral ligaments.* J Biomech Eng, 1999. **121**(3): p. 311-5.

62. Novotny, J.E., B.D. Beynnon, and C.E. Nichols, *Modeling the stability of the human glenohumeral joint during external rotation.* J Biomech, 2000. **33**(3): p. 345-54.

63. Debski, R.E., et al., *The collagen fibers of the anteroinferior capsulolabrum have multi-axial orientation to resist shoulder dislocation.* J Shoulder Elbow Surg, 2002. **in press**.

64. Drury, N.J., et al., *The Inferior Stability Provided by the Glenohumeral Capsule Increases with External Rotation in the Abducted Glenohumeral Joint.* ASME 2008 Summer Bioengineering Conference, SBC2008-192857. Marco Island, FL, 2008.

65. Rowe, C.R., B. Zarins, and J.V. Ciullo, *Recurrent anterior dislocation of the shoulder after surgical repair. Apparent causes of failure and treatment.* J Bone Joint Surg Am, 1984. **66**(2): p. 159-68.

66. Rockwood, C.A., et al., *The Shoulder*. 2nd ed. 1998, Philadelphia, PA: W. B. Saunders Co.

67. Silliman, J.F. and R.J. Hawkins, *Classification and physical diagnosis of instability of the shoulder.* Clin Orthop Relat Res, 1993(291): p. 7-19.

68. Millett, P.J., et al., *Recurrent posterior shoulder instability.* J Am Acad Orthop Surg, 2006. **14**(8): p. 464-76.

69. Levy, A.S., et al., *Intra- and interobserver reproducibility of the shoulder laxity examination.* Am J Sports Med, 1999. **27**(4): p. 460-3.

70. Warren, R.F., *Subluxation of the shoulder in athletes.* Clin Sports Med, 1983. **2**(2): p. 339-54.

71. Liu, S.H. and M.H. Henry, *Anterior shoulder instability. Current review.* Clin Orthop, 1996(323): p. 327-37.

72. Henry, J.H. and J.A. Genung, *Natural history of glenohumeral dislocation--revisited.* Am J Sports Med, 1982. **10**(3): p. 135-7.

73. Hovelius, L., *Anterior dislocation of the shoulder in teen-agers and young adults. Five-year prognosis.* J Bone Joint Surg Am, 1987. **69**(3): p. 393-9.

74. McLaughlin, H.L. and D.I. MacLellan, *Recurrent anterior dislocation of the shoulder. II. A comparative study.* J Trauma, 1967. **7**(2): p. 191-201.

75. Simonet, W.T. and R.H. Cofield, *Prognosis in anterior shoulder dislocation.* Am J Sports Med, 1984. **12**(1): p. 19-24.

76. Wheeler, J.H., et al., *Arthroscopic versus nonoperative treatment of acute shoulder dislocations in young athletes.* Arthroscopy, 1989. **5**(3): p. 213-7.

77. Neer, C.S., 2nd and C.R. Foster, *Inferior capsular shift for involuntary inferior and multidirectional instability of the shoulder. A preliminary report.* J Bone Joint Surg Am, 1980. **62**(6): p. 897-908.

78. Deutsch, A., et al., *Anterior-inferior capsular shift of the shoulder: a biomechanical comparison of glenoid-based versus humeral-based shift strategies.* J Shoulder Elbow Surg, 2001. **10**(4): p. 340-52.

79. Speer, K.P., et al., *Strategies for an anterior capsular shift of the shoulder. A biomechanical comparison.* Am J Sports Med, 1995. **23**(3): p. 264-9.

80. Sperber, A., et al., *Comparison of an arthroscopic and an open procedure for posttraumatic instability of the shoulder: a prospective, randomized multicenter study.* J Shoulder Elbow Surg, 2001. **10**(2): p. 105-8.

81. Montgomery, W.H., 3rd and F.W. Jobe, *Functional outcomes in athletes after modified anterior capsulolabral reconstruction.* Am J Sports Med, 1994. **22**(3): p. 352-8.

82. Bigliani, L.U., et al., *Inferior capsular shift procedure for anterior-inferior shoulder instability in athletes.* Am J Sports Med, 1994. **22**(5): p. 578-84.

83. Harryman, D.T., 2nd, et al., *The role of the rotator interval capsule in passive motion and stability of the shoulder.* J Bone Joint Surg Am, 1992. **74**(1): p. 53-66.

84. Boardman, N.D., et al., *Tensile properties of the superior glenohumeral and coracohumeral ligaments.* J Shoulder Elbow Surg, 1996. **5**(4): p. 249-54.

85. Provencher, M.T., et al., *Arthroscopic versus open rotator interval closure: biomechanical evaluation of stability and motion.* Arthroscopy, 2007. **23**(6): p. 583-92.

86. Harryman, D.T., 2nd, et al., *Translation of the humeral head on the glenoid with passive glenohumeral motion.* J Bone Joint Surg Am, 1990. **72**(9): p. 1334-43.

87. Mahaffey, B.L. and P.A. Smith, *Shoulder instability in young athletes.* Am Fam Physician, 1999. **59**(10): p. 2773-82, 2787.

88. Beynnon, B., et al., *The measurement of anterior cruciate ligament strain in vivo.* Int Orthop, 1992. **16**(1): p. 1-12.

89. Beynnon, B.D., et al., *Anterior cruciate ligament strain behavior during rehabilitation exercises in vivo.* Am J Sports Med, 1995. **23**(1): p. 24-34.

90. Debski, R.E., et al., *Stress and strain in the anterior band of the inferior glenohumeral ligament during a simulated clinical examination.* J Shoulder Elbow Surg, 2005. **14**(1 Suppl S): p. 24S-31S.

91. Musahl, V., et al., *The use of porcine small intestinal submucosa to enhance the healing of the medial collateral ligament--a functional tissue engineering study in rabbits.* Journal of Orthopaedic Research, 2004. **22**(1): p. 214-20.

92. Race, A. and A.A. Amis, *The mechanical properties of the two bundles of the human posterior cruciate ligament.* J Biomech, 1994. **27**(1): p. 13-24.

93. Woo, S.L., *Mechanical properties of tendons and ligaments. I. Quasi-static and nonlinear viscoelastic properties.* Biorheology, 1982. **19**(3): p. 385-96.

94. Woo, S.L., K.J. Ohland, and J.A. Weiss, *Aging and sex-related changes in the biomechanical properties of the rabbit medial collateral ligament.* Mech Ageing Dev, 1990. **56**(2): p. 129-42.

95. Gardiner, J.C. and J.A. Weiss, *Subject-specific finite element models can predict strain in the human medial collateral ligament during valgus knee loading.* J Orthop Res, 2002. **In press**.

96. Malicky, D.M., et al., *Total strain fields of the antero-inferior shoulder capsule under subluxation: a stereoradiogrammetric study.* J Biomech Eng, 2001. **123**(5): p. 425-31.

97. McMahon, P.J., et al., *The anterior band of the inferior glenohumeral ligament: biomechanical properties from tensile testing in the position of apprehension.* J Shoulder Elbow Surg, 1998. **7**(5): p. 467-71.

98. Quapp, K.M. and J.A. Weiss, *Material characterization of human medial collateral ligament.* Journal of Biomechanical Engineering, 1998. **120**(6): p. 757-63.

99. Soslowsky, L.J., et al. *Total and non-recoverable strain fields of the glenohumeral joint capsule under shoulder subluxation.* in *Open Meeting, American Shoulder Elbow Surgeons*. 2000. Orlando, FL.

100. Ticker, J.B., et al., *Inferior glenohumeral ligament: geometric and strain-rate dependent properties.* J Shoulder Elbow Surg, 1996. **5**(4): p. 269-79.

101. Urayama, M., et al., *Function of the 3 portions of the inferior glenohumeral ligament: a cadaveric study.* J Shoulder Elbow Surg, 2001. **10**(6): p. 589-94.

102. Newman, W.J., et al. *Function of the anterior band of the inferior glenohumeral ligament during the load and shift test*. in *ASME Advances in Bioengineering*. 2002.

103. Ellis, B.J., et al., *Methodology and Sensitivity Studies for Finite Element Modeling of the Inferior Glenohumeral Ligament Complex.* J Biomech, 2006. **In Press**.

104. Maker, B.N., R.M. Ferencz, and J.O. Hallquist, *NIKE3D: A nonlinear, implicit, three-dimensional finite element code for solid and structural mechanics*. 1990, Lawrence Livermore National Laboratory.

105. Weiss, J.A., D.A. Schauer, and J.C. Gardiner. *Modeling contact in biological joints using penalty and augmented Lagrangian methods*. in *ASME Winter Annual Meeting*. 1996.

106. Weiss, J.A., B.N. Maker, and D.A. Schauer. *Treatment of initial stress in hyperelastic finite element models of soft tissues*. in *ASME Summer Bioengineering Conference*. 1995.

107. Weiss, J.A., B.N. Maker, and S. Govindjee, *Finite element implementation of incompressible, transversely isotropic hyperelasticity*. Comp Meth Appl Mech Eng, 1996. **135**: p. 107-28.

108. Weiss, J.A., J.C. Gardiner, and C. Bonifasi-Lista, *Ligament material behavior is nonlinear, viscoelastic and rate-independent under shear loading.* J Biomech, 2002. **35**(7): p. 943-50.

109. Gardiner, J.C. and J.A. Weiss, *Simple shear testing of parallel-fibered planar soft tissues.* Journal of Biomechanics, 2001. **123**: p. 1-5.

110. Anderson, A.E., et al., *Subject-specific finite element model of the pelvis: development, validation and sensitivity studies.* J Biomech Eng, 2005. **127**(3): p. 364-73.

111. Drury, N.J., et al., *The Impact of Glenoid Labrum Thickness and Modulus on Labrum and Glenohumeral Capsule Pathology*. ORS 2008 Annual Meeting. San Francisco, CA, 2008.

112. Ellis, B.J., et al., *Methodology and sensitivity studies for finite element modeling of the inferior glenohumeral ligament complex.* J Biomech, 2007. **40**(3): p. 603-12.

113. Veronda, D.R. and R.A. Westmann, *Mechanical characterization of skin-finite deformations.* Journal of Biomechanics, 1970. **3**: p. 111-124.

114. Engelmann, B.E., Whirley, R.G., Goudreau, G.L., *A simple shell element formulation for large-scale elastoplastic analysis, in "Analytical and Computational Models of Shells," CED-Vol 3, The American Society of Mechanical Engineers, New York, 1989.*

115. Matthies, H. and G. Strang, *The solution of nonlinear finite element equations.* Int J Numer Methods Engng, 1979. **14**: p. 1613-26.

116. Maker, B.N., *Rigid bodies for metal forming analysis with NIKE3D*. 1995, University of California, Lawrence Livermore Laboratory. p. 1-8.

117. Malicky, D.M., et al., *Neer Award 2001: nonrecoverable strain fields of the anteroinferior glenohumeral capsule under subluxation.* J Shoulder Elbow Surg, 2002. **11**(6): p. 529-40.

118. Burkart, A., et al., *Glenohumeral translations are only partially restored after repair of the type II SLAP lesion.* American Journal of Sports Medicine, 2002. **In press**.

119. Li, G., J. Suggs, and T. Gill, *The effect of anterior cruciate ligament injury on knee joint function under a simulated muscle load: a three-dimensional computational simulation.* Ann Biomed Eng, 2002. **30**(5): p. 713-20.

120. Li, G., et al., *A validated three-dimensional computational model of a human knee joint.* J Biomech Eng, 1999. **121**(6): p. 657-62.

121. Song, Y., et al., *A three-dimensional finite element model of the human anterior cruciate ligament: a computational analysis with experimental validation.* J Biomech, 2004. **37**(3): p. 383-90.

122. Bey, M.J., et al., *Structural and mechanical properties of the glenohumeral joint posterior capsule.* J Shoulder Elbow Surg, 2005. **14**(2): p. 201-6.

123. McMahon, P.J., et al., *Variation in the histologic anatomy of the glenoid origin of the anterior band of the IGHL.* Transcripts of the Orthopaedic Research Society, 1999. **24**.

124. Bourne, D.A., et al., *Three-dimensional rotation of the scapula during functional movements: an in vivo study in healthy volunteers.* J Shoulder Elbow Surg, 2007. **16**(2): p. 150-62.

125. Ebaugh, D.D., P.W. McClure, and A.R. Karduna, *Three-dimensional scapulothoracic motion during active and passive arm elevation.* Clin Biomech (Bristol, Avon), 2005. **20**(7): p. 700-9.

126. McClure, P.W., et al., *Direct 3-dimensional measurement of scapular kinematics during dynamic movements in vivo.* J Shoulder Elbow Surg, 2001. **10**(3): p. 269-77.

127. Rudy, T.W., et al., *A combined robotic/universal force sensor approach to determine in situ forces of knee ligaments.* J Biomech, 1996. **29**(10): p. 1357-60.

128. Livesay, G.A., et al., *Evaluation of the effect of joint constraints on the in situ force distribution in the anterior cruciate ligament.* J Orthop Res, 1997. **15**(2): p. 278-84.

129. Livesay, G.A., et al., *Determination of the in situ forces and force distribution within the human anterior cruciate ligament.* Ann Biomed Eng, 1995. **23**(4): p. 467-74.

130. Zeminski, J., *Development of a combined analytical and experimental approach to reproduce knee kinematics for the evaluation of anterior cruciate ligament function,* in *Mechanical Engineering*. 2001, University of Pittsburgh: Pittsburgh, PA.

131. Fujie, H., et al., *The use of a universal force-moment sensor to determine in-situ forces in ligaments: a new methodology.* J Biomech Eng, 1995. **117**(1): p. 1-7.

132. Ferguson, S.J., J.T. Bryant, and K. Ito, *The material properties of the bovine acetabular labrum.* J Orthop Res, 2001. **19**(5): p. 887-96.

133. Gohlke, F., B. Essigkrug, and F. Schmitz, *The patterns of the collagen fiber bundles of the capsule of the glenohumeral joint.* J Shoulder Elbow Surg, 1994. **3**(3): p. 111-28.

134. Prodromos, C.C., et al., *Histological studies of the glenoid labrum from fetal life to old age.* J Bone Joint Surg Am, 1990. **72**(9): p. 1344-8.

135. Smith, C.D., et al., *Tensile properties of the human glenoid labrum.* J Anat, 2007.

136. Ishiko, T., M. Naito, and S. Moriyama, *Tensile properties of the human acetabular labrum-the first report.* J Orthop Res, 2005. **23**(6): p. 1448-53.

137. Joshi, M.D., et al., *Interspecies variation of compressive biomechanical properties of the meniscus.* J Biomed Mater Res, 1995. **29**(7): p. 823-8.

138. Lechner, K., M.L. Hull, and S.M. Howell, *Is the circumferential tensile modulus within a human medial meniscus affected by the test sample location and cross-sectional area?* J Orthop Res, 2000. **18**(6): p. 945-51.

139. Fithian, D.C., M.A. Kelly, and V.C. Mow, *Material properties and structure-function relationships in the menisci.* Clin Orthop Relat Res, 1990(252): p. 19-31.

140. Tissakht, M. and A.M. Ahmed, *Tensile stress-strain characteristics of the human meniscal material.* J Biomech, 1995. **28**(4): p. 411-22.

141. Fischer, K.J., et al., *A method for measuring joint kinematics designed for accurate registration of kinematic data to models constructed from CT data.* J Biomech, 2001. **34**(3): p. 377-83.

142. Simo, J.C., *On the dynamics in space of rods undergoing large motions: A geometrically exact approach.* Comp Meth Appl Mech Eng, 1988. **66**: p. 125-161.

143. Munro, B.H., *Statistical Methods for Health Care Research*. 5th ed. 2005, Philadelphia, PA: Lippincott-Raven Publishers.

144. Gardiner, J.C. and J.A. Weiss, *Subject-specific finite element analysis of the human medial collateral ligament during valgus knee loading.* J Orthop Res, 2003. **21**(6): p. 1098-106.

145. Ellis, B.J., et al., *Medial collateral ligament insertion site and contact forces in the ACL-deficient knee.* J Orthop Res, 2006. **24**(4): p. 800-10.

146. Gardiner, J.C. and J.A. Weiss, *Simple shear testing of parallel-fibered planar soft tissues.* J Biomech Eng, 2001. **123**(2): p. 170-5.

147. Chen, S., et al., *The effects of thermal capsular shrinkage on the outcomes of arthroscopic stabilization for primary anterior shoulder instability.* Am J Sports Med, 2005. **33**(5): p. 705-11.

148. Levine, W.N., L.U. Bigliani, and C.S. Ahmad, *Thermal capsulorrhaphy.* Orthopedics, 2004. **27**(8): p. 823-6.